Analysis of the epigenetics of meiotic silencing and its role in germ cell loss

Jeffrey M Cloutier

University College London
and
National Institute for Medical Research
PhD Supervisor: James MA Turner

A thesis submitted for the degree of
Doctor of Philosophy
University College London
2016

Declaration

I, Jeffrey M Cloutier, confirm that the work presented in this thesis is my own. Where information has been derived from other sources, I confirm that this has been indicated in the thesis.

Abstract

Numerical and structural chromosome abnormalities are common in the human population and cause infertility associated with germ cell losses during meiotic prophase I. The precise trigger of germ cell loss in response to chromosome abnormalities in mammals is still unclear, but several models have been postulated, including a DNA damage checkpoint, an asynapsis checkpoint, and meiotic silencing of asynapsed chromosomes. Here, I investigate the contribution of these mechanisms to oocyte loss in mice with chromosome abnormalities, such as X chromosome monosomy (XO). First, I show that asynapsed chromosomes trigger oocyte elimination during diplonema of meiotic prophase I, later than predicted by the pachytene checkpoint model that has been characterized in other organisms. Markers of DNA double-strand break repair disappear from asynapsed chromosomes during pachynema, suggesting that persistent DNA damage is unlikely to be the proximal cause of diplotene oocyte losses in chromosomally abnormal mice. I also show that oocytes with asynapsed accessory (i.e. supernumerary) chromosomes are not eliminated during diplonema, suggesting that asynapsis *per se* is not sufficient to cause germ cell loss. In support of the meiotic silencing model of germ cell loss, I find that deletion of the meiotic silencing factor *H2afx* prevents diplotene oocyte elimination in XO females. I show that meiotic silencing is less robust in oocytes compared to spermatocytes, and that this may be associated with sex-specific differences in the epigenetics of meiotic silencing. Finally, I report on the meiotic characterization of *Brca1* and *Hormad2* mutant mouse models, and in doing so ascribe critical roles for them in the meiotic silencing pathway. Together, these studies inform a meiotic silencing-based mechanism of prophase I surveillance against asynapsis.

Acknowledgements

First and foremost, I thank James Turner for his unwavering support and mentorship throughout my PhD, and for his technical expertise, countless ideas and suggestions, and endless patience. I also thank Daniel Camerini-Otero for his mentorship and support during my time at the NIH.

I thank Shantha Mahadevaiah for her technical assistance and Kevin Brick for his computation analysis assistance. I thank members of the Turner laboratory, including Helene Royo, Greg Polikiewicz, Elias Elinati, and Mahesh Sangrithi, and members of the Camerini-Otero laboratory, especially Flor Pratto and Kevin Brick, for their support and help. I am very thankful to my family for their encouragement throughout this process.

I am grateful to many people for providing critical resources, including Jiří Forejt for providing T43H ovaries, Victor Tybulewicz for providing Tc1 mice, Chu-Xia Deng for the BRCA1 antibody, Attila Tóth for *Hormad2*-/- mice and HORMAD1/2 antibodies. I thank Greg Polikiewicz for assistance with genotyping, Paul Burgoyne for maintenance of the Tc1 mouse line, and NIMR Biological Services for animal husbandry and technical support.

Finally, I am indebted to the MRC National Institutes of Health, National Institutes of Health, and the Marshall Commission for providing the opportunity and funding to pursue this PhD.

Table of Contents

Abstract **3**

Acknowledgements **4**

List of Figures **8**

List of Tables **10**

1 Introduction **11**

1.1 Mammalian meiosis: an overview **11**

1.1.1 Developmental timing and duration of meiosis 12

1.1.2 Meiotic prophase I events: an overview 14

1.1.3 Aneuploidy and meiotic errors 15

1.1.4 Meiotic surveillance mechanisms: an overview 18

1.2 Meiotic DNA double-strand breaks and repair **19**

1.2.1 Meiotic DNA DSBs initiation 19

1.2.2 Distribution of meiotic DNA DSBs 20

1.2.3 Regulation of meiotic DNA DSB formation 21

1.2.4 Repair of DNA DSBs by homologous recombination 22

1.2.5 DNA DSB cytological analysis by chromosome spreads 25

1.2.6 Meiotic DNA DSB repair proteins 25

1.2.7 Meiotic DNA DSBs on the X and Y chromosomes 32

1.3 Meiotic chromosome synapsis **36**

1.3.1 Synapsis: an overview 36

1.3.2 Components of the synaptonemal complex 36

1.3.3 Synaptonemal complex assembly and dynamics 37

1.4 Meiotic silencing **42**

1.4.1 Meiotic Sex Chromosome Inactivation (MSCI) 42

1.4.2 Meiotic silencing of unsynapsed chromatin (MSUC) 44

1.4.2 Epigenetics of meiotic silencing in mice 46

1.4.3 Meiotic silencing from an evolutionary perspective 56

1.4.4 Role of meiotic silencing in mammalian germ cells 58

1.5 Meiotic surveillance mechanisms **62**

1.5.1 The eukaryotic cell cycle 62

1.5.2 The DNA damage checkpoint: a mitotic perspective 64

1.5.3 Meiotic DNA damage checkpoint: insight from other organisms 66

1.5.4 DNA damage checkpoint model in mice 67

1.5.5 Asynapsis checkpoint model 72

1.5.6 Meiotic silencing model of meiotic surveillance 77

1.6 Aims of thesis **81**

2 Materials and Methods **82**

2.1. Mice **82**

2.1.1 XO mice 82

2.1.2 In(X)1H mice 83

2.1.3 T(16;17)43H mice 83

2.1.4 Tc1 mice 84

2.1.5 XY^{d1} mice 84

2.1.6 XXY^{d1} mice 85

2.1.7 *H2afx*-/- and XO *H2afx*-/- mice 85

2.1.8 *Spo11*-/- and XO *Spo11*+/- 86

2.1.9 *H2afx*-/- *Spo11*-/- mice 87

2.1.10 *Dmc1*-/- and *H2afx*-/- *Dmc1*-/- mice 88

2.1.11 *Hormad2*-/- mice 89

2.1.12 *Brca1-/- 53bp1-/-* mice ... 89
2.1.13 *Brca1*Δ11/Δ11 *p53+/-* ... 90
2.2 Genotyping ... 90
2.3 Chromosome spreads and immunofluorescence ... 94
2.4 Chromosome painting ... 95
2.5 RNA fluorescent *in-situ* hybridization (RNA FISH) and immunofluorescence ... 96
2.6 Ovarian sectioning and oocyte counting ... 97
2.7 Imaging ... 97
2.8 Statistics ... 98
2.9 Chromatin immunoprecipitation and sequencing (ChIP-seq) ... 98
2.10 ChIP-seq data analysis ... 101

3 Results: Characterization of oocyte losses in chromosomally abnormal mice ... 102
3.1 Timing of oocyte losses in mice with chromosome abnormalities ... 103
3.1.1 Classification of oocytes into meiotic prophase I sub-stages ... 103
3.1.2 γH2AFX marks the asynapsed X chromosome in XO oocytes ... 107
3.1.3 Elimination of XO oocytes with an asynapsed X chromosome ... 110
3.1.4 Elimination of In(X)1H oocytes with asynapsed X chromosomes ... 113
3.1.5 Elimination of T(16;17)43H oocytes with asynapsed autosomes ... 115
3.1.6 Elimination of XX oocytes with asynapsis ... 117
3.2 The role of meiotic DNA DSBs in oocyte losses in chromosomally abnormal mice ... 120
3.2.1 DNA DSB repair proteins do not persist on the asynapsed X chromosome in XO oocytes ... 120
3.2.2 DNA DSB repair proteins do not persist on multiple asynapsed chromosomes in PWDxB6 F1 oocytes ... 123
3.2.3 *Spo11* heterozygosity does not attenuate XO oocyte losses ... 126
3.3 The role of an asynapsis checkpoint in oocyte losses in chromosomally abnormal mice ... 128
3.3.1 Predictions under asynapsis checkpoint model ... 128
3.3.2 RNA FISH analysis of transcription in XX oocytes ... 131
3.3.3 Meiotic characterization of Tc1 mouse model of Down syndrome ... 134
3.3.4 Tc1 oocytes with an asynapsed h21 chromosomes persist into diplonema ... 138
3.3.5 XXY^{d1} oocytes with an asynapsed accessory Y chromosome persist to late diplonema ... 140
3.4 Discussion ... 142

4 Results: The role of H2AFX in oocyte losses in chromosomally abnormal mice ... 147
4.1 A role for H2AFX in XO oocyte losses ... 148
4.1.1 Sub-staging XO *H2afx-/-* oocytes and identifying the asynapsed X chromosome ... 148
4.1.2 Autosomal synapsis and DNA DSB repair in XO *H2afx-/-* oocytes ... 151
4.1.3 XO *H2afx-/-* oocytes persist to late diplotene ... 154
4.1.4 XO *H2afx-/-* oocytes with a non-phosphorylatable *H2afx* transgene persist to late diplonema ... 155
4.1.5 XO *H2afx-/-* females have more oocytes than XO females perinatally ... 156
4.2 A role for H2AFX in *Spo11-/-* oocyte losses ... 160
4.2.1 γH2AFX domain frequency in *Spo11-/-* oocytes ... 160
4.2.2 *H2afx* nullizygosity increases *Spo11-/-* oocyte numbers perinatally ... 161
4.2.3 SPO11-independent DNA DSBs in oocytes ... 164

4.3 H2AFX is not required for elimination of *Dmc1*-/- oocytes 167
4.4 Discussion 170

5 Results: Characterization of meiotic silencing in oocytes 175
5.1 RNA FISH analysis of the X chromosome in germ cells 175
5.1.1 Silencing of the X chromosome in XY spermatocytes 175
5.1.2. Silencing of the X chromosome in XO oocytes 179
5.1.3 Mosaic gene inactivation of the X chromosome in XO oocytes 183
5.2 RNA FISH analysis of the h21 chromosome in Tc1 germ cells 185
5.2.1 Silencing of the h21 chromosome in Tc1 spermatocytes 185
5.2.2 Silencing of the h21 chromosome in Tc1 oocytes 186
5.2.3 Mosaic gene silencing of the h21 chromosome in Tc1 oocytes 189
5.3 Characterization of the sexually dimorphic silencing response 191
5.3.1 The Y chromosome does not improve X silencing in oocytes 191
5.3.2 γH2AFX domain intensity in XO spermatocytes and oocytes. 194
5.3.3 X chromatin compaction in XO spermatocytes and oocytes 194
5.4 Discussion 197

6 Results: Examination of factors involved in meiotic silencing 202
6.1 Role of BRCA1 during meiotic prophase I 203
6.1.1 BRCA1 localization during male meiotic prophase I 203
6.1.2 Localization of BRCA1 in meiotic mutant spermatocytes 205
6.1.3 RAD51 localization in *Brca1* mutants 208
6.1.4 ChIP-seq in wildtype spermatocytes 211
6.1.5 Anti-BRCA1 ChIP-seq in *Spo11*-/- mice 216
6.1.6 Anti-DMC1 ChIP-seq in *Brca1*-/- spermatocytes 220
6.1.7 ATR localization in *Brca1*-/- spermatocytes 222
6.2. Role of *Hormad2* in meiotic silencing 225
6.2.1 Localization of silencing factors in *Hormad2-/-* mice 225
6.2.2 RNA FISH analysis of X gene transcription in Hormad2-/- mice 228
6.3 Discussion 232

7 General discussion 239
7.1 Overall summary 239
7.2 H2AFX-dependent meiotic surveillance 240
7.3 Limitations of an H2AFX-based surveillance mechanism 242
7.4 DNA DSB repair and the DNA damage checkpoint in mice 244
7.5 Other factors involved in meiotic silencing and surveillance 245
7.6 Sexual dimorphism in meiotic silencing 248

References 251

List of Figures

Introduction Figure 1: Meiosis in male and female mice. 13
Introduction Figure 2: Meiotic non-disjunction and aneuploidy. 17
Introduction Figure 3: Meiotic homologous recombination. 24
Introduction Figure 4: Synaptonemal complex dynamics. 40
Introduction Figure 5: Factors involved in meiotic silencing in mice. 55
Introduction Figure 6: Meiotic surveillance mechanisms in mice. 63
Introduction Figure 7: Meiotic DNA damage checkpoint model of germ cell loss in mice. 71
Introduction Figure 8: Asynapsis checkpoint model of germ cell loss in mice. 76
Introduction Figure 9: Meiotic silencing model of germ cell loss in mice. 80
Figure 1.1. Oocyte sub-staging criteria. 105
Figure 1.2. Oocyte sub-stages at different gestational ages. 106
Figure 1.3. XO oocytes with an asynapsed X chromosome. 109
Figure 1.4. Elimination of XO oocytes with an asynapsed X chromosome. 112
Figure 1.5. Elimination of In(X)1H oocytes with asynapsis. 114
Figure 1.6. Elimination of T(16;17)43H oocytes with asynapsed autosomes 116
Figure 1.7. Elimination of XX oocytes with asynapsis. 118
Figure 1.8. Schematic depicting fate of prophase I oocytes with chromosome abnormalities. 119
Figure 2.1 DNA DSB repair proteins do not persist on the asynapsed X chromosome in XO oocytes. 122
Figure 2.2. DNA DSB repair proteins do not persist on multiple asynapsed chromosomes in PWDxB6 F1 oocytes. 125
Figure 2.3. Elimination of XO *Spo11*+/- oocytes. 127
Figure 2.4. Predictions for fate of oocytes with asynapsed chromosomes containing non-essential genes. 130
Figure 2.5. Cot-1 RNA FISH analysis of wildtype XX oocytes. 133
Figure 2.6. Meiotic characterization of Tc1 oocytes with an asynapsed h21 chromosome. 136
Figure 2.7. Tc1 oocytes with an asynapsed h21 persist to late diplonema. 139
Figure 2.8. XXY^{d1} oocytes with an asynapsed Y^{d1} chromosome persist to late diplonema. 141
Figure 3.1. Characterization of XO *H2afx*+/- and XO *H2afx*-/- females. 150
Figure 3.2. Autosomal synapsis and DNA DSB repair are unaffected in XO *H2afx*-/- oocytes. 153
Figure 3.3. *H2afx* is required for the elimination of XO oocytes with an asynapsed X chromosome. 158
Figure 3.4. *H2afx* nullizygosity increases *Spo11*-/- oocyte numbers perinatally. 163
Figure 3.5. DNA DSB repair foci in *Spo11*-/- oocytes. 166
Figure 3.6. *H2afx* is not required for the elimination of *Dmc1*-/- oocytes. 169
Figure 3.7. Meiotic silencing model of prophase I oocyte elimination. 174
Figure 4.1. RNA FISH analysis of wildtype and *H2afx*-/- spermatocytes. 178
Figure 4.2. Incomplete silencing of the X chromosome in XO oocytes. 181
Figure 4.3. Mosaic silencing of the X chromosome in XO oocytes. 184
Figure 4.4. Incomplete silencing of the h21 chromosome in Tc1 oocytes. 187
Figure 4.5. Mosaic silencing of the h21 chromosome in Tc1 oocytes. 190
Figure 4.6. RNA FISH analysis of XY^{d1} oocytes. 193
Figure 4.7. γH2AFX domains in XO oocytes versus spermatocytes. 196

Figure 5.1. BRCA1 localization in wildtype, *Dmc1*-/-, and *Spo11*-/- spermatocytes. 206
Figure 5.2. RAD51 localization in *Brca1*Δ11/Δ11 mutant spermatocytes. ... 209
Figure 5.3. Control anti-DMC1 ChIP-seq in wildtype spermatocytes. 212
Figure 5.4. Anti-BRCA1 ChIP-seq in wildtype spermatocytes. 214
Figure 5.5. Anti-BRCA1 ChIP-seq in *Spo11*-/- spermatocytes..... 218
Figure 5.6. Anti-DMC1 ChIP-seq in *Brca1*-/- spermatocytes..... 221
Figure 5.7. ATR localization in wildtype and *Brca1*-/- spermatocytes. 224
Figure 5.8. Abnormal BRCA1 and γH2AFX staining in *Hormad2*-/- spermatocytes. 226
Figure 5.9. RNA FISH analysis of *Hormad2*-/- spermatocytes. 230
Figure 5.10. Model for mechanism of meiotic silencing in wildtype and mutant meiosis. 237

List of Tables

Table 1. Proteins involved in meiotic DNA DSB events 34
Table 2. Proteins involved in the meiotic synaptonemal complex 41
Table 3. Description of factors involved in meiotic silencing 53
Table 4: Genotyping primers and PCR conditions. 92
Table 5: Antibodies used for immunofluorescence experiments 95
Table 6: Antibodies used for ChIP-seq 99

1 Introduction

Aneuploidy is a common chromosome abnormality in humans, affecting 7-10% of clinically recognized pregnancies (Hunt and Hassold, 2008). Many aneuploid conditions, such as Turner syndrome (chromosome X monosomy; XO), are associated with germ cell loss and infertility (Burgoyne et al., 2009). The underlying molecular basis for germ cell loss associated with chromosome abnormalities is still not well understood (Hall et al., 2006). The primary goal of this thesis is to examine and characterize the mechanisms that respond to chromosome abnormalities and lead to germ cell losses.

1.1 Mammalian meiosis: an overview

Meiosis is an integral step of gametogenesis, the process of forming mature eggs and sperm for reproduction (Handel and Schimenti, 2010). Meiosis is characterized by one round of DNA replication, an extended prophase I stage, and two successive cell divisions (**Intro Figure 1**). Meiotic prophase I consists of several meiosis-specific events that are essential for the production of viable gametes. Two such events are the physical pairing of maternal and paternal homologous chromosomes, called synapsis, and the reshuffling of genetic material between them by meiotic recombination (Bolcun-Filas and Schimenti, 2012). Together, these events result in the establishment of crossovers (CO) between homologs, which are required for accurate chromosome segregation (Bolcun-Filas and Schimenti, 2012). Additionally, meiotic recombination creates new genetic combinations from maternal and paternal genomes.

During metaphase I, homologous chromosomes align at the equatorial plate in a bi-oriented fashion (Handel and Schimenti, 2010). Chromosome bi-orientation ensures that homologs are segregated faithfully into different daughter cells during the first meiotic division (Wang and Sun, 2006). The first division yields two daughter cells, each with one chromosome (two chromatids) from every homologous pair. These daughter cells then undergo meiosis II, which involves the alignment of

paired sister chromatids, followed by their separation into two more daughter cells. At the end of one cycle of meiosis, genetically unique haploid gametes are produced (Handel and Schimenti, 2010).

1.1.1 Developmental timing and duration of meiosis

The timing and duration of meiosis vary widely between different species and even between sexes (**Intro Figure 1**). In mammals, male meiosis occurs in a series of uninterrupted steps beginning during early post-natal life. In juvenile male mice, the first subset of germ cells enters meiosis at 10.5 d*pp* and completes meiotic prophase I at 21 d*pp* (Cohen et al., 2006). At 21 d*pp*, spermatocytes enter metaphase I and subsequently progress through meiosis I and meiosis II. Following the second meiotic division, male germ cells undergo significant morphological changes in a process called spermiogenesis (for review see (Jan et al., 2012)). By 27 d*pp*, mature sperm (i.e. spermatozoa) are formed, and continuous cycles of meiosis ensue thereafter (Cohen et al., 2006). Therefore, at the end of each cycle each germ cell produces four haploid spermatozoa.

By contrast, female meiosis – the main focus of this thesis – takes place predominantly during embryonic development and occurs over a significantly longer timeframe (**Intro Figure 1**). Meiotic prophase I begins at 13 days *post coitum* (d*pc*), and germ cells reach pachynema by 17 d*pc* (Speed, 1982). Oocytes complete prophase I by 21 d*pc* (i.e. 1-2 days *post partum* (d*pp*)), and soon after enter an extended arrest period called the dictyate stage (Pepling and Spradling, 2001; Speed, 1986). Dictyate oocytes remain quiescent until sexual maturation (6-8 weeks old in mouse), after which point a subset of arrested oocytes re-enter meiosis at each estrus cycle (Morelli and Cohen, 2005). These ovulated oocytes undergo the first meiotic division, extruding a polar body in the process, and then temporarily arrest again before metaphase II (Morelli and Cohen, 2005). Upon fertilization, these oocytes resume meiosis and complete the final meiotic division, extruding another polar body. In contrast to male meiosis, female meiosis produces only one haploid oocyte per cycle.

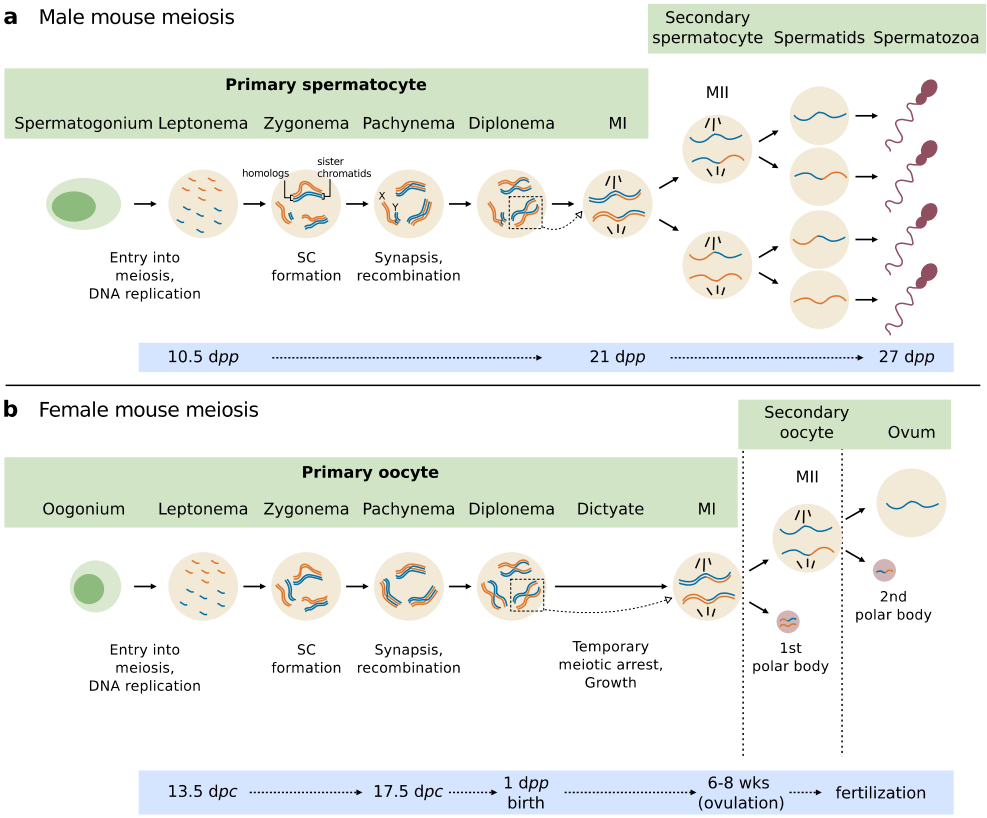

Introduction Figure 1: Meiosis in male and female mice.

(**a**) Overview of male mouse meiosis. In mice, the first wave of male meiosis occurs at 10.5 days *post partum* (d*pp*), when a spermatogonium duplicates its DNA. Prophase I, subdivided into leptonema, zygonema, pachynema, and diplonema, occurs over the subsequent 10 days. From leptonema to zygonema, components of the synaptonemal complex begin to form, leading to synapsis of paternal (blue) and maternal (orange) homologs at pachynema. The heterologous X and Y chromosomes achieve only partial synapsis at the pseudoautosomal region (PAR). Recombination between homologs during pachynema leads new genetic combinations. Chromosomes desynapse at diplonema, remaining physically attached at sites of crossing over, called chiasmata. Metaphase I (MI) is achieved by 21 d*pp* and results in separation of homologs into two secondary spermatocytes. The second meiotic division divides the sister chromatids to form four haploid spermatids. Spermatids then undergo spermiogenesis to produce spermatozoa. This process occurs continuously throughout male reproductive lifespan. (**b**) Overview of female mouse meiosis. In mice, all oogonia enter prophase I at 13.5 d*pc*. Prophase I occurs in one synchronous wave over the next 7-8 days, at which point primary oocytes arrest at the dictyate growth stage. Cohorts of arrested oocytes re-enter meiosis I at each estrus cycle, leading to the first meiotic division and the formation of a secondary oocyte and one polar body. This secondary oocyte arrests at metaphase II and only resumes meiosis II at fertilization, if such should occur. Fertilization triggers the second meiotic division and formation of another polar body. The fertilized egg then gives rise to a diploid embryo.

Unlike in mouse, where meiosis progression is synchronous, initiation of female meiotic prophase I in humans occurs over a broader period of time (Gondos et al., 1971). The first cohort of oocytes enter prophase I at week 12 of gestation, while the remaining oocytes enter prophase I over the subsequent 18 weeks (Gondos et al., 1971). By birth, most oocytes have completed prophase I and entered the dictyate stage (Gondos et al., 1971). Compared to the mouse, female meiosis in humans is less synchronous and much more challenging to study. The mouse, therefore, is a commonly used experimental model for studying mammalian meiosis.

1.1.2 Meiotic prophase I events: an overview

One goal of meiotic prophase I is to form physical connections, called chiasmata, between maternal and paternal homologous chromosomes. Chiasmata are formed from COs made during meiotic recombination, and they are a prerequisite for faithful chromosome segregation at metaphase I (Cohen et al., 2006). Another important consequence of meiotic recombination is the creation of new allelic combinations from parental genomes, leading to genetic diversity (Bolcun-Filas and Schimenti, 2012).

Prophase I is divided into four sub-stages: leptonema, zygonema, pachynema, and diplonema (**Intro Figure 1**). First, DNA is replicated during meiotic S phase (Lima-de-Faria and Borum, 1962). Then, at leptonema, programmed DNA double-strand breaks (DSBs) are introduced throughout the germ cell genome (Cohen and Pollard, 2001). These DNA DSBs are the substrates for meiotic recombination and are essential for prophase I progression (Baudat et al., 2000; Romanienko and Camerini-Otero, 2000).

During zygonema, the second stage of prophase I, homologous chromosomes begin to physically pair in a process called synapsis (Handel and Schimenti, 2010). Synapsis is mediated by a multi-partite proteinaceous structure called the synaptonemal complex (SC) (Fraune et al., 2012). During this process of synapsis, the intimate association of homologs allows for DNA DSBs to be repaired via homologous recombination (Handel and Schimenti, 2010). At pachynema, homologous chromosomes are fully

synapsed along their lengths. At diplonema, the SC breaks down in a process called desynapsis, but homologs remain physically connected at chiasmata.

1.1.3 Aneuploidy and meiotic errors

Aneuploidy is the state of having an abnormal number of chromosomes, such as an extra chromosome or a missing chromosome. It does not, however, include states in which an organism or cell has a change in the number of complete sets of chromosomes. Aneuploidy can result from non-disjunction of chromosomes during meiosis I or meiosis II (**Intro Figure 2a-e**).

In humans, the most prevalent class of aneuploidies involves the sex chromosomes (Hall et al., 2006). In males, the most common sex chromosome aneuploidies are 47,XXY (Klinefelter syndrome; 0.1%) and 47,XYY (Double Y syndrome; 0.1%) (Heard and Turner, 2011). In females, the most common sex chromosome abnormality is 46,XO (Turner syndrome; 0.04%) (Heard and Turner, 2011). Sex chromosome aneuploidies more commonly arise from XY non-disjunction occurring in the paternal germ line (Hall et al., 2006). For example, sex chromosome non-disjunction can produce sperm harboring both the X and Y chromosomes or no sex chromosomes, which can result in several different sex chromosome aneuploidy conditions (**Intro Figure 2d,e**).

On the other hand, most autosomal trisomies, such as Trisomy 21 (i.e. Down syndrome; 47,XX/XY+21; 0.1%) result from non-disjunction occurring in the maternal germ line (Hassold and Hunt, 2001; Shin et al., 2009). Trisomy 21 arises due to non-disjunction related to improper crossover positioning and/or loss of sister chromatid cohesion. Chromosome crossovers that form too proximal or too distal to the centromere are thought predispose germ cells to non-disjunction (Lynn et al., 2004). Increasing maternal age also predisposes to chromosome non-disjunction due to progressive deterioration of the cohesin complex that maintains sister chromatids cohesion (Herbert et al., 2015). This mechanism is thought to be responsible for the majority of human trisomy 21

conceptions from older women however there is likely interaction between the advancing age and crossover positioning risk factors (Oliver et al., 2008).

Aneuploidy in germ cells presents major challenges during meiosis (Jones and Lane, 2013). For example, if one chromosome is missing, as in Turner syndrome (46,XO), there is no homolog for the univalent chromosome to synapse with or repair its DNA DSBs from during prophase I. An unpaired chromosome, therefore, cannot generate chiasmata, leading to non-disjunction and the subsequent development of aneuploid gametes (**Intro Figure 2**) (Hodges et al., 2001). Similarly, meiotic events can be disrupted if one chromosome exists in too many copies, as in Down syndrome (47,XX/XY+21) (Hall et al., 2006). In summary, meiotic errors and aneuploidies are intimately related (Hall et al., 2006; Hassold and Hunt, 2001).

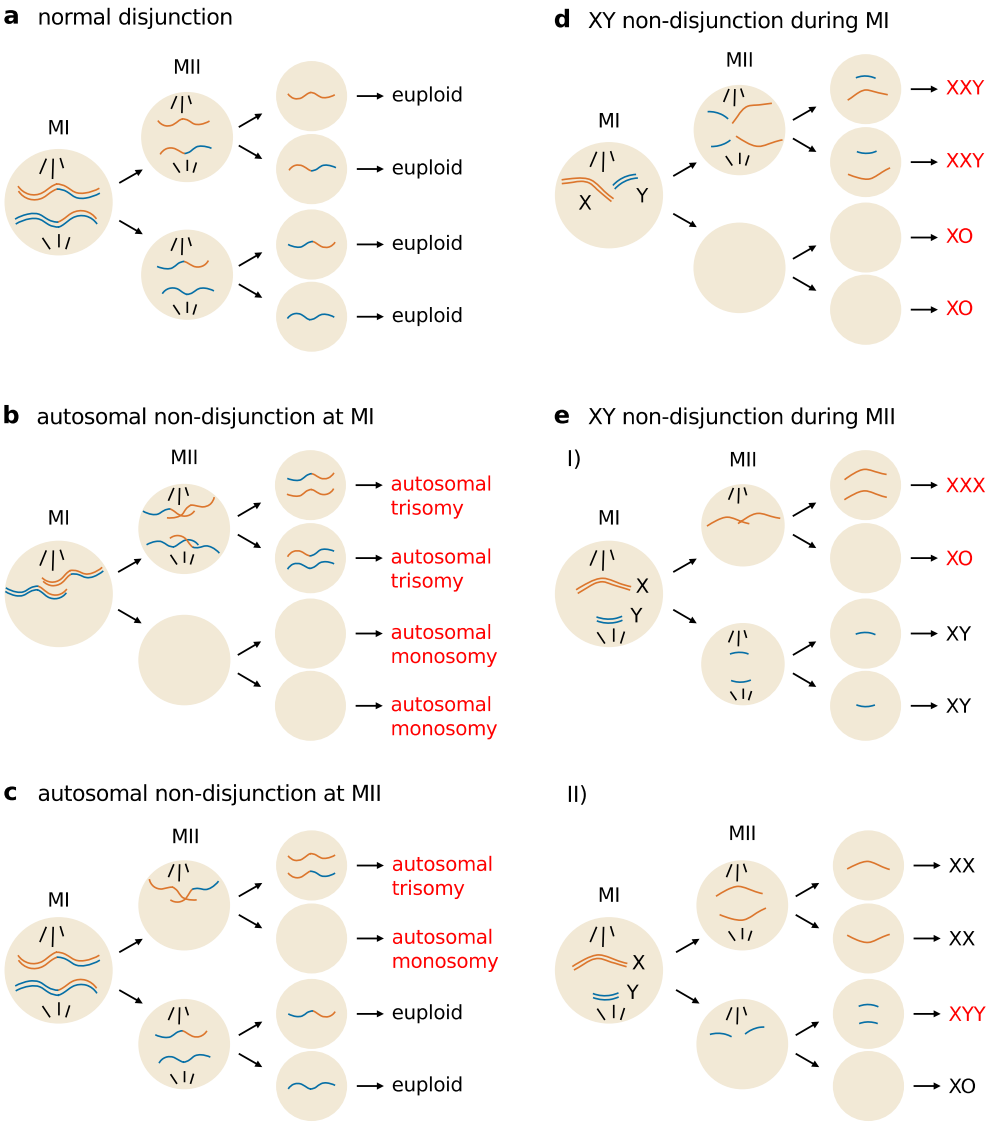

Introduction Figure 2: Meiotic non-disjunction and aneuploidy.

(**a**) Normal disjunction during meiosis I and II. Each meiosis product has one copy of each chromosome, which can generate euploid embryos. (**b**) Autosomal non-disjunction at meiosis I. Half the products have two complements of one autosome, which leads to trisomic embryos. The other half are missing this autosome, resulting in monosomic embryos. (**c**) Autosomal non-disjunction at meiosis II. One product contains two copies of an autosome, leading to trisomies. Another product is missing the autosome, leading to monosomies. (**d**) Meiosis I non-disjunction of the XY chromosomes. Half of the products contain both X and Y chromosomes, leading to XXY embryos, and the other half contain no sex chromosome, leading to XO embryos. (**e**) Two cases of XY non-disjunction during MII. In the first case, there is non-disjunction of the X chromosomes, resulting in XXX and XO embryos. In the second case, there is non-disjunction of the Y chromosomes, leading to XYY and XO embryos. Red indicates aneuploid conditions.

1.1.4 Meiotic surveillance mechanisms: an overview

In order to minimize potentially deleterious meiotic errors that could lead to aneuploidies, germ cells have developed a system of checks and balances, called meiotic surveillance mechanisms. These are cellular pathways that actively monitor the fidelity of meiotic events (MacQueen and Hochwagen, 2011). Meiotic quality control mechanisms are triggered by specific meiotic defects, such as asynapsed chromosomes (Burgoyne et al., 2009), persistent unrepaired DNA DSBs (Di Giacomo et al., 2005), and improper meiotic spindle tension (Sun and Kim, 2012). By eliminating defective germ cells, surveillance mechanisms prevent the formation of aneuploid gametes and offspring. However, these mechanisms can also have deleterious reproductive consequences, including infertility, if they cause total germ cell elimination. Therefore, studying the surveillance mechanisms that operate in mammals has important implications for our understanding of aneuploidy and infertility.

Surveillance mechanisms operate at several different developmental points during meiosis. One important quality control mechanism, called the spindle assembly checkpoint (SAC), operates at metaphase I and monitors the tension of microtubule attachments to kinetochores of homologous chromosomes (Sun and Kim, 2012). The SAC is activated when a kinetochore is unattached or when there is loss of tension, and it arrests the germ cell until chromosomes are properly aligned (Sun and Kim, 2012).

Interestingly, in mammals, the stringency of the SAC is sexually dimorphic, being more sensitive to tension defects in males than in females (Hunt and Hassold, 2002; Nagaoka et al., 2011). The reduced stringency of the SAC in oocytes may explain why autosomal trisomies are predominately maternally derived (Hall et al., 2006; Hunt and Hassold, 2002). The precise reason for the SAC sexual dimorphism remains unclear.

In addition to the SAC, other important surveillance mechanisms operate earlier in germ cell development, particularly during meiotic prophase I. While the details of these mechanisms remain to be worked out in mammals, they are believed to monitor important prophase I events, including chromosome synapsis and meiotic DNA repair (Burgoyne et al.,

2009; Di Giacomo et al., 2005), similar to what has been described in other organisms (MacQueen and Hochwagen, 2011).

Like the SAC, there is some evidence that the prophase I surveillance mechanism is less stringent in females than males (Di Giacomo et al., 2005). Despite the importance of meiotic prophase I surveillance mechanisms, the molecular details of these pathways remain poorly understood. Identifying and characterizing prophase I surveillance mechanisms in mammals is a major aim of this thesis.

1.2 Meiotic DNA double-strand breaks and repair

One of the earliest events in mammalian meiosis is the formation of programmed DNA DSBs throughout the genome (Baudat et al., 2013). This process initiates meiotic recombination, facilitates homologous chromosome synapsis, and helps create new genetic combinations from parental genomes. However, persistent unrepaired meiotic DSBs are deleterious, and have been implicated as a trigger of a prophase I surveillance mechanism (Di Giacomo et al., 2005). Therefore, a detailed discussion of meiotic DNA DSB metabolism is important for understanding prophase I quality control.

1.2.1 Meiotic DNA DSBs initiation

During leptonema of prophase I, programmed DNA DSBs are generated by the topoisomerase II-like enzyme sporulation-specific 11 (SPO11) (Baudat et al., 2000; Keeney et al., 1997; Romanienko and Camerini-Otero, 2000). SPO11 is a highly evolutionarily conserved protein (Keeney, 2008) that is expressed predominantly in germ cells (Metzler-Guillemain and de Massy, 2000; Shannon et al., 1999).

In mice, *Spo11* has two primary alternative splice transcripts, *Spo11*α and *Spo11*β (Bellani et al., 2010). In spermatocytes, SPO11β is expressed in early prophase I, implicating it as the major isoform for DNA DSB formation at leptonema (Bellani et al., 2010; Kauppi et al., 2011). By contrast, the smaller SPO11 isoform, SPO11*α* (exon 2 skipped), is expressed later in prophase I, during pachynema and diplonema, and recent work suggests

that SPO11α may be involved in DNA DSB formation on the small region of homology shared between the X and Y chromosomes, called the pseudoautosomal region (PAR) (Kauppi et al., 2011). Mice that express only the *Spo11β* isoform have normal numbers of nuclear DNA DSBs at leptonema, but reduced numbers of X-Y PAR-associated DNA DSBs (Kauppi et al., 2011). This suggests that *Spo11α* and *Spo11β* have temporally and functionally distinct roles during meiosis.

Deletion of *Spo11 in mice* leads to infertility in both sexes (Baudat et al., 2000; Romanienko and Camerini-Otero, 2000). Phenotypically, *Spo11-/-* mice do not form programmed DNA DSBs at leptonema, and consequently have severe chromosome asynapsis at late zygonema-pachynema (Baudat et al., 2000; Romanienko and Camerini-Otero, 2000). Therefore, SPO11-dependent DNA DSBs are required for homologous chromosome synapsis in mouse.

In mice, *Spo11*-/- spermatocytes fail to progress beyond the mid-pachytene stage (Baudat et al., 2000; Romanienko and Camerini-Otero, 2000). By contrast, in *Spo11*-/- females, oocyte arrest occur later, with some oocytes reaching diplonema (Baudat et al., 2000). Nevertheless, at birth *Spo11*-/- females have 40% fewer oocytes than wildtype females (Di Giacomo et al., 2005), indicating that a substantial wave of oocytes are eliminated during prophase I. The remaining oocytes in *Spo11*-/- females are subsequently eliminated over several weeks after birth, resulting in infertility (Baudat et al., 2000; Di Giacomo et al., 2005).

1.2.2 Distribution of meiotic DNA DSBs

SPO11-induced DNA DSBs are non-randomly distributed, occurring at higher frequencies in specific regions of the genome called “hot spots” (Paigen and Petkov, 2010). In mice, hotspots are defined by PR domain-containing 9 (PRDM9) (Baudat et al., 2010; Mihola et al., 2009; Parvanov et al., 2010; Smagulova et al., 2011). PRDM9 is a meiosis-specific histone H3 methyltransferase, which adds methyl moieties to histone H3. Consistent with PRDM9’s role in designating DNA DSB locations, studies using chromatin immunoprecipitation with sequencing (ChIP-seq) have shown

that hotspot co-localize with sites of histone H3 trimethylation at lysine 4 (H3K4me3) (Smagulova et al., 2011).

The zinc finger domain of *Prdm9* is critical for determining hotspot location (Grey et al., 2011). Mutating the zinc finger array alters the genomic location of DNA DSB hotspots and H3K9me3 marks (Grey et al., 2011). The current model for meiotic DNA DSB initiation posits that PRDM9 first binds to specific regions of the genome determined by its zinc finger domain where it then generates H3K4me3 marks, which in turn recruit SPO11 to generate DNA DSBs (Brick et al., 2012).

1.2.3 Regulation of meiotic DNA DSB formation

Faithful segregation of chromosomes requires that at least one CO be generated on each homologous chromosome pair. Regulating the number of DNA DSBs introduced in the genome is referred to as DSB homeostasis. The goal of DSB homeostasis is to ensure that neither too few nor too many DNA DSBs are generated, both of which could have deleterious outcomes (Lange et al., 2011).

In mouse, on average 200-300 DNA DSBs per nucleus are generated during early prophase I (Cole et al., 2012). This is 10x in excess the number of crossovers formed (20-25 CO events per nucleus) (Moens et al., 2002). This indicates that the vast majority of meiotic DNA DSBs resolve as non-crossover (NCO) products rather than CO products (Cole et al., 2012). Furthermore, while individual germ cells show variability in the number of DNA DSBs, the number of COs is held constant (Cole et al., 2012). A high ratio of meiotic DNA DSBs to COs is also observed in other organisms, including humans (150 DSBs), *Saccharomyces cerevisiae* (140-170 DSBs), and *Arabidopsis thaliana* (230 DSBs) (Cole et al., 2012). Therefore, DNA DSB homeostasis is highly conserved.

What factors are involved in meiotic DSB homeostasis? Recently, the kinase ataxia telangiectasia mutated (ATM) was implicated in inhibiting DNA DSB formation in the vicinity of existing DNA DSBs (Lange et al., 2011). This model is consistent with the phenotype of *Atm*-deficient mice, which show higher than normal numbers of meiotic DNA DSBs (Lange et al., 2011).

A similar role for ATM has been described in *S. cerevisiae* (Zhang et al., 2011) and *Drosophila melangastor* (Joyce et al., 2011), suggesting an evolutionarily conserved function for ATM in limiting DNA DSB numbers. While the mechanism of ATM-dependent homeostasis is unclear mammals, a recent study in yeast has shown that ATM promotes phosphorylation of Rec114 meiotic recombination protein (Rec114), which in turn inhibits further DNA DSB formation (Carballo et al., 2013). This mechanism is likely important because having too many DNA DSBs can create genomic damage.

There also appear to be mechanisms that promote DNA DSB formation during meiosis. In the case of the X and Y chromosomes in mammals, crossing over is limited to a small region of X-Y homology, the PAR (Burgoyne, 1982). Insufficient DNA DSBs within the PAR can result in failed CO formation and X-Y non-disjunction. *Spo11α* is thought to induce DNA DSBs on the PARs of the X and Y chromosomes, thereby ensuring that sufficient breaks are generated for CO formation (Kauppi et al., 2013). Furthermore, in *S. cerevisiae* a group of factors called ZMM proteins are involved in complex feedback loops that coordinate homolog engagement with meiotic DNA DSB formation (Thacker et al., 2014). In summary, meiotic DNA DSBs are tightly controlled temporally, quantitatively, and spatially.

1.2.4 Repair of DNA DSBs by homologous recombination

In somatic cells, DNA DSBs are repaired predominantly via non-homologous end-joining (NHEJ). During meiosis, however, DNA DSBs are repaired via homologous recombination (HR) (Andersen and Sekelsky, 2010). Components of the NHEJ pathway are down-regulated during meiosis, leaving HR as the default repair pathway (Goedecke et al., 1999). HR is the preferred repair mechanism in meiosis because it is less error prone than NHEJ and it generates the necessary COs between homologs (Andersen and Sekelsky, 2010).

Meiotic DNA DSBs are catalyzed by SPO11 via endonuclease cleavage of DNA (Keeney et al., 1997). This results in SPO11 covalently bound to the break site (**Intro Figure 3**). Processing first involves cleavage of SPO11-DNA complex (Neale et al., 2005). This reaction is mediated by the MRN

complex, composed of MRE11 meiotic recombination 11 (MRE11), RAD50 homolog (RAD50), and Nibrin (NBS1), as well as other factors such as the nuclease retinoblastoma binding protein 8 (RBBP8, CTIP) (Farah et al., 2009; Hartsuiker et al., 2009; Milman et al., 2009).

After SPO11 removal, the 5'-end of the break is resected by exonucleases, including CTIP and exonuclease 1 (EXO1), to form 3' single-stranded DNA (ssDNA) overhangs (**Intro Figure 3**) (Farah et al., 2009; Sun et al., 1991). These ssDNA ends then invade the neighboring intact DNA molecule on the homologous chromosome, catalyzed by DNA strand exchange proteins RAD51 and disrupted meiotic cDNA1 (DMC1) (Neale and Keeney, 2006). RAD51/DMC1-ssDNA nucleoprotein filaments support DNA homology search and strand invasion of the intact homolog, and results in the formation a heteroduplex intermediate called the displacement loop (D-loop) (Hunter and Kleckner, 2001).

After D-loop formation, the resected DNA strand is then resynthesized using the homolog as a template (**Intro Figure 3**) (Neale and Keeney, 2006). Finally, the DNA DSB is resolved into either a CO or NCO (Neale and Keeney, 2006). Resolution into a CO involves formation of an intermediate structure called the double Holliday junction (dHJ) (Collins and Newlon, 1994; Schwacha and Kleckner, 1994, 1995). By contrast, NCOs are generated through synthesis-dependent strand annealing (SDSA) (McMahill et al., 2007), where the re-synthesized strand is displaced from the intact homolog and re-anneals with the complementary end of its original homolog (Andersen and Sekelsky, 2010). The factors that control the decision to resolve DNA DSBs as COs or NCOs are not well understood (Guillon et al., 2005).

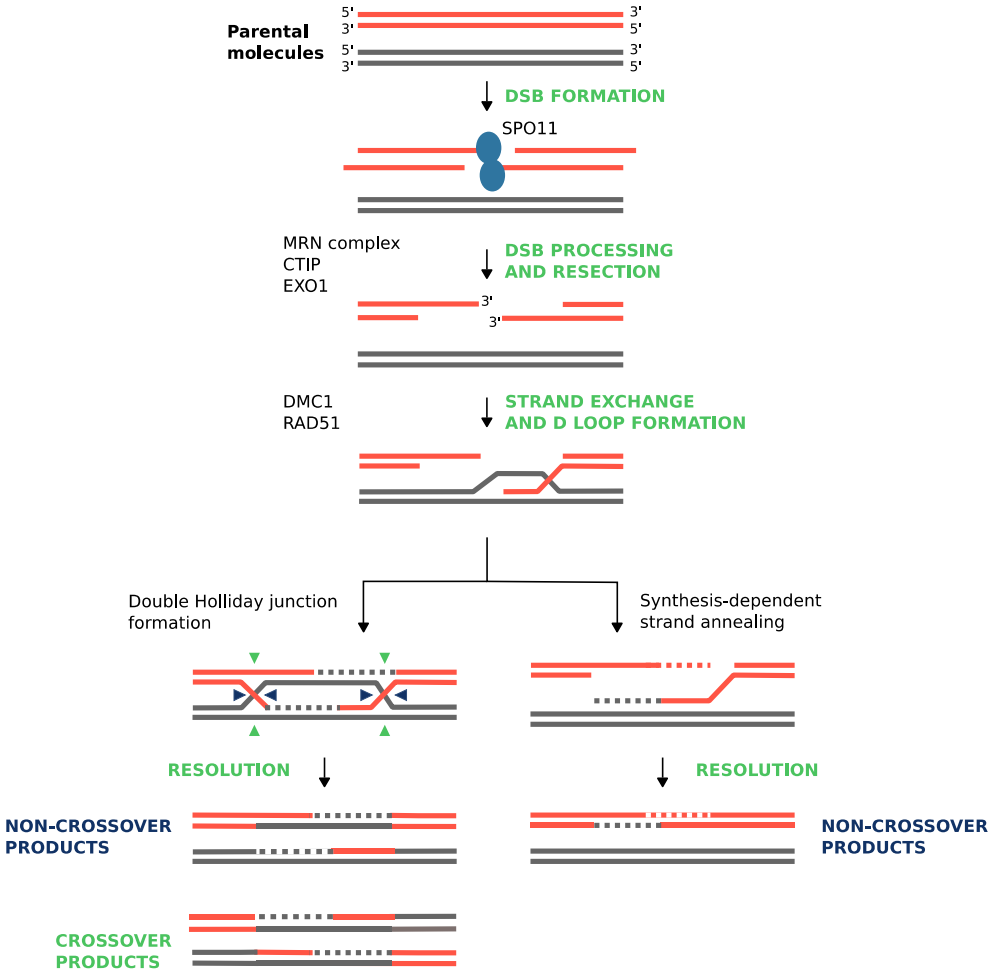

Introduction Figure 3: Meiotic homologous recombination.

Meiotic homologous recombination begins with introduction of DNA DSBs on a parental molecule by the enzyme SPO11. The SPO11-DNA complex is cleaved by the MRN complex and CTIP, and the free DNA ends are then resected 5'-to-3' by exonucleases, leaving 3' overhangs. With the aid of single stranded DNA binding proteins DMC1 and RAD51, the 3' overhang then invades the neighboring molecule, forming a D loop. In the canonical recombination pathway, the second end is captured leading to the formation of a double Holliday junction, which is processed to a crossover or a non-crossover. In an alternative recombination pathway, called synthesis-dependent strand annealing, the extended D loop is dissolved and the newly synthesized strand reanneals with the second end of the DSB, resulting in non-crossover product.

1.2.5 DNA DSB cytological analysis by chromosome spreads

In yeast, meiotic DNA DSB events such as initiation and repair can be analyzed directly using established biochemical assays (Murakami and Keeney, 2008). However, these techniques are less feasible in mouse due to low bioavailability of meiotic tissue and higher cellular heterogeneity. More commonly, meiotic DNA DSBs are studied indirectly in mice using surrogate markers of DNA DSBs, such as DNA repair proteins (Moens et al., 2002). A common method to visualize meiotic events, such as DNA DSB repair, is called meiotic chromosome spreads (Peters et al., 1997). This involves permeablizing and fixing germ cell nuclei onto glass slides, followed by antibody-mediated immunofluorescence to detect meiotic proteins (Peters et al., 1997). Fluorescence microscopy is then used to visualize the staining pattern of immunofluorescently-labeled proteins within individual germ cell nuclei (see Materials and Methods for more details).

Meiotic chromosome spreads have greatly advanced our understanding of mouse meiosis. For example, chromosome spreads have allowed for estimation of DNA DSB numbers, by quantifying foci of DNA repair proteins, especially RAD51 and DMC1 (Tarsounas et al., 1999). This approach has also provided a wealth of information about the timing of events and proteins involved in meiotic processes. In this thesis, I used meiotic chromosome spreads to answer important questions about meiotic DNA DSB repair and meiotic prophase I surveillance.

1.2.6 Meiotic DNA DSB repair proteins

H2AFX and its interacting proteins

One of the earliest markers of DNA DSBs in meiotic and mitotic cells is the serine-139 phosphorylated histone H2A family member X (γH2AFX) (Mahadevaiah et al., 2001; Rogakou et al., 1998) (**Table 1**). H2AFX is a ubiquitously expressed histone variant, making up approximately 25% of histone H2A (Redon et al., 2002), and it is enriched in germ cell nuclei compared to other tissues (Mahadevaiah et al., 2001).

Early studies have shown that upon induction of DNA DSBs by laser, H2AFX becomes rapidly phosphorylated at serine-139 within the carboxy-terminal SQ motif (Rogakou et al., 1998). Immunocytologically, this appears as discreet foci of γH2AFX (Pilch et al., 2003; Rogakou et al., 1999). In mammalian cells, γH2AFX accumulates in the nearby chromatin up to a megabase around DNA DSBs, forming large domains (Rogakou et al., 1999; Shroff et al., 2004). γH2AFX domains have been hypothesized to create a chromatin microenvironment suitable for DNA DSB repair (Srivastava et al., 2009).

In eukaryotes, ATM is involved in phosphorylation of histone protein H2AFX at serine-139 in response to DNA DSBs (Burma et al., 2001). However, H2AFX can also be phosphorylated by other kinases, including ataxia telangiectasia and Rad3-related (ATR) and DNA-dependent protein kinase (DNA-PKcs) (Wang et al., 2005a).

Much of our understanding of γH2AFX in the context of DNA DSB repair has been gained from studies of mitotic mammalian cells and yeast cells. Such studies have shown that γH2AFX recruits a downstream DNA damage response (DDR) protein called mediator of checkpoint signaling 1 (MDC1) (Stucki et al., 2005). γH2AFX-MDC1 complexes promote retention and amplification of additional downstream DDR factors at DNA DSB sites. These DDR proteins include ATM, NBS1, breast cancer 1 (BRCA1), and p53 binding protein 1 (53BP1) (Bekker-Jensen et al., 2005; Lukas et al., 2004; Paull et al., 2000; Stucki et al., 2005).

Other studies have implicated H2AFX in the recruitment of cohesion to DNA DSBs (Unal et al., 2004) and maintenance of checkpoint arrest until DNA DSB repair is complete (Fillingham et al., 2006). In yeast, γH2AFX is involved in recruitment of chromatin modifiers (Downs et al., 2004). In summary, γH2AFX has multiple roles in DNA DSB repair, including modifying chromatin structure and promoting the recruitment, retention, and amplification of downstream DNA DSB repair proteins.

In mitotic cells, upon completion of DNA DSB repair γH2AFX is dephosphorylated by protein phosphatase 2A (Chowdhury et al., 2005). This

dephosphorylation event is necessary for recovery from the checkpoint arrest established by γH2AFX (Keogh et al., 2006).

Despite its myriad roles in DDR, *H2afx* is not necessary for viability of cells or animals (Bassing et al., 2002; Celeste et al., 2002). Nevertheless, *H2afx-/-* mice show growth retardation, immune deficiencies, cancer predisposition, and male-specific sterility (Celeste et al., 2002). *H2afx*-/- cells have genomic instability and DNA repair defects (Bassing et al., 2002; Celeste et al., 2003b), including impaired recruitment of NBS1, 53BP1, and BRCA1, but not RAD51, to irradiation-induced DNA DSBs (Bassing et al., 2002; Celeste et al., 2002).

H2afx heterozygous mice also have a phenotype, specifically genomic instability and increased predisposition to cancer in a *p53*-deficient background (Celeste et al., 2003a; Srivastava et al., 2009). Furthermore, *H2afx* mutations and copy number variations are implicated in human cancers (Parikh et al., 2007; Srivastava et al., 2008). In summary, H2AFX is critical for a proper DDR in mitotic cells and mutations in *H2afx* have deleterious genomic consequences.

Despite these studies, the role of H2AFX in meiosis is less well understood. Importantly, *H2afx*-/- male mice are sterile and experience a germ cell arrest at mid-pachynema (Celeste et al., 2002), suggesting that H2AFX has an important meiotic function. By contrast, *H2afx*-/- female mice are fertile, but have reduced litter sizes (Celeste et al., 2002). This suggests that H2AFX's essential meiotic role is limited to spermatogenesis. A reduced litter size in *H2afx*-/- females may reflect embryo loss during pregnancy or a reduction in oocytes ovulated, but this has yet to be worked out.

In leptotene-staged germ cells, γH2AFX diffusely stains the chromatin of germ cell nuclei (Mahadevaiah et al., 2001). This staining pattern disappears in *Spo11*-/- spermatocytes, indicating that leptotene γH2AFX is a direct response to SPO11-induced DNA DSB formation (Mahadevaiah et al., 2001). Leptotene γH2AFX-staining is also disrupted in *Atm*-/- mice (Bellani et al., 2005), implicating ATM as the primary kinase involved in H2AFX phosphorylation in response to meiotic DNA DSB formation (Burma et al., 2001).

This diffuse nuclear γH2AFX staining disappears with chromosome synapsis, when meiotic DNA DSBs are repaired, during zygonema (Mahadevaiah et al., 2001). In spermatocytes, however, there is a second wave of γH2AFX, which occurs during pachynema to late diplonema. During this period, γH2AFX accumulates throughout the chromatin of the X and Y chromosomes (Mahadevaiah et al., 2001). Unlike the first wave, which is driven by ATM, this second wave of γH2AFX formation is predominately mediated by the kinase ATR (Royo et al., 2013). As discussed later, this sex chromosome-associated γH2AFX is necessary for meiotic silencing of the sex chromosomes, called meiotic sex chromosome inactivation (MSCI) (Fernandez-Capetillo et al., 2003).

Despite its role in DNA DSB repair in somatic cells, H2AFX does not appear to be essential for meiotic DNA DSB repair. *H2afx*-/- females are fertile (Celeste et al., 2002), which would not be expected if H2AFX had an essential role in meiotic DNA DSB repair. For example, DNA DSB repair proteins such as RAD51 are not affected by *H2afx* deletion (Fernandez-Capetillo et al., 2003). Furthermore, autosomal synapsis, which is often disrupted when DNA DSB is compromised, is not defective in *H2afx*-/- spermatocytes (Fernandez-Capetillo et al., 2003). By contrast, the X and Y chromosomes frequently fail to synapse at the PAR (Fernandez-Capetillo et al., 2003), again suggestive of a role for H2AFX in sex chromosome events.

RAD51, DMC1, and RPA

The recombinases RAD51 and DMC1 are highly conserved proteins involved in meiotic DNA DSB repair (Handel and Schimenti, 2010) (**Table 1**). RAD51 and DMC1 together form ssDNA-protein filaments that facilitate strand invasion during homologous recombination (Neale and Keeney, 2006). Since they represent early intermediates in homologous recombination, RAD51 and DMC1 are frequently used as surrogate markers to monitor the DNA DSB repair process (Tarsounas et al., 1999). Immunocytologically, RAD51 and DMC1 form distinct foci on asynapsed chromosome axes in germ cell nuclei at zygonema, and foci on asynapsed chromosomes during pachynema (Moens et al., 2002). Furthermore, ChIP-

seq using anti-RAD51 antibodies has been performed to map meiotic hotspots throughout the genome in germ cells (Smagulova et al., 2011).

Unlike RAD51, which is expressed in both somatic and germ cells (Lim and Hasty, 1996), DMC1 is a meiosis-specific recombinase (Bishop et al., 1992). In mouse, DMC1 is required for proficient repair of DNA DSBs during meiosis (Pittman et al., 1998; Yoshida et al., 1998). *Dmc1*-/- spermatocytes have persistent RAD51 foci (Pittman et al., 1998) and persistent diffuse γH2AFX staining at early/mid-pachynema (Mahadevaiah et al., 2008), indicating stalled DNA DSB repair. *Dmc1*-/- mice also have extensive chromosome asynapsis, germ cell apoptosis, and infertility in both sexes (Pittman et al., 1998; Yoshida et al., 1998). By contrast, *Rad51* deletion is embryonic lethal in mice, challenging efforts to understand its precise meiotic function (Lim and Hasty, 1996).

The ssDNA-binding protein replication protein A (RPA) also forms foci in close proximity to RAD51 and DMC1 (Moens et al., 2002). RPA is a three-protein complex comprising the subunits RPA1, RPA2 and RPA3 (Wold, 1997). During homologous recombination, RPA loads onto newly formed 3' ssDNA tails before RAD51 and DMC1, where it also helps stabilize the ssDNA tails and remove secondary structure (Wang and Haber, 2004). This event may also facilitate subsequent RAD51 and DMC1 loading to ssDNA ends (Wang and Haber, 2004).

During meiosis, RAD51 and DMC1 foci reach maximum numbers between late leptonema and early zygonema (Burgoyne et al., 2007; Moens et al., 2002). While RAD51 and DMC1 foci are rapidly depleted from chromosome cores following synapsis, RPA foci are also observed on synapsed chromosomes (Burgoyne et al., 2007; Moens et al., 2002; Plug et al., 1997). In fact, RPA numbers peak between zygonema and pachynema, when chromosomes are becoming increasingly synapsed (Moens et al., 2002; Plug et al., 1997). This post-synaptic localization is thought to represent RPA bound to the D-loop intermediate of DNA molecules engaging in meiotic homologous recombination (Burgoyne et al., 2007). RPA is usually depleted from chromosomes by mid-pachynema (Moens et al., 2002).

BRCA1

Breast cancer susceptibility gene *1* (BRCA1) is a tumor suppressor protein involved DDR and homologous recombination (Moynahan et al., 1999) (**Table 1**). *Brca1* was first described as a gene that is associated with an increased risk to breast cancer (Hall et al., 1990). BRCA1's role in DNA repair is thought to be critical for genomic stability and cancer (Caestecker and Van de Walle, 2013).

Immunocytologically, BRCA1 forms foci at DNA DSB sites in both mitotic and meiotic cells (Scully et al., 1997). Similar to RAD51 and DMC1, BRCA1 only localizes to pre-synaptic (i.e. asynapsed) chromosomes (Mahadevaiah et al., 2008). At leptonema and early zygonema, BRCA1 foci co-localize with RAD51 (Mahadevaiah et al., 2008), consistent with a role for BRCA1 in DNA DSB repair events. BRCA1 foci disappear once chromosomes synapse (Turner et al., 2004).

In spermatocytes, there is a second wave of BRCA1 staining during pachynema to diplonema. At this time, BRCA1 accumulates along the cores of asynapsed X and Y chromosome (Turner et al., 2004). Furthermore, if autosomal regions are abnormally asynapsed at pachynema, as in translocation carriers, they also accumulate BRCA1 (Turner et al., 2005). As discussed later, this BRCA1 localization pattern is consistent with a role for BRCA1 in meiotic silencing (Turner et al., 2004).

Mouse embryonic stem cells with mutations in *Brca1* show genomic instability and defects in homologous recombination (Moynahan et al., 1999). Single *Brca1* null mutations are not compatible with mouse survival (Xu et al., 2001). However, embryo viability can be restored by combining *Brca1* mutations with mutations in either *tumor protein p53* (*Tp53*, or *p53*) (Xu et al., 2001) or *tumor protein p53 binding protein 1* (Tp*53bp1*, or *53bp1*) (Bunting et al., 2012). Deletion of exon 11 of *Brca1* on a *p53*+/- background (i.e. *Brca1*Δ11 *p53*+/-) produces viable mice with an increased risk for development of mammary tumors (Xu et al., 2001). Exon 11 of *Brca1* is 3.4kb and encodes protein-binding sites for RAD51 and other interacting proteins (Deng and Brodie, 2000). Interestingly, *Brca1*Δ11 *p53*+/- mice have male-specific infertility associated with pachytene-stage germ cell arrest (Xu

et al., 2003). By contrast, *Brca1*Δ11 *p53*+/- females are fertile and have no germ cell arrest phenotype (Xu et al., 2003).

According to the original characterization study (Xu et al., 2003), *Brca1*Δ11 *p53*+/- spermatocytes fail to load RAD51 to asynapsed chromosomes at leptonema-zygonema, but have normal DMC1 loading (Xu et al., 2003). A recent study, however, reported normal localization of RAD51 in a *Brca1* conditionally deleted mouse model (*Brca1cKO*) (Broering et al., 2014). At early and mid pachynema, when RAD51 is restricted to the X and Y chromosomes, there was a slight but significant reduction in RAD51 foci numbers in *Brca1cKO* mice and *Brca1*Δ11 *53bp1*-/- mice (Broering et al., 2014). Proteins involved in later stages of meiotic DSB repair, including MutS homolog 4 (MSH4), which promotes crossover formation at late zygonema and pachynema (Kneitz et al., 2000), and MutL homolog 1 (MLH1), which labels crossovers at pachynema (Edelmann et al., 1996), show minor perturbations in *Brca1* mutants (Broering et al., 2014). MSH4 numbers are normal in *Brca1*Δ11 *53bp1*-/- mice, but somewhat reduced in *Brca1cKO* mice, and MLH1 levels are normal (Broering et al., 2014). Together, these data suggest that BRCA1 probably has a minor role in meiotic DNA DSB repair events.

Other DNA repair proteins

After homologous chromosomes have synapsed, early recombination proteins RAD51 and DMC1 are displaced by post-synaptic recombination proteins (Moens et al., 2002). These post-synaptic proteins include RPA, as discussed above, and others, such as MSH4 and mutS homolog 5 (MSH5) (Moens et al., 2002), testis expressed 11 (TEX11) (Adelman and Petrini, 2008; Yang et al., 2008), and the pro-crossover factor ring finger protein 212 (RNF212) (Reynolds et al., 2013) (**Table 1**). MSH4 and MSH5 are mismatch repair proteins that are required for chromosome synapsis, crossing over, and progression through prophase I (de Vries et al., 1999; Edelmann et al., 1999; Kneitz et al., 2000; Tsubouchi et al., 2006). TEX11 is required for timely DNA DSB repair, proper synapsis, and CO formation in mice (Adelman and Petrini, 2008; Yang et al., 2008). RNF212, while

dispensable for chromosome synapsis, is essential for CO formation, presumably by stabilizing other CO factors such as MSH4 and MSH5 (Reynolds et al., 2013).

In addition to these factors, there are even later recombination nodule proteins, including as MLH1 and MutL homolog 3 (MLH3), which form complexes on synapsed chromosome cores during mid-pachynema (Kolas et al., 2005; Plug et al., 1998), where they are thought to promote CO formation (Baker et al., 1996; Lipkin et al., 2002). *Mlh1* and *Mlh3* deficient mice show sterility in both sexes (Baker et al., 1996; Lipkin et al., 2002). While synapsis occurs normally at pachynema in *Mlh1*-/- and *Mlh3*-/- mice, chromosomes desynapse prematurely owing to failed CO formation, leading to univalents at diplonema (Baker et al., 1996; Lipkin et al., 2002).

1.2.7 Meiotic DNA DSBs on the X and Y chromosomes

In mammalian males, the X and Y chromosomes are largely non-homologous and remain asynapsed during meiosis except at the PAR (Burgoyne, 1982). Both the PAR and the asynapsed regions of the X and Y chromosomes are subject to DNA DSBs (Kauppi et al., 2011). Germ cells, therefore, must have mechanisms to repair DNA DSBs on asynapsed cores.

Based on immunocytology, the asynapsed X chromosome accumulates RAD51, DMC1, and RPA foci in mouse spermatocytes (Ashley et al., 1995; Barlow et al., 1997; Mahadevaiah et al., 2001; Moens et al., 1997; Plug et al., 1998; Tarsounas et al., 1999). RAD51 and DMC1 foci are observed on the asynapsed X chromosome at zygonema and persist into mid-pachynema, when RAD51 is no longer present on synapsed autosomes (Barlow et al., 1997; Moens et al., 1997; Plug et al., 1998). Interestingly, RAD51 and DMC1 foci are rarely observed on the asynapsed region of the Y chromosome, but are restricted to the PAR (Kauppi et al., 2011). RPA foci persist on the asynapsed X chromosome into mid-late pachynema, i.e. later than RAD51 and DMC1 (Plug et al., 1998). By the end of pachynema, however, RPA is depleted from asynapsed X chromosome (Plug et al., 1998).

Therefore, DNA DSB repair is protracted on the asynapsed X chromosome compared to autosomes. These delayed kinetics of DNA DSB

repair are not limited to the asynapsed X chromosome, but are observed on asynapsed autosomes as well. In Tc1 mouse model of Down syndrome (O'Doherty et al., 2005), RAD51 persists on the asynapsed human chromosome 21 into late pachynema (Mahadevaiah et al., 2008). The reason for delayed repair on asynapsed chromosomes is unclear, but may be linked to the fact that asynapsed chromosomes are heterochromatic and transcriptionally silenced at pachynema (Turner, 2007), since DNA repair is influenced by chromatin environment (van Attikum and Gasser, 2009).

Two different mechanisms have been proposed to facilitate DNA DSB repair on asynapsed chromosomes: (1) homologous recombination, using the sister chromatid as a template; (2) non-homologous end joining (Inagaki et al., 2010). Since components of the NHEJ pathway are suppressed during mammalian meiosis (Goedecke et al., 1999), however, it is believed that sister chromatid-mediated HR is a key mechanism acting on asynapsed chromosomes (Kauppi et al., 2011). However, recent work in *C. elegan* males has shown that DNA DSBs on the hemizygous (i.e. asynapsed) X chromosome can be repaired in the absence of HR machinery, indicating that other mechanisms, such as an error-prone single-strand annealing (SSA) pathway may also operate (Checchi et al., 2014).

Table 1. Proteins involved in meiotic DNA DSB events

Protein	Function(s)	Mouse mutant meiotic phenotype	Reference
53BP1	Tumor suppressor protein, interacts with p53, involved in the DNA damage response	Normal fertility	(Ward et al., 2003)
ATM	Kinase involved in phosphorylation of H2AFX at DNA DSBs, and DNA DSB homeostasis	Asynapsis, persistent unrepaired DNA DSBs	(Burma et al., 2001; Lange et al., 2011)
ATR	Kinase involved in DNA DSB repair, cell cycle progression/checkpoints, and meiotic silencing	MSCI defects	(Royo et al., 2013; Traven and Heierhorst, 2005)
BRCA1	Tumor suppressor protein involved in DNA repair, cell cycle, and meiotic silencing.	MSCI defects	(Boulton, 2006; Turner et al., 2004)
DMC1	Meiosis-specific recombinase, HR strand exchange	Persistent unrepaired DNA DSBs, asynapsis	(Pittman et al., 1998; Yoshida et al., 1998)
H2AFX	Phosphorylated H2AFX modification (γH2AFX) involved in somatic DNA DSB repair and meiotic silencing	MSCI failure	(Fernandez-Capetillo et al., 2003; Fillingham et al., 2006)
MDC1	DNA repair protein, interacts with γH2AFX at DNA DSBs, necessary for meiotic silencing.	MSCI defects	(Ichijima et al., 2011; Stucki et al., 2005)
MLH1/3	MutL homolog mismatch repair proteins, marks crossover sites at pachynema	Failed crossover/ chiasmata formation and premature separation of homologs, metaphase I univalents	(Baker et al., 1996; Lipkin et al., 2002)
MSH4/5	MutS homolog mismatch repair protein	Aberrant chromosome synapsis and crossing over, persistent unrepaired DNA DSBs	(de Vries et al., 1999; Edelmann et al., 1999; Kneitz et al., 2000)
PRDM9	H3 methyltransferase, dictates DNA DSB location	Altered hotspot locations, asynapsis, unrepaired DNA DSBs	(Baudat et al., 2010)
RAD51	Recombinase, HR strand exchange	Not viable	(Cloud et al., 2012)
RNF212	Pro-crossover protein	DNA DSB repair and	(Reynolds et al.,

		crossover defects	2013)
RPA	Single-stranded DNA binding protein involved in DNA repair and strand exchange	Not viable	(Sakaguchi et al., 2009)
SPO11	Generates DNA DSBs at leptonema	Failed programmed DNA DSB formation, asynapsis, MSCI failure	(Keeney et al., 1997)
TEX11	MRE11-interacting protein required for DNA DSB repair and crossing over	Asynapsis, persistant unrepaired DNA DSBs, MSCI defects	(Hartsuiker et al., 2009)

1.3 Meiotic chromosome synapsis

1.3.1 Synapsis: an overview

Homologous chromosome synapsis is a critical and highly conserved meiotic event during which homologs become physical paired via a proteinaceous structure called the synaptonemal complex (SC) (Cohen et al., 2006). Synapsis begins during zygonema and is completed upon entry into pachynema, defined as the stage when homologous chromosomes have synapsed along their lengths (Cohen et al., 2006). The SC is composed of several meiosis-specific proteins that come together in a zipper-like fashion to stabilize homologous chromosomes as one unit, called a bivalent.

Synapsis is essential for meiotic progression through meiosis and for faithful chromosome segregation (Fraune et al., 2012). Defects in synapsis result in aneuploid gametes, germ cell arrest, and infertility (Burgoyne et al., 2009; Wang and Hoog, 2006). In mammals, synapsis and meiotic recombination are intimately linked processes: synapsis requires meiotic DNA DSBs (Baudat et al., 2000), and efficient repair of DNA DSBs requires homologous chromosome synapsis (Fraune et al., 2012). The SC is thought to facilitate the formation of COs by keeping homologs in close proximity (de Vries et al., 2005; Wang and Hoog, 2006; Yuan et al., 2002).

Given the importance of the SC, the faithful completion of synapsis is monitored by specific, yet currently undefined meiotic surveillance mechanisms. In the following section, I will introduce SC morphogenesis and homologous chromosome recognition, alignment, and synapsis. My results presented later in this thesis sheds important new insight into how synaptic defects are monitored in germ cells.

1.3.2 Components of the synaptonemal complex

Components of the SC begin forming at leptonema of prophase I (**Intro Figure 4**). At this stage, axial elements (AEs) begin to assemble along the length of each chromosome (Fraune et al., 2012). At zygonema, homologous chromosomes start to align along their AEs, and gradually

synapse via a central region (CR) composed of transverse filaments (TFs) and the central elements (CE) (Fraune et al., 2012). At this stage, AEs are termed lateral elements (LEs). The mature SC is assembled at pachynema when two LEs are connected along their entire lengths by TFs and the CE. Chromosomes that have completed SC assembly are considered to have synapsed.

In mammals, the SC is composed of at least seven meiosis-specific protein components (Fraune et al., 2012) (**Table 2**). These components are: synaptonemal complex protein 1 (SYCP1), synaptonemal complex protein 2 (SYCP2), synaptonemal complex protein 3 (SYCP3), synaptonemal complex central element protein 1 (SYCE1), synaptonemal complex central element protein 2 (SYCE2), synaptonemal complex central element protein 3 (SYCE3), and testis expressed 12 (TEX12) (Fraune et al., 2012). The AE/LE portion of the SC is composed of SYCP3 (Lammers et al., 1994) and SYCP2 (Offenberg et al., 1998; Yang et al., 2006). The TF is made of SYCP1 (Meuwissen et al., 1992). The remaining SC components, including SYCE1 (Costa et al., 2005), SYCE2 (Costa et al., 2005), SYCE3 (Schramm et al., 2011), and TEX12 (Hamer et al., 2006), are part of the CE.

1.3.3 Synaptonemal complex assembly and dynamics

Synapsis entails the pairing of AEs, comprised of SYCP3 and SYCP2, and the loading of SYCP1 between them (Handel and Schimenti, 2010). Structurally, SYCP1 contains two globular domains separated by a coiled-coil segment (Ollinger et al., 2005). One globular domains of SYCP1 binds the SYCP2-portion of the AE, while the other binds the CE (Liu et al., 1996; Tarsounas et al., 1997). In mice, deletion of *Sycp1* results in defective synapsis and infertility in both sexes (de Vries et al., 2005). *Sycp3*-/- mice have severe defects in SC morphogenesis, meiotic arrest, and male-specific infertility (Yuan et al., 2002; Yuan et al., 2000).

Components of the CE are also critical for SC morphogenesis. SYCE1, SYCE2, and SYCE3 interact to form complexes (Costa et al., 2005; Schramm et al., 2011), and each component of the CE is required for stability of SYCP1 (Bolcun-Filas et al., 2007; Bolcun-Filas et al., 2009; Hamer et al., 2008;

Schramm et al., 2011). Therefore, components of the SC are highly interdependent.

Unlike AEs, which are visible during all stages of prophase I, the CE part of the SC is only present when chromosomes are synapsed (de Vries et al., 2005; Yuan et al., 2000). Desynapsis of homologues during diplonema is associated with loss of CR proteins, but retention of AE components (Handel and Schimenti, 2010). Since SYCP3 is present throughout prophase I, it is a commonly used marker to visualize meiotic chromosomes and substage germ cells (Cohen et al., 2006).

In addition to the SC structural components, there is a cohort of proteins that localize to the SC in a stage-specific manner. In mouse, two such proteins are HORMA-domain containing 1 (HORMAD1) and HORMA-domain containing 2 (HORMAD2) (Wojtasz et al., 2009). In early prophase I, HORMAD1 and HORMAD2 preferentially associate with pre-synaptic chromosome axes (Wojtasz et al., 2009). At pachynema, HORMAD1 and HORMAD2 are restricted to asynapsed chromosomes, i.e. the asynapsed regions of the X and Y chromosomes (Fukuda et al., 2009; Wojtasz et al., 2009). By contrast, in normal females, since all chromosomes have homologs for synapsis at pachynema, HORMAD1 and HORMAD2 are only found on pre-synaptic axes (Wojtasz et al., 2009).

During diplonema, the localization pattern of HORMAD1 and HORMAD2 diverge (Wojtasz et al., 2009). At this stage, HORMAD1 accumulates along the asynapsed regions of the desynapsing chromosomes and is retained on the X and Y chromosomes (Fukuda et al., 2009; Wojtasz et al., 2009). By contrast, HORMAD2 remains preferentially bound to the X and Y chromosomes, but does not label desynapsed axes at diplonema (Wojtasz et al., 2009). Therefore, HORMAD2 is a marker that is retained on chromosomes that were previously asynapsed at pachynema, whereas HORMAD1 localizes to all unsynapsed axes (Wojtasz et al., 2009).

Deletion of *Hormad1* in mice disrupts several meiotic processes and results in infertility in both sexes (Daniel et al., 2011; Shin et al., 2010). *Hormad1*-/- mice show defects in synapsis and SC formation, suggesting that it is required for SC assembly (Daniel et al., 2011; Shin et al., 2010).

Hormad1-/- mice also have reduced numbers of DNA DSBs and lower numbers of meiotic recombination protein foci compared to wildtype (Daniel et al., 2011; Shin et al., 2010). It is believed that HORMAD1 helps coordinate the progression of chromosome synapsis with meiotic recombination (Daniel et al., 2011). Under this model, HORMAD1 might ensure that there are sufficient numbers of DNA DSBs to engage in homology search and synapsis. With homolog engagement, HORMAD1 is displaced from the chromosome cores, permitting progression through prophase I (Daniel et al., 2011). By contrast, the role of HORMAD2 is not clear. Dissecting the role of HORMAD2 in mammalian meiosis is an objective of this thesis.

In summary, the SC is composed of a variety of proteins that together facilitate synapsis of homologous chromosomes and the repair of meiotic DNA DSBs. Understanding the interplay between components of the SC and the meiotic recombination pathway and how they are regulated remains an important challenge in the field of meiosis.

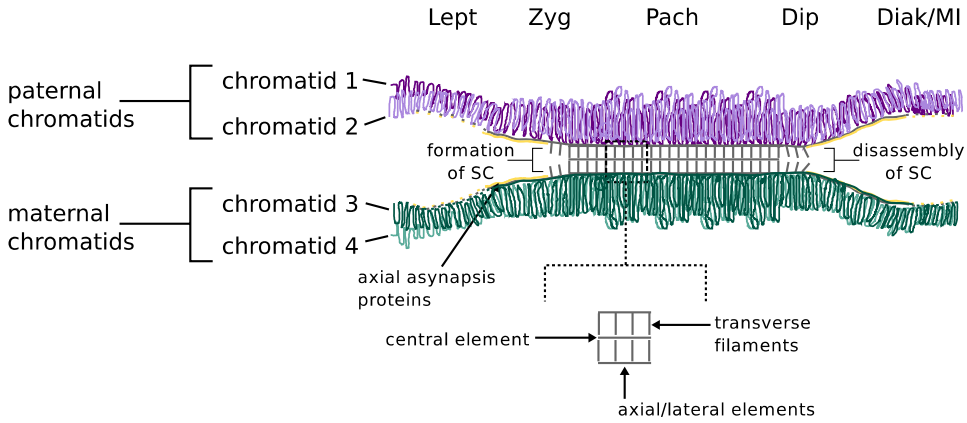

Introduction Figure 4: Synaptonemal complex dynamics.

During meiotic S phase, the DNA of each parental chromosome is replicated (not shown), forming two sister chromatids per chromosome which are held together by cohesins. At leptonema, each pair of sister chromatids begins to assemble a proteinaceous axis, called axial elements. At zygonema the axes of each homolog begin to synapse via transverse filaments. At pachynema, the synaptonemal complex is complete, with lateral elements, transverse filaments, and a central element. During diplonema, the synaptonemal complex disassembles, but the axial elements and asynapsis axial proteins (i.e. HORMAD1) remain. Between diakenesis and the first meiotic metaphase (MI) the axial elements are disassembled and cohesins are removed, separating the sister chromatids.

Table 2. Proteins involved in the meiotic synaptonemal complex

Protein	Function(s)	Mouse mutant meiotic phenotype	Reference
HORMAD1	SC morphogenesis, DNA DSB processing, meiotic silencing, and meiotic surveillance	SC defects, reduced DNA DSB formation/intermediates, meiotic silencing failure	(Daniel et al., 2011; Shin et al., 2010)
SYCE1	Central element component of SC	SC and recombination defects	(Bolcun-Filas et al., 2009; Costa et al., 2005; Hamer et al., 2006)
SYCE2	Central element component of SC	SC, recombination, and MSCI defects	(Bolcun-Filas et al., 2007)
SYCE3	Central element component of SC	SC and recombination defects	(Schramm et al., 2011)
SYCP1	Transverse filament component of SC	SC and recombination defects	(de Vries et al., 2005)
SYCP2	Axial/lateral element component of SC	SC defects	(Yang et al., 2006)
SYCP3	Axial/lateral element component of SC	SC and recombination defects	(Yuan et al., 2000)
TEX12	Central element component of SC	SC and recombination defects	(Hamer et al., 2006)

1.4 Meiotic silencing

In this section, I will introduce meiotic silencing, another critical event of mammalian meiotic prophase I. In mammals, meiotic silencing refers to the transcriptional inactivation of genes on asynapsed chromosomes (Turner, 2007). In the following section, the process of meiotic silencing in mammals will be introduced in the context of the X and Y chromosomes, and then examined as a more general mechanism affecting any asynapsed chromosome. Then, the epigenetics of the meiotic silencing response will be discussed, building off the previous sections of DDR and chromosome synapsis. Finally, various theories will be addressed to explain the role of meiotic silencing in germ cell development and fertility.

1.4.1 Meiotic Sex Chromosome Inactivation (MSCI)

In mammals, the X and Y chromosomes are unique in that they are largely heteromorphic and have only a small region of genetic homology, the PAR (Burgoyne, 1982; Ellis and Goodfellow, 1989). The PAR is where the X and Y chromosomes form a requisite CO that is necessary for proper segregation of homologs at metaphase I. In mouse, the PAR spans less than 1Mb (Perry et al., 2001), which is short relative to the full length of the X chromosome (171 Mb) and Y chromosome (91 Mb). In mice, the PAR has several unique properties, including a higher than expected frequency of DNA DSBs and a distinct chromatin loop size (Kauppi et al., 2011). Furthermore, one particular isoform of *Spo11*, namely *Spo11*α, is thought to be important for the formation of DNA DSBs at the PAR and the subsequent pairing of the X and Y chromosomes (Kauppi et al., 2013). Together, these properties of the PAR ensure that an obligatory crossover forms between the X and Y chromosomes (Kauppi et al., 2011).

In addition to these distinct features of the PAR, the non-PAR regions of the X and Y chromosomes have unique properties during prophase I of meiosis. Given that they are non-homologous, the non-PAR X-Y regions do not synapse during pachynema. In other words, the vast majority of the X and Y chromosomes remains asynapsed during pachynema. Very early

studies showed that the X-Y chromosomes form a dense staining structure in pachytene nuclei, and this was originally termed the “sex vesicle” (Sachs, 1954; Solari, 1964). Later cytological work revealed that rather than being enveloped in a vesicular compartment, the X-Y chromosomes instead attain a dense chromatin structure during pachynema (Solari, 1974). This lead to the renaming of the X-Y chromosomes at pachynema as the “sex body” (Solari, 1974).

Early studies of transcription in germ cells revealed that the sex body does not incorporate [^{3}H]uridine at pachynema, indicating that the X and Y chromosomes are transcriptionally inactive (Henderson, 1964 ; Kierszenbaum and Tres, 1974; Monesi, 1965). This inactivity of the X and Y chromosomes during male meiotic prophase I was later termed meiotic sex chromosome inactivation (MSCI) (McKee and Handel, 1993). Since these early studies, MSCI has been confirmed using several other methods, including RNA fluorescent *in situ* hybridization (RNA FISH) (Turner et al., 2005), micro-arrays (Ichijima et al., 2011), RNA polymerase II immunostaining (Baarends et al., 2005), and high throughput sequencing (Modzelewski et al., 2012).

MSCI initiates during the zygonema to pachynema transition (McKee and Handel, 1993; Turner, 2007), and this is associated with the accumulation of repressive chromatin marks and meiotic silencing proteins within the chromatin of the sex chromosomes (Baarends et al., 2005; Turner et al., 2004). This results in the complete suppression of X- and Y-linked genes at mid-pachynema (Turner et al., 2006). In spermatocytes, the repressive effects of MSCI are maintained to the end of prophase I and also to a substantial degree into spermatid development (Greaves et al., 2006; Namekawa et al., 2006; Turner et al., 2006).

In contrast to X chromosome inactivation (XCI) in female somatic cells, where 25-30% of X-linked genes escape silencing (Carrel and Willard, 2005), previous studies using RNA microarrays (Namekawa et al., 2006), reverse transcriptase polymerase chain reaction (RT-PCR) (Wang et al., 2005b), and RNA FISH (Mueller et al., 2008) have failed to identify any X- or Y-linked gene that escapes MSCI in the male germ line. Therefore, MSCI

causes the complete silencing all of X- and Y-linked protein-coding genes at pachynema (Turner, 2007).

According to a recent study, however, the majority of miRNAs on the X chromosome are expressed throughout prophase I (Song et al., 2009). By RT-PCR, RNA FISH, and RNA polymerase II ChIP followed by quantitative PCR (ChIP-qPCR), Song et al. detected *de novo* transcription of X-linked miRNAs in samples enriched for pachytene spermatocytes. This was the first report of transcription occurring from the X chromosome during pachynema in mice. Based on these findings, it was suggested that X-linked miRNAs may function in MSCI itself, by promoting gene repression, or may have a role in autosomal gene regulation (Song et al., 2009).

Another recent analysis (Mueller et al., 2008) revealed that not all X-linked genes are subject to the same level of repression in post-meiotic cells. Using both RNA FISH and microarrays, it was discovered that many X-genes, particularly multicopy genes, are re-activated in spermatids (Mueller et al., 2008). Indeed, an estimated 18% of X-linked genes are expressed in spermatids, and the majority of these are multicopy genes (Mueller et al., 2008). Gene amplification is believed to be a mechanism by which important post-meiotic X-linked genes escape the repressive effects imposed by MSCI (Mueller et al., 2008).

In summary, MSCI initiates at pachynema and causes the inactivation of all protein-coding genes in spermatocytes. After pachynema, the majority of genes remain repressed into diplonema, but a subset of X-linked genes, particularly multicopy genes, is reactivated in round spermatids.

1.4.2 Meiotic silencing of unsynapsed chromatin (MSUC)

Meiotic silencing is a response that is not limited to the asynapsed X and Y chromosomes, but also occurs on asynapsed autosomes (Baarends et al., 2005; Turner et al., 2005). This more general silencing response is called meiotic silencing of unsynapsed chromatin (MSUC), or simply meiotic silencing. Evidence for MSUC came from analysis of T(X;16)16H translocation mice (Turner et al., 2005), which have a translocation involving chromosomes X and 16 that creates a X;16 fusion chromosome

(Ford and Evands, 1964). During meiosis, the X;16 translocation disrupts synapsis, leaving segments of chromosome 16 asynapsed at pachynema (Turner et al., 2005). This asynapsed autosomal region is enriched in silencing factors and transcriptionally silent in pachytene spermatocytes (Turner et al., 2005).

An independent group analyzed T(1;13)70H/T(1;13)1Wa mice, which have a translocation involving chromosomes 1 and 13 that disrupts synapsis at pachynema (Baarends et al., 2005). These asynapsed autosomal regions are subject to transcriptional inactivation and are enriched in silencing proteins (Baarends et al., 2005). Together, these studies revealed that meiotic silencing occurs in response to asynapsis in general, not just X and Y asynapsis. MSCI was thereafter recognized as the manifestation of a general meiotic silencing response specifically affecting the X and Y chromosomes (Schimenti, 2005).

Importantly, meiotic silencing is not restricted to the male germ, but also can occur in females. While normal XX oocytes contain fully homologous chromosomes, if a chromosome is missing, in excess, or structurally abnormal, asynapsis can be present (Burgoyne et al., 2009). In such circumstances, asynapsed chromosomes accumulate meiotic silencing proteins and are subject to transcriptional inactivation at pachynema (Turner et al., 2005).

Evidence for MSUC in females came from analysis of female mice carrying a single X chromosome, called XO mice (Evans and Phillips, 1975). The asynapsed X chromosome in XO pachytene oocytes was shown to be transcriptionally repressed, as measured by Cot-1 RNA FISH (Turner et al., 2005) and RNA polymerase II immunostaining (Baarends et al., 2005). Furthermore, the asynapsed X chromosome in XO pachytene oocytes is enriched in silencing factors, such as γH2AFX and ubiquitinated histone H2A (ubi-H2A) (Baarends et al., 2005; Turner et al., 2005). In summary, meiotic silencing is a general response to asynapsis that operates in both sexes.

1.4.2 Epigenetics of meiotic silencing in mice

γH2AFX

One of the earliest meiotic silencing factors discovered in mammals was S-139 phosphorylated H2AFX (γH2AFX) (Celeste et al., 2002; Fernandez-Capetillo et al., 2003) (**Table 3, Intro Figure 5**). As mentioned above, γH2AFX has two temporally distinct patterns of localization during prophase I in spermatocytes (Mahadevaiah et al., 2001). The first wave occurs at early prophase during leptonema, when γH2AFX diffusely stains chromatin, consistent with a response to meiotic DNA DSBs (Mahadevaiah et al., 2001). As meiotic prophase I continues, γH2AFX disappears in a manner that is temporally linked to chromosome synapsis and DSB repair (Mahadevaiah et al., 2001).

The second wave of γH2AFX staining in spermatocytes occurs at pachynema, when it forms a chromatin domain around asynapsed X and Y chromosomes (Mahadevaiah et al., 2001). This X-Y chromosome γH2AFX-domain persists from pachynema until late diplonema, and disappears upon entry into metaphase I (Mahadevaiah et al., 2001). Importantly, these γH2AFX-domains also form on asynapsed autosomes, and on the asynapsed X chromosome in XO pachytene oocytes, suggesting that this is a general response to asynapsis in both male and female germ cells (Turner et al., 2005). This localization pattern of γH2AFX is consistent with a role in meiotic silencing.

Genetic evidence supporting that γH2AFX is involved in meiotic silencing came from studies of mice carrying a null mutation of *H2afx* (Fernandez-Capetillo et al., 2003). *H2afx*-/- male mice have defective X-Y chromatin compaction and over expression of X- and Y-linked genes, indicative of MSCI failure (Celeste et al., 2002; Fernandez-Capetillo et al., 2003). Therefore, *H2afx* is essential for meiotic silencing in mice.

As described above, *H2afx*-/- male mice are infertile, but female mutants are fertile (Celeste et al., 2002). This sexually dimorphic infertility phenotype indicates that *H2afx* has an essential role in a male-specific process. It is now believed that abnormal MSCI is the underlying cause of

infertility in *H2afx*-/- male mice, and in many other mouse mutants that have MSCI defects (Mahadevaiah et al., 2008; Royo et al., 2010). In support of this, there are no obvious meiotic defects outside of MSCI failure in *H2afx*-/- mice (Celeste et al., 2002; Fernandez-Capetillo et al., 2003).

Additional support for the MSCI-failure model of male-specific infertility comes from recent transgenic mouse experiments (Royo et al., 2010). XY male mice carrying autosomal transgenes for two Y-linked genes, namely *Zfy1* and *Zfy2,* experience a pachytene germ cell arrest similar to that observed in *H2afx*-/- mice (Royo et al., 2010). This suggests that mis-expression of two Y-linked genes alone is sufficient to trigger pachytene germ cell arrest. Indeed, several mutant mouse models with defective γH2AFX domains show mis-expression of *Zfy1/2* (Royo et al., 2010). Therefore, γH2AFX accumulation and MSCI are intimately linked, and defects in either can result in germ cell arrest and infertility.

ATR

Like γH2AFX, ATR has two distinct localization patterns during meiotic prophase I (Keegan et al., 1996; Moens et al., 1999). During zygonema, ATR localizes as foci to asynapsed chromosome cores (Keegan et al., 1996; Moens et al., 1999). These ATR foci overlap with γH2AFX staining (Moens et al., 1999) and RPA (Burgoyne et al., 2007), suggesting that ATR accumulates near DNA DSB repair sites. At early pachynema, ATR foci are no longer present, but instead ATR accumulates within the chromatin of the asynapsed X and Y chromosomes (Moens et al., 1999), where it co-localizes with γH2AFX (**Intro Figure 5**) (Turner et al., 2004). These ATR chromatin domains also occur on the asynapsed X chromosome in XO oocytes (Turner et al., 2005). In addition to ATR, the ATR co-factors ATR interacting protein (ATRIP) and topoisomerase II binding protein 1 (TOPBP1) are enriched in the sex body in spermatocytes (Perera et al., 2004; Refolio et al., 2011; Reini et al., 2004). (Table 3)

ATR-enrichment in the chromatin of the X and Y chromosomes is suggestive of a role in H2AFX phosphorylation and meiotic silencing. Recent genetic studies have confirmed that ATR is the key meiotic silencing kinase

(**Table 3**). Conditional deletion of *Atr* during early meiotic prophase I disrupts γH2AFX domain formation and meiotic silencing (Royo et al., 2013). However, ablation of *Atr* after meiotic silencing initiates does not affect γH2AFX, indicating that once the γH2AFX domain and silencing are established it is stable and irreversible (Royo et al., 2013).

BRCA1

Like ATR and γH2AFX, BRCA1 has two distinct localization patterns during meiotic prophase I in mice. At zygonema, BRCA1 forms distinct foci on pre-synaptic chromosome axes (Scully et al., 1997; Turner et al., 2004), and these foci overlap with RAD51, indicating an association with meiotic DNA DSBs (Mahadevaiah et al., 2008; Scully et al., 1997). Interestingly, however, similar BRCA1 foci are also observed in *Spo11*-/- DNA DSB-deficient mice (Mahadevaiah et al., 2008). The presence of BRCA1 in *Spo11*-/- spermatocytes suggests a role for BRCA1 outside of meiotic DNA DSB events.

At pachynema, BRCA1 localizes along the length of asynapsed chromosome axes (**Intro Figure 5**) (Scully et al., 1997; Turner et al., 2004; Turner et al., 2005). In spermatocytes, BRCA1 is restricted to the asynapsed axes of the X and Y chromosomes, suggestive of a role in meiotic silencing (Turner et al., 2004). Several mutant mouse models of *Brca1* have been developed to understand BRCA1's role in meiosis. *Brca1*Δ11/Δ11 *p53+/-* mutant mice, which have a deletion in exon 11 of *Brca1*, show defective targeting of ATR to the asynapsed X and Y chromosomes (Broering et al., 2014; Turner et al., 2004). This is associated with absence of γH2AFX and failed meiotic silencing (Broering et al., 2014; Turner et al., 2004). Similar meiotic silencing defects were also observed in a conditional deletion mutant of *Brca1* (Broering et al., 2014).

Based upon these findings, it was postulated that BRCA1 is necessary for recruitment and retention of ATR to asynapsed chromosome axes (Table 3). Interestingly, recent work has also shown that loss of *Atr* compromises the loading of BRCA1 on asynapsed axes, indicating an interdependence of ATR and BRCA1 in meiotic silencing (Royo et al., 2013). Additionally,

BRCA1, ATR, and γH2AFX accumulation on asynapsed chromosomes is dependent on the SC component SYCP3 (Fukuda et al., 2012; Kouznetsova et al., 2009). This indicates that SYCP3 is upstream of BRCA1 in the meiotic silencing cascade.

HORMAD1

In addition to BRCA1 and ATR, several other proteins have been recently implicated in meiotic silencing, including the HORMA-domain protein HORMAD1 (Daniel et al., 2011; Shin et al., 2010) (**Table 3, Intro Figure 5**). As discussed above, HORMAD1 associates with pre-synapsed, asynapsed, and desynapsed chromosome axes in both spermatocytes and oocytes (Fukuda et al., 2009; Shin et al., 2010; Wojtasz et al., 2009). HORMAD1 likely has multiple functions in mammalian meiosis, including regulation of synapsis, DNA DSB formation and/or repair, and meiotic silencing (Daniel et al., 2011).

Mice with a deletion of *Hormad1* have meiotic silencing defects. In *Hormad1*-/- spermatocytes, BRCA1 and ATR does not localize properly to asynapsed chromosome axes (Daniel et al., 2011; Shin et al., 2010). This leads to disrupted γH2AFX domains and failed X- and Y-linked gene silencing (Daniel et al., 2011; Shin et al., 2010). In wildtype spermatocytes, HORMAD1 associated with asynapsed axes becomes phosphorylated at serine-375 (Fukuda et al., 2012). Reduced phosphorylation leads to an impaired meiotic silencing response (Fukuda et al., 2012). Therefore, HORMAD1 recruitment to asynapsed axes and HORMAD1 post-translational modifications are critical for meiotic silencing.

Another related HORMA-domain protein, HORMAD2, also accumulates on asynapsed chromosome axes in mouse spermatocytes and oocytes (Wojtasz et al., 2009). The function of HORMAD2 in mammalian meiosis remains unclear. As part of my goal to better understand the meiotic silencing pathway in mammals, I will present novel data on the meiotic silencing phenotype of *Hormad2*-/- mice (see below)**.**

MDC1

Another protein involved in meiotic silencing in mammals is MDC1 (**Table 3**). MDC1 directly interacts with γH2AFX and mediates the DDR in mammals (Stewart et al., 2003; Stucki et al., 2005). Like many factors involved in meiotic silencing, MDC1 labels the chromatin over the asynapsed X and Y chromosomes (**Intro Figure 5**), which overlaps γH2AFX and other sex body-associated proteins (Ichijima et al., 2011; Lu et al., 2013).

Deletion of *Mdc1* in mice results in male-specific infertility, suggesting an essential role for MDC1 in male-specific events (Lou et al., 2006). *Mdc1*-/- males have defects in the meiotic silencing pathway, including reduced spreading of the silencing factors ATR, TOPBP1, and γH2AFX throughout the X-Y chromatin (Ichijima et al., 2011). This is associated with mis-expression of X- and Y-linked genes, indicating that MDC1 is essential for meiotic silencing (Ichijima et al., 2011). γH2AFX, ATR, and MDC1 are interdependent in meiotic silencing – genetic ablation of any of these factors leads to defective loading of the others (Ichijima et al., 2011; Royo et al., 2013).

AGO4

Recent work implicated a component of the RNAi pathway, argonaute4 (AGO4), in meiotic silencing in mammals (Table 3) (Modzelewski et al., 2012). AGO4 is highly expressed in the male germ line (González-González et al., 2008), and AGO4 localizes to chromatin of the asynapsed X and Y chromosomes and asynapsed autosomes, suggestive of a role in silencing (Modzelewski et al., 2012). While *Ago4*-/- males are fertile, they have increased spermatocyte apoptosis, reduced testis weight, and reduced spermatozoa counts (Modzelewski et al., 2012). Pachytene spermatocytes from *Ago4*-/- mice show defects in ATR and γH2AFX staining, and loss of silencing of sex-linked genes (Modzelewski et al., 2012). In the absence of *Ago4*, there is also a general down-regulation of X-linked miRNAs (Modzelewski et al., 2012), many of which have been previously reported to escape MSCI (Song et al., 2009). Based on these data, the authors speculate

that AGO4 may help coordinate silencing in conjunction with X-linked miRNAs, by promoting their production and/or stability (Song et al., 2009).

SETX

Another protein recently implicated in silencing in mice is senataxin (SETX) (**Table 3**). SETX has multiple biological functions, including regulation of DDR, transcription, and DNA replication (Becherel et al., 2013). In mouse spermatocytes, SETX co-localizes with ATR, MDC1, and γH2AFX in the X-Y chromatin (Becherel et al., 2013). *Setx*-/- mice have defective accumulation of several silencing proteins, including ATR, MDC1, and γH2AFX (Becherel et al., 2013). These sex body abnormalities are associated with upregulation of X- and Y-linked genes and male-specific infertility (Becherel et al., 2013). SETX's role in MSCI is still unclear, but it maybe linked to its action on transcription, RNA processing, or DDR (Becherel et al., 2013).

SUMO

Sumoylation is a post-translational modification associated with transcriptional regulation (Gill, 2005). Several small ubiquitin-like modifier (SUMO) proteins are enriched in the sex body in spermatocytes (La Salle et al., 2008; Rogers et al., 2004; Vigodner and Morris, 2005) (**Table 3**). Like many meiotic silencing components, SUMO also localizes to meiotic DNA DSBs in spermatocytes (Shrivastava et al., 2010). One study reported that SUMO localizes to the sex chromatin even before γH2AFX (Vigodner, 2009), however subsequent studies refuted this claim (Ichijima et al., 2011; Royo et al., 2013).

Other sex body associated factors

As described above, specific epigenetic marks and histone modifications associate with the sex body in spermatocytes. Additional marks that localize to the sex body in mice include: di- and tri-methylation of histone H3 at lysine-9 (H3K9me2 and H3K9me3, respectively) (Khalil et al., 2004; van der Heijden et al., 2007); phosphorylated cyclin dependent

kinase 2 (p-CDK2) isoform 1 at threonine 160 (Wang et al., 2014); heterochromatin protein 1 beta and gamma isoforms (HP1β and HP1γ) (Metzler-Guillemain et al., 2003)(Metzler-Guillemain et al., 2003)(Metzler-Guillemain et al., 2003)(Metzler-Guillemain et al., 2003)(Metzler-Guillemain et al., 2003)(Metzler-Guillemain et al., 2003)(Metzler-Guillemain et al., 2003)(Metzler-Guillemain et al., 2003)(Metzler-Guillemain et al., 2003)(Metzler-Guillemain et al., 2003); histone macroH2A1.2 (Hoyer-Fender et al., 2000); histone H2A.Z (Greaves et al., 2006); ubiquitin conjugates (FK2) (Baarends et al., 2005; Ichijima et al., 2011); and, ubiquitinated histone H2A (uH2A) (Baarends et al., 1999; Baarends et al., 2005), formed by the action of ubiquitin protein ligase E3 component n-recognin 2 (UBR2) (An et al., 2010) (**Table 3**). Additionally, the histone H3 variants, H3.1 and H3.2, are removed and replaced by histone H3.3 in the sex body of pachytene spermatocytes (van der Heijden et al., 2007) (**Table 3**). Deletion of one gene encoding H3.3 results in male specific infertility associated with spermatocyte loss (Yuen et al., 2014). The function of these sex body-associated chromatin modifications and proteins remain largely unclear.

In summary, a multitude of factors interact with the sex chromosomes during late prophase I to establish a unique chromatin environment to facilitate the transcriptional silencing of X- and Y-linked genes (**Intro Figure 5**).

Table 3. Description of factors involved in meiotic silencing

Protein	Function(s)	Mouse mutant phenotype	Reference
AGO4	Argonaute RNAi processing protein, enriched in sex body, meiotic silencing.	Premature meiotic entry, sex body defects, MSCI failure, reduced X-linked miRNAs.	(Modzelewski et al., 2012)
ATR	Kinase involved DNA DSB repair, cell cycle progression/checkpoints, and meiotic silencing. Enriched in the sex body.	Defective accumulation of BRCA1, γH2AFX, MDC1, SUMO, ATRIP, and TOPBP1; MSCI failure.	(Royo et al., 2013; Traven and Heierhorst, 2005)
ATRIP	ATR interacting protein. Enriched on asynapsed sex chromosome axes.	-	(Royo et al., 2013; Zou and Elledge, 2003)
BRCA1	Tumor suppressor protein involved in DNA repair, cell cycle, and meiotic silencing.	Defective accumulation of ATR and γH2AFX; MSCI failure.	(Boulton, 2006; Turner et al., 2004)
CDK2	Kinase involved in cell cycle progression. Phosphorylated CDK2 at threonine 160 enriched in sex body. CDK2 also localized to crossovers.	Synaptic defects, unrepaired DNA DSBs, sex body defects, including impaired loading of BRCA1 and ATR.	(Viera et al., 2009; Wang et al., 2014)
FK2	Ubiquitin conjugate enriched in sex body.	-	(Ichijima et al., 2011)
H2A.Z	Histone variant enriched in sex body. Implicated in chromosome segregation and heterochromatin formation.	-	(Greaves et al., 2006)
H2AFX	γH2AFX involved in somatic DNA DSB repair and meiotic silencing. Enriched in sex body.	Failed accumulation of MDC1 and ATR, MSCI failure.	(Celeste et al., 2002; Royo et al., 2013)
H3.3	Histone variant involved in transcriptional reprogramming, enriched in sex body.	Deletion of one gene encoding H3.3 results in spermatocyte arrest.	(van der Heijden et al., 2007; Yuen et al., 2014)
H3K9me2/3	Repressive methylation modification on histone H3. Enriched in sex body.	-	(Khalil et al., 2004; van der Heijden et al., 2007)
HORMAD1	SC morphogenesis, DNA DSB processing, meiotic silencing, and meiotic	SC defects, reduced DNA DSB formation/intermedi	(Daniel et al., 2011; Shin et al., 2010)

	surveillance.	ates, meiotic silencing failure.	
HP1β/γ	Heterochromatin protein 1 isoforms associated with sex body.	Deletion of *Hp1γ* leads to reduction in number of primordial germ cells.	(Abe, 2011; Metzler-Guillemain et al., 2003)
MacroH2A1.2	Histone variant enriched in sex body.	-	(Hoyer-Fender et al., 2000)
MDC1	DNA repair protein, interacts with γH2AFX at DNA DSBs, necessary for meiotic silencing.	Defective accumulation of ATR and γH2AFX.	(Ichijima et al., 2011; Stucki et al., 2005)
SETX	DDR, transcriptional regulation, and replication; enriched in sex body.	Defective accumulation of ATR, MDC1, γH2AFX, and MSCI failure.	(Becherel et al., 2013)
SUMO	Transcriptional regulation, enriched in sex body and meiotic DNA DSBs.	-	(La Salle et al., 2008; Royo et al., 2013; Vigodner and Morris, 2005)
TOPBP1	ATR co-factor. Enriched on asynapsed sex chromosome axes.	-	(Perera et al., 2004)
uH2A	Ubiquitylated H2A modification, formed by UBR2, involved in transcriptional regulation. Enriched in sex body.	Deletion of *Ubr2* results in impaired meiotic silencing.	(An et al., 2010; Baarends et al., 1999)

- indicates that mutant is not viable, available, or information unknown

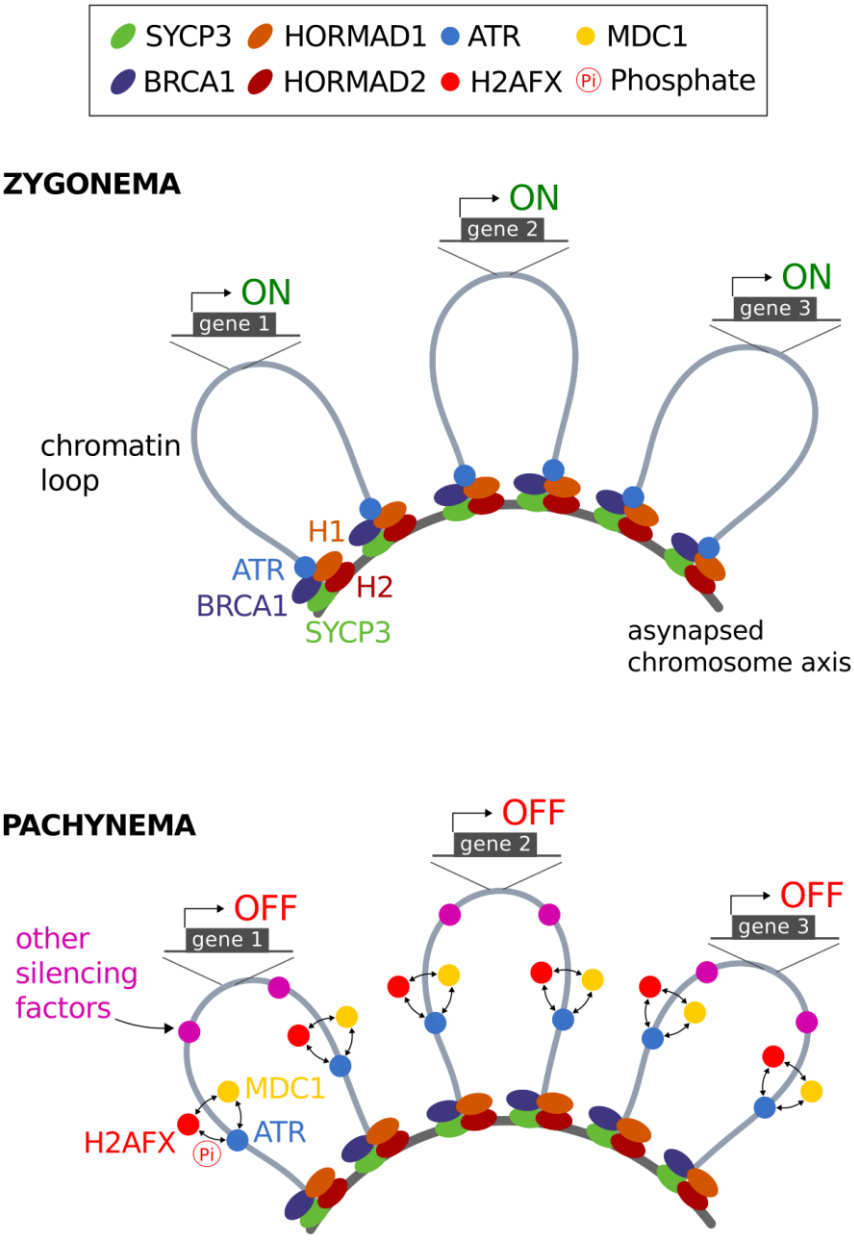

Introduction Figure 5: Factors involved in meiotic silencing in mice.

During zygonema, SYCP3, HORMAD1 (H1), HORMAD1 (H2), BRCA1, and ATR accumulate along the asynapsed chromosome axis. At this stage genes remain transcriptionally active. During pachynema, ATR spreads into the chromatin loops, where it phosphorylates H2AFX in a positive feedback loop involving H2AFX and MCD1. The resultant chromatin-wide γH2AFX domain, in concert with other silencing factors, leads to chromosome-wide gene inactivation.

1.4.3 Meiotic silencing from an evolutionary perspective

Meiotic silencing is conserved across many taxa, including eutherian mammals (Baarends et al., 2005; de Vries et al., 2012; Turner et al., 2005), metatherian mammals (Hornecker et al., 2007), fungi (Shiu et al., 2001), nematodes (Kelly et al., 2002), and insects (Cabrero et al., 2007b).

The first report of meiotic silencing was described in the fungus *Neurospora crassa* (Shiu et al., 2001). Any unpaired DNA during meiosis in *N. crassa* becomes transcriptionally inactivated, along with any sequences of DNA that are homologous to it (Shiu et al., 2001). Meiotic silencing in *N. crassa* has been termed meiotic silencing by unpaired DNA (MSUD). In contrast to meiotic silencing in mammals, MSUD is mediated by post-transcriptional mechanisms, which involves components of the RNA interference pathway (Alexander et al., 2008; Lee et al., 2003; Shiu et al., 2001). MSUD has been proposed to function in genome defense, by silencing potentially mutagenic transposable elements (Shiu et al., 2001).

A mechanistically and functionally distinct form of meiotic silencing has been reported in the nematode *Caenorhabditis elegans*. In *C. elegans*, males have a single X chromosome (XO), compared to their hermaphroditic XX counterparts. Early immunostaining experiments reveled that the asynapsed X chromosome in XO males is devoid of RNA polymerase, suggesting gene inactivation (Kelly et al., 2002).

Like in mammals, meiotic silencing in *C. elegans* is mediated in large part by chromatin modifications (Maine, 2010). The asynapsed X chromosome in XO males is deficient in active transcription histone marks and enriched in repressive histone marks, including tri-methylation of histone H3 at lysine 27 (H3K27me3) and H3K9me2 (Bean et al., 2004; Bender et al., 2004; Kelly et al., 2002). In *C. elegans*, silencing and heterochromatin formation have been proposed to shield the asynapsed X chromosome from a checkpoint. Indeed, mutants lacking *met-2*, which encodes the histone methyltransferase responsible for generating the repressive H2K9me2 mark, results in increased apoptosis and activation of a recombination checkpoint (Checchi and Engebrecht, 2011). Thus, meiotic silencing may have evolved distinct functions in different organisms.

Meiotic silencing may also operate in the grasshopper *Eyprepocnemis plorans* (Cabrero et al., 2007a). The asynapsed X chromosome in *E. plorans* accumulates γH2AFX at pachynema (Cabrero et al., 2007a). However, the X chromosome in *E. plorans* is already heterochromatic and silenced at leptonema, even before the presence of γH2AFX at pachynema (Cabrero et al., 2007b). This suggests that γH2AFX in insects may help maintain a silenced state established in early prophase I, rather than initiating silencing.

In addition to mammals, worms, and insects, MSCI has also been previously reported in birds (Schoenmakers et al., 2009; Schoenmakers et al., 2010). In avian species, females are the heterogametic sex, carrying the Z and W sex chromosomes, and males are ZZ. The Z and W chromosomes are largely non-homologous, but nevertheless achieve transient, near complete synapsis at mid-pachynema (Schoenmakers et al., 2009). An early gene expression study reported that the Z and W chromosome pair are transiently silenced from early pachynema to early diplonema (Schoenmakers et al., 2009). However, a more recent analysis involving epigenetic profiling and RNA FISH found no evidence for MSCI in chickens (Guioli et al., 2012). Therefore, MSCI may not be conserved in avian species.

The status of the sex chromosomes in the germ line of *Drosophila melanogaster* is less well understood. While early genetic studies (Hoyle et al., 1995) and expression analyses (Vibranovski et al., 2009) suggested that meiotic silencing operates in *Drosophila melanogaster,* the latest work supports that it does not occur (Meiklejohn et al., 2011; Mikhaylova and Nurminsky, 2011). The earlier studies are thought to have been confounded by germ cell contamination (Vibranovski, 2014). Owing to the limitations of the methods used to study MSCI in *Drosophila,* more sophisticated approaches are needed to settle these conflicting results.

Surprisingly, meiotic silencing has not been well characterized in humans. Like in mouse, the human X and Y chromosomes are condensed (Solari, 1974) and stain for γH2AFX, BRCA1 (Sciurano et al., 2007), and ATR (de Boer et al., 2004). These meiotic silencing components also localize to asynapsed regions in human oocytes, e.g. the asynapsed chromosome 21 in

trisomy 21 oocytes (Garcia-Cruz et al., 2009). Therefore, the meiotic silencing pathway appears to be active in human germ cells with asynapsis.

A recent study reported a high degree of variation in the meiotic silencing response in human males (de Vries et al., 2012). Immunofluorescent analyses of γH2AFX, histone H3.1/3.2, RNA polymerase II, and Cot-1 RNA FISH in human spermatocytes showed significant heterogeneity in localization and intensity of these silencing components compared to mouse (de Vries et al., 2012). While this suggests that meiotic silencing may be less stringent in humans, this should be verified by direct analysis of transcription using gene-specific RNA FISH, a sensitive method to detect nascent transcription (Mahadevaiah et al., 2009a).

In addition to eutherian mammals (e.g. mouse, humans, etc.), meiotic silencing has also been described in metatherian mammals (e.g. marsupials) (Hornecker et al., 2007; Namekawa et al., 2007). In the marsupial *Monodelphis domestica*, the X and Y chromosomes in pachytene spermatocytes are enriched in γH2AFX and other silencing factors (Namekawa et al., 2007). Like in mouse, the sex chromosomes in *M. domestica* are robustly silenced during pachynema (Hornecker et al., 2007; Mahadevaiah et al., 2009b; Namekawa et al., 2007). While MSCI was previously believed to persist into spermiogenesis in *M. domestica* (Hornecker et al., 2007; Namekawa et al., 2007), a recent RNA FISH analysis debunked this claim, showing that many X-linked genes are reactivated during spermiogenesis (Mahadevaiah et al., 2009b). In summary, meiotic silencing operates in mammals and several other organisms, but there appear to be significant mechanistic differences between species.

1.4.4 Role of meiotic silencing in mammalian germ cells

In mammals, MSCI has an essential role in spermatogenesis (Burgoyne et al., 2009). Chromosome translocations that disrupt MSCI are associated with spermatocyte losses and infertility (Lifschytz and Lindsley, 1972). For example, T43(16;17)H (T43H) mice, which have a translocation involving chromosomes 17 and 16, have incomplete MSCI and are sterile (Homolka et al., 2007; Homolka et al., 2012). Furthermore, deletion of genes

necessary for meiotic silencing, including *Brca1* (Xu et al., 2003), *Atr* (Royo et al., 2013), *Hormad1* (Daniel et al., 2011; Kogo et al., 2012b; Shin et al., 2010), *H2afx* (Celeste et al., 2002), and *Mdc1* (Ichijima et al., 2011; Lou et al., 2006), also cause spermatocyte losses and male infertility. In all of these mutants, germ cell arrest occurs around mid-pachynema of meiotic prophase I.

MSCI is also disrupted in other meiotic mutants that arrest at mid-pachynema (Mahadevaiah et al., 2008; Royo et al., 2010). For example, in meiotic recombination mutants *Dmc1*-/- and *Msh5*-/- mice, the MSCI factors BRCA1 and ATR are abnormally retained at unrepaired DNA DSBs, and fail to accumulate on the asynapsed X and Y chromosomes, leading to disrupted MSCI (Mahadevaiah et al., 2008). In DNA DSB initiation mutants, e.g. *Spo11*-/- mice, MSCI is also disrupted, for reasons that are still unclear (Bellani et al., 2005; Mahadevaiah et al., 2008). Given the overwhelming association between MSCI defects and spermatocyte arrest, it has been speculated that disruption in XY silencing is an underlying mechanism of male infertility (Royo et al., 2010).

A recent study of male mice with an extra Y chromosome, i.e. XYY males, revealed that the X and Y chromosomes harbor genes that are toxic when expressed at pachynema (Royo et al., 2010). XXY mice have a pachytene stage spermatocyte arrest, similar to that observed in the aforementioned meiotic mutants (Burgoyne and Baker, 1984; Burgoyne and Biddle, 1980; Mahadevaiah et al., 2000). In a subset of XYY germ cells, the two Y chromosomes achieve homologous synapsis and are not subject to MSCI, resulting in Y-linked gene expression (Royo et al., 2010). These germ cells are eliminated during pachynema, suggesting that Y-gene expression is toxic. In support of this, transgenic mice mis-expressing the Y-linked genes *zinc finger protein Y-linked 1* (*Zfy1*) and *Zfy2* have pachytene germ cell losses (Royo et al., 2010). Therefore, mis-expression of sex-linked genes can cause spermatocyte losses.

While these studies highlight the importance of MSCI in mice, its raison d'être remains a mystery. Several theories have been postulated to explain the role of MSCI during meiosis. One of the earliest theories

suggested that MSCI prevents recombination from occurring between the non-homologous regions of the X and Y chromosomes (McKee and Handel, 1993). However, genetically ablating MSCI in mice, e.g. disrupting *H2afx* (Fernandez-Capetillo et al., 2003), *Brca1* (Xu et al., 2003), *Atr* (Royo et al., 2013), *Hormad1* (Daniel et al., 2011), or *Mdc1* (Ichijima et al., 2011), does not result in recombination between the X and Y heterologous regions. On the contrary, disrupting MSCI genes commonly result in failure of crossing over at the PAR and sex chromosome asynapsis (Fernandez-Capetillo et al., 2003; Turner et al., 2004; Wojtasz et al., 2012). This indicates that MSCI may actually promote proper pairing and recombination of the sex chromosomes.

Another proposed function of MSCI in mammals is to prevent transcription from DNA templates which have unrepaired meiotic DNA DSBs (Inagaki et al., 2010). As discussed above, DNA DSB repair proteins persist longer on the asynapsed X chromosome in spermatocytes than on synapsed autosomes (Moens et al., 2002). Perhaps MSCI evolved to suppress transcription from these damaged chromosomes. Support for this theory comes from the recent finding that HU-induced DNA DSBs in somatic cells results in local transcriptional repression (Ichijima et al., 2011). However, this theory does not explain why MSCI continues long after DNA DSBs on the asynapsed X chromosome are repaired (i.e. mid-pachynema).

The recent discovery of meiotic silencing (i.e. MSUC) as a general mechanism of silencing asynapsed chromosomes has led to new ideas about the role of silencing (Turner et al., 2005). It is possible that MSUC existed before the emergence of the modern heteromorphic X and Y chromosomes. If this is true, then upon divergence of the proto-X-Y chromosomes into their modern day heteromorphic counterparts, MSCI would have become a permanent feature of spermatogenesis (Cloutier and Turner, 2010). This model would suggest that there was a selective advantage to a general meiotic silencing response even before the heteromorphic sex chromosomes existed.

One theory is that MSUC evolved as an important surveillance mechanism to monitor the synaptic process (Burgoyne et al., 2009; Turner

et al., 2005). Under this model, MSUC would drive the elimination of germ cells with potentially deleterious errors in synapsis (Burgoyne et al., 2009; Schimenti, 2005; Turner et al., 2005). Mechanistically, MSUC could achieve this by silencing critical genes on asynapsed chromosomes (Burgoyne et al., 2009). To date, however, there is very little known about the surveillance mechanisms that operate in mammalian germ cells. The potential role for meiotic silencing in surveillance of the synaptic process will be expanded upon in the following section.

1.5 Meiotic surveillance mechanisms

Meiotic surveillance mechanisms monitor the integrity of meiotic processes to ensure that they are completed successfully before proceeding to cell division (Hochwagen and Amon, 2006). These quality control mechanisms prevent germ cells with defects from progressing through meiosis to produce abnormal gametes. In the absence of such surveillance mechanisms, germ cells with defects could generate aneuploid gametes and embryos.

In contrast to mitosis, meiosis involves several unique steps, namely programmed DNA DSB formation and homologous chromosome synapsis. Ensuring the fidelity of these meiosis-specific processes requires specialized surveillance mechanisms. In mammals, the mechanisms that monitor these meiosis-specific processes are not well understood. This is particularly true in the female germ line, which has been historically less extensively studied. Four specific mechanisms have been proposed to operate in mammalian germ cells: asynapsis checkpoint, DNA damage (recombination) checkpoint, meiotic silencing based mechanism, and the SAC (**Intro Figure 4**). The first three are thought to specifically operate during meiotic prophase I, and they will be discussed more extensively in this section.

1.5.1 The eukaryotic cell cycle

In eukaryotes, the mitotic cell cycle consists of four stages: gap phase 1 (G1), S phase, gap phase 2 (G2), and mitosis (M) (Futcher, 1996). During G1, cells grow and activate genes in preparation for the subsequent S phase (Bähler, 2005). Once the cells have reached a sufficient size, they proceed to S phase, when DNA is replicated (Futcher, 1996). Following S phase, cells enter the G2 phase, a period of cell growth and protein synthesis during which the cell prepares for division (Futcher, 1996). The G2 phase ends with the onset of prophase I, when cells enter into mitosis. Progression through each of these phases of the cell cycle is coordinated by the spatial and temporal activity of cyclins and cyclin dependent kinase (CDK) proteins (Futcher, 1996).

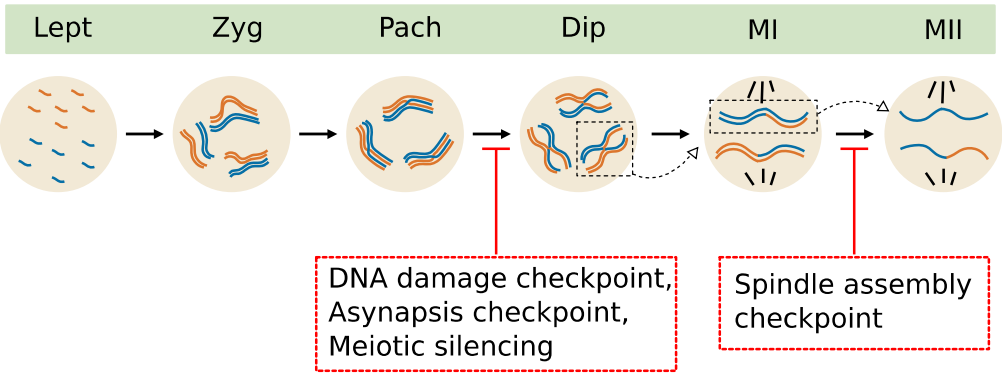

Introduction Figure 6: Meiotic surveillance mechanisms in mice.

In male mice, several different surveillance mechanisms operate to monitor the fidelity of meiotic processes. Three putative mechanisms, namely a DNA damage checkpoint, an asynapsis checkpoint, and a meiotic silencing based mechanism of surveillance, are thought to operate to prevent progression beyond pachynema. In females, the timing and activity of these prophase I mechanisms is not well understood. The spindle assembly checkpoint (SAC) operates in both male and female germ cells to prevent cells from progressing beyond metaphase I if improper spindle tension is detected. For simplicity, only one daughter cell is shown after each meiotic division. The chromosomes/chromatids boxed are those in the subsequent daughter cell.

Similar to mitosis, the meiotic cell cycle begins with commitment into G1, followed by a round of DNA replication during meiotic S phase (Marston and Amon, 2004). Following S phase, germ cells enter prophase I, which is akin to meiotic G2 (Marston and Amon, 2004). This begins with meiotic DNA DSBs being generated throughout the genome by SPO11 (Borde et al., 2000). During meiotic G2, chromosomes synapse and meiotic recombination occurs. After completion of prophase I, the first meiotic division takes place, which segregates homologs, followed by the second meiotic division, which segregates sister chromatids.

1.5.2 The DNA damage checkpoint: a mitotic perspective

Several distinct meiotic surveillance mechanisms are believed to operate in germ cells. One of the first-described models, the pachytene checkpoint model, has been well characterized in yeast meiosis (Roeder and Bailis, 2000). A "checkpoint" is a point in the cell cycle where the integrity of chromosomal processes are monitored (Hartwell and Weinert, 1989). One such checkpoint, called the DNA damage checkpoint, monitors for DNA damage during the G2/M phase of the cell cycle (O'Connell and Cimprich, 2005). When DNA damage is present, it sets off a series of biochemical events that triggers cell cycle delay or arrest until DNA lesions are repaired. If the lesion is too severe or irreparable, cells will undergo senescence or apoptosis (Harper and Elledge, 2007).

DNA DSBs are one of the most hazardous forms of DNA damage, and pose a significant threat to cell viability, survival, and normal cellular processes (Finn et al., 2012). DNA DSBs are capable of inducing gross chromosomal rearrangements and potentially deleterious mutations (Finn et al., 2012). In mitosis, a DNA damage checkpoint operates to delay cell division until DNA DSBs are fully repaired (Hartwell and Weinert, 1989; O'Connell and Cimprich, 2005), thereby preventing the propagation of hazardous lesions (Weinert and Hartwell, 1988).

The DNA damage checkpoint is best understood in the context of mitosis (O'Connell and Cimprich, 2005). During mitosis, DNA damage, such as DNA DSBs, can be made during S phase at replication forks, and these

lesions are subsequently repaired in G2, prior to cell division (Cuddihy and O'Connell, 2003). In the event that DNA DSBs persist at end of the G2 phase, the mitotic G2/M DNA damage checkpoint is triggered, and this delays entry into M phase, allowing more time for DNA repair (Harrison and Haber, 2006).

This mitotic DNA damage checkpoint is mediated by a number of highly conserved proteins that sense DNA damage and signal the cell cycle "effector" machinery (Finn et al., 2012). The first step in the DNA damage checkpoint is sensing the DNA lesion. The phosphoinositide three-kinase-related kinase (PIKK) family proteins ATM, ATR, and DNA-PKcs are the primary sensors in the G2/M DNA damage checkpoint (Lovejoy and Cortez, 2009). These kinases are activated by different DNA lesions: ATM and DNA PKcs are activated predominately by DNA DSBs, while ATR can be activated by a variety of DNA lesions, especially single-strand DNA gaps (Lovejoy and Cortez, 2009).

Each kinase is recruited to DNA lesions by different factors. ATM is recruited by the MRN complex, specifically by the Nbs1 component (Horejsí et al., 2004); ATR is recruited by ATRIP (Zou and Elledge, 2003); and DNA-PKc is recruited by the Ku70/80 heterodimer (Gottlieb and Jackson, 1993), which is composed of X-ray repair complementing defective repair in Chinese hamster cells 6 (XRCC6, or Ku70) and X-ray repair complementing defective repair in Chinese hamster cells 5 (XRCC5, or Ku80) (Falck et al., 2005).

Once recruited to DNA DSBs, ATR and ATM activate and recruit several downstream DDR proteins (Finn et al., 2012). Two important downstream effector kinases involved in the DNA damage checkpoint are checkpoint kinase 1 (CHK1) and checkpoint kinase 2 (CHK2), which are activated by ATR and ATM, respectively (Stracker et al., 2009). Functionally, CHK1 and CHK2 recruit additional downstream DDR factors, amplify the DDR signal, and activate the checkpoint (Stracker et al., 2009).

In eukaryotes, the G2/M DNA damage checkpoint ultimately prevents entry into mitosis by inhibiting the activity of CDK proteins (Finn et al., 2012). In the presence of DNA damage, activated CHK1 and CHK2 trigger a

cascade of events that inactivates CDK1 and CDK2 (Zhou and Bartek, 2004). Specifically, CHK1 phosphorylates the protein phosphatase cell division cycle 25A (CDC25A), leading to its degradation and thereby preventing it from activating CDK1/2 (Zhao et al., 2002). When CDK1/2 is inactivated, the cell cycle is halted at G2, providing additional time for DNA repair (Finn et al., 2012). Upon completion of DNA repair, cells exit the G2 arrest and resume to mitosis (Bartek and Lukas, 2007). Recovery from the checkpoint involves degradation of checkpoint mediator proteins, and activation of cell cycle promoting cyclin-CDK complexes (Bartek and Lukas, 2007).

1.5.3 Meiotic DNA damage checkpoint: insight from other organisms

An analogous DNA damage checkpoint is believed to operate in meiotic cells (Roeder and Bailis, 2000). Studies in the budding yeast *S. cerevisiae* have shown that the ATR and ATM orthologs, mitosis entry checkpoint 1 (Mec1; denoted $Mec1^{ATR}$) and telomere maintenance 1 (Tel1; denoted $Tel1^{ATM}$), respectively, are essential for arresting cells at pachynema in the presence of persistent DNA DSBs (Hochwagen and Amon, 2006).

In *S. cerevisiae*, two distinct DNA damage checkpoints operate during meiosis. The first pathway depends upon $Tel1^{ATM}$ and is activated by DNA DSBs with unprocessed DNA ends (Harrison and Haber, 2006). The second pathway, called the recombination checkpoint, is mediated by $Mec1^{ATR}$ and is activated by DNA DSBs with resected ends (Hong and Roeder, 2002; Lydall et al., 1996). Once activated, $Mec1^{ATR}$ phosphorylates the yeast ortholog of HORMAD1/2, called homolog pairing 1 (Hop1), which subsequently activates the CHK2-related effector kinase meiotic kinase 1 (Mek1; denoted $Mek1^{CHK2}$) (Carballo et al., 2008). Activated $Mek1^{CHK2}$ then phosphorylates and activates saccharomyces wee1 (Swe1). In turn, Swe1 inactivates the yeast ortholog of CDK1, cell division cycle 28 (Cdc28), resulting in meiotic arrest cells at pachynema (Leu and Roeder, 1999).

Following DSB repair, checkpoint recovery is mediated by the transcription factor non-dityrosine 1 (Ndt80). While inactive in the presence of DNA damage, Ndt80 becomes activated once DNA lesions are repaired,

thereby allowing re-entry into meiosis (Chu and Herskowitz, 1998; Tung et al., 2000).

This meiotic DNA damage checkpoint is thought to operate in other organisms. For example, persistent meiotic DSBs also trigger oocyte arrest in *C. elegans*, suggesting that a DNA damage checkpoint is active (Gartner et al., 2000). This checkpoint triggers oocyte death at pachynema and is mediated by the *C. elegan* orthologs of ATR (ATM like 1; ATL-1), HORMAD1 (high incidence of males 3; HIM-3) and CHK2 (CHK-2), among other proteins (Gartner et al., 2000; Jaramillo-Lambert et al., 2010; MacQueen and Villeneuve, 2001; Stergiou and Hengartner, 2004).

A DNA damage checkpoint has also been reported in the fission yeast Schizosaccharomyces *pombe*. This DNA damage checkpoint is dependent on the *S. pombe* orthologs of ATR (Rad3) and CHK2 (Cds1) (Perera et al., 2004; Pérez-Hidalgo et al., 2003; Shimada et al., 2002). Interestingly, some but not all *S. pombe* meiotic mutants with persistent DNA DSBs are subject to checkpoint arrest (Catlett and Forsburg, 2003; Pérez-Hidalgo et al., 2003). This suggests that the meiotic DNA damage checkpoint is less stringent, or more specific to only certain types of DNA lesions, in *S. pombe*.

A DNA damage checkpoint has also been suggested in *Drosophila melanogaster*. Mutant flies with persistent unrepaired DSBs exhibit oocyte arrest (Ghabrial and Schüpbach, 1999; Jang et al., 2003). This arrest is mediated by ATR, indicating a highly conserved role for ATR in the meiotic DNA damage checkpoint (Joyce et al., 2011).

1.5.4 DNA damage checkpoint model in mice

Compelling evidence for a existence of DNA damage checkpoint in mammals comes from studies of mice with persistent unrepaired DNA DSBs. Deletion of genes involved in DNA DSB repair and meiotic recombination, such as *Dmc1*, *Atm,* and *Msh5*, result in persistent unrepaired DNA DSBs and significant germ cell losses and infertility (**Intro Figure 7**) (Barchi et al., 2005; Di Giacomo et al., 2005). In female mice, these germ cell losses are partially reversed when DNA DSBs are abolished, i.e. by mutating *Spo11* or *meiosis 1* (*Mei1*) (Di Giacomo et al., 2005; Reinholdt and Schimenti, 2005).

These experiments provide strong genetic evidence that persistent unrepaired DNA DSBs can trigger oocyte losses in mice.

The role of DNA damage checkpoint proteins in mice is not very well understood. This is in part because deletion of putative checkpoint genes, such as *Atr, Rad9, Rad1* and *Hus1*, are incompatible with life (Brown and Baltimore, 2000; Han et al., 2010; Hopkins et al., 2004; Weiss et al., 2000). However, a recent study has provided evidence that ATM has a role in the meiotic DNA checkpoint in mice (Pacheco et al., 2015). Deletion of *Atm* in mice with recombination defects, i.e. *Trip13* mutants, allows spermatocyte progression to a later stage in pachynema (Pacheco et al., 2015). This implicates ATM in a DNA damage/recombination checkpoint that operates during early pachynema.

Recently, a conserved role for CHK2 in the meiotic DNA damage checkpoint has also been described in mice (Bolcun-Filas et al., 2014; Pacheco et al., 2015). *Chk2* is dispensable for viability and fertility in mice (Takai et al., 2002). Deleting *Chk2* in mouse mutants with persistent unrepaired DNA DSBS, such as *Dmc1*-/- females (Pittman et al., 1998) and *thyroid hormone receptor interactor 13* (*Trip13*) mutant females (Li and Schimenti, 2007), enables prolonged survival of oocytes (Bolcun-Filas et al., 2014). However, while *Chk2*-/- *Trip13*-/- mutants are fertile for several months, they only have a fraction (~25%) of the normal number of oocytes after birth (Bolcun-Filas et al., 2014), suggesting that the rescue is incomplete. CHK2-dependent oocyte losses are hypothesized to be mediated by the upstream kinase ATR and the downstream effectors p53 and p63 (Bolcun-Filas et al., 2014). CHK2 is also thought to mediate the activation of the DNA damage/recombination checkpoint that occurs in *Trip13* mutant spermatocytes (Pacheco et al., 2015).

In mice, the timing and kinetics of germ cell arrest in response to DNA damage is sexually dimorphic. *Atm*-/-, *Dmc1-/-*, and *Msh5*-/- mutant males experience a complete germ cell arrest at early pachynema (Barchi et al., 2005), with no cells progressing beyond. By contrast, in the female germ line, half of the mutant oocytes are eliminated by birth, corresponding to late diplonema/dicytate (Di Giacomo et al., 2005). The remaining oocytes

are eliminated over the next 2-3 postnatal weeks of development (Di Giacomo et al., 2005). This suggests that the meiotic DNA damage checkpoint is less stringent, delayed, and/or operates over a longer developmental period in females compared to males (Nagaoka et al., 2012).

The meiotic DNA damage checkpoint in mammals can also be triggered by other sources of DNA DSBs, such as those derived from retrotransposons. Retrotransposons are mobile genetic elements that utilize an RNA intermediate to facilitate insertion into new sites in the genome (Goodier and Kazazian, 2008). In addition to being an insertional mutagen, retrotransposons can produce hazardous DNA DSBs during the process of retrotransposition (Soper et al., 2008). Therefore, in mice, developing germ cells have mechanisms to suppress the expression of potentially mutagenic retrotransposons (Ollinger et al., 2010). These mechanisms involve DNA methylation (Bourc'his and Bestor, 2004; De La Fuente et al., 2006), Piwi-like proteins (Aravin et al., 2007; Kuramochi-Miyagawa et al., 2008), and other components such as Maelstrom (Mael) (Soper et al., 2008) and testis expressed gene 19.1 (Tex19.1) (Ollinger et al., 2008). Mice lacking any of these factors have increased expression of retrotransposons and defects in meiosis which compromise fertility (Ollinger et al., 2010). For example, *Mael*-/- mutants accumulate retrotransposon-derived DNA DSBs and fail to complete meiotic prophase I (Soper et al., 2008). This highlights that misexpression of retrotransposons can lead to DNA damage checkpoint activation.

Interestingly, retrotransposon-derived DNA DSBs may be important for fetal oocyte attrition (FOA) in wildtype females (Malki et al., 2014). FOA is a normal developmental process in mammals in which ~80% of the initial pool of oocytes are eliminated by birth (Burgoyne and Baker, 1985; Pepling and Spradling, 2001). While the molecular basis of FOA has been long debated (Pepling and Spradling, 2001), recent work showed that widespread derepression of retrotransposons in developing oocytes causes DNA DSBs (Malki et al., 2014). As repressive DNA methylation marks are erased in fetal oocytes during epigenetic reprogramming, retrotransposons are transiently reactivated (Lees-Murdock and Walsh, 2008). This opens up

a period of time in which oocytes are prone to the DNA damaging effects of retrotransposons. A critical role for retrotransposons in FOA is supported by experiments showing that FOA losses increase when LINE-1 retrotransposons are upregulated, and decreased by the reverse transcriptase inhibitor AZT (Malki et al., 2014). In summary, the DNA damage checkpoint is an important process in normal and defective oocytes.

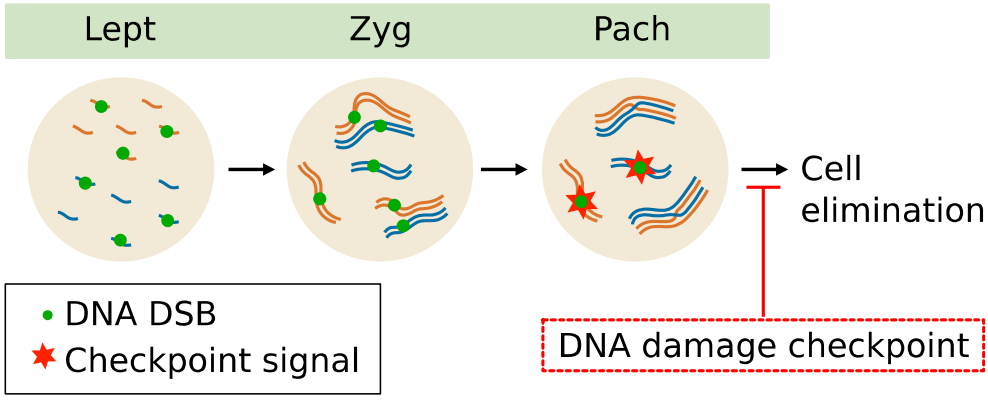

Introduction Figure 7: Meiotic DNA damage checkpoint model of germ cell loss in mice.

Under the DNA damage checkpoint model, endogenous or exogenous DNA DSBs that remain persistently unrepaired activates a signaling cascade that results in cell elimination at pachynema and/or diplonema. This model has been proposed to explain the oocyte losses experienced by female meiotic mutants with persistent unrepaired DNA DSBs (e.g. *Dmc1*-/-, *Msh5*-/-, *Atm*-/-).

1.5.5 Asynapsis checkpoint model

In addition to the DNA damage checkpoint, some organisms also have an asynapsis checkpoint, which monitors the fidelity of synapsis in a DNA damage-independent manner (MacQueen and Hochwagen, 2011). Under the asynapsis checkpoint, defects in chromosome axis structure and/or synaptonemal complex formation trigger germ cell arrest and elimination (**Intro Figure 8**).

In mice, synapsis and meiotic recombination are intimately coupled, such that failed synapsis can result in delayed or defective DNA DSB repair (de Vries et al., 2005). This makes it difficult to determine the precise mechanism responsible for germ cell losses in cells with asynapsis. For example, asynapsed chromosomes could cause germ cell losses through a DNA damage checkpoint that is triggered by persistent unrepaired DNA DSBs. Alternatively, asynapsed chromosomes could directly trigger a DNA damage-independent asynapsis checkpoint. Owing to the difficulties of dissecting the asynapsis checkpoint in mammals, most of our understanding of the asynapsis checkpoint comes from studies of other organisms, such as *C. elegans.*

In *C. elegans*, synapsis and meiotic recombination are mechanistically separable, such that synapsis can occur in the absence of meiotic DNA DSBs (Dernburg et al., 1998). Synapsis in *C. elegans* is mediated by distinct genetic regions called pairing centers (PCs) (MacQueen et al., 2005). If chromosome PCs are asynapsed at pachynema, a checkpoint is elicited and the defective oocytes are eliminated (Bhalla and Dernburg, 2005). These oocyte losses occur via a DNA DSB-independent pathway that involves CHK1 (Jaramillo-Lambert and Engebrecht, 2010; MacQueen and Hochwagen, 2011) and pachytene checkpoint 2 (PCH-2) (Bhalla and Dernburg, 2005).

Interestingly, the normally asynapsed X chromosome in XO *C. elegans* males does not trigger the asynapsis checkpoint (Jaramillo-Lambert and Engebrecht, 2010). Repressive chromatin marks, including H3K9me2, are thought to shield the asynapsed X chromosome from triggering the asynapsis checkpoint (Checchi and Engebrecht, 2011). However, accumulation of H3K9me2 on asynapsed autosomes does not prevent

checkpoint activation, suggesting that there are different functional responses on different chromosomes (Checchi and Engebrecht, 2011).

An asynapsis checkpoint is also suspected to operate in yeast. In *S. cerevisiae*, the checkpoint protein PCH2 is required for germ cell arrest in certain mutants with SC formation defects (San-Segundo and Roeder, 1999; Wu and Burgess, 2006). However, these SC mutations also have meiotic recombination defects, making it difficult to determine the proximal cause of PCH2-dependent arrest in yeast (MacQueen and Hochwagen, 2011).

In mice, evidence for an asynapsis checkpoint comes from studies of mutants lacking meiotic DNA DSBs, i.e. *Spo11*-/- and *Mei1*-/- animals. Both *Spo11*-/- (Baudat et al., 2000; Romanienko and Camerini-Otero, 2000) and *Mei1*-/- mice (Libby et al., 2002) lack programmed meiotic DNA DSBs, have extensive asynapsis, and experience profound germ cell losses resulting in infertility (Baudat et al., 2000; Di Giacomo et al., 2005; Libby et al., 2002; Romanienko and Camerini-Otero, 2000). This suggests a DNA DSB-independent surveillance mechanism operates in mice.

The molecular details of this DNA DSB-independent pathway remain largely unclear. However, recent work has shown that deletion of *Hormad1* rescues oocyte losses in *Spo11*-/- females (Daniel et al., 2011; Kogo et al., 2012b). This implicates HORMAD1 in the meiotic surveillance response to asynapsis. One possibility is that HORMAD1 recruits important asynapsis signaling proteins, such as ATR, which triggers an asynapsis checkpoint (Daniel et al., 2011). Alternatively, since HORMAD1 is necessary for meiotic silencing, it may trigger germ cell losses through meiotic silencing of critical genes (Daniel et al., 2011). The role of the mouse ortholog of the checkpoint protein PCH2, called TRIP13, is not fully understood. However, *Trip13* deficiency in mice does not rescue germ cell arrest in recombination- and synapsis-defective germ cells, suggesting that TRIP13 does not function in an asynapsis checkpoint in mice (Li and Schimenti, 2007; Roig et al., 2010).

The timing of germ cell arrest in *Spo11*-/- and *Mei1*-/- mice is sexually dimorphic. In mutant males, spermatocytes arrest at mid-pachynema, while in mutant females, oocytes are eliminated over a longer time period (Baudat et al., 2000; Di Giacomo et al., 2005; Libby et al., 2002).

Spo11-/- females lose 50% of their total oocyte pool by birth, and the remaining are lost over the next 2-3 weeks, when oocytes are arrested in dictyate (Di Giacomo et al., 2005). Differences in the timing of germ cell arrest imply that the DNA DSB-independent, asynapsis checkpoint is less efficient in females than males, or that different mechanisms operate in each sex.

It is also possible that an asynapsis checkpoint operates in response to chromosome abnormalities, such as monosomies, inversions, and translocations. These chromosome abnormalities disrupt synapsis during meiosis, and thus are useful models for dissecting the asynapsis surveillance mechanisms in mammals. Furthermore, since these models do not have mutations in key meiotic genes, they are valuable for understanding the response to asynapsis in the context of normal biology.

One useful chromosomally abnormal mouse model is the XO female mouse, which has a single X chromosome (Burgoyne and Baker, 1981, 1985). The XO condition in humans leads to Turner syndrome. XO female mice are subfertile, defined as having a shortened reproductive lifespan compared to XX females (Burgoyne and Baker, 1981, 1985). XO subfertility has been linked to a wave of oocyte losses occurring during late prophase I (Burgoyne and Baker, 1985). This wave of oocyte losses correlates with an increased number of atretic or degenerating cells at 19.5 d*pc*, when oocytes are at late pachynema and early diplonema (Burgoyne and Baker, 1985).

Interestingly, electron microscopy analysis of XO oocytes revealed that the single X chromosome in subset of XO oocytes forms a self-synapsed "hairpin" (Speed, 1986). This hairpin represents non-homologous synapsis and is mediated by the synapsis protein SYCP1 (Hodges et al., 2001). The percentage of pachytene XO oocytes with self-synapsed X chromosome increases during the period from 16.5 to 19.5 d*pc*, and the percentage of oocytes with an asynapsed X chromosome decreases (Hodges et al., 2001; Speed, 1986). This suggests that XO oocytes with an asynapsed X chromosome are eliminated during prophase I. It is possible that these oocytes with X chromosome asynapsis are eliminated by an asynapsis checkpoint. However, there are several other possible mechanisms that

could be responsible for XO oocyte losses, including a DNA damage checkpoint and a meiotic silencing-based mechanism (discussed in the next section). Therefore, there are still many unresolved questions concerning the molecular players involved in the asynapsis checkpoint and its contribution to germ cell losses in mice with chromosome abnormalities.

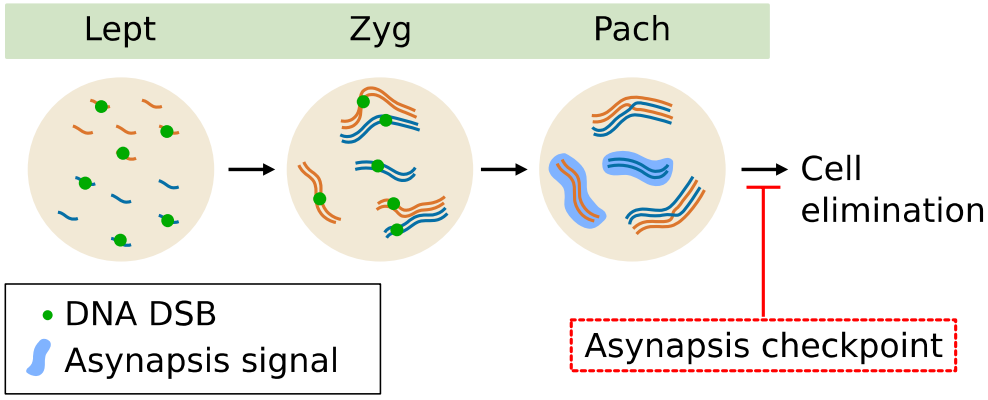

Introduction Figure 8: Asynapsis checkpoint model of germ cell loss in mice.

Under the asynapsis checkpoint model, germ cells with asynapsed chromosomes at pachynema trigger a checkpoint and subsequent germ cell losses. This pathway functions independent of meiotic DNA DSBs. Such a checkpoint may contribute to the oocyte losses observed in *Spo11*-/- females, which lack meiotic DNA DSBs, but have extensive asynapsis. The precise timing and the molecular machinery of this putative checkpoint remain largely unclear. The pathway may involve HORMAD1 and/or ATR (Daniel et al., 2011).

1.5.6 Meiotic silencing model of meiotic surveillance

The discovery of meiotic silencing of asynapsed chromosome in mammals (Baarends et al., 2005; Turner et al., 2005) has lead to another model of synaptic surveillance based on gene silencing (Schimenti, 2005). Under this model, meiotic silencing leads to the elimination of germ cells with asynapsis by inactivating critical genes on asynapsed chromosomes (**Intro Figure 9**) (Burgoyne et al., 2009; Schimenti, 2005).

The meiotic silencing model of germ cell arrest was first proposed based upon studies of XO female mice (Baarends et al., 2005; Turner et al., 2005). These studies showed that the asynapsed X chromosome in XO oocytes accumulates silencing factors, including BRCA1, ATR, γH2AFX, and ubi-H2A (Baarends et al., 2005; Turner et al., 2005). They also provided evidence based on Cot-1 RNA FISH (Turner et al., 2005) and RNA PolII staining (Baarends et al., 2005) that the asynapsed X chromosome in XO oocytes is transcriptional repressed. Since the X chromosome is enriched in genes involved in oogenesis (Khil et al., 2004), silencing of the X chromosome in XO females is likely incompatible with oocyte survival. Therefore, meiotic silencing may be a cause of XO oocyte losses by starving developing oocytes of important gene products (**Intro Figure 9**) (Burgoyne et al., 2009).

Genetics support for the meiotic silencing model comes from an analysis of meiotic mutant female mice (Kouznetsova et al., 2009). Females deficient in the gene *structural maintenance of chromosomes 1B* (*Smc1β*) have variable levels of asynapsis, and experience oocyte losses and infertility (Revenkova et al., 2004). In 30% of *Smc1β*-/- pachytene oocytes, up to 2-3 pairs of chromosomes are asynapsed, and they accumulate the silencing factors BRCA1 and γH2AFX (Kouznetsova et al., 2009). However, when more than 2-3 pairs of asynapsed chromosomes are present, BRCA1 accumulation on asynapsed axes is reduced, suggesting that the BRCA1 pool is limited and that silencing breaks down in oocytes with extensive asynapsis (Kouznetsova et al., 2009). Another study showed that spermatocytes also have limited pool of BRCA1, and suggested that BRCA1

is sequestered at unrepaired DNA DSBs in mutants with extensive asynapsis and recombination defects (Mahadevaiah et al., 2008).

To address whether meiotic silencing or BRCA1/γH2AFX signaling is involved in *Smc1β*–/– oocyte losses, Kouznetsova and colleagues tested whether disrupting *Sycp3*, which is required for silencing (Fukuda et al., 2012), improves survival of *Smc1β*-/- oocytes (Kouznetsova et al., 2009). Indeed, *Sycp3*-/- *Smc1β*-/- females have 25% more oocytes than *Smc1β*-/- females at birth (Kouznetsova et al., 2009). They concluded that the silencing machinery, SYCP3/BRCA1/γH2AFX, is required for a subset *Smc1β*-/- oocyte losses (Kouznetsova et al., 2009). However, *Sycp3*-/- mutants have numerous meiotic defects, including meiotic recombination and synaptonemal complex defects (Yuan et al., 2000), and there is evidence that *Sycp3* may also influence the DNA damage checkpoint in oocytes (Wang and Hoog, 2006). More research is therefore required to clarify the contribution of meiotic silencing and other checkpoints to oocyte losses.

Meiotic silencing has also been invoked as a mechanism responsible for the elimination of synapsis-defective *Spo11*-/- oocytes (Burgoyne et al., 2009). Traditionally, *Spo11*-/- oocyte losses were hypothesized to be driven by an asynapsis checkpoint (Di Giacomo et al., 2005). However, recent studies have revealed that *Spo11*-/- oocytes mount a meiotic silencing response involving a subset of asynapsed chromosomes (Carofiglio et al., 2013; Daniel et al., 2011; Shin et al., 2010). It is therefore conceivable that silencing of critical genes in *Spo11*-/- oocytes could contribute to oocyte losses.

In support of a meiotic silencing mechanism of *Spo11*-/- oocyte losses, disrupting the essential silencing factor HORMAD1 rescues *Spo11*-/- oocyte losses (Daniel et al., 2011; Kogo et al., 2012b). *Hormad1*-/- *Spo11*-/- oocytes do not initiate meiotic silencing due to defects in ATR recruitment and γH2AFX accumulation (Daniel et al., 2011; Kogo et al., 2012a; Kogo et al., 2012b; Wojtasz et al., 2012). While these studies implicate meiotic silencing as the cause of *Spo11*-/- oocyte losses, it is also possible that HORMAD1 facilitates *Spo11*-/- oocyte losses via an alternative pathway, such as an asynapsis checkpoint (Daniel et al., 2011; Kogo et al., 2012b).

In summary, more research is needed to understand the role of meiotic silencing as a potential surveillance mechanism against asynapsis in mice. Furthermore, it is still unclear which of the meiotic surveillance mechanisms contribute to germ cell losses in mice with chromosome abnormalities, such as XO mice. Determining the relative contributions of each putative mechanism of meiotic surveillance – the DNA damage checkpoint, asynapsis checkpoint, and meiotic silencing – to oocyte losses represents an important challenge.

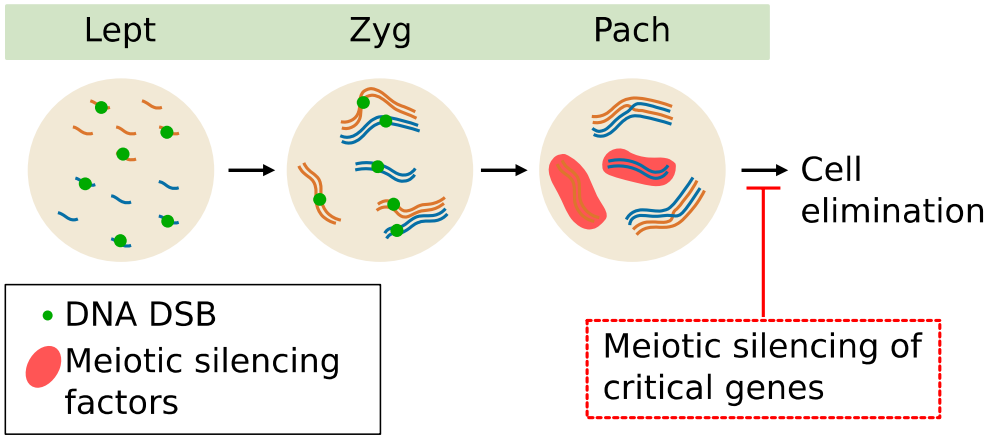

Introduction Figure 9: Meiotic silencing model of germ cell loss in mice.

Under the meiotic silencing model of germ cell loss, asynapsed chromosomes at pachynema trigger a the accumulation of meiotic silencing factors that causes the inactivation of critical genes, such as those required for meiosis and oogenesis. Starving germ cells of essential gene products is expected to lead to germ cell death. This mechanism has been proposed to explain oocyte losses in mice with chromosome abnormalities, i.e. XO female mice (Burgoyne et al., 2009).

1.6 Aims of thesis

The principal goals of this thesis are: (1) to identify and characterize the meiotic surveillance mechanisms that mediate oocyte losses in female mice with chromosome abnormalities; (2) to characterize the meiotic silencing response in oocytes; and (3) to study the molecular factors involved in meiotic silencing pathway.

Specifically, I will address the following aims:

1. **Determine the developmental timing of oocyte losses in mice with chromosome abnormalities.**
2. **Examine the contribution of the following models of meiotic surveillance on oocyte loss in mice with chromosome abnormalities:**
    a. **DNA damage checkpoint**
    b. **Asynapsis checkpoint**
    c. **Meiotic silencing**
3. **Characterize the meiotic silencing response in oocytes at the single gene level.**
4. **Characterize the role of BRCA1 and HORMAD2 in meiotic silencing.**

2 Materials and Methods

2.1. Mice

Unless otherwise noted, all mice were generated on a randomly bred MF1 Swiss albino background at NIMR according to UK Home Office Regulations. Wildtype XX mice used in this thesis were either of MF1 or C57BL/6 origin, as indicated in the particular experiment. A variety of mouse models were used in this study, and the origin of each are described below.

To generate embryos at specific gestational ages, female mice were set up in matings and checked each morning for vaginal plugs. The day that a vaginal plug was identified was considered 0.5 days *post coitum* (d*pc*). Embryos were sacrificed at 17.5, 18.5, 19.5 and 20.5 d*pc* using UK Home Office Schedule I methods. Ovaries were dissected from embryos, flash frozen in liquid nitrogen, and stored at -80°C until later use.

2.1.1 XO mice

XO mice containing a single maternal X chromosome were produced by mating XX females with fertile $X^{Y}O$ males. $X^{Y}O$ males carry an X chromosome fused to a Y chromosome at a shared pseudoautosomal (PAR) region (Eicher et al., 1991). Because the X^{Y} chromosome segregates as one unit, $X^{Y}O$ males produce X^{Y} and O gametes (see Punnett square, below). XO females (red) are generated when an O-bearing sperm from $X^{Y}O$ studs fertilizes an X-bearing egg.

		$X^{Y}O$	
		X^{Y}	O
XX	X	XX^{Y}	XO
	X	XX^{Y}	XO

2.1.2 In(X)1H mice

Heterozygous female carriers of the In(X)1H inversion were generated by crossing wildtype XX females with In(X)1H/Y males (see Punnett square, below) (Evans and Phillips, 1975; Tease and Fisher, 1986). The In(X)1H/Y male was originally derived from a mouse colony that had received radiation treatment (Evans and Phillips, 1975). This inversion encompasses 85% of the X chromosome, which disrupts meiotic pairing in a subset of In(1)1H oocytes (Koehler et al., 2004; Tease and Fisher, 1986).

		In(X)Y	
		In(X)	Y
XX	X	In(X)X	XY
	X	In(X)X	XY

2.1.3 T(16;17)43H mice

T(16;17)43H (referred to as T43H mice) females were a gift from Jiří Forejt (Institute of Molecular Genetics of the ASCR, Czech Republic). These mice were generated on the C57BL/10ScSnPh (B10) background, as previously described (Forejt et al., 1980; Homolka et al., 2007; Searle, 1978). T43H/+ male heterozygote carriers are sterile and cannot be used for colony maintenance (Searle, 1978). By contrast, T43H/T43H male homozygotes are fertile and are breed to wildtype XX females to generate T43H/+ female heterzygotes (See Punnet square, below) (Forejt et al., 1980). T43H/T43H homozygous males were generated by crossing T43H/+ heterozygous females, which are fertile, to males homozygous for a Robertsonian translocation, Rb(16.17)7Brn, as previously described (Forejt et al., 1980; Searle, 1978).

		XY T43H/T43H	
		X T43H	Y T43H
XX +/+	X +	XX T43/+	XY T43/+
	X +	XX T43/+	XY T43/+

2.1.4 Tc1 mice

Tc1 mice (i.e. hemizygous carriers of human chromosome 21) were produced by crossing Tc1 hemizygous males (h21/+) to XX wildtype females (+/+) (see Punnett square, below). The Tc1 transchromosomic mouse (Tc(Hsa21)1TybEmcf), a gift from Victor Tybulewicz, was originally developed as a model of Down syndrome and carries a single and near complete copy of human chromosome 21 (O'Doherty et al., 2005). Due to the irradiation used to generate this mouse model, the h21 chromosome is genetically shuffled and contains 25 structural rearrangements, six duplications and one deletion (Gribble et al., 2013). Since the accessory chromosome freely segregates as a distinct unit, Tc1 males generate both h21-bearing sperm and sperm carrying the wildtype (+) complement of chromosome.

		h21/+	
		h21	+
+/+	+	h21/+	+/+
	+	h21/+	+/+

2.1.5 XY^{d1} mice

XY^{d1} mice contain Y chromosome with a deletion that prevents the expression of the sex-determining gene *Sry* in developing gonads. This causes XY^{d1} mice to develop as females (Capel et al., 1993; Mahadevaiah et al., 1998). The XY^{d1} female was originally produced by crossing XX females with $XSxr^a$/Y males, which contain a duplicated copy of the Y short arm (Yp) transposed on the X chromosome ($XSxr^a$) (Capel et al., 1993).

Asymmetric meiotic recombination between the duplicated regions of the $XSxr^a$ and Y chromosomes generates several variants of the X and Y chromosomes, including the Y^{d1} chromosome (Capel et al., 1993). The Y^{d1} chromosome is missing several copies of Sx1 band C repeat on the Yp region of the chromosome, and this leads to *Sry* silencing by long range position effects (Capel et al., 1993). XY^{d1} females were maintained by mating them

with normal XY males. XY^{d1} females were also used to generate XXY^{d1} females (see Punnett square, next section).

2.1.6 XXY^{d1} mice

XXY^{d1} females were produced by mating a wild type XY stud to a sex-reversed XY^{d1} female. The X and Y chromosomes rarely pair in oocytes (Mahadevaiah et al., 1993), and as a result the X and Y^{d1} chromosomes segregate randomly at metaphase I of meiosis. Because of X-Y^{d1} nondisjunction, XY^{d1} females produce four types of gametes: X, Y^{d1}, XY^{d1} and O (see Punnett square, below). Therefore, the XY x XY^{d1} mating generates eight different genotypes, and XXY^{d1} females (red) are produced when an X-bearing sperm fertilizes an XY^{d1}-bearing egg.

		XY	
		X	Y
XY^{d1}	X	XX	XY
	Y^{d1}	XY^{d1}	$Y^{d1}Y$
	XY^{d1}	XXY^{d1}	$XY^{d1}Y$
	O	XO	YO

2.1.7 *H2afx*-/- and XO *H2afx*-/- mice

H2afx-/- mice were a gift from Andre Nussensweig (National Institutes of Health, USA), and contain a null mutation due to a neomycin resistance cassette inserted within the 5' end of the single exon of the *H2afx* locus (Celeste et al., 2002; Petersen et al., 2001). *H2afx*-/- mice were used to generate XO *H2afx*-/- females (see below), *H2afx*-/- *Spo11*-/- females (Section 2.1.9), and *H2afx*-/- *Dmc1*-/- females (Section 2.1.10).

XO *H2afx*-/- mice were produced in three generations of matings. In the first step, XO *H2afx*+/- females were produced. This was achieved by crossing fertile $X^{Y}O$ males with XX *H2afx*+/- females (see Punnett square, step 1).

Step 1:		X^YO *H2afx+/+*	
		X^Y *H2afx+*	O *H2afx+*
XX *H2afx+/-*	X *H2afx+*	XX^Y *H2afx+/+*	XO *H2afx+/+*
	X *H2afx-*	XX^Y *H2afx+/-*	XO *H2afx+/-*

In the second step, the fertile XO *H2afx*+/- females were then used generate X^YO *H2afx*+/- male mice. This was achieved by crossing XO *H2afx*+/- females with X^YO fertile males (see Punnett square, step 2).

Step 2:		X^YO *H2afx+/+*	
		X^Y *H2afx+*	O *H2afx+*
XO *H2afx+/-*	X *H2afx+*	XX^Y *H2afx+/+*	XO *H2afx+/+*
	O *H2afx-*	X^YO *H2afx+/-*	OO *H2afx+/-*

Finally, fertile X^YO *H2afx*+/- males were crossed with XX *H2afx*+/- females to generate XO *H2afx*-/- females (see Punnett square, step 3).

Step 3:		X^YO *H2afx+/-*			
		X^Y	X^Y	O *H2afx+*	O *H2afx-*
XX *H2afx+/-*	X *H2afx+*	XX^Y *H2afx+/+*	XX^Y *H2afx+/-*	XO *H2afx+/+*	XO *H2afx+/-*
	X *H2afx-*	XX^Y *H2afx+/-*	XX^Y *H2afx-/-*	XO *H2afx+/-*	XO *H2afx-/-*

2.1.8 *Spo11*-/- and XO *Spo11*+/-

Spo11-/- mice were a gift from Scott Keeney (Memorial Sloane-Kettering Cancer Center, USA). The *Spo11* knockout allele contains a neomycin resistance cassette that replaces exons 4 through 6, including the putative catalytic tyrosine encoded in exon 5, as previously described (Baudat et al., 2000). *Spo11*-/- mice were used for two separate purposes, to generate XO *Spo11*+/- females (see below) and *H2afx*-/- *Spo11*-/- females (Section 2.1.9).

XO *Spo11*+/- females were generated on a mixed C57BL/6 and MF1 background by mating fertile $X^{Y}O$ males (MF1) to XX *Spo11*+/- females (C57BL/6) (see Punnett square, below).

		$X^{Y}O$	
		X^{Y} *Spo11*+	O *Spo11*+
XX *Spo11*+/-	X *Spo11*+	XX^{Y} *Spo11*+/+	XO *Spo11*+/+
	X *Spo11*-	XX^{Y} *Spo11*+/-	XO *Spo11*+/-

2.1.9 *H2afx*-/- *Spo11*-/- mice

H2afx-/- *Spo11*-/- females were generated in two generations of matings on a mixed C57BL/6 and MF1 background. In the first step, *H2afx*+/- *Spo11*+/- mice were generated by crossing *Spo11*+/- males and *H2afx*+/- females (see Punnett square, step 1).

Step 1:		*H2afx*+/+ *Spo11*+/-	
		H2afx+ *Spo11*+	*H2afx*+ *Spo11*-
H2afx+/- *Spo11*+/+	*H2afx*+ *Spo11*+	*H2afx*+/+ *Spo11*+/+	*H2afx*+/+ *Spo11*+/-
	H2afx- *Spo11*+	*H2afx*+/- *Spo11*+/+	*H2afx*+/- *Spo11*+/-

Next, *H2afx*-/- *Spo11*-/- females were produced by crossing the double heterozygotes (see Punnett square, step 2).

Step 2:		*H2afx*+/- *Spo11*+/-			
		H2afx+ *Spo11*+	*H2afx*+ *Spo11*-	*H2afx*- *Spo11*+	*H2afx*- *Spo11*-
H2afx+/- *Spo11*+/-	*H2afx*+ *Spo11*+	*H2afx*+/+ *Spo11*+/+	*H2afx*+/+ *Spo11*+/-	*H2afx*+/- *Spo11*+/	*H2afx*+/- *Spo11*+/-
	H2afx+ *Spo11*-	*H2afx*+/+ *Spo11*+/-	*H2afx*+/+ *Spo11*-/-	*H2afx*+/- *Spo11*+/-	*H2afx*+/- *Spo11*-/-
	H2afx- *Spo11*+	*H2afx*+/- *Spo11*+/+	*H2afx*+/- *Spo11*+/-	*H2afx*-/- *Spo11*+/	*H2afx*-/- *Spo11*+/-
	H2afx- *Spo11*-	*H2afx*+/- *Spo11*+/-	*H2afx*+/- *Spo11*-/-	*H2afx*-/- *Spo11*+/-	*H2afx*-/- *Spo11*-/-

2.1.10 *Dmc1*-/- and *H2afx*-/- *Dmc1*-/- mice

Dmc1-/- mice were a gift from Attila Tóth (Technische Universität Dresden, Germany) and were maintained on a mixed genetic background. *Dmc1*-/- mice contain a deletion in the region encoding the conserved DNA binding domain necessary for its RecA-like enzymatic activity (Pittman et al., 1998).

Dmc1-/- mice were used to generate *H2afx*-/- *Dmc1*-/- females in two steps. The first step produced *H2afx*+/- *Dmc1*+/- double heterozygotes (see Punnett square, step 1).

Step 1:

		H2afx+/+ *Dmc1*+/-	
		H2afx+ *Dmc1*+	*H2afx*+ *Dmc1*-
H2afx+/- *Dmc1*+/+	*H2afx*+ *Dmc1*+	*H2afx*+/+ *Dmc1*+/+	*H2afx*+/+ *Dmc1*+/-
	H2afx- *Dmc1*+	*H2afx*+/- *Dmc1*+/+	*H2afx*+/- *Dmc1*+/-

In the second step, the double heterozygotes were crossed (see Punnett square, step 2)

Step 2:

		H2afx+/- *Dmc1*+/-			
		H2afx+ *Dmc1*+	*H2afx*+ *Dmc1*-	*H2afx*- *Dmc1*+	*H2afx*- *Dmc1*-
H2afx+/- *Dmc1*+/-	*H2afx*+ *Dmc1*+	*H2afx*+/+ *Dmc1*+/+	*H2afx*+/+ *Dmc1*+/-	*H2afx*+/- *Dmc1*+/+	*H2afx*+/- *Dmc1*+/-
	H2afx+ *Dmc1*-	*H2afx*+/+ *Dmc1*+/-	*H2afx*+/+ *Dmc1*-/-	*H2afx*+/- *Dmc1*+/-	*H2afx*+/- *Dmc1*-/-
	H2afx- *Dmc1*+	*H2afx*+/- *Dmc1*+/+	*H2afx*+/- *Dmc1*+/-	*H2afx*-/- *Dmc1*+/+	*H2afx*-/- *Dmc1*+/-
	H2afx- *Dmc1*-	*H2afx*+/- *Dmc1*+/-	*H2afx*+/- *Dmc1*-/-	*H2afx*-/- *Dmc1*+/-	*H2afx*-/- *Dmc1*-/-

2.1.11 *Hormad2*-/- mice

Hormad2-/- mice were a gift from Attila Tóth (Technische Universität Dresden, Germany), and were maintained on a mixed background. *Hormad2*-/- mice have a deletion of exon 4 (Wojtasz et al., 2012). *Hormad2*-/- mice were generated by crossing heterozygotes (see Punnett square, below).

		Hormad2+/-	
		Hormad2+	*Hormad2-*
Hormad2+/-	*Hormad2+*	*Hormad2+/+*	*Hormad2+/-*
	Hormad2-	*Hormad2+/-*	*Hormad2-/-*

2.1.12 *Brca1*-/- *53bp1*-/- mice

Deletion of *Brca1* causes embryonic lethality at 5.5-8.5 days *post coitum* (d*pc*) in mice (Ludwig et al., 1997). This embryonic lethality can be overcome with a homozygous null mutation in *53bp1* (Bunting et al., 2012). *Brca1*-/- *53bp1*-/- mice were a gift from Andre Nussenzweig (National Institutes of Health, USA), and were maintained on a genetically mixed background. In these mice, the *Brca1* locus is disrupted by replacement of exon 2 with a neomycin resistance cassette (Ludwig et al., 1997), and *53bp1* locus is disrupted at a 3' exon with a neomycin resistance cassette (Ward et al., 2003). *Brca1*-/- *53bp1*-/- males were generated as shown in the Punnett square below:

		Brca1+/- 53bp1-/-	
		Brca1+ 53bp1-	*Brca1- 53bp1-*
Brca1+/- 53bp1-/-	*Brca1+ 53bp1-*	*Brca1+/+ 53bp1-/-*	*Brca1+/- 53bp1-/-*
	Brca1- 53bp1-	*Brca1+/- 53bp1-/-*	*Brca1-/- 53bp1-/-*

2.1.13 *Brca1*Δ11/Δ11 *p53*+/-

*Brca1*Δ11/Δ11 *p53*+/- mice were generated on a mixed genetic background of 129/FVB/Black Swiss as previously described (Xu et al., 2001). In these *Brca1* mutants, exon 11 of the *Brca1* gene is deleted, resulting in a truncated *Brca1* isoform (Xu et al., 1999). Simultaneous heterozygous mutation of *p53* overcomes the embryonic lethality of *Brca1*Δ11/Δ11 mice (Xu et al., 2001). *Brca1*Δ11/Δ11 *p53*+/- mice were generated as shown below:

Step 1:		*Brca1*+/+ *p53*+/-	
		Brca1+ *p53*+	*Brca1*+ *p53*-
*Brca1*Δ11/- *p53*+/+	*Brca1*Δ11 *p53*+	*Brca1*Δ11/+ *p53*+/+	*Brca1*Δ11/+ *p53*+/-
	Brca1+ *p53*+	*Brca1*+/+ *p53*+/+	*Brca1*+/+ *p53*+/-

Step 2		*Brca1*Δ11/+ *p53*+/-			
		*Brca1*Δ11 *p53*+	*Brca1*Δ11 *p53*-	*Brca1*+ *p53*+	*Brca1*+ *p53*-
*Brca1*Δ11/+ *p53*+/-	*Brca1*Δ11 *p53*+	*Brca1*Δ11/ Δ11 *p53*+/+	*Brca1*Δ11/ Δ11 *p53*+/-	*Brca1*Δ11 /+ *p53*+/+	*Brca1*Δ11 /_ *p53*+/-
	*Brca1*Δ11 *p53*-	*Brca1*Δ11/ Δ11 *p53*+/-	*Brca1*Δ11/ Δ11 *p53*-/-	*Brca1*Δ11 /+ *p53*+/-	*Brca1*Δ11 /+ *p53*-/-
	Brca1+ *p53*+	*Brca1*Δ11/+ *p53*+/+	*Brca1*Δ11/ + *p53*+/-	*Brca1*+/+ *p53*+/+	*Brca1*+/+ *p53*+/-
	Brca1+ *p53*-	*Brca1*Δ11/+ *p53*+/-	*Brca1*Δ11/ + *p53*-/-	*Brca1*+/+ *p53*+/-	*Brca1*+/+ *p53*-/-

2.2 Genotyping

Mice were genotyped using DNA extracted from tail tips. Tail tips were digested in 200 µl GNTK buffer (50mM KCl, 1.5mM $MgCl_2$, 10mM Tris-HCl pH 8.5, 0.45% NP-40 (Fluka), 0.45% TWEEN-20 (Sigma)) and 1 µl Proteinase K (20 mg ml^{-1}) (Roche) overnight at 55°C in a water bath. The next day, reactions were incubated in a heat block at 95°C for 15 min and then centrifuged at maximum speed for 5 min.

Each genotyping PCR reaction had the following contents: Koops Buffer (250mM Tris pH 9, 75mM ammonium sulphate, 35mM $MgCl_2$, 0.85 mg ml^{-1} bovine serum albumin (BSA) (Sigma) and 0.25% NP-40), 250 ng μl^{-1} primers, 1x cresol red, 1.44 mM dNTPs (Invitrogen), Thermoprime Plus DNA Polymerase (ThermoFischer), and 1 µl of DNA. Genotyping PCR primers and cycling conditions are listed below (**Table 4**).

Table 4: Genotyping primers and PCR conditions.

Mouse	Primers 5' --> 3'	Ref.	PCR conditions
H2afx ko	HX5 CTCTTCTACCTCGTACACCATGTCCG RW CTCGGCGCGGGCCCCC KXR GTCACGTCCTGCACGACGCGAGC	(Celeste et al., 2002)	1x: 94°C, 3 min 35x: 96°C, 10 sec 65°C, 30 sec 72°C, 30 sec 1x: 72°C, 10 min
Spo11 ko	PRSF4 CTGAGCCCAGAAAGCGAAGGA SP16R ATGTTAGTCGGCACAGCAGTAG	(Baudat et al., 2000)	1x: 94°C, 5 min 35x: 94°C, 30 sec 58°C, 30 sec 72°C, 45 sec 1x: 72°C, 10 min
Tc1	Neo1 ATTGAACAAGATGGATTGCAC Neo2 TTCGTCCAGATCATCCTGATCGAC	(Marahrens et al., 1997)	1x: 94°C, 3 min 35x: 96°C, 10 sec 60°C, 30 sec 72°C, 30 sec 1x: 72°C, 5 min
Y^{d1} chrom. [*Ymt2b*]	YMTfp1 CTGGAGCTCTACAGTGATGA YMTrc2 CAGTTACCAATCAACACATCAC	(Bishop and Hatat, 1987)	1x: 94°C, 5 min 35x: 96°C, 10 sec 60°C, 30 sec 72°C, 30 sec 1x: 72°C, 5 min
X^{Y} chrom. [*Sts*]	STS F GCTCGCTGACATCATCCTC STS R CACCGATGCCCAGGTCGTC	(Salido et al., 1996)	1x: 94°C, 3 min 35x: 96°C, 10 sec 58°C, 30 sec 72°C, 30 sec 1x: 72°C, 10 min
Hormad2 ko	H2lox3 CACTTTAGCCCATATGAACAGCC H2lox5 AATACTTTATTAGCCCTCTTTCC H2FRT GTCTACAGAGTGAGTTTAAAATGC	(Wojtasz et al., 2012)	Performed by Attila Toth's lab
Brca1 ko [*Brca1-/-*]	WT F GGACGGCAGATAAATCCATTTCTTCC WT R GTACAAAGCCAGTGTGGGTTACATG KO F GGAATGTTTCCACCCAATGTCGAGC KO R CATCAGAGCCGATTGTCTGTTG	(Ludwig et al., 1997)	1x: 94°C, 1 min 35x: 94°C, 60 sec 60°C, 2 min 72°C, 1 min 1x: 72°C, 10 min
53BP1 ko	□□□□□□CTC CAG AGA GAA CCC AGC AG 10694 GAA CTT GGC TCA CAC CCA TT oIMR5316 CTA AAG CGC ATG CTC CAG AC	(Ward et al., 2003)	1x: 94°C, 3 min 35x: 94°C, 30 sec 62°C, 30 sec 72°C, 30 sec 1x: 72°C, 2 min
*Brca1*Δ11/Δ11	□11 F CTGGGTAGTTTGTAAGCATCC □11 R CTGCGAGCAGTCTTCAGAAAG	(Xu et al., 2001)	1x: 95°C, 60 sec 30x: 95°C, 30 sec 60°C, 60 sec 68°C, 1 min 1x: 68°C, 5 min
p53	F TTTACGGAGCCCTGGCGCTCGATGT R ATGACTGCCATGGAGGAGTCACAGTC	(Donehower et al., 1992)	1x: 95°C, 60 sec 30x: 95°C, 30 sec 60°C, 60 sec 68°C, 1 min 1x: 68°C, 5 min
Dmc1 ko/wt [*Dmc1-/-*]	oIMR5332 GCCAGAGGCCACTTGTGTAG oIMR9132 CCGGCCAGATTACATTTCTT oIMR9133 AAAGGGACTGCTGAGGCATA	(Pittman et al., 1998)	1x: 94°C, 3 min 25x: 94°C, 20 sec 54°C, 30 sec 72°C, 20 sec 1x: 72°C, 7 min
In(X)1H [In(X)1H]	DXMit16f CTG CAA TGC CTG CTG TTT TA DXMit16r CCG GAG TAC AAA GGG AGT CA	(Evans and Phillips, 1975)	1x: 94°C, 3 min 35x: 96°C, 10 sec 58°C, 30 sec 72°C, 30 sec 1x: 72°C, 5 min

To genotype for XXY^{d1} females (Section 2.1.6), female offspring were first genotyped for *Ymt2b* to check for the presence of a Y chromosome (see below diagram). Female offspring with a Y chromosome (*Ymt2b*+) were either XY^{d1} or XXY^{d1} females. To distinguish between these karyotypes, an assay was performed to check for the presence of an inactive X chromosome, marked by H3K27me3 antibody staining. An X chromosome is inactivated in XXY^{d1} female somatic tissue but not in XY^{d1} female somatic tissue.

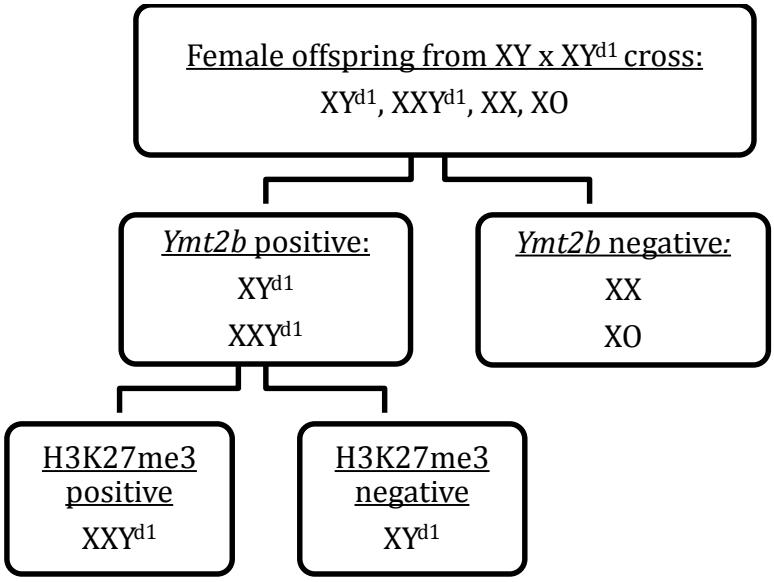

For the H3K27me3 detection assay, livers were removed from mice and were macerated using scalpels in RPMI (+L-glutamatine) (Invitrogen). Six drops of this cell suspension were dropped onto Superfrost Plus slides (ThermoScientific). Cells were simultaneously permeablized and fixed in six drops of a solution of 2% formaldehyde (TAAB), 0.02% sodium dodecyl sulphate (SDS) (Bio-Rad), and 0.05% Triton X-100 (Sigma) in distilled water, for 30 min in a humid chamber at room temperature. Slides were then washed in distilled water six times and allowed to air dry completely. Slides were blocked in PBT (0.15% bovine serum albumin, 0.10% TWEEN-20 in phosphate buffer saline (PBS)) for 60 min at room temperature. Next, 50 µl of rabbit polyclonal anti-H3K27me3 antibody (Millipore, ABE44) was applied at a concentration 1:100 in PBT, and slides were incubated in a

humid chamber overnight at 37°C. The next morning, slides were washed three times in PBS for 5 min, 50 µl of secondary antibody (AlexaFluor 594, Invitrogen) was applied at a concentration of 1:500 in PBS and slides were incubated in a humid chamber for one hour at 37°C. Finally, slides were washed three times in PBS and then mounted in Vectashield with DAPI (Vector).

2.3 Chromosome spreads and immunofluorescence

Chromosome spreads were preformed using a protocol adapted from Barlow and colleagues (Barlow et al., 1997). Briefly, -80°C frozen ovaries were transferred into two drops of chilled RPMI medium (plus L-glutamine) on pre-boiled Superfrost glass slides (ThermoScientific). Ovaries were then macerated using 25G needles (BD), and cells were mechanically dispersed. The cells were permeablized for 10 min in two drops of 0.05% Triton X-100 (Sigma) in distilled water, dropped from approximately 10 cm above the slide. Next, the cells were fixed for 60 min in six drops of 2% formaldehyde, 0.02% SDS in PBS. The slides were rinsed in distilled water, allowed to air dry, and then were blocked in PBT (0.15% BSA, 0.10% TWEEN-20 in PBS) for 60 min.

Next, primary antibodies (**Table 5**) were applied at a concentration of 1:100 in PBT and slides were incubated in a humid chamber overnight at 37°C. The next morning, slides were washed three times in PBS, 50 µl of secondary antibodies (AlexaFluor 488, 594 and 647, Invitrogen) were applied at a concentration of 1:500 in PBS, and slides were incubated in a humid chamber for one hour at 37°C. Finally, slides were washed three times in PBS and then mounted in Vectashield with DAPI.

Table 5: Antibodies used for immunofluorescence experiments

Antibody	Type	Source
anti-SCYP3	Rb polyclonal	Abcam, ab-15092
anti-SYCP3	M polyclonal	Santa Cruz, sc-74569
anti-HORMAD1	Gp polyclonal	Gift, Attila Tóth
anti-HORMAD2	Gp polyclonal	Gift, Attila Tóth
anti-HORMAD2	Rb polyclonal	Gift, Attila Tóth
anti-γH2AFX	M monoclonal	Upstate, 16-193
anti-DMC1	G polyclonal	Santa Cruz (C-20), sc 8973
anti-RPA	Rb polyclonal	Abcam, ab-2175
anti-RAD51 (#1)	Rb polyclonal	Santa Cruz (H92), sc 8349
anti-RAD51 (#2)	Rb polyclonal	Calbiochem, PC130
anti-BRCA1	Rb polyclonal	Gift, Chu-Xia Deng
anti-ATR	G polyclonal	SantaCruz, sc-1887

2.4 Chromosome painting

Chromosome painting was carried out using Cy3 STARFISH paints (Cambio) for mouse chromosome X or human chromosome 21 (pseudocolored in images). Slides were washed once for 5 min in PBS and then once for 5 min in 2x saline sodium citrate (SSC). Slides were pre-warmed for 6 min at 80°C in 2x SSC and then denatured for 5 min at 80°C in 2x SSC and 70% formamide. Slides were quenched in ice cold 70% ethanol for 3 min, dehydrated in a series of ethanol dilutions (70%, 85%, 90%, 95%, 100%) at room temperature and then allowed to air dry. Chromosome paint reactions, consisting of 3 µl concentrated paint and 12 µl hybridization buffer (Cambio), were denatured at 80°C for 10 min, allowed to cool to 37°C and then applied to slides. Coverslips were sealed to slides with Tip-Top Resin (Rema) and slides were incubated overnight in a covered tray in a 37°C water bath. The next day, slides were washed four times for 3 min in 2x SSC at 45°C, four times for 3 min in 0.1x SSC at 60°C and then once for 3

min in 4x SSC and 0.1% TWEEN-20 at 37°C, before mounting in Vectashield with DAPI.

2.5 RNA fluorescent *in-situ* hybridization (RNA FISH) and immunofluorescence

Frozen ovaries (-80°C) were transferred to two drops of RPMI medium (plus L-glutamine) on boiled Superfrost glass slides. Ovaries were macerated using needles, and cells were mechanically dispersed. The cells were then permeablized for 10 min in excess cold CSK buffer (100 mM NaCl, 300 mM sucrose, 3 mM $MgCl_2$, 10 mM PIPES, 0.5% Triton X-100, 1 mM EGTA and 2 mM vanadyl ribonucleoside (NEB), pH 6.8), and then fixed for 10 min in excess ice cold 4% paraformaldehyde (FischerScientific), pH 7-7.4. Slides were then washed in PBS, dehydrated in a series of ethanol dilutions (2 x 70%, 80%, 95%, 100%) and air dried.

RNA FISH digoxigenin-labelled probes were prepared from 1 µg of BAC DNA (from CHORI: *Scml2*, RP24-204O18; *Zfx*, RP24-204018, *USP25,* RP11-296D11; *NRIP1,* RP11-22D1; from ABgene: *TPTE,* CTD-2260D15; *Utx*, gift from Mike Mitchell, University Marseilles) using the Biotin Nick Translation Kit (Roche), according to manufacturer's instructions. For each probe, 100 ng digoxigenin-labelled BAC was prepared in 15 µl formamide (Sigma), with 3 µg mouse (for XO) or human (for Tc1) Cot1 DNA (Invitrogen) and 10 µg sheared salmon sperm DNA (Ambion). Probes were denatured for 10 min at 80°C and then combined with 15 µl pre-warmed (37°C) of 2x hybridization buffer (2x SSC, 10% dextran sulphate (Sigma), 1 mg ml^{-1} BSA and 2 mM vanadyl ribonucleoside) and incubated for 30 min at 37°C. Finally, 30 µl pre-hybridized probes were applied to slides and incubated in a humid chamber overnight at 37°C.

The next day, slides were washed at 42°C, three times in 2x SSC and 50% formamide, and three times in 2x SSC, for 5 min per wash. Slides were then transferred to 4x SSC and 0.1% TWEEN-20, and then blocked (4x SSC, 4 mg ml^{-1} bovine serum albumin and 0.1% TWEEN-20) for 30 min in a humid chamber at 37°C. Probes were detected using 30 µl of 1:10 anti-digoxigenin

fluorescein, diluted in detection buffer (4x SSC, 1mg ml^{-1} bovine serum albumin and 0.1% TWEEN-20) for 60 min in a humid chamber at 37°C.

Slides were washed three times for 2 min in 4x SSC and 0.1% TWEEN-20. For subsequent immunofluorescence, 50 µl of primary antibody against γH2AFX (Upstate, 16-193), diluted 1:100 in 4x SSC and 0.1% TWEEN-20, was added to slides and incubated for 30 min in a humid chamber at room temperature. Slides were washed for 2 min in 4x SSC and 0.1% TWEEN-20. Next, 50 µl of secondary antibody (AlexaFluor 594 conjugated), diluted 1:100 in 4x SSC and 0.1% TWEEN-20, was added to slides and incubated for 30 min in a humid chamber at room temperature. Finally, slides were washed for 2 min in 4x SSC and 0.1% TWEEN-20 and mounted in Vectashield with DAPI.

2.6 Ovarian sectioning and oocyte counting

Ovaries were harvested from females at 20.5 days *post-coitum* (d*pc*), fixed in 4% paraformaldehyde overnight at 4°C and then transferred to 70% ethanol. Fixed ovaries were dehydrated by three successive 5min incubations with 95% ethanol, 100% ethanol, 100% xylene and were then embedded in paraffin wax. Ovaries were serially sectioned at 5-7 µm thickness. Sections were dewaxed using histoclear (2 x 5 min) and 1:1 histoclear:ethanol (1 x 5 min), and then rehydrated using the following ethanol series: 100% ethanol (2 x 5 min), 95% ethanol (1 x 5 min), 80% (1 x 5 min), 70% (1 x 5 min), 50% (1 x 3 min) and PBS (1 x 5 min). Sections were stained with DAPI and oocytes were identified based upon their distinct size and nuclear cytology, as described previously (Burgoyne and Baker, 1985). To quantify the relative number of oocytes in each ovary, I summed the oocyte counts from every tenth section, as described previously (Daniel et al., 2011).

2.7 Imaging

Imaging was performed using an Olympus IX70 inverted microscope with a 100-W mercury arc lamp. For chromosome spread and RNA FISH

imaging, an Olympus UPlanApo 100x/1.35 NA oil immersion objective was used. For ovary section imaging, an Olympus UPlanApo 20x/0.75 NA objective was used. A Deltavision RT computer-assisted Photometrics CoolsnapHQ CCD camera with an ICX285 Progressive scan CCD image sensor was utilized for image capture. 16-bit (1024x1024 pixels) raw images of each channel were captured and later processed using Fiji software. Quantitation of Cot1 and γH2AFX intensities was performed as previously described (Mahadevaiah et al., 2008).

For chromosome spreads, the cells were first categorized into meiotic stages based upon SYCP3 and HORMAD1 staining, as described in Figure 1 and Results Section 3.1. The cells were then assessed for γH2AFX domains or HORMAD2 staining and representative images were captured. For RNA FISH preparations, cells were first categorized based upon the presence or absence of a γH2AFX domain. Next, the FISH signals were examined and representative images were captured. The number of cells counted for each experiment is indicated in figure legends.

2.8 Statistics

Statistical calculations were performed using GraphPad Prism 6.0. For comparison of two means, unpaired t tests were performed. For multiple comparisons (more than two means), ANOVAs followed by the Tukey or Sidak multiple comparison were used, minimizing Type 1 error (i.e. detecting a difference when one is not present). P values are reported in graphs and/or figure legends. Error bars in graphs represent the standard error of the mean (s.e.m).

2.9 Chromatin immunoprecipitation and sequencing (ChIP-seq)

Chromatin immunoprecipitation (ChIP) was performed as described previously (Smagulova et al., 2011). Testes were surgically extracted from mice, and the tunicae albuginea was mechanically removed and discarded. The testis material was then fixed for 10 min in 10ml 1% fresh paraformaldehyde. After quenching the fixative with glycine for 10min,

tissue was homogenised on ice using a dounce homogenizer. The homogenized tissue was then filtered through 40 µm cell strainer, and washed in the following buffers: (1) PBS (twice); (2) 0.25% Triton X-100, 10mM EDTA, 0.5mM EGTA, 10mM Tris pH 8; and (3) 0.2M NaCl, 1mM EDTA, 0.5mM EGTA, 10mM Tris pH 8. Prior to each wash, cells were pelleted by centrifugation at 900g for 5min at 4°C. After the final wash, cells were pelleted and resuspended in 1.5 ml of lysis buffer (1% SDS, 10mM EDTA, 50mM TrisCl pH8, 1X complete protein inhibitor cocktail (Roche)).

The resulting chromatin was then sheared to ~1000 bp by sonication for 15min at 4°C using 15-sec on/45-sec off pulses. The sheared chromatin was then dialyzed against ChIP buffer (0.01% SDS, 1.1% Triton X-100, 1.2mM EDTA, 16.7mM TrisHCl, 167mM NaCl) in a Slide-A-Lyser Dialysis Cassettes, 10K MWCO (ThermoScientific) for 4-5hrs at 4°C with constant rotation.

Prior to addition of antibodies, samples were pre-cleared using 150 µg of magnetic Protein G beads (Sigma) for 1 hr at 4°C, rotating constantly. Beads were pelleted, and the pre-cleared chromatin was removed. 50 µl of the pre-cleared sample was set aside for input controls (i.e. no antibody). The remainder of the sample was incubated with primary antibody overnight (12-16 hrs) at 4°C, rotating constantly (see below table for antibodies).

Table 6: Antibodies used for ChIP-seq.

Antibody	Details	Source
anti-DMC1	Santa Cruz (C-20, sc 9873)	(Smagulova et al., 2011)
anti-BRCA1	Rb polyclonal	Gift, Satoshi Namekawa
anti-BRCA1	M monoclonal	Gift, Andre Nussenzweig

The following day, the sample was incubated with 150 µg of magnetic Protein G beads for 2 hr at 4°C to pull down antibody-bound chromatin. The beads were pelleted and washed in the following buffers: (1) low salt immune complex wash buffer (0.1% SDS, 1% Triton X-100, 2mM EDTA,

20mM TrisHCl, 150mM NaCl); (2) high salt immune complex wash buffer (0.1% SDS, 1% Triton X-100, 2mM EDTA, 20mM TrisCl pH 8, 500mM NaCl); (3) LiCl immune complex wash buffer (0.25M LiCl, 1% Igepal, 1mM EDTA, 10mM TrisCl, pH8, 1% Deoxycholic acid); (4) TE buffer (10mM Tris-HCl, 1mM EDTA pH 8.0) (twice).

Next, the protein/DNA complexes were eluted from magnetic beads using 100 µl of 1% SDS, 0.1M NaHCO3 pH 9 at 65°C for 30 min. Protein/DNA crosslinking was reversed in 12 ul of 5M NaCl at 65°C overnight. The sample was then deproteinized by addition of 6 µl of 0.5M EDTA, 12 µl 1M Tris-HCl pH 6.5, and 5 µl of Proteinase K (20 mg/ml), and incubating for 2 hr at 45°C. Finally, DNA was purified with a MiniElute Reaction Clean up kit (QIAGEN) and eluted in 12 ul of elution buffer.

Standard sequencing library construction was done using New England Biolab reagents according to protocol provided by Illumina, as described previously (Khil et al., 2012). Sequencing libraries were prepared as follows: (1) End repair step: mix 10 µl DNA, 30 µl ddH2O, 5 µl 10X T4 Buffer, 2 µl dNTPs, 1 µl T4 DNA pol, 1 µl Klenow (1:5 dilution), and 1 µl T4 PNK, incubated for 30 min at 20°C, and then purified DNA using Qiagen MiniElute PCR purification kit, eluting in 10 µl; (2) A addition step: 10 µl DNA, 24 µl ddH2O, 5 µl Klenow Buffer, 10 µl 1mM dATP, 1 µl Klenow (exo-), and incubated for 30 min at 37°C, and then purified DNA, eluting in 10 µl; (3) Kinetic enrichment step (if necessary): incubated sample at 95°C for 3 min, then cool to room temperature; (4) Adaptor ligation step: 10 µl DNA, 3 µl ddH2O, 15 µl Ligation Buffer, 1 µl Adaptor mix (1:20 dilution of conc.), 1 µl DNA Ligase, and incubated for 30 min at 20°C, purified, eluted in 10 µl; (5) PCR amplification step: 10 µl DNA, 26 µl H2O, 10 µl 5x Phusion B buffer, 1.5 µl dNTPs, 1 µl Adaptor primer 1, 1 µl Adaptor primer 2, 0.5 µl Phusion Taq pol, and performed PCR under following conditions: (1) 30 sec @ 98°C; (2) 18 cycles of 30 sec @ 98°C, 30 sec @ 65°C, 30 sec @ 72°C; and (3) 5 min @ 72°C. The PCR product was purified using Qiaquick PCR Purification kit. Libraries were sequenced on an Illumina HiSeq 2000 platform at the NIDDK Genomics Core Facility (NIH, Bethesda, MD).

2.10 ChIP-seq data analysis

Raw ChIP-seq data were processed and analyzed by computational biologist Dr. Kevin Brick (NIH, Dr. Camerini-Otero laboratory). Briefly, sequence fragments were aligned to the mm9 mouse reference genome using the Illumina GAII analysis pipeline. Quality filtered reads that mapped uniquely to the genome were utilized for downstream analyses. DMC1 and BRCA1 peaks were identified by comparing the sequence tag coverage for each ChIP sample with that of the tag-count matched control/input sample using MACS.

3 Results: Characterization of oocyte losses in chromosomally abnormal mice

Mice with chromosome abnormalities, such as chromosome aneuploidies and translocations, have asynapsed chromosomes during meiosis and experience germ cell loss and a shortened reproductive lifespan or infertility (Burgoyne, 1979; Burgoyne and Baker, 1984; Forejt, 1976; Homolka et al., 2007). However, many fundamental questions remain about the mechanisms of germ cell loss in chromosomally abnormal mice.

The first objective of this chapter is to define the developmental timing of oocyte arrest in female mice with either asynapsed sex chromosomes or autosomes, using several different chromosome variant mouse models. Previous work on XO females revealed that the proportion of oocytes with an asynapsed X chromosome decrease in proportion during progression through prophase I (Burgoyne and Baker, 1985), although the precise meiotic sub-stage of during which these losses remains unclear. Elucidating the kinetics of oocyte loss in different chromosome variant mouse models, including XO females, is vital for understanding the timing of meiotic surveillance in females.

The next objective of this chapter is to examine the role for persistent unrepaired DNA DSBs in the elimination of chromosomally abnormal oocytes. Mice with persistent unrepaired DNA DSBs (i.e. *Dmc1*-/-) have severe oocyte losses during meiotic prophase I (Pittman et al., 1998; Yoshida et al., 1998). These oocyte losses can be partially relieved by preventing DNA DSB formation, indicating that persistent unrepaired DNA DSBs is the proximal trigger of oocyte losses (Di Giacomo et al., 2005; Reinholdt and Schimenti, 2005). To address the role of persistent DNA damage in oocyte losses in chromosome variant mice I studied markers of unrepaired DNA DSBs, including RAD51, DMC1, and RPA. This study will shed light on whether DNA DSBs contribute to oocyte losses in the context of chromosome abnormalities.

In the final section of this chapter, I examine the role of asynapsis *per se* in oocyte loss by determining the impact of accessory chromosomes on

oocyte survival. If asynapsis *per se* is the proximal trigger of oocyte losses, then any asynapsed chromosome, including asynapsed accessory chromosomes will trigger oocyte arrest. By contrast, if asynapsis alone is not sufficient to cause arrest, but rather depends on gene content or some other factor, then asynapsed accessory chromosomes should not elicit oocyte losses. In summary, determining the impact of persistent unrepaired DNA DSBs and accessory chromosomes will advance our understanding of the meiotic surveillance mechanisms that operate in oocytes.

3.1 Timing of oocyte losses in mice with chromosome abnormalities

3.1.1 Classification of oocytes into meiotic prophase I sub-stages

Chromosome abnormalities lead to asynapsis at pachynema (Burgoyne et al., 2009). To address the impact of asynapsis on oocyte survival, oocytes must be monitored from pachynema to the end of prophase I. Prophase I of female meiosis occurs in a single semi-synchronous wave between 13.5 and 20.5 d*pc* (Pepling and Spradling, 2001; Speed, 1986). Based on studies of wildtype mice, pachytene oocytes are abundant between the gestational ages of 16.5 and 18.5 d*pc* (Speed, 1982). By 18.5 d*pc*, a subset of oocytes have entered diplonema (Speed, 1982). Therefore, with the goal of studying oocytes from pachynema to diplonema, I focused my initial experiments on 18.5 d*pc* ovaries.

To visualize oocytes, meiotic chromosome spreads were performed in combination with immunofluorescence (Peters et al., 1997). An antibody recognizing SYCP3, a component of the axial/lateral element of the SC (Yuan et al., 2000), was used to detect meiotic chromosome axes and identify pachytene oocytes. To aid with substaging diplotene oocytes, I combined anti-SYCP3 with an antibody recognizing HORMAD1, a protein that localizes exclusively to asynapsed chromosome axes (Fukuda et al., 2009; Wojtasz et al., 2009). Using this approach, I defined criteria for substaging oocytes into pachynema, early diplonema, and late diplonema.

At pachynema, SYCP3 clearly labels 20 synapsed chromosome pairs (**Figure 1.1a**). At this meiotic stage HORMAD1 staining is virtually undetectable (**Figure 1.1a**). At early diplonema, homologous chromosomes have begun to desynapse, which manifests as separation of the SYCP3-labeled chromosome axes and accumulation of HORMAD1 (**Figure 1.1b**). Importantly, at this stage, there are still regions of synapsis. At late diplonema, by contrast, all chromosomes have completely desynapsed, shown by more extensive HORMAD1 staining (**Figure 1.1c**). For subsequent experiments, these criteria were used to substage oocytes.

According to studies of female mice of CD1 and Swiss albino genetic backgrounds (Pepling and Spradling, 2001; Speed, 1986), mouse oocytes progress from pachynema and late diplonema between 17.5 to 19.5 d*pc.* Given that genetic background may impact meiotic processes (Koehler et al., 2002), I first confirmed the developmental timing of meiotic prophase I in the NIMR MF1 wildtype mice, by analyzing surface spread oocytes double-stained for SYP3 and HORMAD1.

At 17.5 d*pc*, the vast majority (68%) of oocytes in the XX MF1 ovary were at pachynema (**Figure 1.2**), and the remaining oocytes had progressed to early diplonema (20%) and late diplonema (8%). At 18.5 d*pc*, still half of XX MF1 oocytes were at pachynema, but there was a higher representation of oocytes at early diplonema (33%) and late diplonema (13%) (**Figure 1.2**). At 19.5 d*pc*, the majority of oocytes (49%) were at late diplonema, while a smaller percentage was found in early diplonema (12%) and pachynema (3%) (**Figure 1.2**). The remaining 36% of oocytes at 19.5 d*pc* had progressed to dicytate, where the HORMAD1/SYCP3-labeled chromosomes are extensively fragmented. In summary, consistent with other genetic backgrouds (Pepling and Spradling, 2001; Speed, 1986), wildtype MF1 oocytes progress from pachynema to late diplonema during the timeframe 17.5 to 19.5 d*pc*.

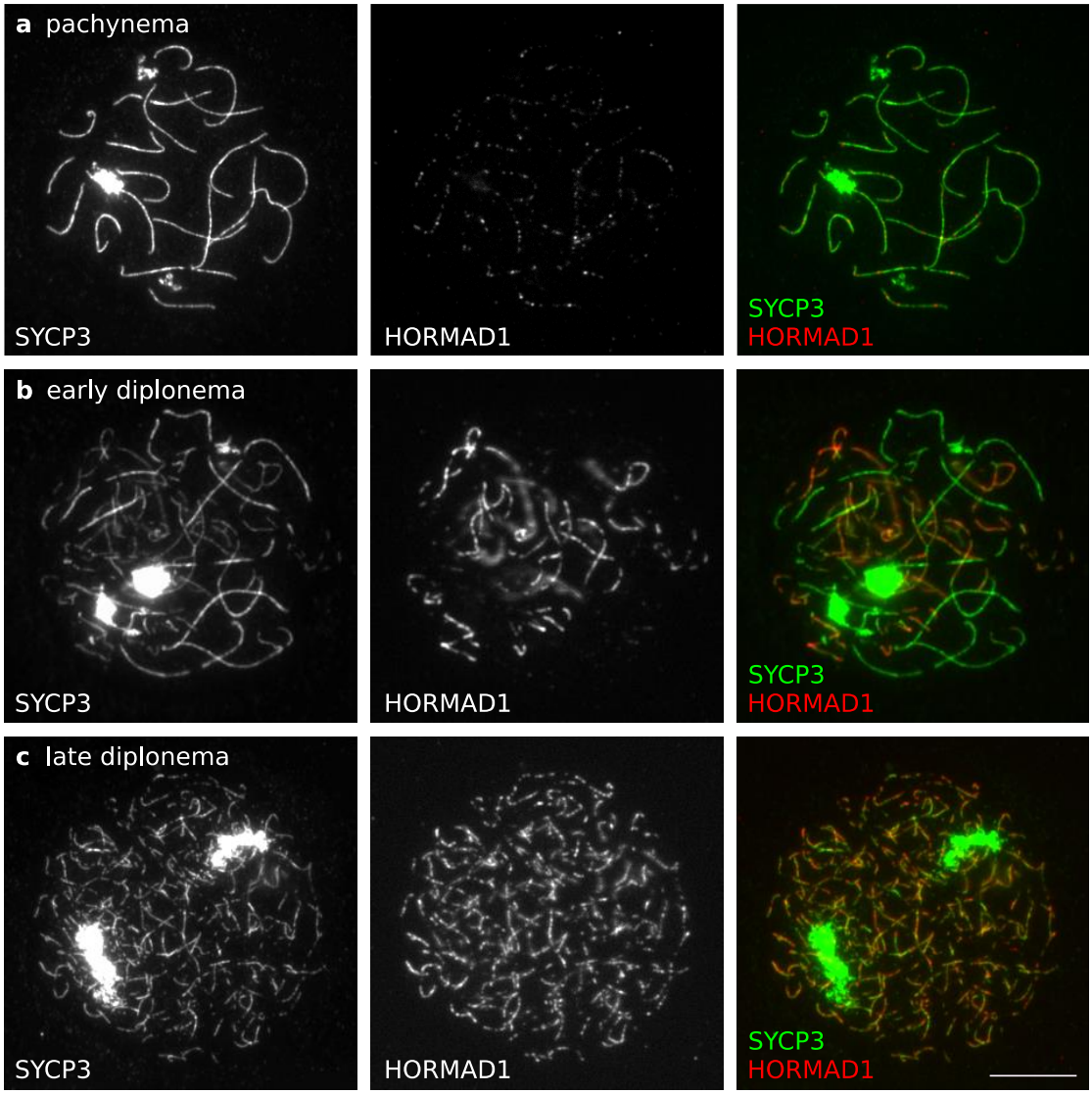

Figure 1.1. Oocyte sub-staging criteria.

(**a**) XX pachytene oocyte. At pachynema, SYCP3 labels 20 fully synapsed chromosome pairs. HORMAD1, if present at all, stains very weakly as foci. (**b**) XX early diplotene oocyte. At early diplonema, homologous chromosomes begin to desynapse, marked by HORMAD1 axial accumulation. At this stage, there are still stretches marked only by SYCP3 (i.e. areas of synapsis). (**c**) XX late diplotene oocytes. At late diplonema, all chromosome pairs have desynapsed, as evident by near complete HORMAD1/SYCP3 co-localization. At this stage SYCP3 and HORMAD1 also begin to show signs of fragmentation. Scale bar represents 10μm.

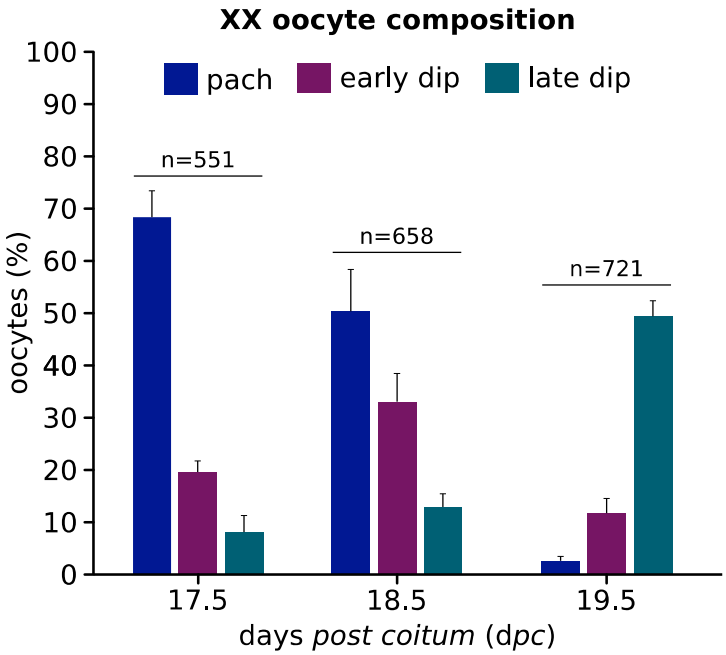

Figure 1.2. Oocyte sub-stages at different gestational ages.

The mean percentage (± s.e.m.) of XX oocytes at pachynema, early diplonema and late diplonema at 17.5 d*pc*, 18.5 d*pc* and 19.5 d*pc*. During this period of gestation, oocytes progress in a semi-synchronous wave between pachynema and late diplonema. n is the total number of oocytes counted in three non-littermate ovaries.

3.1.2 γH2AFX marks the asynapsed X chromosome in XO oocytes

XO females have a shortened reproductive lifespan due to late prophase I oocyte losses (Burgoyne and Baker, 1985). The kinetics and trigger of these prophase I oocyte losses remains unclear, but it has been proposed to be linked to the asynapsed X chromosome (Speed, 1986). Therefore, I sought to determine whether XO oocytes with an asynapsed X chromosome are eliminated, and if so, during what stages of meiotic prophase I.

To address these questions, it is first imperative to be able to identify the asynapsed chromosome in surface spread XO oocytes. Although HORMAD1, which was used for staging oocytes (see **Figure 1.1**), is also enriched on the asynapsed X chromosome at pachynema (**Figure 1.3a**), it was also present on desynapsed axes in diplotene oocytes (**Figure 1.3c-f, insets**). Therefore, HORMAD1 is not useful for distinguishing the asynapsed X chromosome from desynapsed chromosomes at diplonema.

Studies of spermatocytes have shown that the silencing factor and DDR epigenetic mark γH2AFX accumulates within the chromatin of asynapsed chromosomes between pachynema and diplonema (Mahadevaiah et al., 2001). Notably, γH2AFX also marks the asynapsed X chromosome in XO oocytes from pachynema and diplonema (**Figure 1.3**). Therefore, for subsequent surface spread experiments, I combined my substaging antibodies, anti-SYCP3 and anti-HORMAD1, with an antibody against γH2AFX, to allow for both substaging and identification of asynapsis.

I utilized this triple immunostaining approach to analyze the behavior of the single X chromosome in 18.5 d*pc* XO oocytes. At pachynema, I observed two populations of XO oocytes. The first population of XO pachytene oocytes had a γH2AFX domain that marked the asynapsed X chromosome (**Figure 1.3a, arrow**). In these oocytes, the X chromosome was marked with the asynapsis marker HORMAD1 (**Figure 1.3a, inset**), further proof that these oocytes contained an asynapsed X chromosome.

By contrast, the second population of pachytene XO oocytes did not have any markers of asynapsis, i.e. both γH2AFX and HORMAD1 staining was absent (**Figure 1.3b**), as reported previously (Turner et al., 2005). In

this population, the X chromosome had engaged in non-homologous self-synapsis (**Figure 1.3b, arrow**), forming a small "hairpin" chromosome, as observed in previous electron microscopy studies (Speed, 1986). I confirmed that the self-synapsed chromosome was the X chromosome using X-specific chromosome paint (**Figure 1.3b, inset**).

Similar populations of XO oocytes were observed at early diplonema and late diplonema: a γH2AFX-positive population and a γH2AFX-negative population. After late diplonema (i.e. dictyate), γH2AFX was no longer visible in XO oocytes, suggesting that this chromatin mark is removed at the end of prophase I, as observed with spermatocytes (Mahadevaiah et al., 2001). In summary, γH2AFX can be used as a marker of the asynapsed X chromosome in XO oocytes between pachynema and late diplonema.

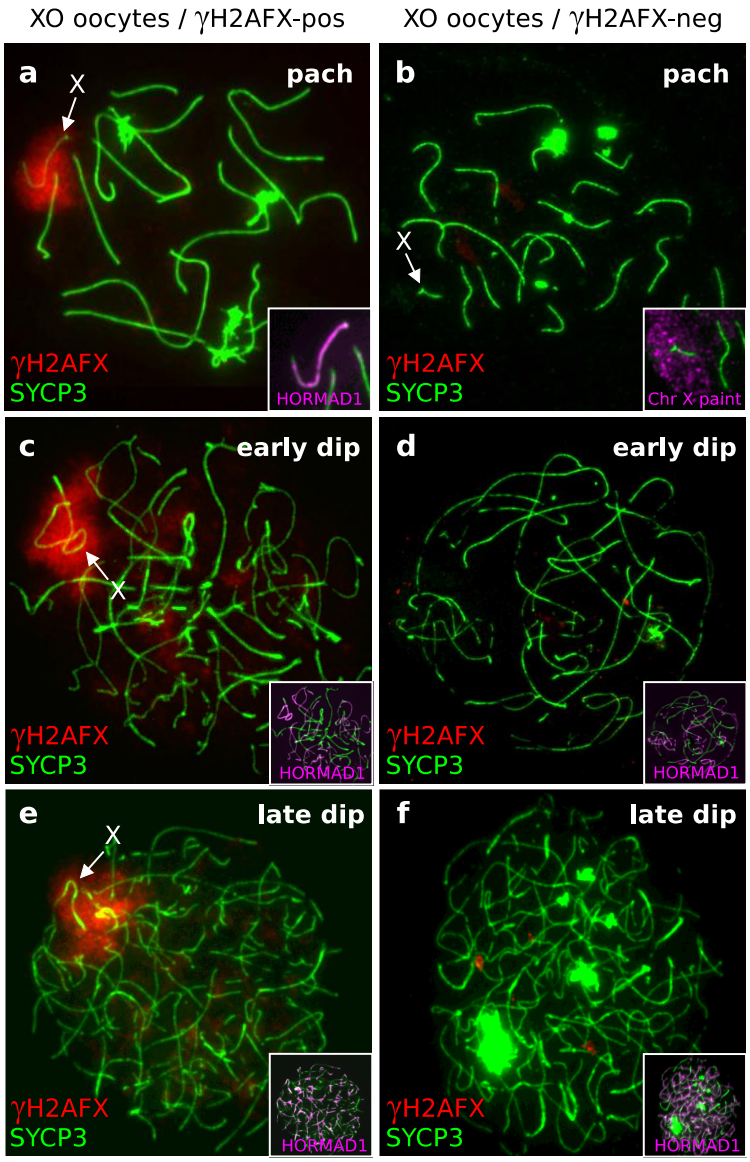

Figure 1.3. XO oocytes with an asynapsed X chromosome.

Surface spread XO oocytes labeled with SYCP3 (green), which marks chromosome cores, γH2AFX (red), which marks chromatin associated with the asynapsed X chromosome, and HORMAD1 (magenta, insets), which marks asynapsed cores. (**a**) Pachytene XO oocyte with γH2AFX domain (asynapsed X chromosome) (arrow). (**b**) Pachytene XO oocyte with self-synapsed X chromosome (γH2AFX-negative). X chromosome painting shown in inset (magenta). (**c**) Early diplotene XO oocyte with a γH2AFX domain (arrow). Both the asynapsed X chromosome and desynapsed axes are labeled with HORMAD1 (inset). (**d**) Early diplotene XO oocyte, γH2AFX-negative. (**e**) Late diplotene XO oocyte (extensive HORMAD1 staining, inset) with γH2AFX domain (arrow). (**f**) Late diplotene XO oocyte, γH2AFX-negative.

3.1.3 Elimination of XO oocytes with an asynapsed X chromosome

Previous studies have shown that compared to XX littermates, XO females lose 50% more oocytes during prophase I (Burgoyne and Baker, 1985). Subsequent work revealed that the frequency of X chromosome self-synapsis increases during prophase I progression (Speed, 1986). Taken together, this suggests that XO oocytes with an asynapsed X chromosome are lost during prophase I progression. To test this hypothesis and to pinpoint the timing of XO oocyte losses, I quantified the percentage of XO oocytes with an asynapsed X chromosome at pachynema, early diplonema, and late diplonema. If the asynapsed X chromosome is associated with XO oocyte losses, the percentage of XO oocytes with an asynapsed X chromosome should decrease by late diplonema.

First, I confirmed that XO and XX females are developmentally matched. At 18.5 d*pc*, XO and XX ovaries contained similar proportions of oocytes at pachynema, early diplonema, and late diplonema (**Figure 1.4a**), indicating that XO oocyte development occurs with the expected kinetics. Next, I quantified the percentage of XO oocytes with an asynapsed X chromosome at 17.5, 18.5, and 19.5 d*pc*, corresponding to progression from pachynema to late diplonema (see **Figure 1.2**).

At 17.5 d*pc*, 51% of XO oocytes had an asynapsed X chromosome, as determined by the presence of a γH2AFX domain (**Figure 1.4b and Figure 1.3a**). The remaining γH2AFX-negative XO oocytes had a self-synapsed X chromosome (**Figure 1.4b and Figure 1.3b**). At 18.5 d*pc*, 43% of XO oocytes had a γH2AFX domain (**Figure 1.4b**). By contrast, at 19.5 d*pc*, 26% of XO oocytes had a γH2AFX domain (Tukey's test, P=0.0002) (**Figure 1.4b**). This drop is consistent with the hypothesis that the asynapsed X chromosome triggers XO oocyte losses during late prophase I.

To determine more precisely the stages during meiosis over which this drop occurs, I next analyzed XO oocytes specifically at pachynema, early diplonema, and late diplonema, by cytologically substaging oocytes within individual ovaries. These meiotic stages are well represented in ovaries from XO females at 18.5 d*pc* (**Figure 1.4a**). For this analysis, XO oocytes

were first classified by meiotic substage based on SYCP3/HORMAD1 immunostaining (**Figure 1.1**), and then I assessed for the presence of a γH2AFX domain (**Figure 1.3**).

Within individual 18.5 d*pc* XO ovaries, 56% of pachytene oocytes had a γH2AFX domain at 18.5 d*pc* (**Figure 1.4c**), which is consistent with our earlier gestational age analysis. Notably, significantly fewer XO oocytes had a γH2AFX domain at early diplonema (39%; Tukey's test, P=0.008), and at late diplonema, only 11% of XO oocytes had a γH2AFX domain (Tukey's test, P<0.0001) (**Figure 1.4c**). This confirms that within individual XO ovaries, oocytes with an asynapsed X chromosome are depleted by late diplonema.

Comparing the two methods of XO analyses, the percentage of XO oocytes with a γH2AFX domain was slightly different depending on whether I studied oocytes based upon gestational age (**Figure 1.4b**) or meiotic sub-stages (**Figure 1.4c**). This discrepancy is expected given that ovaries contain a mixed population of oocytes (**Figure 1.4a**). The less precipitous drop observed between 17.5 to 19.5 d*pc* (two-fold drop), compared to between pachynema and late diplonema (five-fold drop), can be explain by this oocyte heterogeneity.

A drop in XO oocytes with an asynapsed X chromosome could reflect an increase in X chromosome self-synapsis. However, this would not explain the drop at late diplonema because desynapsis, not synapsis, occurs during this transition. This drop could also be due to dephosphorylation of γH2AFX. However, in spermatocytes γH2AFX dephosphorylation occurs after late diplonema (Mahadevaiah et al., 2001). Therefore, this drop is more consistent with XO oocyte losses.

Notably, the XO oocyte composition analysis (**Figure 1.4a**) did not reveal a significant drop in the proportion of late diplotene oocytes at 18.5 d*pc* in XO versus XX females, as would be expected if significant XO oocyte losses occur. However, a significant drop may not be apparent due to the small percentage of oocytes present at late diplonema at 18.5 d*pc*. It may become more evident at an age where more oocytes are at late diplonema. Consistent with this, previous studies have revealed that XO oocytes losses are only evident starting at 19.5 d*pc* (Burgoyne and Baker, 1985).

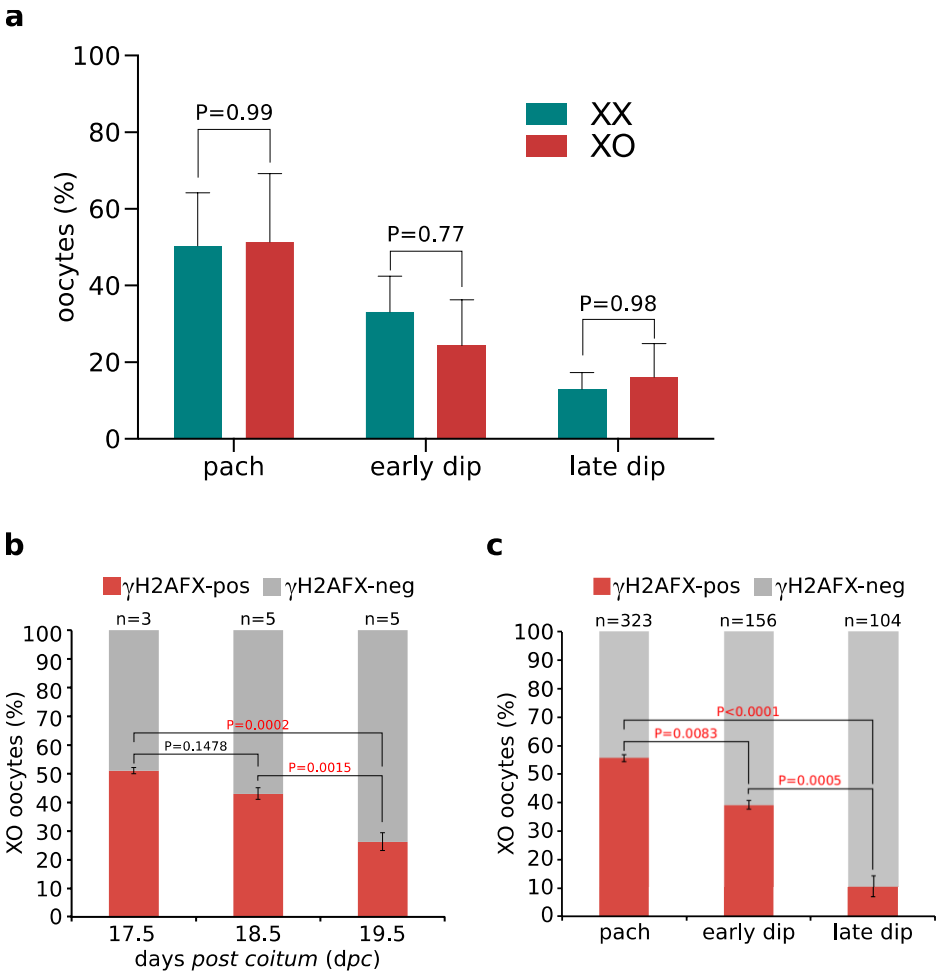

Figure 1.4. Elimination of XO oocytes with an asynapsed X chromosome.

(**a**) The mean percentage of XO oocytes and XX oocytes at pachynema, early diplonema, and late diplonema at 18.5 d*pc*. Three non-littermate ovaries were analyzed per age, and 100-200 oocytes were counted per ovary. (**b**) The mean percentage of XO oocytes with a γH2AFX domain at 17.5, 18.5, and 19.5 d*pc*. n is the number of ovaries analyzed, with 100-200 oocytes analyzed per ovary. (**c**) The mean percentage of XO oocytes with a γH2AFX domain in 18.5 d*pc* ovaries, where oocytes were sub-staged into pachynema, early diplonema, and late diplonema. Three ovaries were analyzed, and n is the number of total oocytes analyzed. P values were generated from Tukey's multiple comparison test, and significant P values ($P<0.05$) are shown in red.

3.1.4 Elimination of In(X)1H oocytes with asynapsed X chromosomes

My previous analysis indicates that X chromosome asynapsis is associated with oocyte losses. To determine if this finding is specific to XO females, I then studied another mouse model with X chromosome asynapsis, the In(X)1H female. In(X)1H heterozygous females have two X chromosomes, but one X chromosome harbors a large inversion that disrupts X-X synapsis in a proportion of oocytes (Tease and Fisher, 1986). As with XO females, perinatal oocyte losses have been reported previously in In(X)1H females (Burgoyne and Baker, 1985; Tease and Fisher, 1986).

Using the SYCP3/HORMAD1/γH2AFX immunostaining, I identified two populations of pachytene In(X)1H oocytes: oocytes with a γH2AFX domain, indicative of X asyanpsis (**Figure 1.5a**), and oocytes with no γH2AFX domain (**Figure 1.5b**). Within those γH2AFX domain-negative oocytes, the In(X) and X chromosomes achieved complete synapsis, presumably through non-homologous pairing (Tease and Fisher, 1986). While at 17.5 d*pc*, 13% of In(X)1H oocytes had a γH2AFX domain, this percentage dropped nearly 2-fold by 19.5 d*pc* (8%) (Tukey's test, P=0.009) (**Figure 1.5c**). Similarly, within substaged In(X)1H oocytes at 18.5 d*pc,* there was a 3.5-fold drop in the percentage of oocytes with a γH2AFX domain between pachynema (17%) and late diplotene (5%) (Tukey's test, P=0.002) (**Figure 1.5d**). Therefore, In(X)1H oocytes with partial X chromosome asynapsis are lost by late diplonema, indicating that X chromosome asynapsis in general is associated with oocyte losses.

It is possible that a subset of In(X)1H oocytes with a γH2AFX domain which I classified as pachytene oocytes are actually late zygotene oocytes that are on their way to achieve full synapsis. Distinguishing these categories of cells more definitively requires use of other markers, such as DNA DSB repair protein makers, e.g. RPA. This DNA DSB marker is much more abundant on synapsed autosomes in zygotene nuclei compared to pachytene nuclei (Guioli et al., 2012).

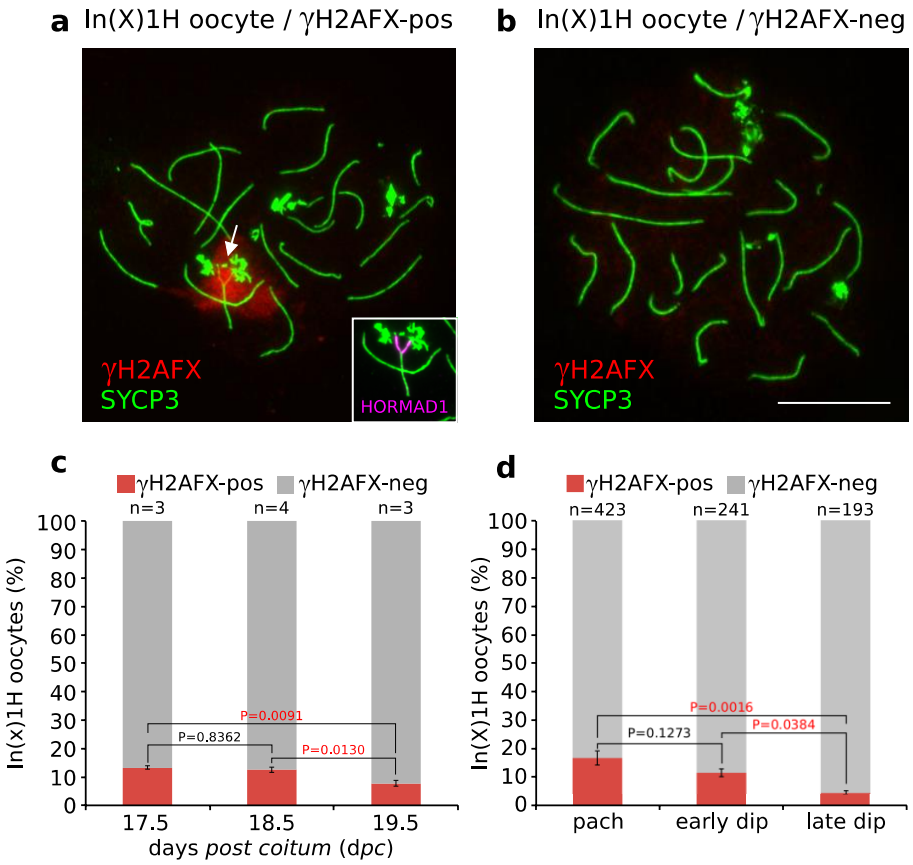

Figure 1.5. Elimination of In(X)1H oocytes with asynapsis.

(**a**) In(X)1H pachytene oocyte showing partial X chromosome asynapsis (arrow), marked by γH2AFX (red) and HORMAD1 (magenta, inset). (**b**) In(X)1H pachytene oocyte with complete synapsis, and no γH2AFX or HORMAD1 staining. (**c**) The mean percentage of In(X)1H oocytes with a γH2AFX domain at 17.5, 18.5, and 19.5 d*pc*. n is the number of ovaries analyzed, with 100-200 oocytes analyzed per ovary. (**d**) The mean percentage of In(X)1H oocytes with a γH2AFX domain in 18.5 d*pc* ovaries, where oocytes were sub-staged into pachynema, early diplonema, and late diplonema. Three ovaries were analyzed, and n equals the number of total oocytes analyzed. P values were generated from Tukey's multiple comparison test, and significant P values ($P<0.05$) are shown in red. Scale bar = 10μm.

3.1.5 Elimination of T(16;17)43H oocytes with asynapsed autosomes

To determine whether oocyte loss is specific to X chromosome asynapsis or can also occur in the presence of asynapsed autosomes, I then analysed oocytes carrying asynapsed autosomes. To address this, I studied T(16;17)43H (designated T43H) female mice, which have an autosomal translocation involving chromosomes 16 and 17 (Forejt et al., 1980). This translocation disrupts chromosomes 16 and 17 synapsis in a subset of T43H oocytes, and this is associated with γH2AFX chromatin enrichment and HORMAD1 axial staining (**Figure 1.6a**), as reported recently (Bhattacharyya et al., 2013). However, in a subset of T43H oocytes the translocation product achieves a fully synapsed quadrivalent configuration via non-homologous synapsis. The structure of this quadrivalent configuration has been previously reported (Homolka et al., 2007). These oocytes are negative for the asynapsis marker γH2AFX (**Figure 1.6b, arrow**).

To evaluate the consequence of autosomal asynapsis in T43H oocytes, I quantified the percentage of T34H oocytes with asynapsis between 17.5 and 19.5 d*pc*. At 17.5 dpc, 45% of T43H oocytes had a γH2AFX domain (**Figure 1.6c**), consistent with a recent study (Bhattacharyya et al., 2013). At 19.5 dpc, there was a two-fold drop in oocytes with a γH2AFX domain (23%; Tukey's test, P=0.0007) (**Figure 1.6c**), indicating that T43H oocytes with autosomal asynapsis are depleted by late diplonema.

Similar results were obtained when I analyzed sub-staged oocytes at 18.5 d*pc*. The percentage of T34H oocytes with asynapsis dropped nearly three-fold between pachynema (41%) and late diplonema (14%) (Tukey's test, P=0.003) (**Figure 1.6d**). These results, in conjunction with the results from XO and In(X)1H females, indicate that oocytes with asynapsed chromosomes, whether it involves the X chromosome or autosomes, are eliminated by the end of prophase I.

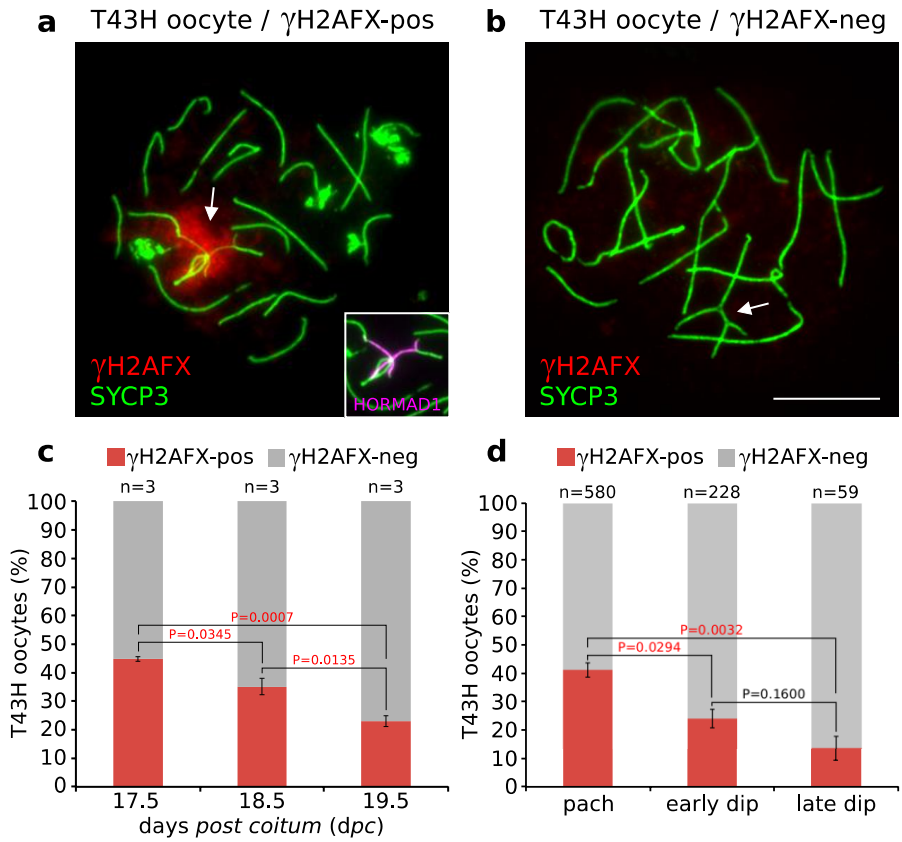

Figure 1.6. Elimination of T(16;17)43H oocytes with asynapsed autosomes.

(**a**) T43H pachytene oocyte with autosomal asynapsis (arrow), marked by γH2AFX (red) and HORMAD1 (magenta, inset). (**b**) T43H pachytene oocyte with complete synapsis, involving a quadrivalent structure (arrow), showing no γH2AFX or HORMAD1 staining. (**c**) The mean percentage of T43H oocytes with a γH2AFX domain at 17.5, 18.5, and 19.5 d*pc*. n is the number of ovaries analyzed, with 100-200 oocytes analyzed per ovary. (**d**) The mean percentage of T43H oocytes with a γH2AFX domain in 18.5 d*pc* ovaries, where oocytes were sub-staged into pachynema, early diplonema, and late diplonema. Three ovaries were analyzed, and n is the number of total oocytes analyzed. P values were generated from Tukey's multiple comparison test, and significant P values (P<0.05) are shown in red. Scale bar = 10μm.

3.1.6 Elimination of XX oocytes with asynapsis

Synaptic errors have previously been reported to occur in a small percentage of oocytes in wildtype XX females (Alton et al., 2008; Kouznetsova et al., 2009). I therefore tested whether asynapsis in normal XX females also lead to oocyte losses. Using SYCP3/HORMAD1/γH2AFX triple-immunofluorescence on chromosome spreads, I examined the prevalence of asynapsed chromosomes in XX females. Consistent with these previous studies, I observed a small population of XX pachytene oocytes with γH2AFX domains (**Figure 1.7a**), indicative of synaptic errors. However, the majority of XX pachytene oocytes had no γH2AFX domains, showing complete synapsis (**Figure 1.7b**).

I quantified the percentage of XX oocytes with a γH2AFX domain as a function of meiotic prophase I progression. At 17.5 d*pc*, 10% of XX oocytes had a γH2AFX domain (**Figure 1.7c**). Notably, only 4% of XX oocytes had a γH2AFX domain at 19.5 d*pc* (Tukey's test, P=0.02) (**Figure 1.7c**). More strikingly, analysis of sub-staged XX oocytes at 18.5 d*pc* revealed a 10-fold drop in the percentage of oocytes with a γH2AFX domain between pachynema (10%) and late diplonema (1%) (Tukey's test, P=0.03) (**Figure 1.7d**).

Therefore, XX oocytes with synaptic defects are also depleted by late diplonema. In summary, based upon my analyses of several chromosomally variant mouse models as well as normal females, I conclude that a meiotic surveillance mechanism operates to eliminate oocytes with asynapsis during diplonema (**Figure 1.8**).

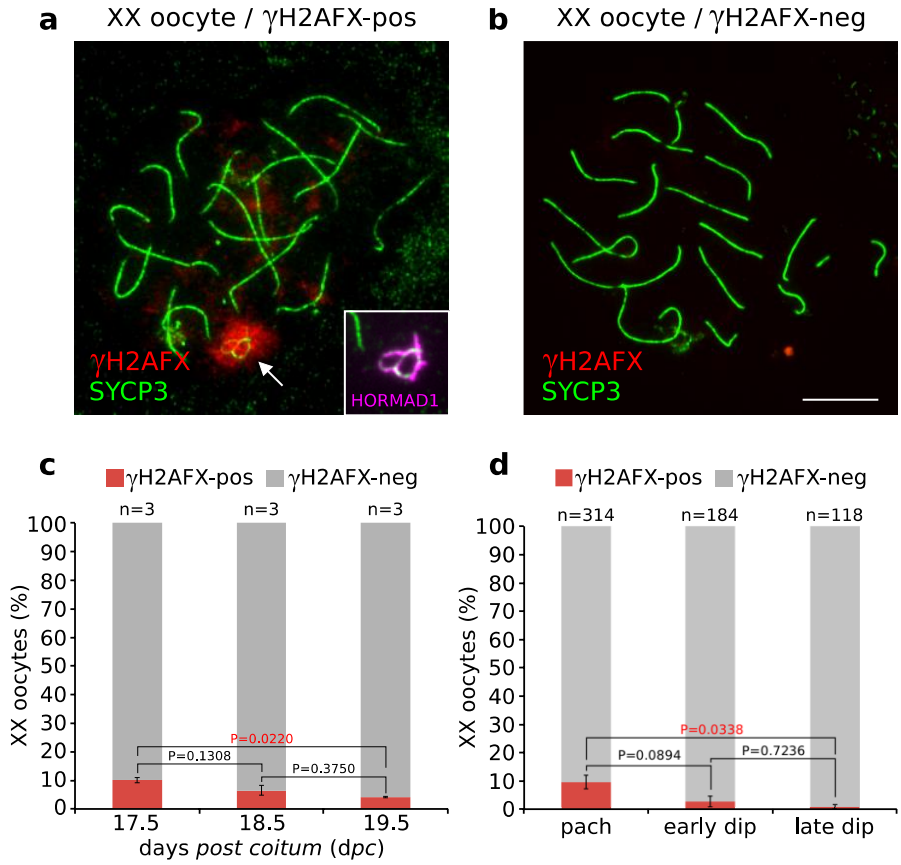

Figure 1.7. Elimination of XX oocytes with asynapsis.

(**a**) XX pachytene oocyte with asynapsis (arrow), marked by γH2AFX (red) and HORMAD1 (magenta, inset). (**b**) XX pachytene oocyte with complete synapsis showing no γH2AFX or HORMAD1 staining. (**c**) The mean percentage of XX oocytes with a γH2AFX domain at 17.5, 18.5, and 19.5 d*pc*. n is the number of ovaries analyzed, with 100-200 oocytes analyzed per ovary. (**d**) The mean percentage of XX oocytes with a γH2AFX domain from 18.5 d*pc* ovaries, where oocytes were sub-staged into pachynema, early diplonema, and late diplonema. Three ovaries were analyzed, and n is the number of total oocytes analyzed. P values were generated from Tukey's multiple comparison test, and significant P values ($P<0.05$) are shown in red. Scale bar = 10μm.

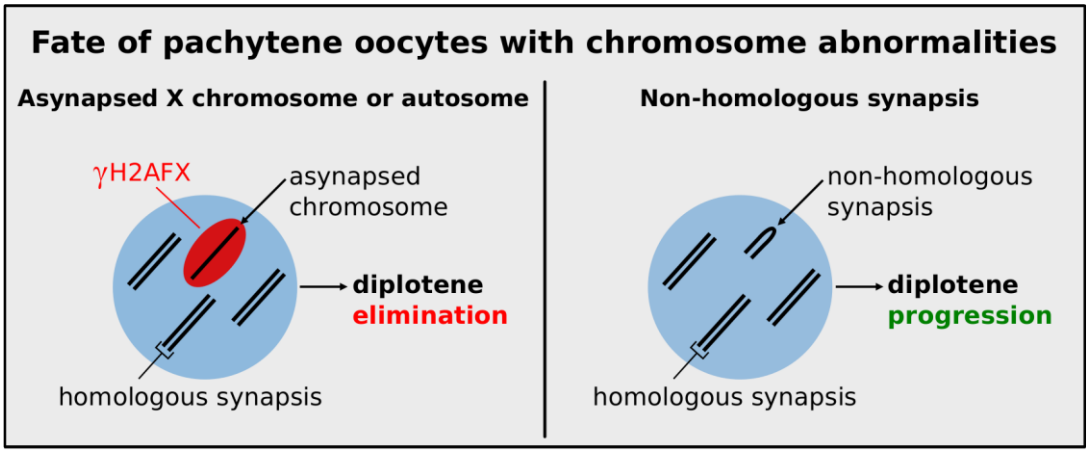

Figure 1.8. Schematic depicting fate of prophase I oocytes with chromosome abnormalities.

Left panel: pachytene oocyte with an asynapsed X chromosome or autosome labelled with the silencing factor γH2AFX are subject to elimination during diplonema. Right panel: pachytene oocyte with homologous synapsis and non-homologous self-synapsis do not elicit γH2AFX domain formation or oocyte elimination.

3.2 The role of meiotic DNA DSBs in oocyte losses in chromosomally abnormal mice

3.2.1 DNA DSB repair proteins do not persist on the asynapsed X chromosome in XO oocytes

After determining that oocytes with asynapsis are eliminated during diplonema, I then sought to understand the mechanism by which this occurs. I first tested the DNA damage model of oocyte arrest in chromosomally abnormal females. To examine this model, I first looked for the presence of persistent unrepaired DNA DSBs, which is the presumed trigger of the DNA damage checkpoint (Di Giacomo et al., 2005), in XO mice.

I studied the localization of three DNA repair proteins, namely RAD51, DMC1, and RPA, which are commonly used as proxy markers for DNA DSB repair in mammalian germ cells (Moens et al., 2002). First, I examined surface spread XO oocyte from 18.5 d*pc* ovaries and performed immunofluorescence for three proteins: SYCP3, to sub-stage oocytes; HORMAD2, to identify the asynapsed X chromosome, and RPA (**Figure 2.1**). HORMAD2 labels asynapsed chromosome axes, but not desynapsed axes, between pachynema and late diplonema (Wojtasz et al., 2009). HORMAD2 was used instead of γH2AFX to identify the asynapsed X chromosome because it identifies specifically the asynapsed core with which RPA foci are located.

Using this approach, I found that the asynapsed X chromosome in XO oocytes has variable numbers of RPA foci depending upon the substage of prophase I. At pachynema, there were on average 5 ±0.5 RPA foci on the asynapsed X chromosome, although the range (0-15 foci) was wide (**Figure 2.1**). At early diplonema, there were significantly fewer RPA foci on the asynapsed X chromosome (1 ±0.5), with a narrower range (0 to 4) (P=0.0435). By late diplonema, most oocytes had no RPA foci on the asynapsed X chromosome (mean=0.5 ±0.3 foci, range=0 to 1). Therefore, the majority of XO oocytes do not have X chromosome-associated RPA foci after pachynema.

Next, I examined whether the drop in the number of RPA foci on the asynapsed X chromosome occurs specifically during pachynema. To test this, I compared the number of RPA foci on the asynapsed X chromosome in XO oocytes further substaged into early pachynema and late pachynema. With the help of Dr. Shantha Mahadevaiah, I categorized oocytes into pachytene sub-stages based on the number of RPA foci on the synapsed autosomes, as described previously (Guioli et al., 2012). Numerous foci of RPA are present on synapsed autosomes at early pachynema (**Figure 2.1a**) but disappear thereafter, with few left by late pachynema (**Figure 2.1b**) (Guioli et al., 2012). Therefore, I subdivided XO pachytene oocytes into those with >30 autosomal RPA foci (early pachynema) and those with ≤30 autosomal RPA foci (late pachynema). Based on these sub-staging criteria, I observed abundant RPA foci on the asynapsed X chromosome in XO oocytes at early pachynema (**Figure 2.1a,d**), but significantly lower RPA counts at late pachynema (**Figure 2.1b,d**).

To verify these results, I also assessed the behavior of recombinases RAD51 and DMC1 on the asynapsed X chromosome in XO oocytes. In accordance with my RPA analyses, both RAD51 and DMC1 were abundant on the asynapsed X chromosome during pachynema in a subset of oocytes (**Figure 2.1e,g**). However, in many pachytene oocytes there were few or no RAD51 and DMC1 foci on the asynapsed X chromosome (**Figure 2.1f,h**). This second population of oocytes represented later pachytene oocytes in which DNA DSB repair has completed on the asynapsed X chromosome. This suggests that most RAD51/DMC1 foci are lost by late pachynema. In accordance with this, RAD51 and DMC1 were not observed on the asynapsed X chromosome at early diplonema (data not shown).

Together, these data reveal that DNA DSBs markers disappear by late pachynema. Therefore, the asynapsed X chromosome does not harbor persistent unrepaired DNA DSBs during the stage when XO oocyte losses are observed (i.e. diplonema). This suggests that persistent unrepaired DNA DSBs are not the proximal cause of oocyte losses in XO mice.

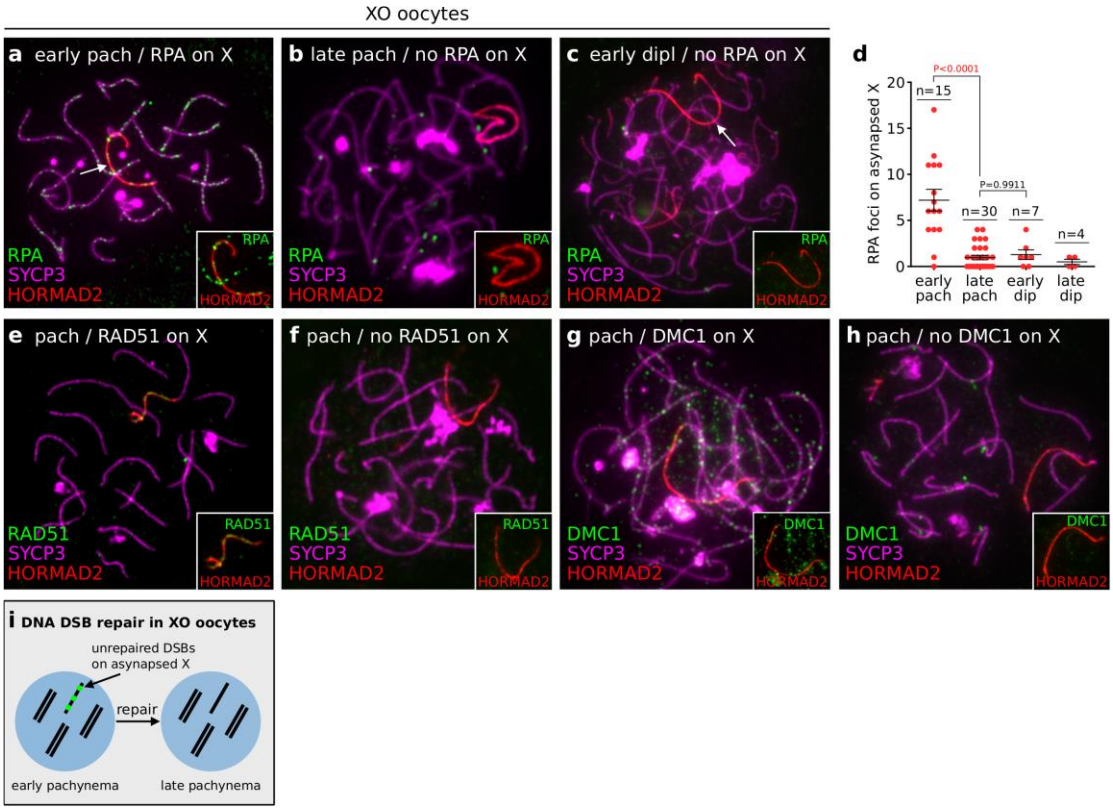

Figure 2.1 DNA DSB repair proteins do not persist on the asynapsed X chromosome in XO oocytes.

(**a**) Early pachytene XO oocyte with numerous RPA foci (green) on asynapsed X chromosome (arrow, and inset). RPA foci are abundant on all synaptic axes at early pachytene, but rapidly decrease by late pachynema. (**b**) Late pachytene XO oocyte with no RPA foci on the asynapsed X chromosome (arrow and inset), and few autosomal foci. (**c**) Early diplotene XO oocytes with no RPA foci on asynapsed X chromosome. (**d**) Number of RPA foci on asynapsed X chromosome at pachynema, early diplonema, and late diplonema. P value determined by Tukey's multiple comparison test. (**e**) Early pachytene XO oocyte with several RAD51 foci on asynapsed X (arrow). (**f**) Late pachytene XO oocyte with no RAD51 foci. (**g**) Early pachytene XO oocyte with numerous DMC1 foci on asynapsed X (arrow) and autosomes. (**h**) Late pachytene XO oocyte with no DMC1 foci. (**i**) Schematic showing RPA turnover from the asynapsed X chromosome by late pachynema.

3.2.2 DNA DSB repair proteins do not persist on multiple asynapsed chromosomes in PWDxB6 F1 oocytes

The analysis of DNA repair in XO oocytes suggests that meiotic DNA DSBs are repaired even in the absence of a homolog. To better characterize this DNA repair response, I next examined whether more extensive asynapsis challenges this DNA DSB repair pathway. To address this, with help from Dr. Shantha Mahadevaiah, I examined RPA turnover in oocytes that contain multiple asynapsed chromosomes. For unknown reasons, progeny from PWD females and C57BL/6 males, which are highly genetically divergent, show extensive and variable levels of asynapsis in germ cells (Bhattacharyya et al., 2013; Mihola et al., 2009). Therefore, I assessed RPA turnover in PWDxB6 F1 oocytes.

First, I estimated the number of asynapsed chromosomes present in PWDxB6 F1 oocytes by SYCP3/HORMAD2 immunostaining. At 18.5 d*pc*, 77% of oocytes from F1 PWDxB6 females had HORMAD2-positive asynapsed chromosomes (**Figure 2.2a-c, arrows**). At pachynema, there were on average nine asynapsed chromosomes (**Figure 2.2a**). A similarly high level of asynapsis was observed at early diplonema (mean=9 asynapsed chromosomes) (**Figure 2.2a**) and late diplonema (mean=8 asynapsed chromosomes). In summary, PWDxB6 F1 females have extensive asynapsis between pachynema and late diplonema. It is possible that some oocytes that I classified as pachytene nuclei with asynapsis are actually zygotene nuclei. However, zygotene oocytes tend to have longer SC cores compared to pachytene oocytes (Wojtasz et al., 2009). Furthermore, the majority of oocytes at 18.5 d*pc* have progressed beyond zygonema (see Figure 1.2). Use of other markers more prevalent on zygotene nuclei, such as DNA DSB markers, could be used to confirm this substaging.

Next, I quantified the number of RPA foci on asynapsed chromosomes in PWDxB6 F1 oocytes between pachynema and late diplonema. As with the XO RPA analysis, I subdivided PWDxB6 F1 pachytene oocytes into early pachynema (**Figure 2.2b**) and late pachynema (**Figure 2.2c**) based on the decreasing number of RPA foci on synapsed chromosomes with pachytene progression. At early pachynema, there were

on average 7 RPA foci associated with all asynapsed chromosomes (**Figure 2.2b,d**). Notably, at late pachynema there were significantly fewer RPA foci on asynapsed chromosomes (mean=1 RPA focus; Tukey's test, $P<0.0001$) (**Figure 2.2c-d**). In fact, most oocytes had no RPA foci on asynapsed chromosomes at late pachynema. Very low RPA counts were also observed at early diplonema (mean=1 focus) and late diplonema (mean=0.5 foci) (**Figure 2.2d**).

These data reveal that, like in XO oocytes, most RPA foci are resolved from multiple asynapsed chromosomes in F1 PWDxB6 oocytes by late pachynema (**Figure 2.2e**). Therefore, oocytes have the capacity to efficiently repair DNA DSBs when an extensive number of chromosomes are asynapsed. Importantly, these data support the theory that unrepaired DNA DSBs do not persist into diplonema in chromosomally abnormal mice, and therefore that DNA damage is unlikely to contribute to oocyte losses in mice with asynapsed chromosomes.

a

PWDxB6 F1 oocytes	number (%)	avg. # of asyn chr.
oocytes with asynapsis at 18.5 dpc	95/123 (77%)	8.5
pachyene oocytes with asynapsis	60/74 (81%)	8.8
early diplotene oocytes with asynapsis	16/16 (100%)	9.0
late diplotene oocytes with asynapsis	19/33 (58%)	7.6
oocytes with no asynapsis	28/123 (23%)	0

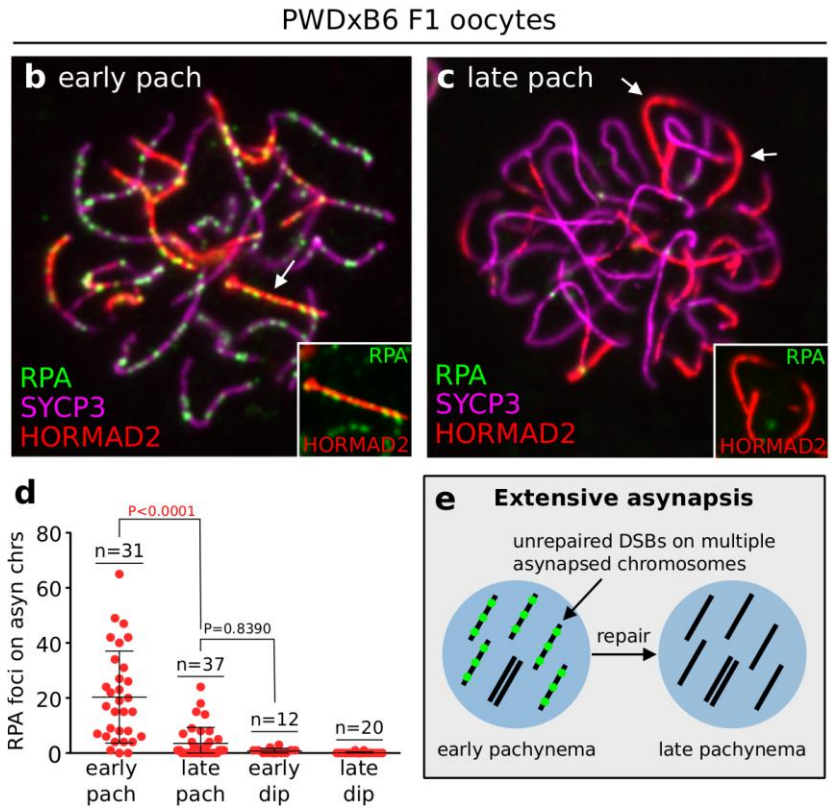

Figure 2.2. DNA DSB repair proteins do not persist on multiple asynapsed chromosomes in PWDxB6 F1 oocytes.

(**a**) Characterization of PWDxB6 F1 oocytes with asynapsed chromosomes at pachynema, early diplonema, and late diplonema. (**b**) Early pachytene PWDxB6 F1 oocyte with numerous asynapsed chromosomes (approx. 8), marked by HORMAD2 and containing abundant RPA foci. (**c**) Late pachytene PWDxB6 F1 oocyte with numerous asynapsed chromosomes (approx. 9) containing much fewer RPA foci. Late pachytene stage is indicated by the dearth of RPA foci on synapsed bivalents. (**d**) Number of RPA foci on asynapsed axes in PWDxB6 F1 oocytes. (**e**) Schematic showing repair of DNA DSBs from numerous asynapsed axes.

3.2.3 *Spo11* heterozygosity does not attenuate XO oocyte losses

To further examine the role of DNA DSBs in oocyte loss in chromosomally abnormal mice, I assessed the effect of genetically reducing meiotic DNA DSBs on XO oocyte elimination. Studies of *Spo11*+/- mouse spermatocytes have shown that *Spo11* heterozygosity reduces the number of RAD51 foci at leptonema by 18-30%, suggesting a reduction in DNA DSB formation (Bellani et al., 2010; Carofiglio et al., 2013). There is a similar reduction in RAD51 foci numbers at leptonema in oocytes heterozygous for *Spo11* (Carofiglio et al., 2013).

I studied XO *Spo11*+/- females to examine whether reducing meiotic DNA DSBs effects the elimination of XO oocyte with an asynapsed X chromosome. I quantified the percentage of XO *Spo11+/-* oocytes with an asynapsed X chromosome at pachynema, early diplonema, and late diplonema. As with my previous analyses, I studied SYCP3/HORMAD2/γH2AFX triple-immunostained oocyte spreads from 18.5 d*pc* XO *Spo11*+/- females. At pachynema, nearly half of XO *Spo11*+/- oocytes had a γH2AFX domain, consistent with age-matched XO *Spo11*+/+ females (**Figure 2.3**). At early diplonema, only 20% of XO *Spo11*+/- oocytes had a γH2AFX domain, indicating that significant oocyte losses occur from pachynema to early diplonema (**Figure 2.3**). Additional oocyte losses are observed by late diplonema (**Figure 2.3**).

Therefore, *Spo11* heterozygosity does not alleviate XO oocyte losses. It is possible, however, that *Spo11* heterozygosity does not sufficiently reduce DNA DSBs to significantly alter the number of DNA DSBs on the asynapsed X chromosome. Addressing this requires quantitation of the number of RAD51 foci on the asynapsed X chromosome in XO *Spo11*+/- oocytes. Nevertheless, combined with my earlier analyses of RPA/RAD51/DMC1 turnover, these data suggest that persistent DNA damage on asynapsed chromosomes is unlikely to trigger oocyte loss in chromosomally abnormal mice.

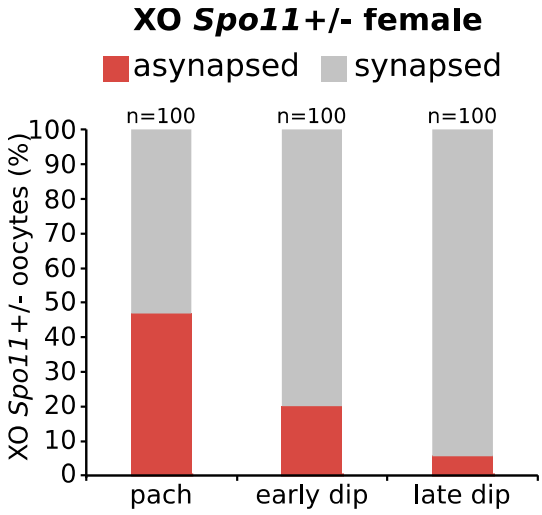

Figure 2.3. Elimination of XO *Spo11*+/- oocytes.

The mean percentage of XO *Spo11*+/- oocytes with a γH2AFX domain in 18.5 d*pc* ovaries. n is the number of oocytes analyzed at each stage from one ovary.

3.3 The role of an asynapsis checkpoint in oocyte losses in chromosomally abnormal mice

Given that my above analyses suggested that DNA damage is unlikely to contribute to oocyte losses in chromosomally abnormal females, I then tested the role of an asynapsis checkpoint. Evidence for an asynapsis checkpoint comes from mice lacking DNA DSBs, i.e. *Spo11*-/- mice. Specifically, *Spo11*-/- oocytes have extensive asynapsis and suffer oocyte losses resulting in infertility (Di Giacomo et al., 2005). The molecular details of this DNA DSB-independent mechanism remain unclear.

One putative pathway for DNA DSB-independent oocyte losses is an asynapsis checkpoint (Di Giacomo et al., 2005). Asynapsis checkpoints are triggered by some feature of asynapsed chromosomes, such as defective SC morphogenesis, and lead to meiotic prophase I arrest (MacQueen and Hochwagen, 2011). Although asynapsis checkpoints have been well characterized in *C. elegans* (Bhalla and Dernburg, 2005) and *S. cerevesiae* (Roeder and Bailis, 2000), it is unclear whether an analogous system operates in mammals. In the next section, I test whether an asynapsis checkpoint operates in mice with chromosome abnormalities.

3.3.1 Predictions under asynapsis checkpoint model

Ascertaining whether an asynapsis checkpoint operates in mammals is not trivial. Genes with putative asynapsis checkpoint functions, e.g. HORMAD1 and ATR, are also required for meiotic silencing (Daniel et al., 2011; Royo et al., 2013). Meiotic silencing has been also proposed to cause germ cell arrest by inactivating essential genes on asynapsed chromosomes (Burgoyne et al., 2009) (see Chapter 4). Owing to the interdependence of proteins involved in the putative asynapsis checkpoint and meiotic silencing pathways, distinguishing between them as triggers of oocyte loss is challenging.

Importantly, however, these two models predict different outcomes depending on whether the asynapsed chromosome contains essential genes. Under the asynapsis checkpoint model, any asynapsed chromosome will

lead to oocyte losses, irrespective of the genes that are associated with the asynapsed chromosome. By contrast, under the meiotic silencing model, oocyte arrest will only occur when asynapsed chromosomes contain essential genes. If asynapsed chromosomes contain non-essential genes, meiotic silencing would not have an effect on transcription that would be detrimental to developing oocytes.

Therefore, it is possible to distinguish between these two models by examining the fate of oocytes containing asynapsed chromosomes that harbor no essential genes, i.e. accessory/supernumerary chromosomes. If the asynapsis checkpoint operates in oocytes, then such oocytes would be eliminated by diplonema (**Figure 2.4**). However, if meiotic silencing is the primary mechanism driving oocyte losses, then these oocytes would escape elimination and survive into diplonema (**Figure 2.4**).

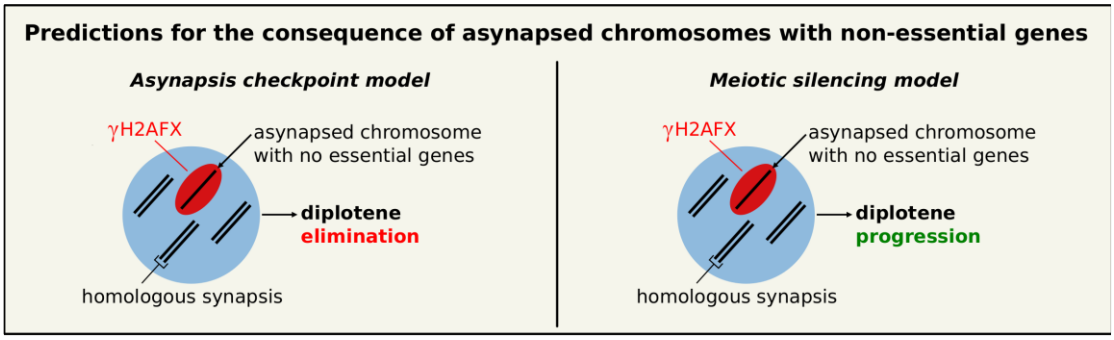

Figure 2.4. Predictions for fate of oocytes with asynapsed chromosomes containing non-essential genes.

Asynapsis checkpoint model: oocytes with asynapsed chromosomes are eliminated, irrespective if the chromosomes contain non-essential or essential genes. Meiotic silencing model: oocytes with asynapsed chromosomes containing non-essential genes are not eliminated, because this model predicts that silencing only causes loses when it silences essential genes.

3.3.2 RNA FISH analysis of transcription in XX oocytes

As discussed above, distinguishing between the asynapsis checkpoint and the meiotic silencing models of oocyte loss requires analysis of chromosomes that do not express genes essential for oocyte survival. Such an analysis can be performed on XX wildtype oocytes provided that they harbor chromosomes, or chromosome regions, that are underrepresented in oocyte-expressed genes (i.e. non-essential genes).

To assess for underexpressed chromosomes, I first examined the nuclear-wide transcriptional status of wildtype oocytes. In collaboration with Dr. Shantha Mahadevaiah (NIMR), Cot-1 RNA FISH was performed in 18.5 d*pc* XX oocytes to estimate global transcription levels in prophase I sub-staged oocytes. Cot-1 DNA is enriched for repetitive sequence that can be used as a probe to detect repeat-rich regions of nascent RNA transcripts, such as intronic and 3' untranslated regions (Turner et al., 2005). The intensity of nuclear Cot-1 RNA FISH immunofluorescence correlates with the level of nuclear transcription (Bellani et al., 2010). Therefore, I used Cot-1 RNA FISH to assess whether oocytes have any chromosomes showing underexpression.

Using HORMAD1 for substaging, I analyzed Cot-1 staining at pachynema, early diplonema, and late diplonema (**Figure 2.5**). As expected, Cot-1 staining was low at sites of DAPI-dense constitutive heterochromatin (i.e. centromeres, telomeres, etc.) (**Figure 2.5c,** asterisks). Outside of sites of constitutive heterochromatin, there was diffuse nuclear-wide Cot-1 staining (**Figure 2.5a-c**), indicative of global transcription. This staining pattern is in contrast to that observed in previous studies of XO oocytes, which have a Cot-1 negative "hole" corresponding to the inactive asynapsed X chromosomes (Turner et al., 2005). This indicates that all mouse chromosomes are transcriptionally active except at sites of constitutive heterochromatin.

To determine if oocyte transcription levels change during meiotic prophase I progression, I then measured the intensity of Cot-1 signal, corrected for background, in XX oocytes at pachynema, early diplonema, and late diplonema. Cot-1 staining intensity increased significantly from

pachynema and late diplonema (**Figure 2.5d**) (Tukey's test, $P<0.0001$), indicating a rise in nuclear-wide transcription during prophase I progression.

These results suggest that the oocyte genome is highly transcriptionally active, especially at diplonema. Therefore, it would be challenging to identify a single endogenous chromosomes or chromosome region that would satisfy the criteria of having non-essential oocyte genes. To distinguish between the asynapsis checkpoint versus meiotic silencing models of meiotic surveillance, therefore, requires analysis of an exogenous, accessory chromosome, which by definition has no essential genes.

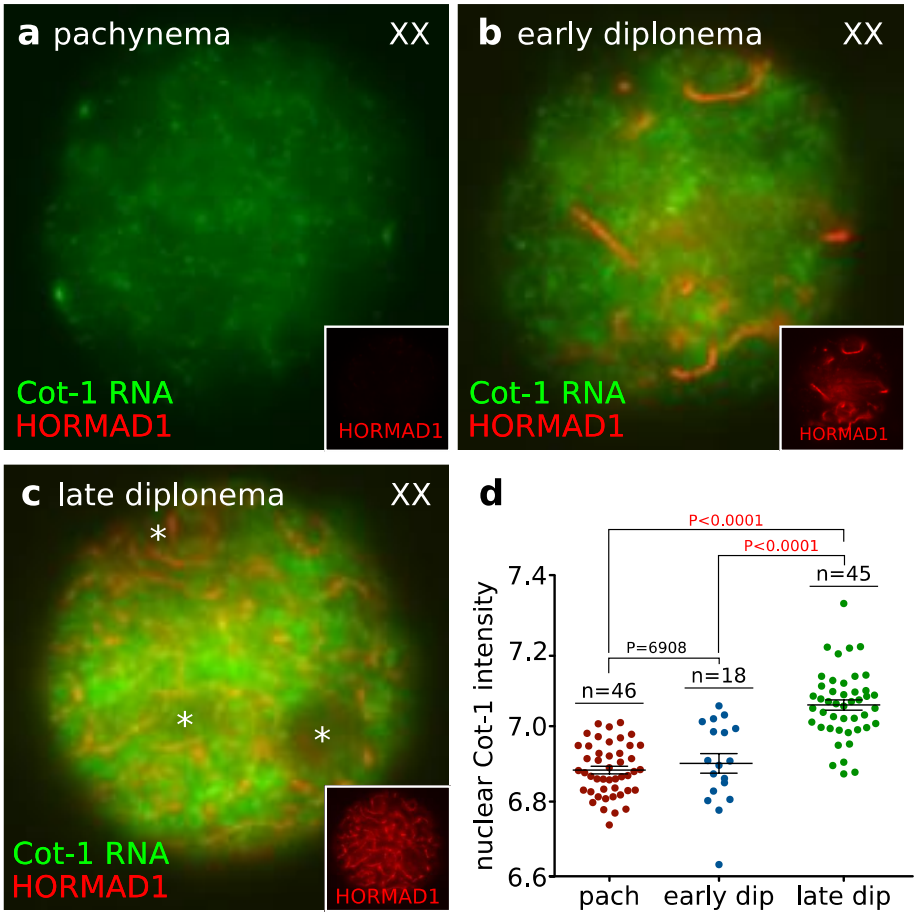

Figure 2.5. Cot-1 RNA FISH analysis of wildtype XX oocytes.

(**a**) Representative pachytene XX oocyte subject to Cot-1 RNA FISH (green), substaged based on the absence of the asynapsis marker HORMAD1 (inset). (**b**) Representative early diplotene oocyte, sub-staged by intermediate levels of HORMAD1. (**c**) Representative late diplotene oocyte, substaged by extensive HORMAD1 staining. Note the higher levels of Cot-1 staining compared to pachytene and early diplotene oocytes. Asterisks represent sites of constitutive heterochromatin. (**d**) Quantitation of nuclear Cot-1 RNA FISH staining intensity. n is the number of oocytes analyzed. P values were generated from Tukey's multiple comparison test, and significant P values ($P<0.05$) are shown in red.

3.3.3 Meiotic characterization of Tc1 mouse model of Down syndrome

I studied two different accessory chromosome mouse models to help distinguish between the asynapsis checkpoint model and the meiotic silencing model of meiotic surveillance. The first accessory chromosome mouse model that I studied was the Tc1 mouse model of Down syndrome, which contains a hemizygous copy of the human chromosome 21 (h21) (O'Doherty et al., 2005). Given that the asynapsed h21 chromosome is accessory it by definition contains only non-essential genes. Therefore, the Tc1 mouse model satisfies the criteria for distinguishing between the two DNA DSB-independent models of meiotic surveillance.

Before assessing the consequence of the accessory h21 on oocyte survival, I first verified that meiotic events occur normally in Tc1 oocytes. To assess whether the kinetics of meiotic progression are changed by the exogenous h21 chromosome, I substaged Tc1 oocytes at 18.5 d*pc* and compared the results to my previous analysis of XX oocytes. The percentage of pachytene, early diplotene, and late diplotene oocytes at 18.5 d*pc* was not significantly different between Tc1 and XX ovaries (**Figure 2.6a**), implying that meiotic progression occurs with normal kinetics in Tc1 ovaries.

Second, I assessed whether the components involved in the asynapsis responses are unchanged in Tc1 oocytes. Using chromosome spreads and immunostaining, I analyzed the localization of BRCA1, ATR, HORMAD1, and γH2AFX in Tc1 oocytes. Importantly, all of these proteins localized as expected to the asynapsed h21 chromosome in pachytene oocytes (**Figure 2.6b-e**). This confirms that asynapsis signalling is proficient in Tc1 oocytes.

Next, I examined the synaptic behavior of the accessory h21 chromosome in Tc1 pachytene oocytes. Using SYCP3/HORMAD1/γH2AFX triple-immunostaining, I found that one population of Tc1 pachytene oocytes contained a γH2AFX chromatin domain, which marked the asynapsed h21 chromosome (**Figure 2.6d, arrow**), as verified by h21 painting (not shown). A second population of Tc1 oocytes had a self-synapsed and γH2AFX-negative h21 chromosome (**Figure 2.6e, arrow**). Therefore, the synaptic behavior of the h21 is similar to that observed for the X chromosome in XO oocytes.

To assure the comparability of the Tc1 model to the XO model, I also determined whether the level/intensity of γH2AFX signalling on the h21 was comparable to that of the asynapsed X in XO oocytes. The h21 (42Mb) in Tc1 oocytes is significantly smaller than the mouse X chromosome (171Mb) in XO oocytes. To assess whether this size difference affects the level/intensity of γH2AFX chromatin signalling, Dr. Shantha Mahadevaiah and I quantified the background-normalized intensity of the γH2AFX domain associated with the asynapsed X chromosome and h21 chromosome, respectively. This analysis was performed specifically on diplotene oocytes, the stage when oocyte losses occur in our chromosomally abnormal mice (see Figure 1). Notably, despite the difference in size of each chromosome, the intensity of γH2AFX signalling was not significantly different between XO and Tc1 oocytes (T test, two-way, P=0.9489) (**Figure 2.6f**).

Finally, I examined whether DNA DSB repair proteins persist on the asynapsed h21, or if they are resolved with normal kinetics. In XO oocytes, RPA on the asynapsed X chromosome were resolved in the majority of oocytes by late pachynema. In Tc1 oocytes, the asynapsed h21 had on average 3 ±0.4 RPA foci (range=0-10 foci) at pachynema (**Figure 2.5i**). At early diplonema the majority of Tc1 oocytes did not have RPA foci on the asynapsed h21 (mean=0.3 ±0.1) (Tukey's test, P=0.0002) (**Figure 2.5i**). This indicates that like in XO females the asynapsed h21 does not harbor persistent DNA DSBs beyond late pachynema.

In summary, my analyses of meiotic kinetics, the asynapsis response, and DNA DSB repair did not reveal any differences between Tc1 and XO oocytes. Therefore, Tc1 oocytes are a suitable model with which to compare to XO oocytes.

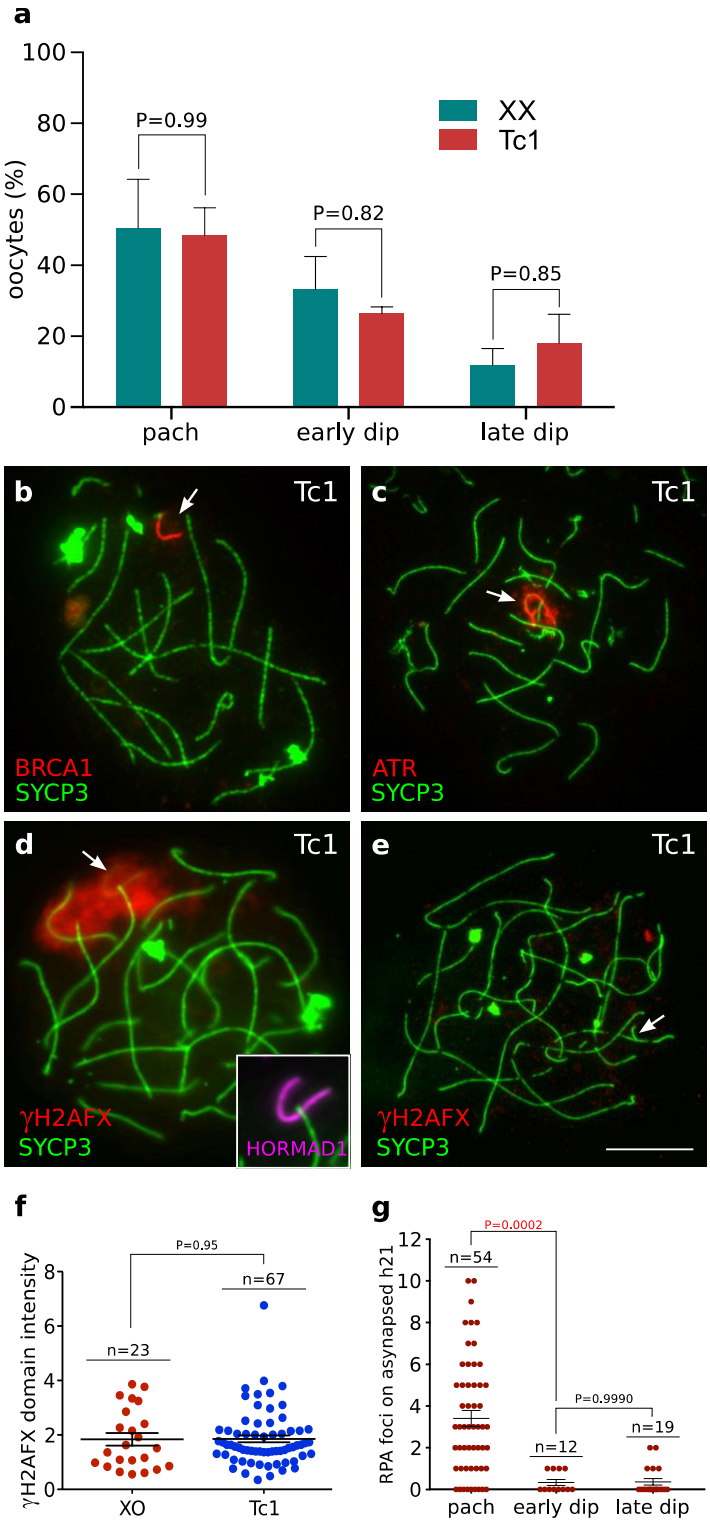

Figure 2.6. Meiotic characterization of Tc1 oocytes with an asynapsed h21 chromosome.

(**a**) Comparison of the mean percentage of oocytes at pachynema, early diplonema, and late diplonema between XX and Tc1 females at 18.5 d*pc*. (**b**) Pachytene Tc1 oocyte showing BRCA1 enrichment on the asynapsed h21 chromosome (arrow). (**c**) Tc1 pachytene oocyte showing ATR enrichment on the asynapsed h21 chromosome (arrow). (**d**) Tc1 pachytene oocyte

showing γH2AFX (arrow) and HORMAD1 (inset) enrichment on the asynapsed h21 chromosome. (**e**) Tc1 pachytene oocyte with a self-synapsed h21 chromosome, lacking γH2AFX staining. Scale bar=10μm. (**f**) Comparison of γH2AFX domain integrated intensity in XO and Tc1 early diplotene oocytes at 19.5 d*pc*. n is the number of oocytes analyzed. P value determined from unpaired T test. (**g**) Number of RPA foci on asynapsed h21 chromosome at pachynema, early diplonema, and late diplonema. Tukey's multiple comparison test, P value significance shown in red.

3.3.4 Tc1 oocytes with an asynapsed h21 chromosomes persist into diplonema

After verifying that meiotic events occur as expected in Tc1 oocytes, I then examined the fate of oocytes with an asynapsed h21. If asynapsis *per se* is sufficient to trigger oocyte losses, as expected by an asynapsis checkpoint, then Tc1 oocytes with an asynapsed h21 should be eliminated by late diplonema, as observed with XO, In(X)1H, T43H, and XX oocytes (**Figure 2.4, left panel**). On the other hand, if meiotic silencing, rather than an asynapsis checkpoint, is the underlying cause of oocyte arrest, then oocytes with an asynapsed h21 chromosome should persist through diplonema, since the h21 chromosome contains only non-essential genes (**Figure 2.4, right panel**).

To test these predictions, I quantified the percentage of Tc1 oocytes with an asynapsed, γH2AFX-positive h21 chromosome between pachynema and late diplonema. At 17.5 d*pc*, on average 36% of Tc1 oocytes had an asynapsed h21 chromosome (**Figure 2.7a**). Notably, at 18.5 and 19.5 d*pc*, the percentage of oocytes with an asynapsed h21 chromosome remained unchanged (34% and 35%, respectively) (Tukey's test, P=0.9504 and P=0.9820, respectively) (**Figure 2.5l**).

To confirm this result, I also analyzed substaged Tc1 oocytes from 18.5 d*pc* ovaries. At pachynema, 40% of Tc1 oocytes had an asynapsed h21 chromosome (**Figure 2.7b**). Notably, this was not significantly different from the percentage of oocytes with an asynapsed h21 chromosome at early diplonema (37%; Tukey's test, P=0.9788) or late diplonema (31%, Tukey's test, P=0.8026) (**Figure 2.7b**).

In conclusion, Tc1 oocytes with an asynapsed h21 chromosome persist into late diplonema (**Figure 2.7c**). This result suggests that asynapsis *per se* is not sufficient to trigger significant oocyte losses, thus supporting the meiotic silencing model of meiotic surveillance.

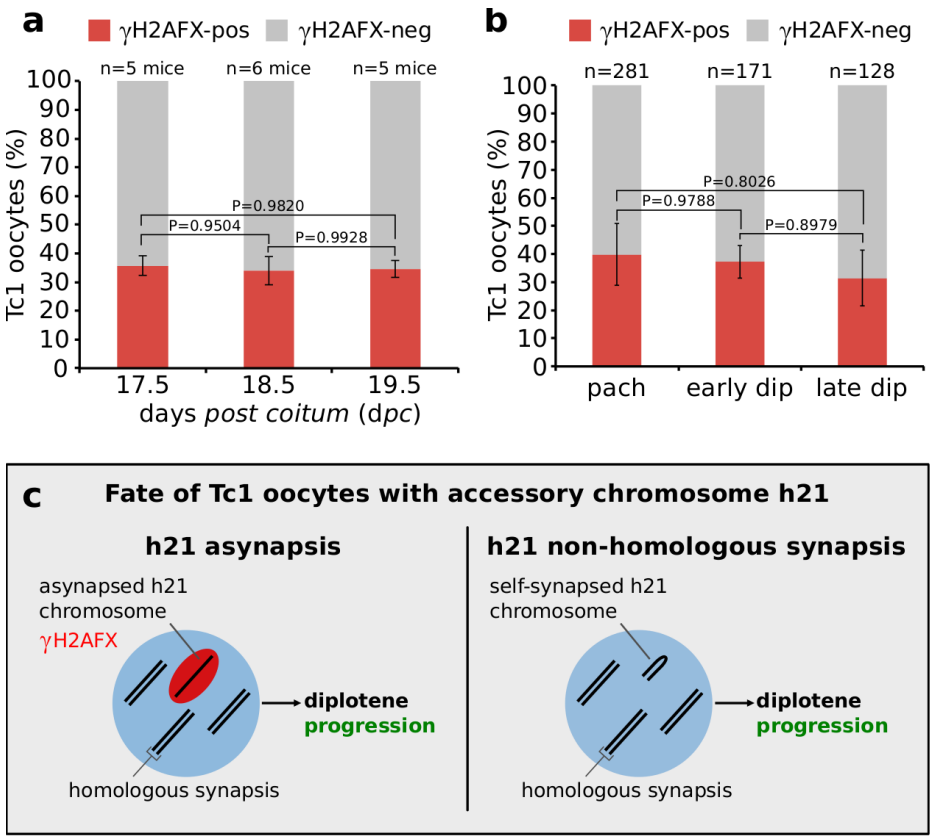

Figure 2.7. Tc1 oocytes with an asynapsed h21 persist to late diplonema.

(**a**) The mean percentage of Tc1 oocytes with a γH2AFX domain, representing the asynapsed h21 chromosome, at 17.5, 18.5, and 19.5 d*pc*. n is the number of ovaries analyzed, with 100-200 oocytes analyzed per ovary. (**b**) The mean percentage of Tc1 oocytes with a γH2AFX domain from 18.5 d*pc* ovaries, where oocytes were substaged into pachynema, early diplonema, and late diplonema. Three ovaries were analyzed, and n is the total number of oocytes analyzed. P values were generated from Tukey's multiple comparison test, and significant P values ($P<0.05$) are shown in red. (**c**) Schematic showing fate of Tc1 oocytes with either an asynapsed h21 chromosome or self-synapsed h21 chromosome. In both cases, oocytes progress to late diplonema.

3.3.5 XXY^{d1} oocytes with an asynapsed accessory Y chromosome persist to late diplonema

To verify the results of the Tc1 mouse model, I also analyzed another accessory chromosome mouse model in which the accessory chromosome was of mouse origin: the sex-reversed XXY^{d1} mouse. XXY^{d1} females harbor a single accessory copy of the mouse Y chromosome (denoted Y^{d1}) containing a 3-4Mb repeat deletion that results in positional inactivation of the male-determining factor *Sry* in the developing gonad, such that XXY^{d1} embryos develop as females (Capel et al., 1993; Mahadevaiah et al., 1998).

To study the synaptic status of the accessory Y^{d1} chromosome, I immmunostained surface spread XXY^{d1} oocytes with SYCP3/HORMAD1/γH2AFX. In a subset of XXY^{d1} pachytene oocytes, the accessory Y^{d1} chromosome remained asynapsed, and was positive for both γH2AFX and HORMAD1 (**Figure 2.8a, arrow, inset**). In the remaining XXY^{d1} oocytes, the single Y^{d1} chromosome was self-synapsed and γH2AFX- and HORMAD1-negative (**Figure 2.8b, arrow**).

Next, I quantified the percentage of XXY^{d1} oocytes with a γH2AFX domain (i.e. asynapsed Y^{d1} chromosome) in substaged oocytes from 18.5 d*pc* ovaries. Notably, the percentage of XXY^{d1} oocytes with an asynapsed Y^{d1} chromosome was unchanged between pachynema (38%), early diplonema (39%), and late diplonema (36%) (**Figure 2.8c**). Therefore, the asynapsed Y^{d1} chromosome does not trigger oocyte losses during prophase I (**Figure 2.8d**).

Taking into account both accessory chromosome mouse models, these data strongly suggest that an asynapsis *per se* is not sufficient to trigger oocyte arrest,. Furthermore, these data support the meiotic silencing model, rather than the asynapsis checkpoint model of meiotic surveillance.

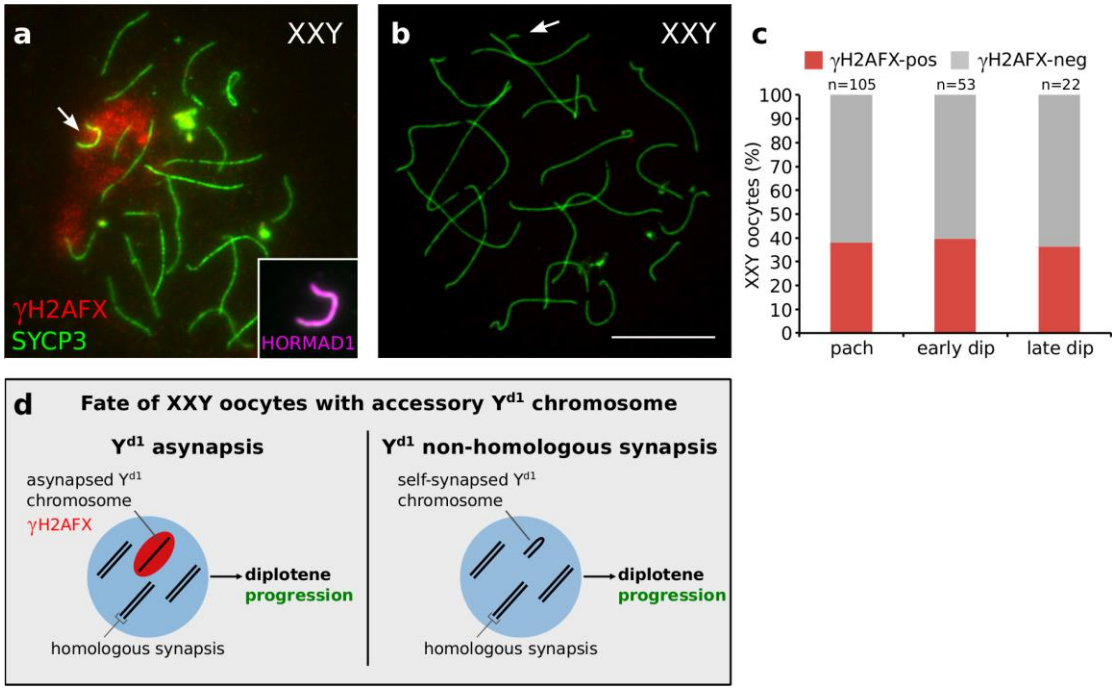

Figure 2.8. XXY^{d1} oocytes with an asynapsed Y^{d1} chromosome persist to late diplonema.

(**a**) Pachytene XXY oocyte showing γH2AFX (arrow) and HORMAD1 (inset) enrichment on the asynapsed Y^{d1} chromosome. (**b**) Pachytene XXY oocyte with a self-synapsed Y^{d1} chromosome (arrow), devoid of γH2AFX. Scale bar=10μm. (**c**) The percentage of XXY oocytes with a γH2AFX domain at pachynema, early diplonema, and late diplonema in an 18.5 d*pc* ovary. (**d**) Schematic showing fate of XXY oocytes with either an asynapsed Y^{d1} chromosome or self-synapsed Y^{d1} chromosome. In both cases, oocytes progress to late diplonema.

3.4 Discussion

A primary goal of this thesis was to determine the molecular basis of prophase I surveillance in mice with chromosome abnormalities. In this section, I studied several mouse models of common human conditions, including a model of Turner syndrome (X chromosome monosomy) and Down syndrome (accessory human chromosome 21), and other structural and numerical chromosome abnormalities, including inversions, translocations and sex chromosome additions. Turner syndrome, in particular, is strikingly prevalent in humans, accounting for 1-2% of all clinically recognized pregnancies (Hall et al., 2006). It has been clear since as early as 1959 that Turner syndrome females experience gonadal dysgenesis and infertility (Ford et al., 1959). Nevertheless, the precise mechanism basis for infertility in these and other patients with chromosome abnormalities remains to be worked out.

To date, our understanding of meiotic prophase I surveillance mechanisms operating in mammals has been informed predominantly from studies of targeted meiotic mutants. Studies of several meiotic mutants have shown that at least two surveillance mechanisms operate in mammalian oocytes. Analysis of mutants with defects in DNA repair, i.e. *Dmc1*-/-, *Msh5*-/- and *Atm*-/- mice, has revealed the existence of a surveillance mechanism that responds to persistent unrepaired DNA DSBs (Di Giacomo et al., 2005; Reinholdt and Schimenti, 2005). There is also evidence for a DNA damage-independent meiotic prophase I surveillance mechanism that is triggered by some feature of asynapsis (Di Giacomo et al., 2005). This DNA DSB-independent pathway has been invoked to explain the severe oocyte loss in *Spo11*-/- and *Mei1*-/- DSB-deficient oocytes, which lack meiotic DNA DSBs but still experience oocyte losses and infertility (Di Giacomo et al., 2005; Reinholdt and Schimenti, 2005). It is unclear whether either of these pathways have a role in germ cell loss in mice with numerical or structural chromosome abnormalities.

Studies of chromosomally variant mice are particularly valuable for understanding wildtype biology because these mouse models do not contain mutations in important genes. Most meiotic mutant mice may have defects

in critical meiotic processes, and these genetic changes may impact the behavior of surveillance mechanisms. Therefore, chromosomally variant mouse models are perhaps more applicable for understanding the mechanisms that operate in the context of normal mammalian biology.

Using an extensive array of these mouse models, I first determined the timing of oocyte losses in a variety of mice with chromosome abnormalities. In XO, In(X)1H, T(16;17)43H, and normal XX females, I observed a significant drop in the percentage oocytes with an asynapsed chromosomes, marked by γH2AFX, from pachynema to late diplonema. Importantly, this drop cannot reflect an increase in the frequency of self-synapsis, because chromosomes desynapse during this period of meiosis. Furthermore, this drop is unlikely due to progressive dephosphorylation of γH2AFX for several reasons: (1) γH2AFX does not disappear until metaphase I in male germ cells (Mahadevaiah et al., 2001), and (2) oocytes with asynapsis that do not drop in frequency during meiotic prophase I (i.e. Tc1 and XXY oocytes) retain γH2AFX until late diplonema. Therefore, I conclude that the drop in the percentage of oocytes with asynapsed chromosomes reflects oocyte elimination.

Taken together, these findings indicate that both an asynapsed X chromosome and asynapsed autosomes trigger oocyte losses during diplonema. This implies that a general mechanism operates in females with chromosome abnormalities and normal females to drive the elimination of oocytes with chromosome synaptic defects.

Notably, oocyte arrest occurring during diplonema is inconsistent with the traditional pachytene checkpoint model of germ cell loss, which has been commonly invoked to explain germ cell arrest in male mice (Barchi et al., 2005). In spermatocytes, meiotic defects, including asynapsis, typically cause a strict arrest at mid-pachynema (Barchi et al., 2005; Burgoyne et al., 2009). This indicates that there is a sexual dimorphism in the timing of arrest in mammals, with oocytes being eliminated later than spermatocytes.

Furthermore, not all oocytes with asynapsis were eliminated by late diplonema, perhaps indicating that the prophase I surveillance mechanism in females is not 100% efficient. This has also been observed in several

meiotic mutants, such as *Spo11*-/- and *Dmc1*-/- females, which retain still 50% of their oocytes at birth, corresponding to diplonema (Di Giacomo et al., 2005). My work confirms the sexual dimorphism in the timing of germ cell arrest between the sexes, and suggests that distinct mechanisms operate in spermatocytes and oocytes and/or that common ones operate with different stringencies.

Persistent unrepaired meiotic DNA DSBs, as found in recombination mutants, e.g. *Dmc1*-/- females, are associated with severe germ cell loss and infertility (Pittman et al., 1998; Yoshida et al., 1998). I therefore considered the possibility that persistent unrepaired DNA DSBs occur on the asynapsed chromosomes in chromosomally variant mouse models. I addressed this possibility by studying the turnover of DNA repair proteins, i.e. RPA, RAD51, and DMC1, in XO mice. I found that the majority of X chromosome DNA DSBs, marked by RAD51/DMC1/RPA, are resolved by exit from pachynema. This drop in foci counts in XO oocytes cannot reflect elimination of XO oocytes with numerous foci because this RPA counts decreased before diplonema, the stage when oocyte losses were observed. Therefore, DNA DSBs do not persist on the asynapsed X chromosome in XO oocytes, and therefore are unlikely to contribute to oocyte arrest in XO females. I also found that DNA DSBs associated with greater than one asynapsed chromosome, as in PWD/Ph x C57Bl/6 F1 hybrid females, are resolved by late pachynema. This is in contrast to the situation in DNA DSB repair-deficient mutant mice, like *Dmc1*-/- oocytes, where unrepaired breaks persist and cause oocyte arrest (Pittman et al., 1998; Yoshida et al., 1998). These pathways leading to oocyte arrest in chromosomally abnormal mice and those with persistent DNA damage are, therefore, mechanistically distinct.

These results also suggest that a mechanism operates in oocytes to repair DNA DSBs in the absence of a homologous chromosome. This is consistent with previous immunocytological studies of the male germ line, which showed that DNA DSB markers disappear from the asynapsed X chromosome by mid-late pachynema (Mahadevaiah et al., 2008). Additional

work will be required to identify the molecular nature of this mechanism of DNA DSB repair in oocytes.

After discounting the DNA damage checkpoint as a likely mechanism for oocyte elimination in our chromosome variant mouse models, I then assessed the potential role of asynapsis *per se* in oocyte arrest. In mammals, asynapsis has been proposed to cause oocyte arrest through meiotic silencing or a checkpoint monitoring asynapsis, but distinguishing between these models has proved challenging because putative synapsis checkpoint proteins are necessary for silencing (Daniel et al., 2011; Kogo et al., 2012a; Shin et al., 2010; Wojtasz et al., 2012).

The silencing model predicts that asynapsed chromosomes will trigger arrest only if they contain oogenesis-expressed genes, while the checkpoint model predicts that they will cause arrest irrespective of their gene content. My Cot1 RNA FISH analysis revealed high global gene expression levels in XX prophase I oocytes, especially during diplonema, indicating that all mouse chromosomes harbor oogenesis-expressed genes. To separate the effects of asynapsis and silencing, I therefore studied mice carrying additional, so-called "accessory" chromosomes, which harbor non-essential genes.

In Tc1 females, oocytes with a single accessory h21 chromosome were not eliminated during diplonema, despite the presence of BRCA1, HORMAD1, ATR, and γH2AFX on the h21 chromosome. There was also no selection against XXY^{d1} oocytes with an asynapsed accessory Y^{d1} chromosome (**Figure 2.8**). This demonstrates that presence of asynapsed chromosomes and asynapsis-associated factors, e.g. HORMAD1, HORMAD2, BRCA1, ATR and γH2AFX, is insufficient to cause diplotene oocyte elimination.

I consistently found that oocyte losses occurs only when asynapsed chromosomes carry oogenesis-expressed genes, as in XO, In(X)1H, T43H, and XX females. While it is conceivable that accessory chromosomes do not efficiently activate a putative synapsis checkpoint, it seems unlikely, since my experiments revealed no qualitative or quantitative differences in the asynapsis response between these models and those that exhibit diplotene

oocyte arrest. Thus, my data cannot be readily explained by either a DNA damage checkpoint or an asynapsis checkpoint, and instead suggest a role for meiotic silencing in oocyte loss in chromosomally abnormal mice.

4 Results: The role of H2AFX in oocyte losses in chromosomally abnormal mice

As described in the previous chapter, oocyte arrest in chromosomally abnormal mice is unlikely to be triggered by persistent unrepaired DNA DSBs or an asynapsis checkpoint. In this chapter, therefore, I will examine the role of meiotic silencing in the elimination of oocytes with asynapsed chromosomes. First, I will test whether disrupting meiotic silencing prevents oocyte losses in chromosomally abnormal mice. To do this, I will examine the consequence of deleting *H2afx*, a histone variant essential for silencing (Fernandez-Capetillo et al., 2003), on XO oocyte survival.

Following this, I will also test the role for H2AFX in the elimination of oocytes in targeted mutant mouse models, specifically *Spo11*-/- and *Dmc1*-/- females. *Spo11*-/- germ cells lack programmed DNA DSBs and have extensive asynapsis associated with γH2AFX domain formation (Baudat et al., 2000; Carofiglio et al., 2013; Daniel et al., 2011; Romanienko and Camerini-Otero, 2000). *Spo11-/-* females experience prophase I oocyte losses, resulting in fewer oocytes compared to wildtype females at birth (Di Giacomo et al., 2005).

Deletion of *Hormad1* rescues oocyte losses in *Spo11-/-* female mice (Daniel et al., 2011; Kogo et al., 2012b). HORMAD1 has been proposed to mediate *Spo11*-/- oocyte losses by being in involved in an asynapsis checkpoint, or via its role in meiotic silencing (Daniel et al., 2011; Kogo et al., 2012b). I test the role of the silencing model of *Spo11*-/- oocyte losses by *H2afx*-/- deletion experiments.

Finally, I test the role for H2AFX in the elimination of *Dmc1*-/- oocytes. *Dmc1*-/- mice fail to repair meiotic DNA DSBs, and *Dmc1*-/- oocytes are eliminated by a DNA damage checkpoint. To examine whether H2AFX is involved in this DNA damage checkpoint, I test whether *H2afx* ablation rescues *Dmc1*-/- oocyte losses.

4.1 A role for H2AFX in XO oocyte losses

4.1.1 Sub-staging XO *H2afx*-/- oocytes and identifying the asynapsed X chromosome

To address the role for meiotic silencing in XO oocyte losses, I generated and studied XO females lacking the essential silencing factor *H2afx.* XO *H2afx-/-* females were first examined using a chromosome spreads combined with immunostaining. First, I quantified the percentage of XO *H2afx*-/- oocytes with an asynapsed X chromosome between pachynema and late diplonema, the timeframe when XO oocytes are eliminated (**Figure 1.4**). As in my previous experiment, HORMAD1 immunostaining was used to sub-stage XO *H2afx-/-* oocytes into pachynema (**Figure 3.1a**), early diplonema (**Figure 3.1b**), and late diplonema (**Figure 3.1c**), based upon the extent of HORMAD1 staining.

In my previous oocyte elimination analyses, I used γH2AFX as a marker of the asynapsed X chromosome (see Figure 1). Since H2AFX is abolished in XO *H2afx*-/- females, I used another marker of asynapsis, namely HORMAD2, to identify the asynapsed X chromosome. HORMAD2 preferentially marks asynapsed chromosome axes, but unlike HORMAD1 does not accumulate on desynapsed axes, between pachynema and late diplonema (Wojtasz et al., 2009).

Using HORMAD1/HORMAD2 double-immunostaining, I was able to identify XO *H2afx*-/- oocytes with an asynapsed X chromosome at pachynema, early diplonema, and late diplonema. At pachynema, a subset of XO *H2afx*-/- oocytes contained a single asynapsed X chromosome, marked by HORMAD1/HORMAD2 (**Figure 3.1a, arrow**). In the remaining pachytene oocytes, the X chromosome achieved self-synapsis, and therefore the oocyte nucleus was negative for HORMAD1/HORMAD2 (not shown). During early and late diplonema, HORMAD1 accumulates on desynapsed chromosome axes (**Figure 3.1b-c, arrowheads**), and HORMAD2 preferentially mark the asynapsed X chromosome (**Figure 3.1b-c, arrows**).

During the process of breeding XO *H2afx*-/- females, I noticed that XO *H2afx*-/- mice were significantly smaller than XO *H2afx*+/- and XO *H2afx*+/+

littermates (**Figure 3.1d, table**). This was the case at all developmental ages analyzed, from 18.5 to 20.5 d*pc* (**Figure 3.1d, table**). This observation is consistent with previous work, which reported a growth delay in *H2afx*-/- mice (Celeste et al., 2002).

Due to this growth defect, I next examined whether oocyte progression was disrupted or delayed in XO *H2afx*-/- females. To address whether oocytes reach the end of prophase I, I analyzed XO *H2afx-/-* oocytes at 19.5 d*pc*, when a significant number of oocytes have reached late diplonema in wildtype females (**Figure 1.1**). Indeed, a significant percentage of XO *H2afx*-/- oocytes were at late diplonema at 19.5 d*pc*, indicating that *H2afx* is not required for completion of meiotic prophase I (**Figure 3.1e**).

Upon quantification of the percentage of 19.5 d*pc* oocytes at pachynema, early diplonema, and late diplonema, however, there was an apparent delay in oocyte progression, such that a substantial fraction of oocytes were at pachynema at 19.5 d*pc* (**Figure 3.1e**). Indeed, oocyte sub-staging revealed that XO *H2afx*-/- oocyte composition at 19.5 d*pc* was not significantly different from XO oocyte composition at 18.5 d*pc* (**Figure 3.1e**). This slight (~1 day) developmental delay in meiotic progression in XO *H2afx-/-* oocytes is likely linked to the overall growth delay in *H2afx-/-* mice (Celeste et al., 2002). I, therefore, focused the rest of my experiments on XO *H2afx*-/- ovaries from 19.5 d*pc* females.

Notably, I did not observe any significant difference in the proportion of oocytes at late diplonema between XO 18.5 d*pc* and XO *H2afx*-/- 19.5 d*pc* ovaries (**Figure 1.3e**), as might be expected if *H2afx* deletion rescued XO oocyte losses. However, this analysis may not be sensitive enough to identify a difference in oocyte losses, given that only a fraction of oocytes are in late diplonema at these ages. Addressing this requires quantitative analysis of ovaries containing mostly late diplotene oocytes (addressed in Section 4.1.3).

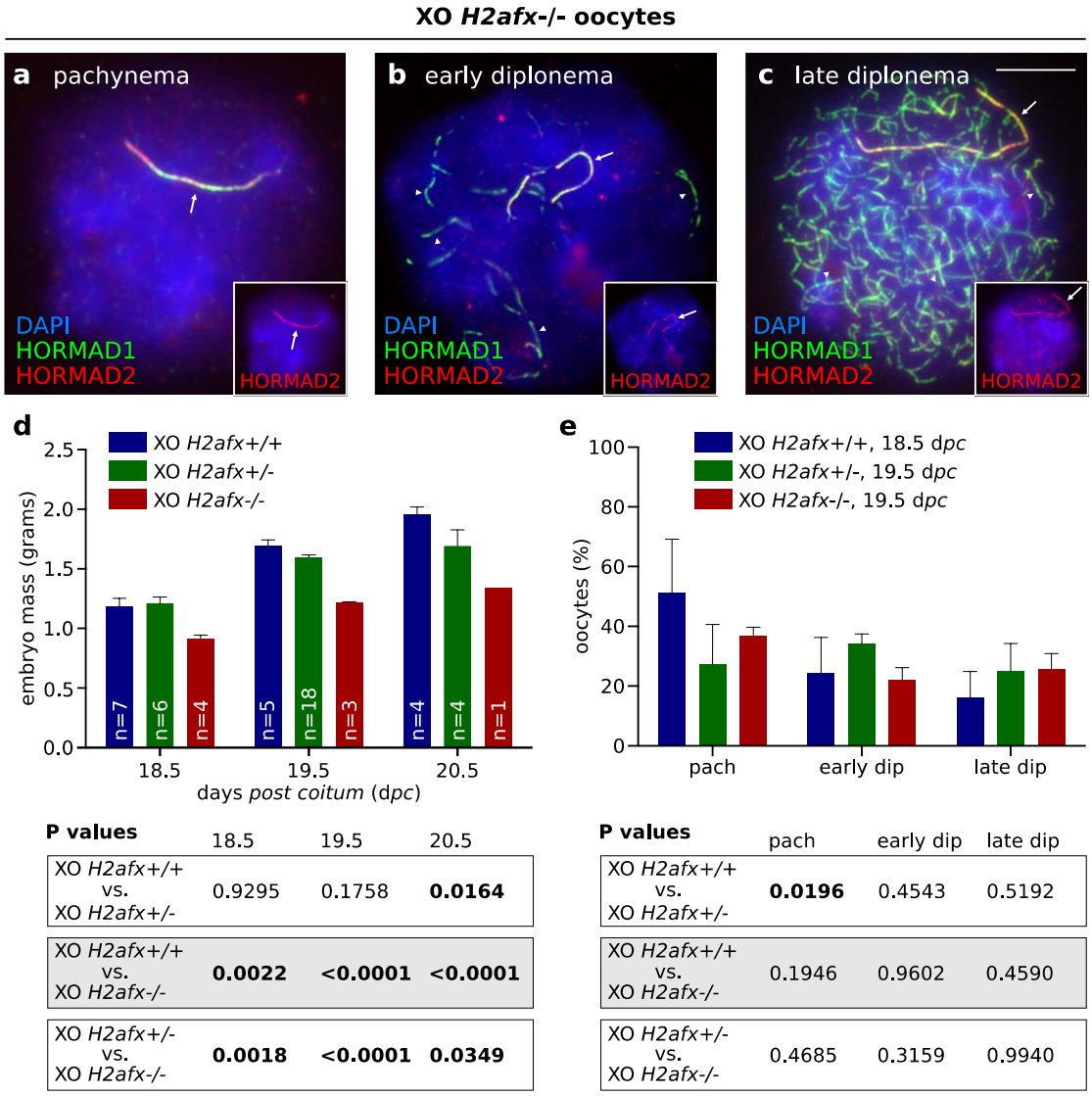

P values	18.5	19.5	20.5
XO *H2afx*+/+ vs. XO *H2afx*+/-	0.9295	0.1758	**0.0164**
XO *H2afx*+/+ vs. XO *H2afx*-/-	**0.0022**	**<0.0001**	**<0.0001**
XO *H2afx*+/- vs. XO *H2afx*-/-	**0.0018**	**<0.0001**	**0.0349**

P values	pach	early dip	late dip
XO *H2afx*+/+ vs. XO *H2afx*+/-	**0.0196**	0.4543	0.5192
XO *H2afx*+/+ vs. XO *H2afx*-/-	0.1946	0.9602	0.4590
XO *H2afx*+/- vs. XO *H2afx*-/-	0.4685	0.3159	0.9940

Figure 3.1. Characterization of XO *H2afx*+/- and XO *H2afx*-/- females.

(**a**) Pachytene XO *H2afx*-/- oocyte with an asynapsed X chromosome (arrow; marked by HORMAD1, green, and HORMAD2, red, and inset). (**b**) Early diplotene XO *H2afx*-/- oocyte, showing intermediate levels of desynapsis (HORMAD1, green) and an asynapsed X chromosome (arrow; marked with both HORMAD1 and HORMAD2, inset). (**c**) Late diplotene XO *H2afx*-/- oocyte, showing extensive desynapsis and an asynapsed X chromosome (arrow). Scale bar is 10μm. (**d**) Mass (g) of embryos of XO *H2afx*+/+, XO *H2afx*+/-, and XO *H2afx*-/- genotypes. Table shows P values from Tukey multiple comparison tests, with significance (P<0.05) shown in bold. (**e**) Mean percentage of oocytes at pachynema, early diplonema, and late diplonema. Table shows that XO *H2afx*+/+ at 18.5 d*pc* and XO *H2afx*-/- females at 19.5 d*pc* are not statistically significantly different in oocyte composition (grey shaded box).

4.1.2 Autosomal synapsis and DNA DSB repair in XO *H2afx*-/- oocytes

H2afx-/- mice have male-specific infertility associated with failed silencing of the X and Y chromosomes (Celeste et al., 2002; Fernandez-Capetillo et al., 2003). Besides the MSCI defect, *H2afx* deletion does not cause defects in autosomal synapsis or meiotic recombination in spermatocytes (Celeste et al., 2002). *H2afx-/-* females, on the other hand, are fertile, but produce a reduced litter size (Celeste et al., 2002). Whether *H2afx* deletion affects meiotic events, such as synapsis or recombination, in the female germ line is unclear.

To determine the effect of *H2afx* deletion on female meiotic events, I studied autosomal synapsis in XO *H2afx-/-* pachytene oocytes. There are two "normal" synaptic configurations expected in XO *H2afx*-/- oocytes: those with an asynapsed X chromosome and those with a self-synapsed X chromosome (**Figure 3.2a, arrow**). I therefore defined XO *H2afx*-/- oocytes as having asynapsed autosomes if they contained more than one asynapsed chromosome (**Figure 3.2b, arrows**).

Using HORMAD2 as a marker of asynapsis, I quantified the percentage of XO *H2afx-/-* oocytes with autosomal synaptic defects (i.e. >1 asynapsed chromosome) at 19.5 d*pc* (**Figure 3.2c**). For a comparison, the same analysis was performed on age-matched XO *H2afx+/-* females (**Figure 3.2c**). Notably, the percentage of pachytene oocytes with autosomal asynapsis was not significantly different between XO *H2afx-/-* and XO *H2afx+/-* females (T test, two-tailed, P=0.9813) (**Figure 3.2c**), indicating that autosomal synapsis is unaffected by *H2afx* deletion.

Next, I studied meiotic DNA DSB repair protein turnover in XO *H2afx*-/- oocytes. Because γH2AFX has been proposed to create a chromatin microenvironment favorable for DNA DSB repair (Srivastava et al., 2009), H2AFX accumulation on the asynapsed X chromosome in XO oocytes may be important for the localization and/or retention of DNA DSB repair proteins. To address this possibility, I analyzed the number of RPA foci on the asynapsed X chromosome in XO *H2afx-/-* oocytes.

To assess RPA turnover, I quantified the number of RPA foci on the asynapsed X chromosome in XO *H2afx*-/- oocytes at pachynema, early

diplonema, and late diplonema. At pachynema, there were on average 6 ±0.5 RPA foci on the X chromosome in XO *H2afx-/-* oocytes (**Figure 3.2d-f**). This is not significantly different from the 5 ±0.5 RPA foci on the asynapsed X chromosome in XO *H2afx+/+* oocytes (Tukey's test, P=0.9559), as determined earlier (see Figure 2.1). Notably, there were also no significant differences in the number of RPA foci on the asynapsed X chromosome between XO *H2afx-/-* and control XO oocytes at early and late diplonema (**Figure 3.2f**) (Tukey's test, P=0.9992 and P>0.9999, respectively).

As in normal XO oocytes, there was also a significant drop in the number of RPA foci on the asynapsed X chromosome between pachynema and early diplonema (mean=1.9 ±0.5 foci) in XO *H2afx-/-* oocytes (Tukey's test, P=0.0016) (**Figure 3.2f**). Thus, RPA foci do not persist on the asynapsed X chromosome beyond late pachynema in XO *H2afx-/-* oocytes. These data suggest that *H2afx* is not required for the resolution of DNA DSBs on the asynapsed X chromosome in XO oocytes, and that DSB repair is unaffected by *H2afx* deletion.

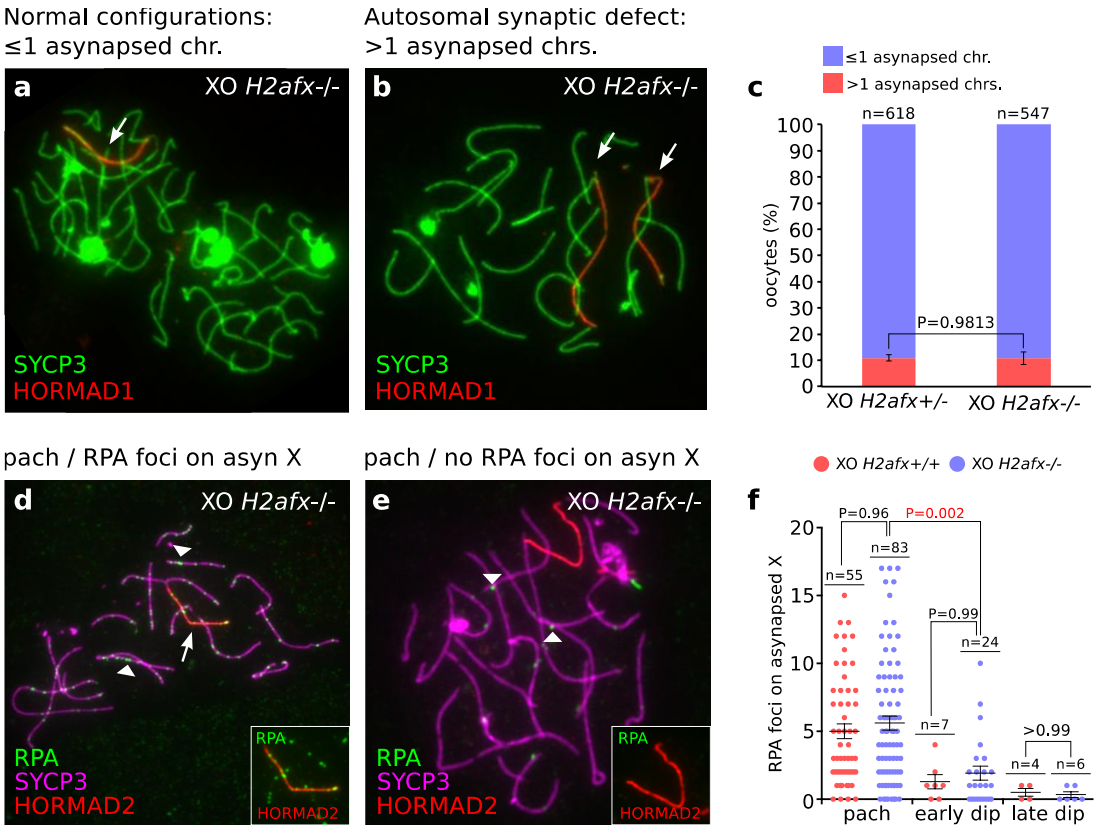

Figure 3.2. Autosomal synapsis and DNA DSB repair are unaffected in XO *H2afx*-/- oocytes.

(**a**) Pachytene XO *H2afx*-/- oocytes with normal synaptic configurations (≤1 asynapsed chromosomes): (top left cell) single asynapsed X chromosome (arrow), and (bottom right cell) self-synapsed X chromosome. (**b**) Pachytene XO *H2afx*-/- oocyte with an autosomal synapsis defect (>1 asynapsed chromosome, arrows). (**c**) The mean percentage of XO *H2afx*+/- and XO *H2afx*-/- pachytene oocytes with autosomal synaptic defects. P value from unpaired t test. (**d**) Pachytene XO *H2afx*-/- oocyte with numerous RPA foci on the asynapsed X chromosome (arrow). (**e**) Pachytene XO *H2afx*-/- oocyte with no RPA foci on the asynapsed X chromosome. (**f**) Number of RPA foci on asynapsed X chromosome in 19.5 d*pc* XO *H2afx*-/- oocytes and 18.5 d*pc* XO *H2afx*+/+ oocytes at pachynema, early diplonema and late diplonema. n is the number of oocytes analyzed. Tukey's multiple comparison test, P value significance (P<0.05) is shown in red.

4.1.3 XO *H2afx*-/- oocytes persist to late diplotene

Next, I tested the meiotic silencing model of oocyte loss by studying the survival of XO *H2afx-/-* oocytes with an asynapsed X chromosome. To address this, I quantified the percentage of oocytes with an asynapsed X chromosome in XO *H2afx*+/- and XO *H2afx*-/- females at 19.5 d*pc*, using HORMAD1/HORMAD2 dual immunostaining.

At pachynema, 52% of XO *H2afx*+/- oocytes had an asynapsed, HORMAD2-positive X chromosome (**Figure 3.3a**). This is similar to the percentage of XO *H2afx*+/+ oocytes with an asynapsed X chromosome at pachynema (56%), in which I used γH2AFX as a marker of the asynapsed X chromosome (**Figure 1.4c**). At early diplonema, 25% of XO *H2afx+/-* oocytes had an asynapsed X chromosome (Tukey's test, P=0.0008), and by late diplonema only 11% of oocytes had one (Tukey's test, P<0.0001) (**Figure 3.3a**). This trend is reminiscent of the oocyte losses in XO wildtype females, indicating that *H2afx* heterozygosity does not improve the survival of XO oocytes with an asynapsed X chromosome during meiotic prophase I.

Next, to evaluate the effect of *H2afx* nullizygosity on XO oocyte survival, I quantified the percentage of oocytes with an asynapsed X chromosome in XO *H2afx-/-* females at pachynema, early diplonema, and late diplonema at 19.5 d*pc*. At pachynema, 49% of XO *H2afx-/-* oocytes had an asynapsed X chromosome (**Figure 3.3b**). This is not significantly different from the percentage of XO *H2afx+/-* pachytene oocytes with an asynapsed X chromosome (Sidak's test, P=0.9625). Notably, at early diplonema, there was no significant drop in the percentage of XO *H2afx-/-* oocytes with an asynapsed X chromosome (47%) (Tukey's test, P=0.8885) (**Figure 3.3b**). At late diplonema, there was also no statistically significant drop in the percentage of XO *H2afx-/-* oocytes with an asynapsed X chromosome (39%) (Tukey's test, P=0.1851) (**Figure 3.3b**).

Therefore, XO *H2afx-/-* oocytes with an asynapsed X chromosome persist to the end of prophase I, such that at late diplonema there are 3.5 times as many oocytes with an asynapsed X chromosome compared to XO *H2afx+/-* females (Sidak's test, P=0.0004) (**Figure 3.3c**). By contrast, at pachynema, the percentage of oocytes with an asynapsed X chromosome

was not significantly different between XO *H2afx*-/- and XO *H2afx*+/- females (Sidak's test, P=0.9625), indicating that *H2afx* deletion has no effect on the percentage of oocytes with an asynapsed X chromosome at pachynema (**Figure 3.3c**). Together, these data suggests that XO oocyte losses are dependent on *H2afx* and occur exclusively during diplonema.

4.1.4 XO *H2afx*-/- oocytes with a non-phosphorylatable *H2afx* transgene persist to late diplonema

Serine-139 phosphorylation of H2AFX is the critical epigenetic event in meiotic silencing (Ichijima et al., 2011). To confirm that the H2AFX-dependent XO oocyte losses occur via S-139 phosphorylation, I examined oocyte survival in XO females carrying a non-phosphorylatable transgene of histone H2AFX (Celeste et al., 2003b). This *H2afx* transgene encodes a serine to alanine substation at position 139 (denoted $H2afx^{S139A}$), which prevents H2AFX phosphorylation at that residue (Celeste et al., 2003b).

For this analysis, I substaged oocytes into pachynema and diplonema using SYCP3 staining, and I identified the asynapsed X chromosome using BRCA1 staining, another marker of asynapsis (Kouznetsova et al., 2009; Turner et al., 2004). Pachytene oocytes have 20 SYCP3-positive chromosome pairs, while oocytes in diplonema show progressive desynapsis of SYCP3 cores (see Figure 1.1). BRCA1 is enriched on asynapsed chromosomes between pachynema and late diplonema in spermatocytes (Turner et al., 2004), and it has been used previously to identify the asynapsed X chromosomes in XO oocytes (Turner et al., 2005).

Unexpectedly, using SYCP3-BRCA1 double-immunostaining, I found that BRCA1 also gradually accumulates on desynapsing chromosome axes in oocytes as diplonema progresses (data not shown). At late diplonema, therefore BRCA1 labels all chromosome axes, in a manner reminiscent of HORMAD1. However, at early diplonema the staining of BRCA1 on the asynapsed X chromosome is more intense that on desynapsed axes (data not shown). Due to this unexpected limitation in substaging, I focused my analysis only at pachynema and early diplonema, the time period when significant H2AFX-dependent XO oocyte losses occur (**Figure 3.3c**).

If H2AFX S-139 phosphorylation is a critical event for XO oocyte losses, then the percentage of XO *H2afx-/- H2afx*^{S139A} oocytes with an asynapsed X chromosome should not change between pachynema and early diplonema. In the control XO *H2afx*+/- *H2afx*^{S139A} females, there was a significant drop in the percentage of oocytes with an asynapsed X chromosome between pachynema and early diplonema (T test, P=0.0432) (**Figure 3.3d**). By contrast, in XO *H2afx*-/- *H2afx*^{S139A} females, the percentage of oocytes with an asynapsed X chromosome did not change between pachynema and diplonema (T test, P=0.1495) (**Figure 3.3d**). While the percentage of oocytes at pachynema was not different between the genotypes (Sidak's test, P=0.3835), there was a substantially higher percentage of diplotene oocytes in XO *H2afx*-/- *H2afx*^{S139A} females (Sidak's test, P=0.0063) (**Figure 3.3d**). This confirms that H2AFX phosphorylation at S-139 is a critical epigenetic event in the elimination of XO oocytes with asynapsis.

4.1.5 XO *H2afx*-/- females have more oocytes than XO females perinatally

Compared to XX females, XO females have approximately half the number of oocytes at birth (19.5-20.5 d*pc*) (Burgoyne and Baker, 1985). I therefore examined whether the oocyte rescue observed in XO *H2afx-/-* females by surface spread analysis results in an increased oocyte pool compared to XO females. To address this, I quantified the number of oocytes in XO and XO *H2afx*-/- ovaries at 20.5 d*pc*, when all oocytes have progressed to late diplonema (Burgoyne and Baker, 1985). I identified oocytes histologically in DAPI-stained ovarian sections based upon their unique nuclear morphology, as described previously (Burgoyne and Baker, 1985). The total oocyte numbers per ovary were estimated by summing oocyte counts from every 10th section in serial sectioned ovaries (Daniel et al., 2011).

Using this approach, I compared the number of oocytes in XX *H2afx*+/+, XO *H2afx*+/-, and XO *H2afx-/-* ovaries at 20.5 d*pc*. In XX *H2afx*+/+ females, there were on average 1223 ±89 oocytes. By comparison, in XO

H2afx+/- females, which experience oocyte losses similar to XO females (see Figure 3.3b), there were 40% fewer oocytes (759 ±72) at 20.5 d*pc* (Sidak's test, P=0.0087) (**Figure 3.3e**), consistent with previous results on XO females (Burgoyne and Baker, 1985).

Notably, XO *H2afx-/-* females had over 40% more oocytes compared to XO *H2afx*+/- females (Sidak's test, P=0.0301) (**Figure 3.3e**). In fact, XO *H2afx-/-* females had oocyte numbers comparable to XX *H2afx*+/+ females (Sidak's test, P=0.2447) (**Figure 3.3e**). In conclusion, abrogating meiotic silencing in XO oocytes by deleting *H2afx* rescues diplotene oocyte losses and increases the perinatal oocyte pool (**Figure 3.3f**). These genetic studies support that H2AFX-dependent meiotic silencing is the proximal trigger of oocyte loss in mice with chromosome abnormalities.

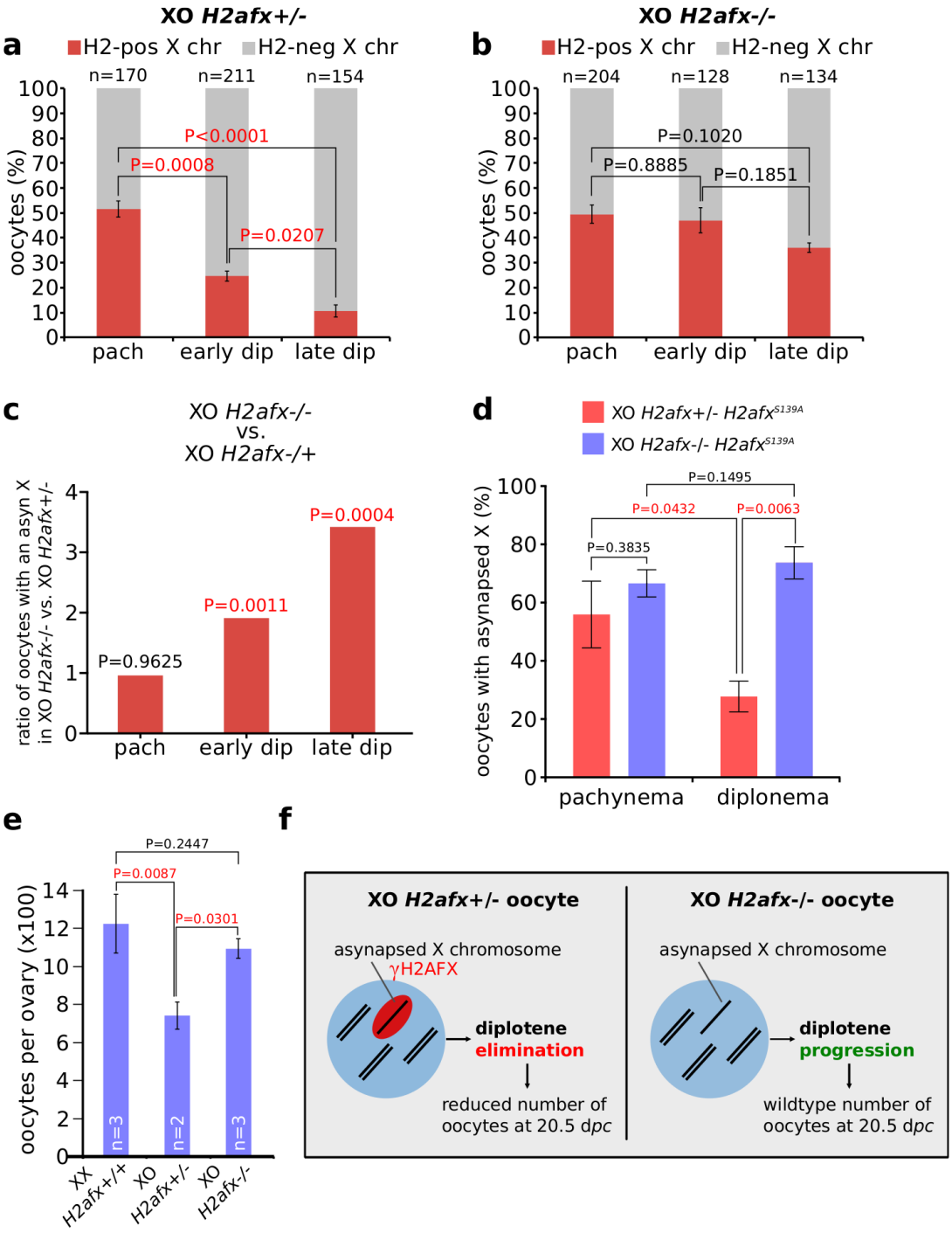

Figure 3.3. *H2afx* is required for the elimination of XO oocytes with an asynapsed X chromosome.

(**a**) Mean percentage of XO *H2afx+/-* oocytes with an asynapsed X chromosome (HORMAD1 and HORMAD2 double-positive) between pachynema and late diplonema at 19.5 d*pc*. Tukey multiple comparison test. (**b**) Mean percentage of XO *H2afx-/-* oocytes with an asynapsed X chromosome between pachynema and late diplonema at 19.5 d*pc*. Tukey test. (**c**) Enrichment of oocytes with an asynapsed X chromosome in XO *H2afx-/-* compared to XO *H2afx+/-*. Enrichment is the ratio of the mean percentage of oocytes with an asynapsed X at each stage in XO *H2afx-/-*

versus XO *H2afx+/-* control. (**d**) The mean percentage of oocytes with an asynapsed X chromosome at pachynema and diplonema (early) in XO *H2afx-/- H2afx*^{S139A} females and XO *H2afx+/- H2afx*^{S139A} controls. The asynapsed X chromosome was identified by BRCA1 staining (not shown). (**e**) Mean number of oocytes in XX *H2afx+/+*, XO *H2afx+/-*, and XO *H2afx-/-* females at 20.5 d*pc*. n is the number of non-littermate ovaries analyzed. Tukey tests. (**f**) Summary demonstrating the importance of H2AFX in XO oocyte elimination.

4.2 A role for H2AFX in *Spo11*-/- oocyte losses

4.2.1 γH2AFX domain frequency in *Spo11*-/- oocytes

I then tested whether H2AFX is also important for the elimination of *Spo11*-/- oocytes, since meiotic silencing has been hypothesized to be a cause of oocyte losses in this mutant (Burgoyne et al., 2009; Daniel et al., 2011). In my analysis of *Spo11*-/- oocytes, I first examined the frequency of γH2AFX domains. Using SYCP3/HORMAD1/γH2AFX triple-immunostaining on chromosome spreads, I found that 62% of *Spo11*-/- oocytes had a γH2AFX domain at 18.5 d*pc* (**Figure 3.4a,c**). The remaining *Spo11*-/- oocytes did not have a γH2AFX domain, despite having high levels of asynapsis (**Figure 3.4b,c**). These results are comparable with an independent analysis of *Spo11*-/- oocytes (Carofiglio et al., 2013).

If meiotic silencing drives *Spo11*-/- oocyte losses, then the frequency of γH2AFX domains in *Spo11*-/- oocytes should decrease during progression to late diplonema. Addressing this possibility in *Spo11*-/- females is challenging because high levels of asynapsis preclude accurate substaging of oocytes. To circumvent this limitation, I estimated pachynema to diplonema progression by analyzing ovaries from 18.5 and 20.5 d*pc*, the developmental period when oocytes progress from pachynema and late diplonema.

Based on previous work, a 40% reduction in oocyte numbers in *Spo11*-/- females is observed at 19.5-20.5 d*pc* (Di Giacomo et al., 2005). Therefore, I expected to see a decrease in γH2AFX domain frequency by 20.5 dpc. Indeed, the percentage of *Spo11*-/- oocytes with a γH2AFX domain dropped to 51% at 19.5 dpc (T test, P=0.0324)(**Figure 3.4c**). Furthermore, at 20.5 dpc, when nearly all oocytes have progressed to late diplonema, only 35% of *Spo11*-/- oocytes had a γH2AFX domain (**Figure 3.4c**). This nearly two-fold drop in the frequency of γH2AFX domains from 18.5 to 20.5 d*pc* indicates that a significant proportion of *Spo11*-/- oocytes with a γH2AFX domain are eliminated by late diplonema.

4.2.2 *H2afx* nullizygosity increases *Spo11*-/- oocyte numbers perinatally

To genetically test a role for H2AFX in *Spo11*-/- oocyte arrest, I generated *Spo11*-/- *H2afx*-/- females and assessed oocyte survival. Since substaging *Spo11*-/- oocytes is challenging, I measured oocyte survival by quantifying the number of oocytes in sectioned ovaries. I counted oocyte numbers histologically using DAPI-stained ovarian sections, and compared the number of oocytes in *Spo11*-/- and *H2afx*-/- *Spo11*-/- females at 20.5 d*pc*, when a 40% oocyte loss was previously reported in *Spo11*-/- females (Di Giacomo et al., 2005).

At 20.5 dpc, *Spo11*-/- females had on average only 339 ±68 oocytes (**Figure 3.4d**), roughly 30% the number of oocytes found in XX *H2afx*+/+ ovaries (**Figure 3.4d**). This more severe reduction in *Spo11*-/- oocyte numbers compared to what was reported previously (Di Giacomo et al., 2005) may reflect methodological counting differences or genetic strain variation. Notably, age-matched *H2afx*-/- *Spo11*-/- females had nearly twice the number of oocytes (mean=622 ±21) as *Spo11-/-* females (T test, P=0.0161) (**Figure 3.4d**). This indicates that *H2afx* deletion alleviates some *Spo11*-/- prenatal oocyte losses.

However, despite the increased number of oocytes in *H2afx*-/- *Spo11*-/- females compared to *Spo11*-/- females, this rescue is only partial. Indeed, *H2afx*-/- *Spo11*-/- females have only 50% the number of oocytes as XX *H2afx*+/+ control females (mean=1223 ±89) (**Figure 3.4d**). This lower oocyte number in *H2afx*-/- *Spo11*-/- may be due to an effect that *H2afx-/-* has on oocyte numbers, which would mask a full rescue. To address this, I compared the number of oocytes in *H2afx*-/- *Spo11*-/- female to age-matched XX *H2afx-/-* females. While XX *H2afx*-/- females have on average more oocytes (mean=1027 ±203) compared to *H2afx*-/- *Spo11*-/- females (**Figure 3.4d**), the difference is not statistically significant (T test, P=0.1176). The mean number of oocytes is also not significantly different between XX *H2afx*-/- and XX *H2afx*+/+ females at 20.5 d*pc* (T test, P=0.4259).

In summary, the 2-fold increase in oocyte numbers in *H2afx*-/- *Spo11*-/- females compared to *Spo11*-/- females suggests that H2AFX has a role in the elimination of *Spo11*-/- oocytes perinatally.

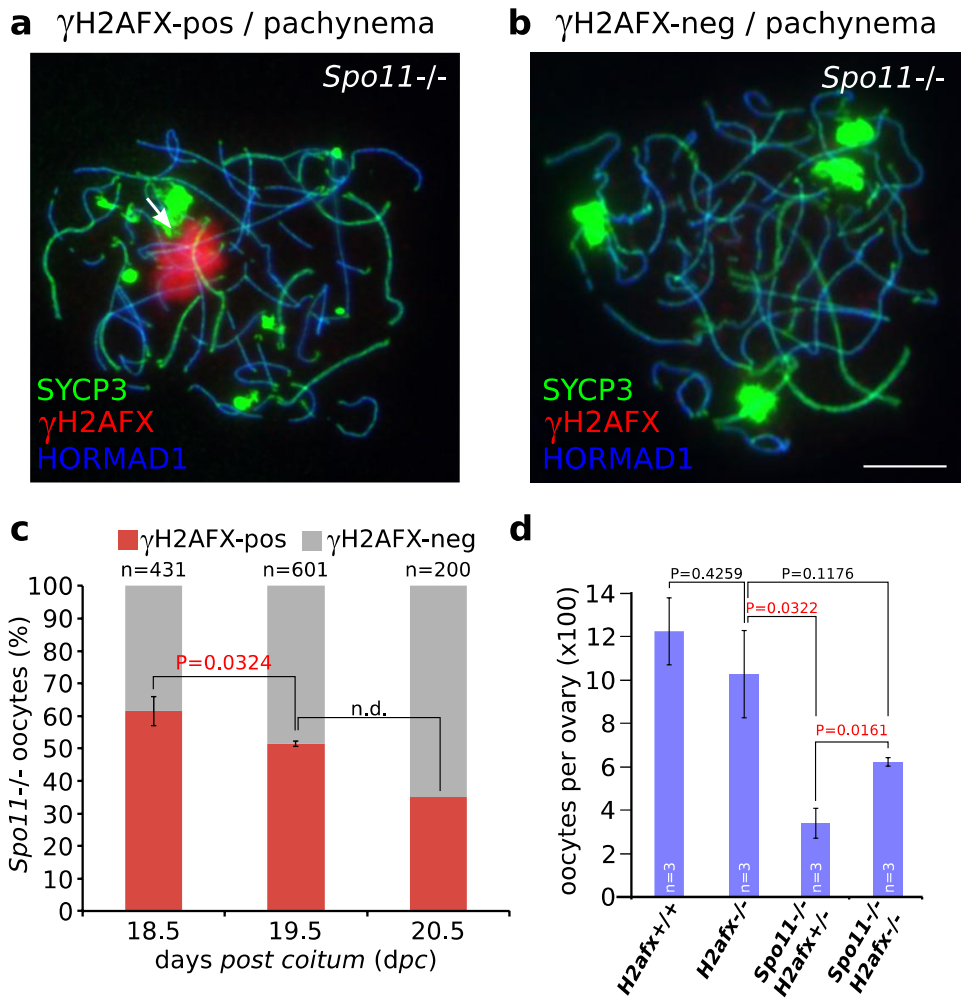

Figure 3.4. *H2afx* nullizygosity increases *Spo11*-/- oocyte numbers perinatally.

(**a**) *Spo11*-/- oocyte with severe asynapsis (HORMAD1-positive chromosomes) and a γH2AFX domain. (**b**) *Spo11*-/- oocyte with severe asynapsis and no γH2AFX domain. (**c**) The mean percentage of *Spo11*-/- oocytes with a γH2AFX domain at 18.5, 19.5, and 20.5 d*pc*, corresponding to the transition from pachynema to late diplonema. (**d**) Mean number of oocytes in *H2afx*+/+, *H2afx*+/-, *Spo11*-/- *H2afx*+/-, and *Spo11*-/- *H2afx*-/- females at 20.5 d*pc*. n is the number of non-littermate ovaries analyzed. Tukey tests were used to calculate P values, significant P values shown in red.

4.2.3 SPO11-independent DNA DSBs in oocytes

Based on other studies, the γH2AFX domains in *Spo11*-/- spermatocytes rarely encompass the X and Y chromosomes, but rather occur on a random subset of asynapsed chromosomes (Bellani et al., 2005; Mahadevaiah et al., 2008). This finding raises the question of what feature of asynapsis targets γH2AFX to a specific region of asynapsis.

Previous work on irradiated mice carrying translocations has suggested that meiotic silencing may be triggered or enhanced by DNA DSBs (Inagaki et al., 2010; Schoenmakers et al., 2008). However, it is difficult to marry this hypothesis with the fact that *Spo11*-/- germ cells have a meiotic silencing response without programmed DNA DSBs. Therefore, I decided to re-examine DNA DSBs in *Spo11*-/- germ cells.

To address this, I immunostained *Spo11*-/- oocytes for SYCP3 to label chromosome axes, γH2AFX to identify regions of silencing, and one of three DSB repair proteins, RAD51, DMC1, and RPA, to identify an potential DNA DSBs. I focused my analysis on *Spo11*-/- oocytes from 18.5 d*pc* females. Strikingly, I observed a small number of RAD51, DMC1, and RPA foci in a subset of *Spo11*-/- oocytes (**Figure 3.5a-c**). Furthermore, 82% of *Spo11*-/- oocytes with a γH2AFX domain contained at least one RPA focus (**Figure 3.5e**). These DNA DSB repair foci were located on chromosome axes, and 48% of the time they were found within the γH2AFX domains (**Figure 3.5e**).

To determine whether a correlation exists between DNA DSBs and meiotic silencing in *Spo11*-/- oocytes, I then assessed the degree of overlap between RPA foci and γH2AFX domains. Of the cells containing RPA foci, 59% (n=29/49) had at least one RPA foci co-localizing with a γH2AFX domain. To determine if this frequency of RPA/γH2AFX overlap was higher than expected by random chance, I compared the percentage area of the γH2AFX domain to the oocyte nucleus to the percentage of RPA foci within γH2AFX domains. Of those cells with at least RPA foci, the percentage of the nuclear RPA foci that co-localized with the γH2AFX domains (21%) was nearly three times greater than the fraction of the nucleus that was covered by the γH2AFX domain (8% of the total area). This suggests a higher

frequency of DNA DSB repair proteins associated with γH2AFX domain than expected due to chance. These findings have also been confirmed by an independent group (Carofiglio et al., 2013)(Carofiglio et al., 2013)(Carofiglio et al., 2013)(Carofiglio et al., 2013)(Carofiglio et al., 2013)(Carofiglio et al., 2013)(Carofiglio et al., 2013)(Carofiglio et al., 2013)(Carofiglio et al., 2013)(Carofiglio et al., 2013).

In summary, DNA DSB repair foci occur in small numbers in *Spo11*-/- oocytes and they are frequently associated with γH2AFX domains. The co-localization of repair foci and γH2AFX domains opens the possibility that meiotic silencing requires DNA DSBs. Furthermore, it is possible that a DNA damage may contribute to some *Spo11*-/- oocyte losses.

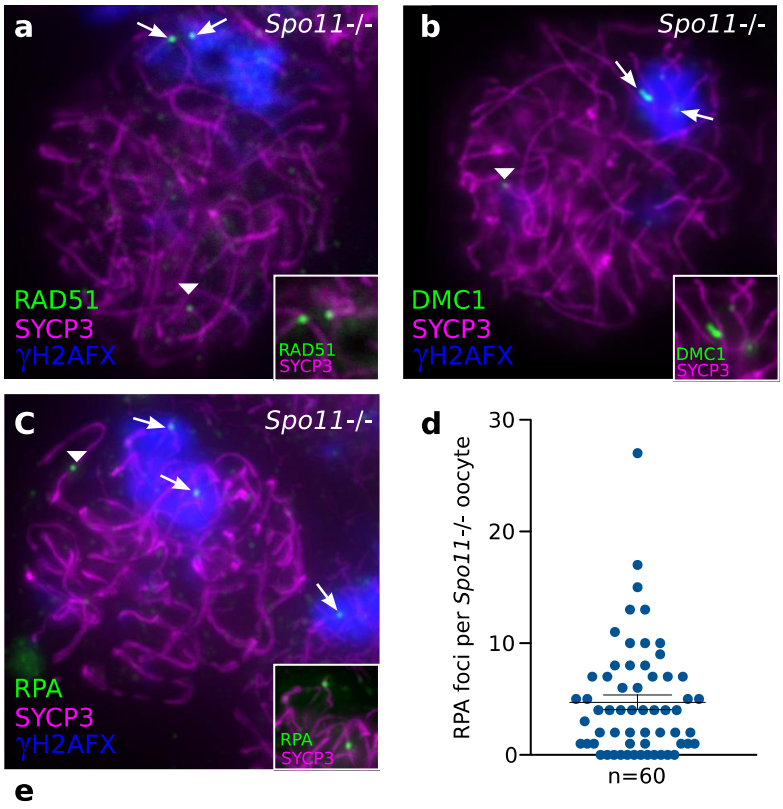

e

Quantitation of RPA foci in *Spo11*-/- oocytes	
Spo11-/- oocytes with a γH2AFX domain	n=60
Oocytes with at least one RPA foci	82% (n=49/60)
Oocytes with no RPA foci	18% (n=11/60)
Spo11-/- oocytes with RPA foci in the γH2AFX domain	48% (n=29/60)
Average number of RPA foci	8.9
Average number of RPA foci in the γH2AFX domain	2.3
RPA foci that co-localize with chromosome axes	99% (n=66/67)
Spo11-/- oocytes with no RPA foci in the γH2AFX domain	53% (n=32/61)
Average number of RPA foci in nuclei	2.0

Figure 3.5. DNA DSB repair foci in *Spo11*-/- oocytes.

(**a**) *Spo11*-/- oocyte with RAD51 foci on chromosome axes surrounded by a γH2AFX domain (arrow, inset), and on chromosome axes outside of the domain (arrowhead). (**b**) *Spo11*-/- oocyte with DMC1 foci on chromosome axes surrounded by a γH2AFX domain (arrow, inset), and on chromosome axes outside of the domain (arrowhead). (**c**) *Spo11*-/- oocyte with RPA foci on chromosome axes surrounded by a γH2AFX domain (arrow, inset), and on chromosome axes outside of the domain (arrowhead). (**d**) Number of RPA foci within *Spo11*-/- nuclei. N=60 oocytes were analyzed. (**e**) Quantitative characterization of RPA foci in *Spo11*-/- oocytes.

4.3 H2AFX is not required for elimination of *Dmc1*-/- oocytes

I next tested if H2AFX has a role in a meiotic DNA damage checkpoint, as has been described in somatic cells (Srivastava et al., 2009). Previous meiotic studies of the DNA damage checkpoint pathway have focused on *Dmc1-/-* female mice (Di Giacomo et al., 2005). *Dmc1-/-* mice fail to repair meiotic DNA DSBs, resulting in persistent unrepaired DNA DSBs, synaptic defects, and infertility in both sexes (Pittman et al., 1998; Yoshida et al., 1998). *Dmc1*-/- females have half the number of oocytes at birth, indicating a significant wave of oocyte loss occurring by the end of meiotic prophase I.

Unlike in the case of the asynapsed X chromosome in XO oocytes, in which RPA foci are resolved by late pachynema, *Dmc1*-/- oocytes have persistent RPA foci into diplonema (**Figure 3.6a**). *Dmc1*-/- oocytes do not form a γH2AFX domain (i.e. do not mount a meiotic silencing response), presumably because the upstream silencing factors BRCA1 and ATR are sequestered at unrepaired DSBs (Mahadevaiah et al., 2008).

Previous work has shown that preventing DNA DSB formation in *Dmc1*-/- females, via *Spo11* mutation, alleviates their oocyte losses, linking persistent unrepaired DSBs to oocyte arrest (Di Giacomo et al., 2005). If H2AFX is also involved in this DNA DSB-dependent mechanism of oocyte losses, *H2afx* deletion should also rescue *Dmc1*-/- oocyte losses.

To test this possibility, I quantified oocyte counts on sectioned ovaries from *Dmc1*-/- females and *H2afx*-/- *Dmc1*-/- females at 20.5 d*pc*. At this age, *Dmc1*-/- females contained on average 246 ±52 oocytes (**Figure 3.6b**). This is similar to the number of oocytes that I found in age-matched *Spo11*-/- females (T test, P=0.3396) (see Figure 3.4d), which have been reported to experience a similar degree of oocyte loss at birth (Di Giacomo et al., 2005).

Notably, age-matched *H2afx*-/- *Dmc1*-/- females had a similar number of oocytes (268 ±109) as *Dmc1*-/- single mutants (Tukey's test, P=0.9996) (**Figure 3.6b**). Therefore, *H2afx* nullizygosity does not alleviate

prenatal *Dmc1*-/- oocyte losses, indicating that *H2afx* does not function in a persistent DNA damage checkpoint in mammalian meiosis.

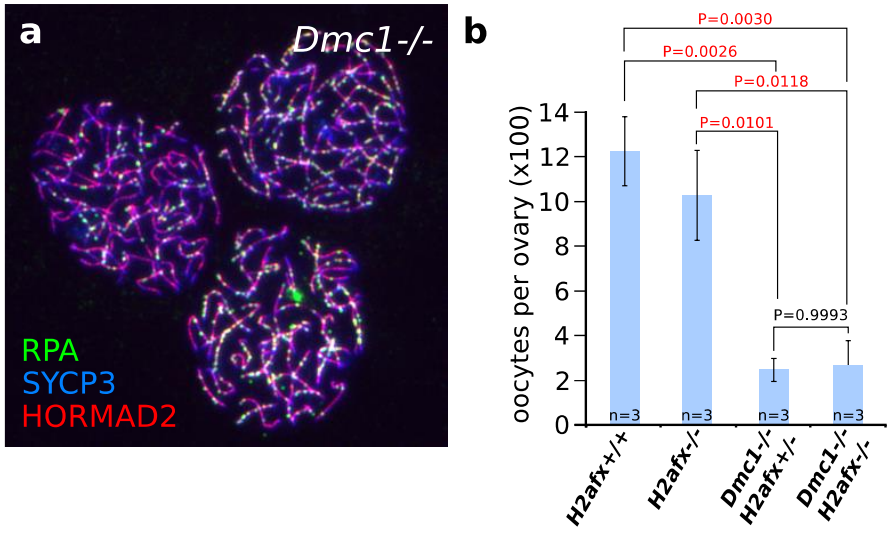

Figure 3.6. *H2afx* is not required for the elimination of *Dmc1*-/- oocytes.

(**a**) Representative image of three *Dmc1*-/- oocytes from 19.5 d*pc* ovaries, when meiosis has reached diplonema. Each oocyte has widespread asynapsis, as shown by SYCP3 (blue) and HORMAD2 (red) co-localization, and persistent RPA foci (green) (n=50 oocytes). (**b**) Mean number of oocytes in *H2afx*+/+, *H2afx*-/-, *Dmc1*-/- *H2afx*+/-, and *Dmc1*-/- *H2afx*-/- females at 20.5 d*pc*. n is the number of non-littermate ovaries analyzed. Tukey multiple comparison tests. Significant P values shown in red.

4.4 Discussion

My results from the previous chapter indicate that neither persistent DNA DSBs nor asynapsis *per se* are likely contributors to oocyte arrest in chromosomally abnormal mice, and instead support a role for meiotic silencing. In this chapter, I directly examined the contribution of the meiotic silencing model of oocyte losses in mice with chromosome abnormalities. To formally address this model, I tested whether genetically ablating meiotic silencing via *H2afx* deletion would prevent diplotene oocyte elimination in the XO mouse model system.

Notably, I found that *H2afx* relieves XO oocyte losses and restored oocyte numbers to wildtype levels at 20.5 d*pc*. Since *H2afx* deletion did not impacted the number of pachytene oocytes with an asynapsed X chromosome, I conclude that H2AFX-dependent oocyte losses occur at diplonema. I also showed XO diplotene oocyte rescue in females carrying a non-phosphorylatable form of histone H2AFX mutated at serine-139. Since serine-139 phosphorylation of H2AFX is the critical epigenetic event in silencing (Ichijima et al., 2011), this implicates meiotic silencing as the mechanism by which XO oocytes with asynapsis are eliminated.

These findings are inconsistent with the hypothesis that silencing shields asynapsed chromosomes from triggering arrest (Checchi and Engebrecht, 2011). Under this scenario, oocytes with silenced, asynapsed chromosomes in XO, In(X)1H, T43H and XX females would be protected from elimation, and genetic ablation of silencing in XO females would trigger, rather than prevent oocyte loss. Based on my rescue data, I suspect that the prophase I meiotic surveillance functions of HORMAD1, HORMAD2, BRCA1, ATR, MDC1, and γH2AFX are executed via meiotic silencing. This would account for the striking fact that all of these proteins have been shown to be essential components of the meiotic silencing pathway (Daniel et al., 2011; Fernandez-Capetillo et al., 2003; Ichijima et al., 2011; Shin et al., 2010; Turner et al., 2004; Wojtasz et al., 2012).

Importantly, *H2afx* nullizygosity did not influence HORMAD1 and HORMAD2 localization to the asynapsed X chromosome (**Figure 3.1a-c**) .

This indicates that the presence of HORMAD1/2 on asynapsed chromosomes is not sufficient to drive oocyte losses. Furthermore, during male meiosis, accumulation of HORMAD1, HORMAD2, BRCA1, ATR, MDC1, and γH2AFX at asynapsed autosomes is associated with prophase I arrest, but localization of the same proteins to the asynapsed X and Y chromosomes is not.

The meiotic silencing model readily explains this paradox. In contrast to the autosomes, the sex chromosomes are dramatically depleted in genes required for male meiosis (Khil et al., 2004; Wang, 2004). Furthermore, the silencing of X-linked housekeeping genes is compensated for by a unique system of autosomally-located, X-derived retrogenes. These are expressed in male but not in female germ cells and are essential for spermatogenesis (Bradley et al., 2004; McCarrey and Thomas, 1987; Wang, 2004).

Therefore, in contrast to silencing of autosomes, silencing of sex chromosomes in the male would not trigger arrest. By extrapolation, I predict that asynapsed accessory chromosomes would also not cause prophase I elimination in the male. Indeed, studies of the Tc1 male mouse indicated that no prophase I losses occur in response to the asynapsed h21 chromosome (Mahadevaiah et al., 2008).

To validate that meiotic silencing is a mechanism by which oocytes with asynapsis are eliminated, I then tested the effect of deleting *H2afx* in *Spo11*-/- females. Indeed, deletion of *H2afx* resulted in a two-fold increase in oocyte numbers in *Spo11-/-* females at 20.5d*pc*. However, in contrast to the complete rescue of *Spo11*-/- oocyte losses by *Hormad1* deletion, loss of *H2afx* only resulted in partial rescue, since *H2afx*-/- *Spo11*-/- had only half the wildtype numbers of oocytes at 20.5 d*pc*. This suggests that multiple mechanisms may be functioning to eliminate *Spo11*-/- oocytes.

In agreement with a recent report (Carofiglio et al., 2013)(Carofiglio et al., 2013)(Carofiglio et al., 2013)(Carofiglio et al., 2013)(Carofiglio et al., 2013)(Carofiglio et al., 2013)(Carofiglio et al., 2013)(Carofiglio et al., 2013)(Carofiglio et al., 2013)(Carofiglio et al., 2013), I observed the presence of DNA repair foci indicative of DNA DSBs in *Spo11*-/- oocytes (**Figure 3.5**). The origin of non-programmed DNA DSBs in *Spo11*-

/- germ cells is unclear, but may involve several different mechanisms. First, DNA DSBs generated at stalled replication forks may be carried over from meiotic S phase (Inagaki et al., 2009). Second, DNA DSBs have been shown to occur at sites of active transcription (Aguilera, 2002). Third, there may be de-repression of transposable genetic elements, such as *Line1* elements, which are capable of generating *Spo11*-independent DNA DSBs (Malki et al., 2014; Soper et al., 2008). Other possibilities include exogenous DNA damage agents, include reactive oxygen species or dysregulation of topoisomerase activity (Carofiglio et al., 2013)(Carofiglio et al., 2013)(Carofiglio et al., 2013)(Carofiglio et al., 2013)(Carofiglio et al., 2013)(Carofiglio et al., 2013)(Carofiglio et al., 2013)(Carofiglio et al., 2013)(Carofiglio et al., 2013)(Carofiglio et al., 2013)(Carofiglio et al., 2013). More work is required to further characterize the nature and origin of *Spo11*-independent DNA DSBs.

Surprisingly, DNA repair foci were located within the γH2AFX silencing domain more often than would be expected due to random chance, in agreement with a recent report (Carofiglio et al., 2013)(Carofiglio et al., 2013)(Carofiglio et al., 2013)(Carofiglio et al., 2013)(Carofiglio et al., 2013)(Carofiglio et al., 2013)(Carofiglio et al., 2013)(Carofiglio et al., 2013)(Carofiglio et al., 2013)(Carofiglio et al., 2013)(Carofiglio et al., 2013). Historically, it was believed that the meiotic silencing occurs independent of DNA DSBs since a meiotic silencing response occurs in *Spo11*-/- oocytes (Mahadevaiah et al., 2001). However, these new observations that *Spo11*-/- oocytes have small numbers of DNA DSB repair foci opens up the possibility the meiotic silencing requires DNA DSBs.

Interestingly, HORMAD1 regulates both meiotic silencing and DNA repair, and loss of *Hormad1* can rescue both *Spo11*-/- and *Dmc1*-/- oocyte losses (Daniel et al., 2011; Kogo et al., 2012b; Shin et al., 2013). It is possible, therefore, that *Hormad1* deletion fully rescues *Spo11*-/- oocyte losses because HORMAD1 functions in two or more distinct meiotic surveillance mechanisms. By contrast, the partial rescue observed in *H2afx*-/- *Spo11*-/- mutants suggests that H2AFX-dependent losses occur through disruption of a single pathway (i.e. meiotic silencing).

Additional proof that H2AFX-dependent oocyte losses occur through meiotic silencing and not a DNA damage checkpoint mechanism comes from my analysis of *Dmc1*-/- mutant females. In *Dmc1*-/- females, oocyte losses are triggered by persistent unrepaired DNA DSBs, and while γH2AFX is observed at these DNA DSBs, it does not spread to surrounding chromatin or induce meiotic silencing (Mahadevaiah et al., 2008). Notably, deletion of *H2afx* had no effect on oocyte numbers in *Dmc1*-/- females. This suggests that H2AFX acts at the level of asynapsed chromatin to exert its role in oocyte elimination, and that H2AFX plays an important role in the response to asynapsis but not in the response to persistent DNA damage. In summary, the data in this chapter strongly support a mechanism of prophase I surveillance of asynapsis that is mediated through an H2AFX-dependent meiotic silencing mechanism (**Figure 3.7**).

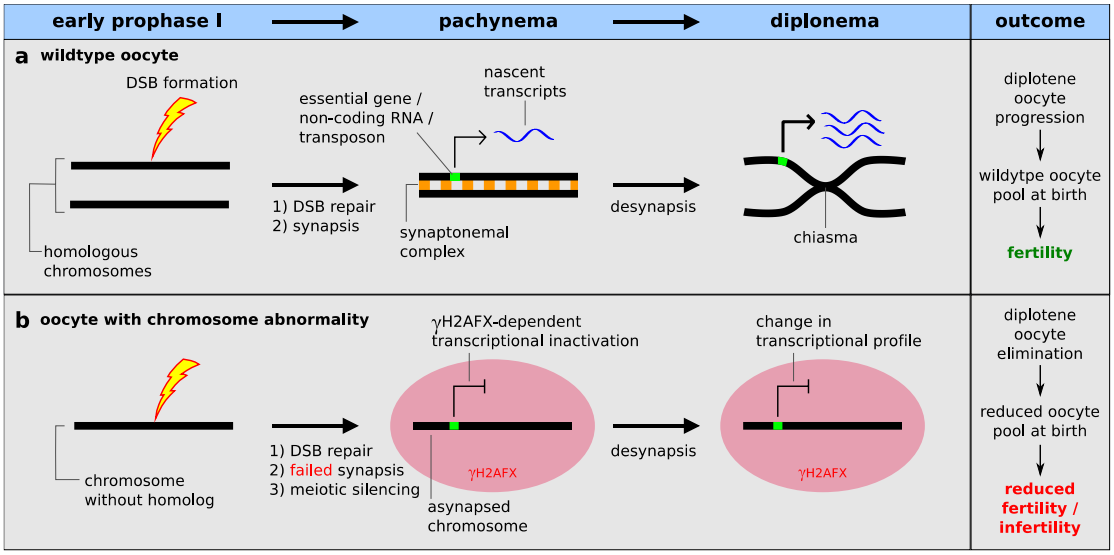

Figure 3.7. Meiotic silencing model of prophase I oocyte elimination.

(**a**) Wildtype oocyte. Meiotic DNA DSBs are formed during early prophase I by SPO11 (lightening bolt). During pachynema, homologous chromosomes synapse and meiotic DNA DSB are repaired (DNA DSB repair proteins shown as a red star). At diplonema, homologs desynapse but remain connected at crossover sites (chiasma). Transcription of genes (green) increases between pachynema and diplonema (nascent transcripts=blue ribbon). (**b**) Events in oocytes containing a chromosome abnormality that disrupts meiotic synapsis. Meiotic DNA DSBs, formed in early prophase I, are repaired on both synapsed and asynapsed chromosomes during pachynema. At this point, the asynapsed chromosome, triggers meiotic silencing, marked by chromatin enrichment of γH2AFX (red domain). The downstream consequence of this would be silencing of essential genes and oocyte elimination.

5 Results: Characterization of meiotic silencing in oocytes

Chromosome abnormalities confer more severe germ cell loss in males than in females (Burgoyne et al., 2009; Hunt and Hassold, 2002). This is due in part to the reduced stringency of the metaphase I spindle checkpoint in females (LeMaire-Adkins et al., 1997; Nagaoka et al., 2011), but is also thought to reflect ill-defined sex differences in the efficacy of the prophase I response to asynapsis (Hunt and Hassold, 2002; Nagaoka et al., 2012). Consistent with this, I noted that not all XO, In(X)1H, T43H, and XX oocytes with asynapsis were eliminated by late diplonema (see Figure 1). In this chapter, I attempt to identify a possible mechanistic basis for the sexual dimorphism in prophase I germ cell losses.

In the previous chapter, I provided evidence that supports the meiotic silencing model of oocyte loss in mice with chromosome abnormalities. With the overall goal of understanding sex-specific differences in prophase I surveillance, I therefore set out to characterize the meiotic silencing response in mammalian germ cells at the transcriptional and epigenetic levels.

In this chapter, I will study the efficiency of meiotic silencing in oocytes compared to spermatocytes using single and triple gene-specific RNA FISH in a variety of chromosomally variant mouse models. I will then evaluate for sex-specific differences in chromatin compaction and epigenetic marks associated with silencing.

5.1 RNA FISH analysis of the X chromosome in germ cells

5.1.1 Silencing of the X chromosome in XY spermatocytes

Previous analyses of X gene transcription using several different approaches has revealed that in the spermatocytes meiotic silencing in the male germ line is robust and complete, i.e. no coding genes are transcribed

from the sex chromosomes at pachynema (Kierszenbaum and Tres, 1974; Mahadevaiah et al., 2009b; Margolin et al., 2014; Mueller et al., 2008).

Initially, I sought to confirm the robustness of meiotic X chromosome silencing in spermatocytes using gene-specific RNA FISH for three X-linked genes: *Scml2* (*sex comb on midleg-like 2*), *Utx* (*ubiquitously transcribed tetratricopeptide repeat X*), and *Zfx* (*zinc finger protein, X-linked*). *Scml2*, *Utx*, and *Zfx* are located in different regions of the mouse X chromosome, allowing for assessment of transcription across the length of the chromosome (**Figure 4.1a**). *Utx* encodes an H3K27-specific demethylase (Agger et al., 2007), *Zfx* encodes a putative transcription factor (Luoh et al., 1997), and *Scml2* encodes a polycomb repressor protein (Montini et al., 1999).

A previous RNA FISH analysis using a different subset of X-linked genes revealed no RNA FISH signals in pachytene spermatocytes (Mahadevaiah et al., 2008). To verify these results, I performed RNA FISH on XY wildtype spermatocytes. For these experiment, RNA FISH preparations were immunostained for HORMAD1 and γH2AFX to unambiguously identify the axis and chromatin of the asynapsed X chromosome (**Figure 4.1b-c**). HORMAD1 staining also helped distinguish between spermatocytes at the pachytene stage from other prophase I stages – at pachynema, HORMAD1 marks only the asynapsed X and Y chromosomes (**Figure 4.1b-d, arrow**). I focused my RNA FISH analysis specifically on spermatocytes at early pachytene, when silencing initiates. Compared to mid-late pachytene spermatocytes, in which the X and Y chromosomes are highly condensed, at early pachytene spermatocytes the X and Y chromosomes are more extended (Wojtasz et al., 2012), as shown by HORMAD1 staining (**Figure 4.1b**). Furthermore, at early pachynema, late recombination foci associated with γH2AFX staining are oftentimes visible, especially at higher exposure times (not shown). Together, these criteria were used to identify spermatocytes at early pachynema.

I first assessed X-gene transcription in wildtype early pachytene spermatocytes. As expected, for all three X-linked genes, the vast majority of early pachytene XY spermatocytes did not contain an RNA FISH signal,

indicative of a silent X chromosome (**Figure 4.1b,e-f**). However, in a small subset (15%) of early pachytene spermatocytes *Smcl2* was expressed (**Figure 4.1c,e-f**). For *Utx* and *Zfx*, a much smaller subset of spermatocytes (3% and 2%, respectively) showed expression (**Figure 4.1e-f**). I did not observe any RNA FISH signals in mid-late pachynema spermatocytes for any of the three genes, indicating that silencing is complete at mid-late pachynema (data not shown).

I then compared this wildtype level of silencing to that of *H2afx*-/- mutants, which have defective MSCI (Fernandez-Capetillo et al., 2003). Silencing in *H2afx*-/- mice was also examined at early pachynema, which is before *H2afx*-/- cells arrest and undergo apoptosis (mid-pachytene) (Celeste et al., 2002). In comparison to XY wildtype spermatocytes, the majority of *H2afx*-/- early pachytene spermatocytes (74%) expressed *Smcl2* (**Figure 4.1d-f, arrow**). The X-linked genes *Utx* and *Zfx* were expressed in 27% and 24% of early pachytene spermatocytes, respectively (**Figure 4.1e-f**).

In conclusion, X-linked genes are robustly silenced in wildtype spermatocytes compared to *H2afx*-/- spermatocytes during early pachynema. These data highlight the efficiency of sex chromosome silencing in the male germ line, and confirm that H2AFX is a critical silencing factor

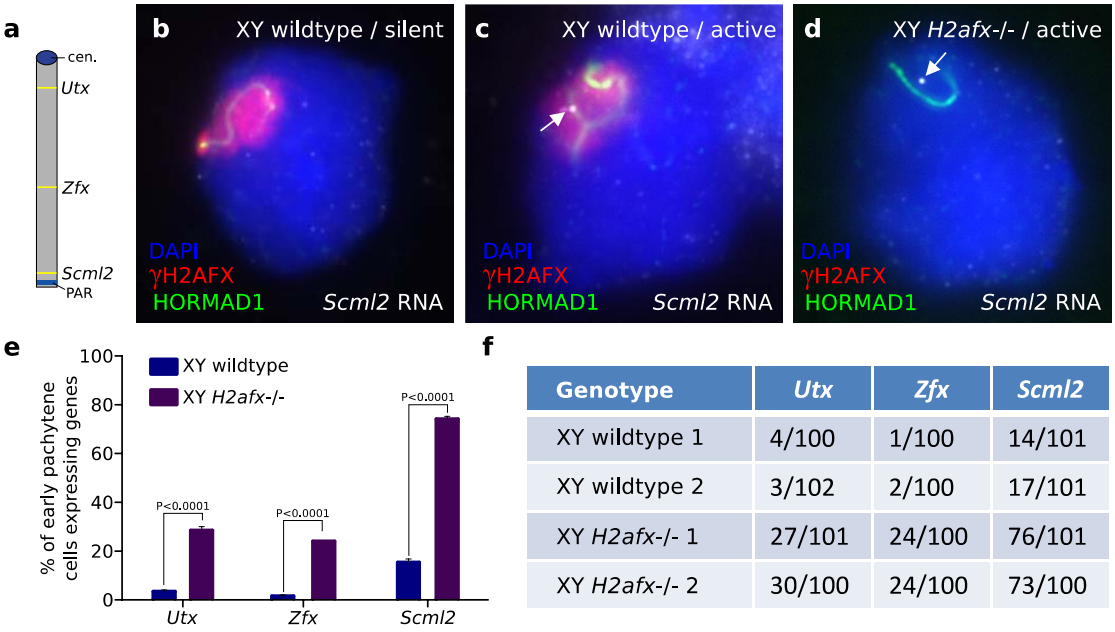

f

Genotype	*Utx*	*Zfx*	*Scml2*
XY wildtype 1	4/100	1/100	14/101
XY wildtype 2	3/102	2/100	17/101
XY *H2afx*-/- 1	27/101	24/100	76/101
XY *H2afx*-/- 2	30/100	24/100	73/100

Figure 4.1. RNA FISH analysis of wildtype and *H2afx*-/- spermatocytes.

(**a**) Schematic of mouse X chromosome showing the location of three genes, *Utx, Zfx,* and *Scml2*, which were used as RNA FISH probes to assess X chromosome transcription. PAR = pseudoautosomal region; cen. = centromere. (**b**) Early pachytene XY spermatocyte nucleus (DAPI, blue) subject to *Scml2* RNA FISH, and HORMAD1 (green) and γH2AFX immunostaining (red). This nucleus does not express *Scml2*. (**c**) Early pachytene XY spermatocyte showing *Scml2* expression (white focus, arrow) near the asynapsed X chromosome (marked by HORMAD1/γH2AFX) (**d**) Early pachytene XY *H2afx*-/- spermatocyte with an asynapsed X chromosome (marked by HORMAD1, green) showing expression of *Smcl2* (arrow). (**e**) Percentage of XY wildtype and XY *H2afx*-/- early pachytene spermatocytes expressing *Utx*, *Zfx*, and *Scml2* in adult mice. (**f**) Raw data showing number of early pachytene spermatocytes expressing *Utx*, *Zfx*, and *Scml2*. Each row represents a different mouse.

5.1.2. Silencing of the X chromosome in XO oocytes

After establishing the efficiency of meiotic silencing in the male germ line, I examined the level of silencing in XO oocytes. For comparison sake, X-linked transcription was measured in XO oocytes using RNA FISH for *Scml2*, *Utx*, and *Zfx* genes. Taking advantage of the synchronous nature of oocyte development, I focused my initial analysis on 17.5 d*pc* ovaries, which are enriched in pachytene oocytes (see Figure 1.2).

For analyses of XO oocytes, RNA FISH preparations were immunostained for γH2AFX to identify XO oocytes with an asynapsed X chromosome, as done in previous experiments (see Figure 1.3). Using this approach, I classified XO oocytes into two populations: (1) XO oocytes with a γH2AFX domain, indicative of an asynapsed X chromosome (**Figure 4.2a-b**); and (2) XO oocytes devoid of a γH2AFX domain, reflecting a self-synapsed X chromosome (**Figure 4.2c**). For all RNA FISH analyses, I first categorized XO oocytes as γH2AFX domain-positive or γH2AFX domain-negative, and then examined for an RNA FISH signal.

First, I assessed X-linked gene transcription in γH2AFX domain-negative XO oocytes (**Figure 4.2c**) to establish the level of X gene expression in the absence of silencing. Consistent with my previous Cot-1 RNA FISH analysis suggesting high transcription levels in oocytes (see Figure 2.5), I found that the self-synapsed X chromosome in XO oocytes was transcriptionally active. At 17.5 d*pc,* 100% of γH2AFX domain-negative XO oocytes expressed *Scml2* (**Figure 4.2d-e**). Similarly, 68% and 72% of γH2AFX domain-negative XO oocytes expressed *Utx* and *Zfx*, respectively (**Figure 4.2d-e**).

I predicted that the percentage of oocytes with an RNA FISH signal would be significantly lower in XO oocytes with a γH2AFX domain due to meiotic silencing. Indeed, a smaller percentage of XO oocytes with a γH2AFX domain had an RNA FISH signal (**Figure 4.2d,e**), indicating silencing. However, the level of silencing in XO oocytes with a γH2AFX domain was not as robust as that observed in spermatocytes (see Figure 4.1 for comparison). Remarkably, 85% of γH2AFX domain-positive XO oocytes at 17.5 d*pc*

expressed *Scml2* (**Figure 4.2c-e**), compared to 15% of pachytene spermatocytes (**Figure 4.1e-f**). While a greater proportion of γH2AFX domain-positive XO oocytes showed silencing of *Utx* and *Zfx*, still 30% and 27% of oocytes showed expression, respectively (**Figure 4.2d,e**). These data suggest that silencing of the asynapsed X chromosome is less complete in females compared to males.

I then examined whether the incompleteness of X chromosome silencing in oocytes is related to shortened length of prophase I in females compared to males. Pachynema of male meiosis lasts seven days (Bennett, 1977), compared to the three day length of pachynema in females (Cohen et al., 2006). To address this, I examined whether the degree of meiotic silencing improves over time in female. I therefore assessed X gene silencing in XO oocytes at later time points, namely 18.5-20.5 d*pc*, when oocytes progress from pachynema to the end of prophase I.

At 18.5, 19.5, and 20.5 d*pc*, the majority of XO oocytes (67-98%) with a self-synapsed X chromosome expressed the genes *Scml2*, *Utx,* and *Zfx* (**Figure 4.2d,e**), consistent with a transcriptional active X chromosome in the absence of silencing. In oocytes with a γH2AFX domain, a smaller percentage (40-71%) expressed these three X-linked genes (**Figure 4.2d,e**). Nevertheless, a substantial percentage of γH2AFX domain-positive XO oocytes at late prophase I, i.e. 19.5 and 20.5 d*pc*, expressed these genes (**Figure 4.2d,e**). This indicates that silencing of the X chromosome in XO oocytes does not improve substantially during prophase I progression.

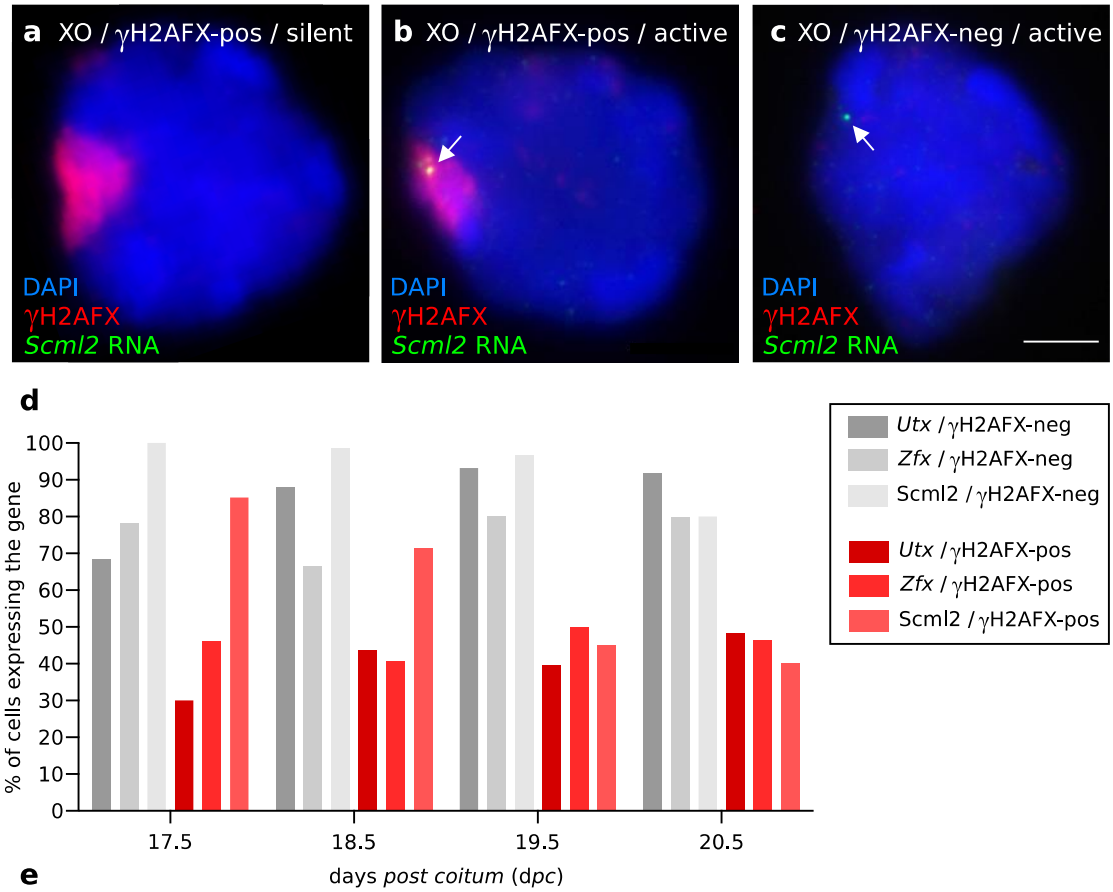

e

Genotype	*Utx*		*Zfx*		*Scml2*	
	γH2AFX-neg	γH2AFX-pos	γH2AFX-neg	γH2AFX-pos	γH2AFX-neg	γH2AFX-pos
XO 17.5 d*pc*	13/19	6/20	13/18	4/15	36/36	69/81
XO 18.5 d*pc*	95/108	35/80	54/81	32/79	74/75	45/63
XO 19.5 d*pc*	110/118	17/43	89/111	16/40	61/63	14/31
XO 20.5 d*pc*	101/110	28/58	79/99	26/56	24/30	8/20

Figure 4.2. Incomplete silencing of the X chromosome in XO oocytes.

(a-c) Representative images of XO oocyte nuclei (DAPI, blue) subject to RNA FISH (green) and γH2AFX immunostaining (red). (a) XO oocyte with an asynapsed X chromosome (γH2AFX domain-positive) with no RNA FISH signal, demonstrating silencing of Scml2. (b) XO oocyte with an asynapsed X chromosome (γH2AFX domain-positive) with an RNA FISH signal (arrow), demonstrating expression of Scml2 and incomplete X silencing. (c) Control XO oocyte with a self-synapsed X chromosome (γH2AFX domain-negative) with an RNA FISH signal (arrow), indicating expression of the X-linked gene Scml2. Oocytes were distinguished from somatic cells based upon DAPI staining and nuclear morphology. Scale bar represents 5μm. (d) The percentage of XO oocytes expressing Utx, Zfx, and Smcl2 at 17.5, 18.5, 19.5 and 20.5 dpc. XO oocytes were subdivided into those with a γH2AFX domain

(red bars) and those without a γH2AFX domain (gray bars). (e) Raw data showing number of XO oocytes expressing *Utx*, *Zfx*, and *Scml2* at 17.5, 18.5, 19.5, and 20.5 d*pc.*

5.1.3 Mosaic gene inactivation of the X chromosome in XO oocytes

Next, I examined whether silencing in XO oocytes is mosaic in individual cells. Mosaic silencing would manifest as inactivity of some X-linked genes and expression of others within individual cells. By contrast, non-mosaic silencing would manifest as all X-linked genes being either active or inactive within individual cells.

To distinguish between these possibilities, I performed simultaneous three-gene RNA FISH on 19.5 d*pc* XO oocytes for *Scml1, Utx,* and *Zfx*. Of the XO oocytes with self-synapsed X chromosomes (γH2AFX domain-negative XO oocytes) (**Figure 4.3a**), 60% expressed all three X-linked genes simultaneously at 19.5 d*pc* (**Figure 4.3c**). By contrast, only 12% of XO oocytes with an asynapsed X chromosome (γH2AFX domain-positive XO oocytes) expressed all three genes simultaneously (**Figure 4.3c**). Notably, only 29% of XO oocytes with a γH2AFX domain had all three genes inactive (**Figure 4.3c**), indicating that multi-gene silencing occurs in only a subset of XO oocytes. Notably, the vast majority (88%) of XO oocytes with an asynapsed X chromosome had at least one of the three genes inactive (**Figure 4.3c**). Therefore, even when an XO oocyte with a γH2AFX domain has one active X-linked gene, usually at least one other X-linked gene is inactive. This indicates that the silence response in oocytes leads to stochastic/mosaic X-linked gene silencing patterns (**Figure 4.3d**).

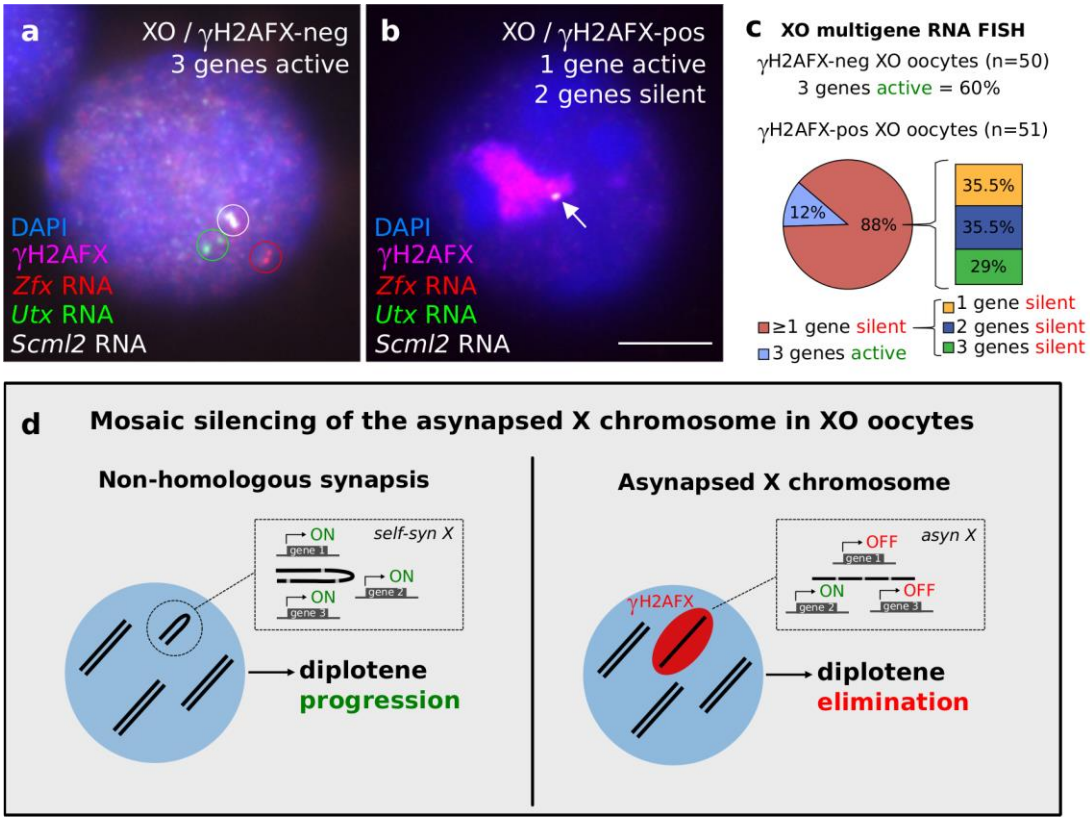

Figure 4.3. Mosaic silencing of the X chromosome in XO oocytes.

(**a**,**b**) Representative images of 19.5 dpc XO oocyte nuclei (DAPI, blue) subject to three-gene RNA FISH for *Utx* (green), *Zfx* (red), and *Scml2* (white), and γH2AFX immunostaining (magenta) to identify the asynapsed X chromosome. (**a**) XO oocyte with a self-synapsed X chromosome (γH2AFX-negative) showing RNA FISH signals for all three genes, indicative of a transcriptionally active X chromosome. (**b**) XO oocyte with an asynapsed X chromosome (γH2AFX-positive) showing an RNA FISH signal only for *Scml2* (white, arrow), indicating that two of three genes are silent. Scale bar = 5μm. (**c**) Quantitation of three-gene RNA FISH. Pie chart: the percentage of XO oocytes with an asynapsed X chromosome (γH2AFX-positive) that have at least one gene silenced (88%). Bar chart: breakdown of the percentage of oocytes with one, two, and three genes silenced. n is the number of oocytes analyzed. (**d**) Schematic showing differential gene expression between the γH2AFX-negative self-synapsed X chromosome (highly transcriptionally active) and the γH2AFX-positive asynapsed X chromosome (mosaically silenced X genes).

5.2 RNA FISH analysis of the h21 chromosome in Tc1 germ cells

5.2.1 Silencing of the h21 chromosome in Tc1 spermatocytes

I next tested the possibility that XO oocytes with complete X chromosome silencing were eliminated, thus overestimating the prevalence of escape from silencing in XO oocytes. Distinguishing between this artefact and a true mosaic silencing phenotype is possible using the Tc1 mouse model, because Tc1 oocytes with an asynapsed h21 are not eliminated during prophase I (see Figure 2.7). I therefore performed a similar RNA FISH study on Tc1 males and females.

First, I established the degree of silencing in Tc1 males. Previously Cot-1 RNA FISH work showed that the asynapsed h21 chromosome in Tc1 spermatocytes is Cot-1 negative, indicative of transcriptional silencing (Mahadevaiah et al., 2008). By contrast, when the h21 is self-synapsed, it is Cot-1 positive, and therefore transcriptionally active (Mahadevaiah et al., 2008). I confirmed the silencing of the asynapsed h21 using gene-specific RNA FISH for three h21 genes: *USP25* (*ubiquitin specific peptidase 25*), which encodes a protease; *NRIP1* (*nuclear receptor interacting protein 1*), which encodes a transcriptional modulator of the estrogen receptor; and *TPTE* (*transmembrane phosphatase with tensin homology*), which encodes a tyrosine phosphatase (**Figure 4.4a**).

I identified the asynapsed h21 in Tc1 oocytes using γH2AFX; those with a self-synapsed h21 were devoid of γH2AFX. I focused my analysis on Tc1 pachytene spermatocyte. In pachytene Tc1 spermatocytes with a self-synapsed h21 chromosome (γH2AFX domain-negative), *USP25* and *TPTE* were expressed in 93% (n=27/29) and 100% (n=26/26) of spermatocytes, respectively (data not shown). No RNA FISH signals were observed for *NRIP1*, suggesting that it is not expressed in spermatocytes.

By contrast, in pachytene Tc1 spermatocytes with an asynapsed h21 chromosome (γH2AFX domain-positive), only 7% of early pachytene spermatocytes with a γH2AFX domain expressed *Usp25* (n=1/14) and zero expressed *TPTE* (n=0/16) (data not shown). These data confirm that silencing of the asynapsed h21 chromosome in spermatocytes is robust.

5.2.2 Silencing of the h21 chromosome in Tc1 oocytes

Next, I assessed transcription in Tc1 oocytes using RNA FISH and γH2AFX immunostaining. I identified two populations of Tc1 oocytes: those with a γH2AFX domain, indicative of an asynapsed h21 chromosome (**Figure 4.4b,c**); and those with no γH2AFX domain, indicative of self-synapsis (**Figure 4.4d**).

At 17.5 d*pc*, nearly all Tc1 oocytes with a self-synapsed h21 expressed *USP25* (94%), *NRIP1* (96%), and *TPTE* (93%) (**Figure 4.4e,f**), indicating that the self-synapsed h21 chromosome is highly transcriptionally active. By contrast, the percentage of Tc1 oocytes with a γH2AFX domain and an RNA FISH signal for *USP25*, *NRIP1*, or *TPTE* was lower (**Figure 4.4e,f**), consistent with meiotic silencing. Nevertheless, in the majority of γH2AFX domain-positive oocytes an RNA FISH signal was visible (75%, 81% and 65%, respectively) (**Figure 4.4e,f**).

To address whether the degree of silencing in Tc1 oocytes is influenced by gestational age, I then performed h21 RNA FISH in oocytes from 18.5, 19.5, and 20.5 d*pc* Tc1 ovaries. At all of these time points, the majority of Tc1 oocytes with a self-synapsed h21 expressed *USP25*, *NRIP1,* and *TPTE* (**Figure 4.4e,f**). By contrast, the percentage of Tc1 oocytes with a γH2AFX domain that express an h21 gene was between 30-76%, depending upon the gene and developmental age (**Figure 4.4e-f**). Therefore, at least 30% of the oocytes showed an RNA FISH signal at all developmental ages. These data, combined with results from the XO oocyte analysis, suggest that meiotic silencing is less complete in the female germ line.

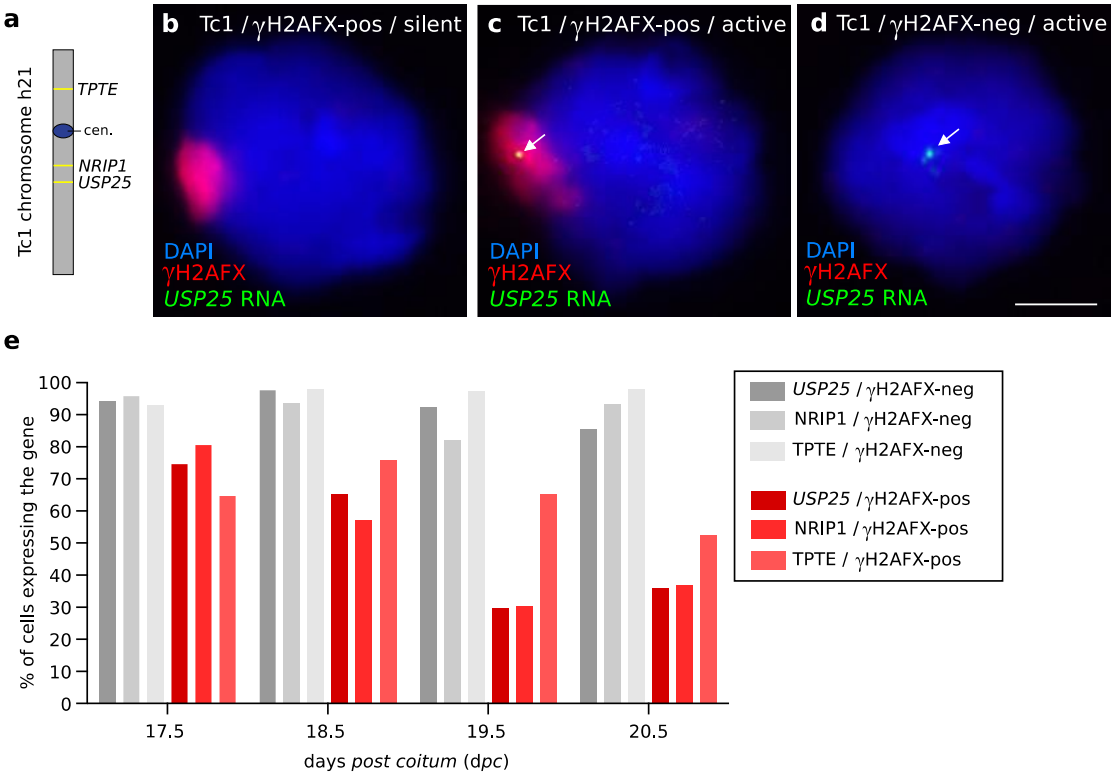

Genotype	USP25		NRIP1		TPTE	
	γH2AFX-neg	γH2AFX-pos	γH2AFX-neg	γH2AFX-pos	γH2AFX-neg	γH2AFX-pos
Tc1 17.5 d*pc*	79/84	50/67	68/71	33/41	13/14	22/34
Tc1 18.5 d*pc*	120/123	51/78	59/63	20/35	104/106	76/100
Tc1 19.5 d*pc*	84/91	8/27	152/182	7/23	177/182	15/23
Tc1 20.5 d*pc*	89/104	22/61	142/152	7/19	149/152	10/19

Figure 4.4. Incomplete silencing of the h21 chromosome in Tc1 oocytes.

(**a**) Schematic of the Tc1 human chromosome 21 (h21) showing the location of three genes, *USP25*, *NRIP1*, and *TPTE*, which were used as RNA FISH probes to assess h21 gene transcription. cen. = centromere. (**b-d**) Representative images of Tc1 oocytes (DAPI, blue) subject to RNA FISH (green) and γH2AFX immunostaining (red). (**b**) Tc1 oocyte with an asynapsed h21 chromosome (γH2AFX domain-positive) and no RNA FISH signal, demonstrating silencing of *USP25*. (**c**) Tc1 oocyte with an asynapsed h21 chromosome (γH2AFX domain-positive) and an RNA FISH signal (arrow), demonstrating expression of *USP25*. (**d**) Control Tc1 oocyte with a self-synapsed h21 chromosome (γH2AFX domain-negative) with an RNA FISH signal (arrow), showing expression of *USP25*. Scale bar represents 5μm. (**e**) The percentage of Tc1 oocytes expressing *USP25*, *NRIP1*, and *TPTE* at 17.5, 18.5, 19.5, and 20.5 d*pc*. Tc1 oocytes were subdivided into those with a γH2AFX domain (red bars) and those without a γH2AFX domain (gray

bars). (**f**) Raw data showing number of Tc1 oocytes expressing *USP25*, *NRIP1*, and *TPTE* at 17.5, 18.5, 19.5, and 20.5 d*pc.*

5.2.3 Mosaic gene silencing of the h21 chromosome in Tc1 oocytes

Next, I examined whether meiotic silencing in Tc1 oocytes leads to stochastic inactivation of genes, as observed in XO oocytes. I performed triple RNA FISH for the genes *USP25*, *NRIP1,* and *TPTE* in oocytes from 19.5 d*pc* Tc1 ovaries. Importantly, of the γH2AFX domain-negative Tc1 oocytes (**Figure 4.5a**), 89% had RNA FISH signals for all three genes (**Figure 4.5c**). This confirms that in the absence of meiotic silencing the h21 is highly transcriptionally active.

By contrast, a much smaller percentage of γH2AFX domain-positive Tc1 oocytes (21%) had RNA FISH signals for all three genes simultaneous (**Figure 4.5c**). Importantly, while only a subset (23%) of γH2AFX domain-positive oocytes had no RNA FISH signals (i.e. no genes expressed), the majority (79%) had at least one RNA FISH signal missing (i.e. ≥1 gene silenced) (**Figure 4.5b-c**). Therefore, the silencing response in Tc1 oocytes results in mosaic gene inactivation.

In summary, in contrast to the situation in spermatocytes, where silencing is robust and complete, meiotic silencing in oocytes leads to an incomplete and mosaic pattern of gene inactivation.

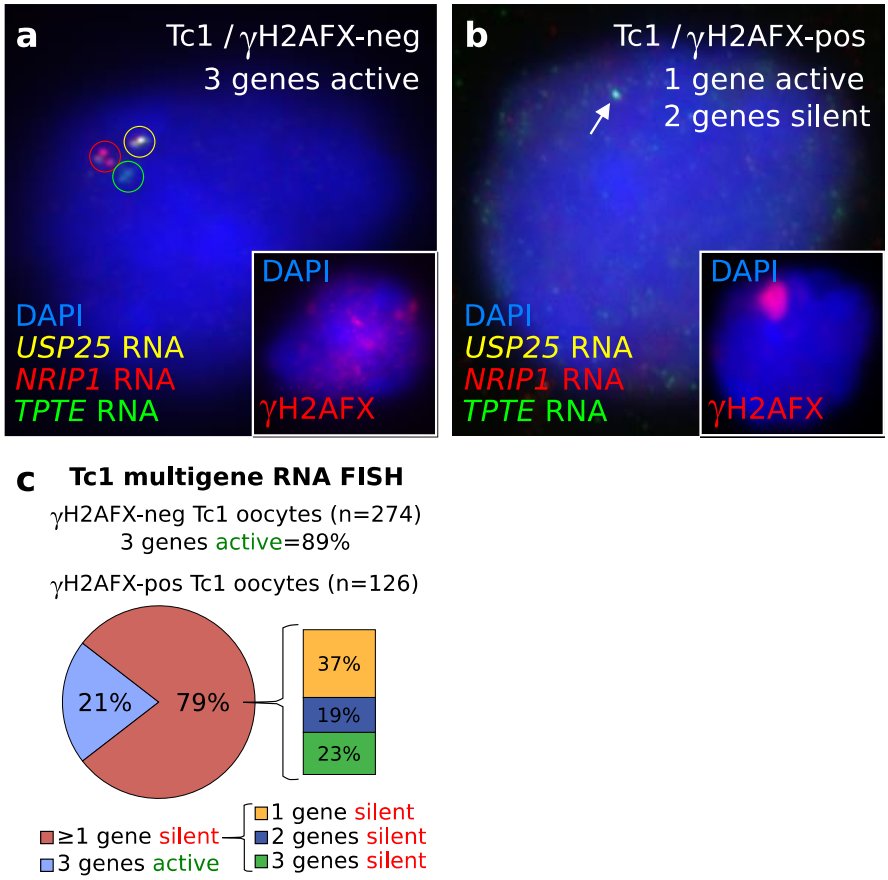

Figure 4.5. Mosaic silencing of the h21 chromosome in Tc1 oocytes.

(**a**,**b**) Representative images of 19.5 d*pc* Tc1 oocyte nuclei (DAPI, blue) subject to three-gene RNA FISH for *USP25* (yellow), *NRIP1* (red), and *TPTE* (green), and γH2AFX immunostaining (inset, red) to identify the asynapsed h21 chromosome. (**a**) Tc1 oocyte with a self-synapsed h21 chromosome (γH2AFX-negative) showing RNA FISH signals for all three genes, indicative of an active h21 chromosome. (**b**) Tc1 oocyte with an asynapsed h21 chromosome (γH2AFX-positive) showing only an RNA FISH signal for *TPTE* (green, arrow), indicating that two of three genes are silenced. (**c**) Quantitation of three-gene RNA FISH. Pie chart: the percentage of Tc1 oocytes with an asynapsed h21 chromosome (γH2AFX-positive) that have at least one gene silenced (79%). Bar chart: breakdown of the percentage of oocytes with one, two and three genes silenced. n is the number of oocytes analyzed.

5.3 Characterization of the sexually dimorphic silencing response

5.3.1 The Y chromosome does not improve X silencing in oocytes

After establishing that meiotic silencing is sexually dimorphic, I examined potential factors that may contribute to this sex-based difference. A fundamental difference between males and females is the contribution of the Y chromosome in males. It is possible, therefore, that the Y chromosome encodes certain factors necessary for a robust silencing response. To address this hypothesis, I examined whether the efficiency of silencing in oocytes improves in the presence of a mouse Y chromosome.

To examine this possibility, I analyzed silencing in XY^{d1} females, which contain a mouse Y chromosome variant that does not express the male-determining factor *Sry* (Capel et al., 1993; Mahadevaiah et al., 1998). Unlike in XY spermatocytes, where the X and Y chromosomes synapse at the PAR in >90% of cases (Kauppi et al., 2011), in the majority of XY oocytes the X and Y chromosomes remain asynapsed (Mahadevaiah et al., 1993).

To address whether the Y^{d1} chromosome improves X chromosome meiotic silencing, I performed RNA FISH for the X-linked gene *Scml2* on XY^{d1} oocytes from 18.5 d*pc* females. As done previously, I identified oocytes with an asynapsed X chromosome using γH2AFX. The majority of XY^{d1} oocytes with a γH2AFX domain had an asynapsed X chromosome, but a small fraction had an asynapsed Y chromosome and a self-synapsed X chromosome. Since the self-synapsed X chromosome is highly transcriptionally active, I was able to identify these oocytes because they contained an *Scml2* RNA FISH signal outside of a γH2AFX domain (not shown). I excluded these oocytes from my analysis, since these oocytes had a self-synapsed X chromosome.

As expected, 91% of the γH2AFX domain-negative XY^{d1} oocytes expressed *Scml2* (**Figure 4.6**). This is consistent with the percentage of XO oocytes with a self-synapsed X chromosome that expresses *Scml2* at 18.5 d*pc* (see Figure 4.2d-e). Based on my earlier analysis of XO females, 71% of XO oocytes with an γH2AFX domain expressed *Scml2* at 18.5 d*pc* (**Figure 4.2d-e**). If the Y chromosome is important for an efficient meiotic silencing

response, then the percentage of XY^{d1} oocytes that express *Scml2* would be dramatically reduced. Contrary to this, the majority (57%) of XY^{d1} oocytes with an asynapsed X chromosome expressed *Scml2* (**Figure 4.6**). This is much higher than the percentage early pachytene XY spermatocytes that express *Scml2* (15%) (**Figure 4.6**). Therefore, the degree of *Scml2* silencing in oocytes is not dramatically improved in the presence of the Y^{d1} chromosome.

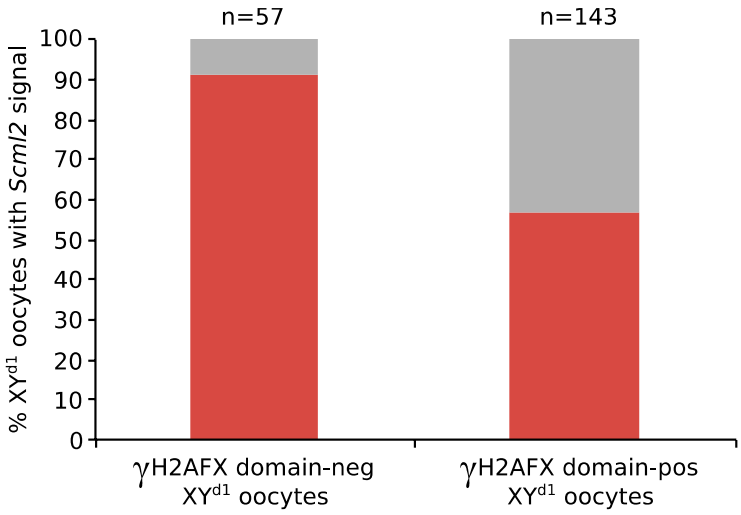

Figure 4.6. RNA FISH analysis of XY^{d1} oocytes.

The percentage of XY^{d1} oocytes at 18.5 d*pc* with an RNA FISH signal for the X-linked gene *Scml2*. XY^{d1} oocytes were subdivided into γH2AFX domain-positive and –negative oocytes. n is the number of oocytes analyzed from one ovary.

5.3.2 γH2AFX domain intensity in XO spermatocytes and oocytes.

I next looked for differences in the epigenetics of asynapsed chromatin between male and female germ cells. A critical factor in the initiation of meiotic silencing in mammals is γH2AFX (Fernandez-Capetillo et al., 2003; Ichijima et al., 2011). To determine whether γH2AFX is sexually dimorphic, I measured the γH2AFX signal on the asynapsed X chromosome in oocytes and spermatocytes.

With assistance from Dr. Shantha Mahadevaiah, I measured the intensity of the γH2AFX domain associated with an asynapsed X chromosome on surface spread XO oocytes and spermatocytes. To control for the amount of sex chromosome asynapsis, I compared XO oocytes to spermatocytes lacking a Y chromosome (i.e. XO males). These particular XO mice differentiate into males because they have a copy of *Sry* on the X chromosome (Mazeyrat et al., 2001).

To evaluate γH2AFX domain intensity, I compared γH2AFX domain intensity in surface spread XO oocytes and XO diplotene spermatocytes (**Figure 4.7a-b**). I analyzed diplotene germ cells because this is the stage when silencing is well established and when oocyte losses occur in XO females (see Figure 1). Germ cells were substaged based up the characteristic staining of SYCP3 at diplonema (see Figure 1).

Notably, there was no significant difference in the integrated intensity of the γH2AFX domain in XO oocytes compared to XO spermatocytes (unpaired T test, P=0.5376) (**Figure 4.7c**). This indicates that γH2AFX signalling/intensity in response to X chromosome asynapsis is not different between the sexes, and that it unlikely accounts for the sexually-dimorphic silencing phenotype.

5.3.3 X chromatin compaction in XO spermatocytes and oocytes

As part of the previous analysis on γH2AFX domain intensity, I also measured the area of the γH2AFX domains. This area corresponds to the degree of chromatin compaction of the asynapsed X chromosome, since γH2AFX marks the chromatin domain. As described above, I compared the

normalized size of the γH2AFX domains between XO diplotene oocytes and XO diplotene spermatocytes. Notably, the mean γH2AFX domain area, normalized to total cell area, was significantly smaller in XO spermatocytes compared to XO oocytes (T test, $P<0.0001$) (**Figure 4.7d**). The greater normalized γH2AFX domain size in oocytes suggests reduced chromatin compaction of the asynapsed X chromosome in oocytes compared to spermatocytes. Therefore, there is a significant difference in asynapsed X chromosome compaction between XO oocytes and spermatocytes.

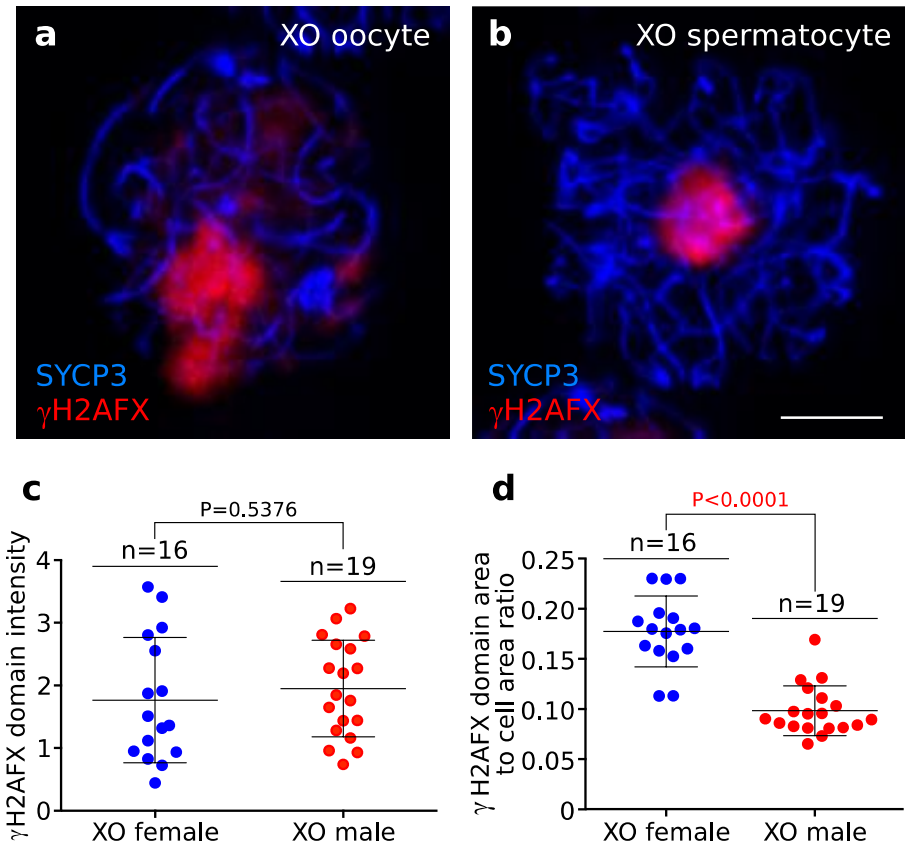

Figure 4.7. γH2AFX domains in XO oocytes versus spermatocytes.

(**a**) Diplotene XO oocyte stained with SYCP3 (blue) and γH2AFX (red), showing a typical γH2AFX domain. (**b**) Diplotene XO spermatocyte showing a typical γH2AFX domain. XO males are also known as XO *Eif2s3y* tg, *Sry* tg males (Vernet et al., 2011), and were chosen because they have the same amount of sex chromosome material as XO females. Scale bar = 10μm. (**c**) Quantitation of γH2AFX domain integrated intensity in XO diplotene oocytes and XO diplotene spermatocytes. (**d**) Quantitation of γH2AFX domain area normalized to germ cell area in XO diplotene oocytes and XO diplotene spermatocytes, revealing increased compaction of asynapsed X chromosome in males compared to females. n is the number of germ cells analyzed. Unpaired t test were performed to compare means, and P values are reported.

5.4 Discussion

Chromosome abnormalities confer greater germ cell losses in males than females (Burgoyne et al., 2009). This is due in part to the reduced stringency of the metaphase I spindle checkpoint in females (LeMaire-Adkins et al., 1997; Nagaoka et al., 2011), but is also thought to reflect ill-defined sex differences in the efficiency of the prophase I response to asynapsis (Hunt and Hassold, 2002; Morelli and Cohen, 2005; Nagaoka et al., 2012). In this chapter, I explored the mechanistic basis for the sex-specific differences in the meiotic prophase I surveillance response.

I provide evidence that meiotic silencing is less efficient/robust in oocytes compared to spermatocytes. A significant number of XO oocytes that have an asynapsed X chromosome still had active X-linked genes, despite the presence of a γH2AFX domain. This is in stark contrast to the situation in males, whereby silencing causes the complete inactivation of all sex-linked protein-coding genes by mid-pachynema (Turner et al., 2006).

Using simultaneous triple-gene RNA FISH, I showed that meiotic silencing in oocytes leads to the stochastic inactivation of genes, in which some X-linked genes are inactivated, while others remain active. Given that the mouse X chromosome has ~940 genes and is enriched for genes involved in oogenesis (Khil et al., 2004), including one gene that I analyzed, namely *Zfx* (Luoh et al., 1997), mosaic silencing of the X chromosome is expected to cause the inactivation of a large number of essential genes, which would presumably be deleterious for XO oocyte survival.

My conclusion that silencing is more heterogeneous in oocytes compared to spermatocytes is further supported by analysis of Tc1 oocytes, and also a recent published analysis of sex-reversed XY oocytes (Taketo and Naumova, 2013). In this independent study, the efficiency of silencing of the X and Y chromosomes in XY oocytes was estimated indirectly by measurement of sex-linked gene products. They found a lower percentage of XY oocytes with staining for the protein ATRX in the presence of silencing; however, the level of staining was not completely abolished, suggesting

leaky gene expression. These results are consistent with my observations that meiotic silencing is sexually dimorphic.

This mosaic nature of silencing in oocytes may have several important implications. First, the impact of silencing on oocyte survival is expected to be dependent on the kind and combinations of genes that are inactivated in each oocyte. For example, oocytes with many critical genes inactivated would be starved of important cellular factors and thus subject to elimination sooner than oocytes that have no or few important genes silenced. Overall, this stochastic nature of silencing may lead to oocyte elimination occurring over a more extended period than predicted by a traditional checkpoint model (Barchi et al., 2005).

Second, mosaic silencing could lead to inability to eliminate all oocytes that have asynapsed chromosomes, especially if silencing fails to inactivate sufficient numbers of critical genes to be deleterious. This could explain why there remained a fraction of late diplotene oocytes with γH2AFX domains in the XO, In(X)1H, T(16;17)43H, and XX mouse models. Based on my current data, however, it is difficult to determine whether these remaining oocytes are subject to elimination by the end of late diplonema, or whether they will survive and continue to metaphase I. Additional studies are required to make this distinction.

In addition to identifying a sexual dimorphism in the degree of silencing, I also observed differences in the degree of compaction of the asynapsed X chromosome between XO oocytes and spermatocytes. This result suggests that the chromatin of asynapsed chromosomes is less heterochromatic in oocytes, which may contribute to weaker silencing response. Less condensed chromatin in oocytes is also consistent with a previous study of chromosome length in oocytes, which revealed that SC is twice as long in oocytes compared to spermatocytes (Wallace and Hultén, 1985). In summary, the sexual dimorphism in the efficiency of meiotic silencing is associated with sex-specific chromatin features.

It is possible that there are also sex-specific epigenetic features that contribute to the differential efficiency of silencing in oocytes vs. spermatocytes. Many silencing components have been shown to be localize

to asynapsed chromosomes in oocytes, including γH2AFX (Turner et al., 2005), BRCA1 (Turner et al., 2005), ATR (Turner et al., 2005), HORMAD1 (Wojtasz et al., 2009), HORMAD2 (Wojtasz et al., 2009), and ubi-H2A (Baarends et al., 2005).

Other important silencing factors that operate in spermatocytes include MDC1 (Ichijima et al., 2011), SUMO-1 (Rogers et al., 2004), and H3K9me3 (van der Heijden et al., 2007). Notably, a recent study of silencing-related epigenetic marks in sex-reversed XY oocytes, reported that H3K9me3 is not enriched on the asynapsed X chromosome in XY oocytes (Taketo and Naumova, 2013). This result has also been confirmed by members of the Turner laboratory (unpublished data). This suggests that accumulation of H3K9me3 on asynapsed chromatin may be important for establishing a fully inactive chromatin domain, and that its absence in oocytes contributes to leaky silencing.

The sex-specific H3K9me3 staining pattern in mammalian germ cells may be indicative of a spermatocyte-specific histone methyltransferase. One potential methytransferase involved in meiotic silencing is Suppressor Of Variegation 3-9 Homolog 2 (SUV39-h2) (O'Carroll et al., 2000). SUV39-h2 is preferentially expressed in the testis and localizes to the sex body in pachytene spermatocytes (O'Carroll et al., 2000). Whether this methyltransferase is present on the asynapsed X chromosome in XO oocytes is unclear.

Another candidate silencing methyltransferase is Set Domain Bifurcated 1 (SETDB1), which has recently been implicated in the maintenance of X chromosome inactivation (XCI) in female somatic cells (Minkovsky et al., 2014). It is possible that SETDB1 is not expressed in oocytes to owning to reactivation of the X chromosome in oocytes (Monk and McLaren, 1981). Future work should address the putative roles of methyltransferases, and other silencing-related epigenetic marks, as they relate to the sexually dimorphic meiotic silencing response.

Chromosome abnormalities cause prophase I loss in both males and females, but the effects are usually less severe in females (Nagaoka et al., 2012). Based on the results from this chapter, I suspect that the sexually

dimorphism in prophase I surveillance may also be associated with fundamental differences in meiotic silencing in the sexes. In spermatocytes, meiotic silencing normally results in robust inactivation of the asynapsed X and Y chromosomes, called MSCI (Turner, 2007). In the presence of small levels of asynapsis, such as the accessory human chromosome 21 in Tc1 spermatocytes, meiotic silencing also affects non-XY asynapsis (Mahadevaiah et al., 2008). If this segment of asynapsis contains critical spermatogenesis genes, then silencing would be expected to cause spermatocyte losses. Therefore, meiotic silencing likely also function to eliminate male germ cells with autosomal asynapsis.

However, in the context autosomal asynapsis, meiotic silencing of the asynapsed X-Y (i.e. MSCI) in spermatocytes typically breaks down (Mahadevaiah et al., 2008). Silencing factors are titrated away from the XY bivalent, which leads to defective MSCI and subsequent mis-expression of a small number of sex-linked genes that are pachytene-lethal (Mahadevaiah et al., 2008; Royo et al., 2010). In summary, meiotic silencing in males may lead to spermatocyte arrest via two pathways: (1) inactivation of critical genes on asynapsed autosomes, (2) titration of silencing factors from the X and Y, leading to MSCI failure.

By contrast, in oocytes, only the first pathway, the inactivation of critical genes on asynapsed autosomes, is active. Furthermore, I have shown that this pathway is leaky, such that oocytes are not fully capable of inactivating all genes associated with asynapsis. As in spermatocytes, more extensive levels of asynapsis in oocytes (>2-3 pairs of asynapsed chromosomes) leads to aberrant accumulation of silencing factors ATR, BRCA1 and γH2AFX, and disrupted meiotic silencing (Kouznetsova et al., 2009). In these situations of extensive asynapsis, therefore, the abrogated silencing response may result in the inability to eliminate these defective germ cells. Consistent with this prediction, I observed a high percentage of PWD x C57BL/6 F1 oocytes with multiple asynapsed chromosomes from pachynema to late diplonema (see Figure 2.2). Since oocytes with extensive asynapsis persist into diplonema, there may not be safeguard mechanisms outside of meiotic silencing to eliminate cells with defective asynapsis.

In summary, I predict that the decreased efficiency of the prophase I meiotic surveillance mechanism in oocytes is due to a combination of factors, which may involve the inefficiency of the meiotic silencing response in oocytes, and the absence of additional surveillance mechanisms to deal with high levels of asynapsis. Importantly, these sex-specific differences in the prophase I asynapsis surveillance mechanism may contribute the high prevalence of human aneuploidies that arise from maternal meiotic errors (Hunt and Hassold, 2002; Morelli and Cohen, 2005; Nagaoka et al., 2012).

6 Results: Examination of factors involved in meiotic silencing

The last objective of this thesis was to better characterize the role of BRCA1 and HORMAD2 during meiosis, and in particular, in meiotic silencing. First, I will focus on BRCA1. The role of BRCA1 in mammalian meiosis is not well understood, but it is thought to be involved in DNA DSB repair events (Xu et al., 2003) and meiotic silencing (Turner et al., 2004).

In this section, I will first look into the putative role of BRCA1 in meiotic DNA DSB repair. Specifically, I will examine the localization of BRCA1 during normal and DNA DSB-defective meiosis. I will then study the localization of the DNA repair factor RAD51 in *Brca1* mutant spermatocytes. An early study of *Brca1*Δ11/Δ11 *p53*+/- mutant mice reported disrupted localization of RAD51 (Xu et al., 2003), however this finding was disputed by a more recent study (Broering et al., 2014). It is important to clarify this discrepancy. I also will present data from anti-BRCA1 ChIP-seq in normal and DNA DSB-defective germ cells, with the goal of understanding the meiotic localization of BRCA1 on a genome-wide scale.

Subsequently, I will address the role of BRCA1 in the meiotic silencing cascade. Previous work implicating BRCA1 in meiotic silencing were based off of studies of *Brca1*Δ11/Δ11 *p53*+/- mutants, which express a shortened BRCA1 isoform that is still capable of binding to asynapsed chromosomes in spermatocytes (Turner et al., 2004). I wished to evaluate the meiotic silencing phenotype in a *Brca1* null mutant. I will therefore study a recently described *Brca1* null mutant mouse model (Bunting et al., 2012), which harbors a deletion of exon 2 that encodes the conserved ring finger motif (Ludwig et al., 1997). *Brca1* nullizygosity has a much more severe phenotype compared to *Brca1*Δ11/Δ11 mutants, resulting in earlier embryonic lethality (Ludwig et al., 1997), which can be overcome by additional deletion of *53BP1* (Bunting et al., 2012). These *Brca1*-/- *53bp1*-/- males are sterile (Bunting et al., 2012), but the meiotic phenotype has not yet been characterized. In this chapter, I will describe the localization of the

silencing factor ATR, and relate it to an RNA FISH analysis of X gene transcription, in *Brca1*-/- *53bp1*-/- mutant spermatocytes.

In the second part of this chapter, I will study meiotic silencing in a recently generated *Hormad2*-/- mouse model (Wojtasz et al., 2012). Recent expression profiling has shown that the HORMA-domain genes *Hormad1* and *Hormad2* are expressed highly during meiosis (Wojtasz et al., 2009). Two independent groups reported that *Hormad1*-/- mice have defects in meiotic silencing (Daniel et al., 2011; Shin et al., 2010). MSCI failure in *Hormad1*-/- mice is associated with failed recruitment and/or accumulation of the silencing factors BRCA1, ATR, and γH2AFX to the asynapsed X and Y chromosomes (Daniel et al., 2011; Shin et al., 2010). Since both HORMAD1 and HORMAD2 accumulate along the cores of the asynapsed X-Y chromosomes in spermatocytes (Wojtasz et al., 2009), I wished to analyze whether HORMAD2 also functions in meiotic silencing pathway.

I therefore characterized the meiotic silencing response in *Hormad2*-/- mice, developed by Attila Tóth's group (Dresden, Germany). I will examine the localization of three critical meiotic silencing factors, namely BRCA1, HORMAD1, and γH2AFX, in *Hormad2*-/- spermatocytes. Finally, I will study meiotic silencing in *Hormad2*-/- spermatocytes at the transcriptional level using gene-specific RNA FISH. These results on *Hormad2*-/- are published as part of a recent *Hormad2*-/- characterization study (Wojtasz et al., 2012), and shed new light on the meiotic silencing pathway in mammals.

6.1 Role of BRCA1 during meiotic prophase I 6.1.1 BRCA1 localization during male meiotic prophase I

Before analyzing *Brca1* mutant mice, I first wanted to assess the localization of BRCA1 in wildtype spermatocytes. I performed meiotic chromosome spreads on wildtype spermatocytes and double-immunostained for SYCP3, to identify chromosome axes, and BRCA1. At leptonema and zygonema, BRCA1 localized to SYCP3 axes as foci (**Figure 5.1a, arrow**), in a manner reminiscent of DNA DSB repair foci, such as RAD51, DMC1, and RPA. BRCA1 foci were restricted to the asynapsed segments of chromosomes, i.e. were absent on synapsed regions of

chromosomes (**Figure 5.1a, arrowheads**). This indicates that BRCA1 is lost from meiotic chromosome axes upon synapsis.

At pachynema and diplonema, BRCA1 was restricted to the asynapsed cores of the X-Y chromosomes, but not at regions of X-Y synapsis (i.e. at the PAR) (**Figure 5.1b, arrow**). These meiotic prophase I staining patterns of BRCA1 are consistent with previous BRCA1 localization studies (Mahadevaiah et al., 2008; Turner et al., 2004).

Given the putative role for BRCA1 in meiotic DNA DSB repair (Xu et al., 2003), I next analyzed the spatial relationship between BRCA1 and DNA repair factors during meiosis. Previously, it was shown that BRCA1 co-localizes with RAD51 on asynapsed chromosome axes in spermatocytes lacking the gene *Dnmt3l* (Mahadevaiah et al., 2008). I therefore examined whether BRCA1 co-localizes with another DNA repair protein, namely DMC1.

Wildtype chromosome spreads were triple-immunostained with SYCP3, BRCA1, and DMC1. Notably, BRCA1 and DMC1 foci were observed in close proximity on asynapsed chromosome axes at leptonema and zygonema (**Figure 5.1c**). Interestingly, while most BRCA1 foci were localized on SYCP3-labeled chromosome axes, DMC1 foci were spatially distinct, oftentimes localizing slightly off the axes (**Figure 5.1c, arrow**). This spatial difference suggests that BRCA1 and DMC1 may bind different structural elements of chromosomes.

At DNA DSB sites, DMC1 binds ssDNA to facilitate strand exchange in concert with RAD51 (Bishop et al., 1992; Cloud et al., 2012). It is unclear whether BRCA1 binds DNA directly, like DMC1 and RAD51, or binds the proteinaceous synaptonemal complex core. Given the spatial offset between DMC1 and BRCA1, and the fact that BRCA1 co-localizes over the SYCP3 signal, it is possible that BRCA1 associates with the SC .

In addition to their distinct spatial relationships, I observed two distinct types of foci observed in spermatocytes stained for BRCA1 and DMC1. The majority of foci were mixed, containing both BRCA1 and DMC1 in close proximity (**Figure 5.1d, arrows**). However, a subset of foci contained only BRCA1 (**Figure 5.1d, arrowheads**). These BRCA1 foci may represent

functional or structurally distinct regions on chromosomes, or they could represent foci that have yet to recruit DMC1. This could also indicate that BRCA1 foci are in excess of DMC1 foci.

6.1.2 Localization of BRCA1 in meiotic mutant spermatocytes

Given that BRCA1 foci occur in close proximity to DMC1 foci, it is possible that DMC1 recruits BRCA1 to DNA DSB sites. If this is true, BRCA1 foci should be abolished in *Dmc1*-/- germ cells. To test this hypothesis, I performed meiotic chromosome spreads in *Dmc1*-/- spermatocytes and analyzed the localization of BRCA1. *Dmc1*-/- spermatocytes fail to successfully repair meiotic DNA DSBs, and DNA repair proteins such as RAD51 persist and chromosomes fail to synapse (Pittman et al., 1998; Yoshida et al., 1998). Contrary to a role for DMC1 in recruiting DMC1 to chromosomes, I found that BRCA1 foci localized normally to pre-synaptic chromosomes in *Dmc1*-/- spermatocytes (**Figure 5.1e**). Therefore, *Dmc1* is not required for recruiting BRCA1 to asynapsed chromosome axes as foci.

If BRCA1 indeed localizes to meiotic DNA DSB sites, as suggested by it's localization pattern, then BRCA1 foci should disappear in *Spo11*-/- germ cells, which do not initiate programmed DNA DSBs (Mahadevaiah et al., 2001). Contrary to this expectation, a study reported that BRCA1 foci occur in *Spo11*-/- spermatocytes (Mahadevaiah et al., 2008). To confirm this puzzling finding, I repeated this experiment and assessed BRCA1 localization in *Spo11*-/- spermatocytes (Baudat et al., 2000; Romanienko and Camerini-Otero, 2000).

Consistent with the previous study (Mahadevaiah et al., 2008), I also observed BRCA1 foci along pre-synaptic axes in *Spo11*-/- zygotene-like spermatocytes (**Figure 5.1f**). Therefore, despite the fact that BRCA1 foci are located in close proximity DNA DSBs in wildtype germ cells, they do not disappear in the absence of DNA DSBs.

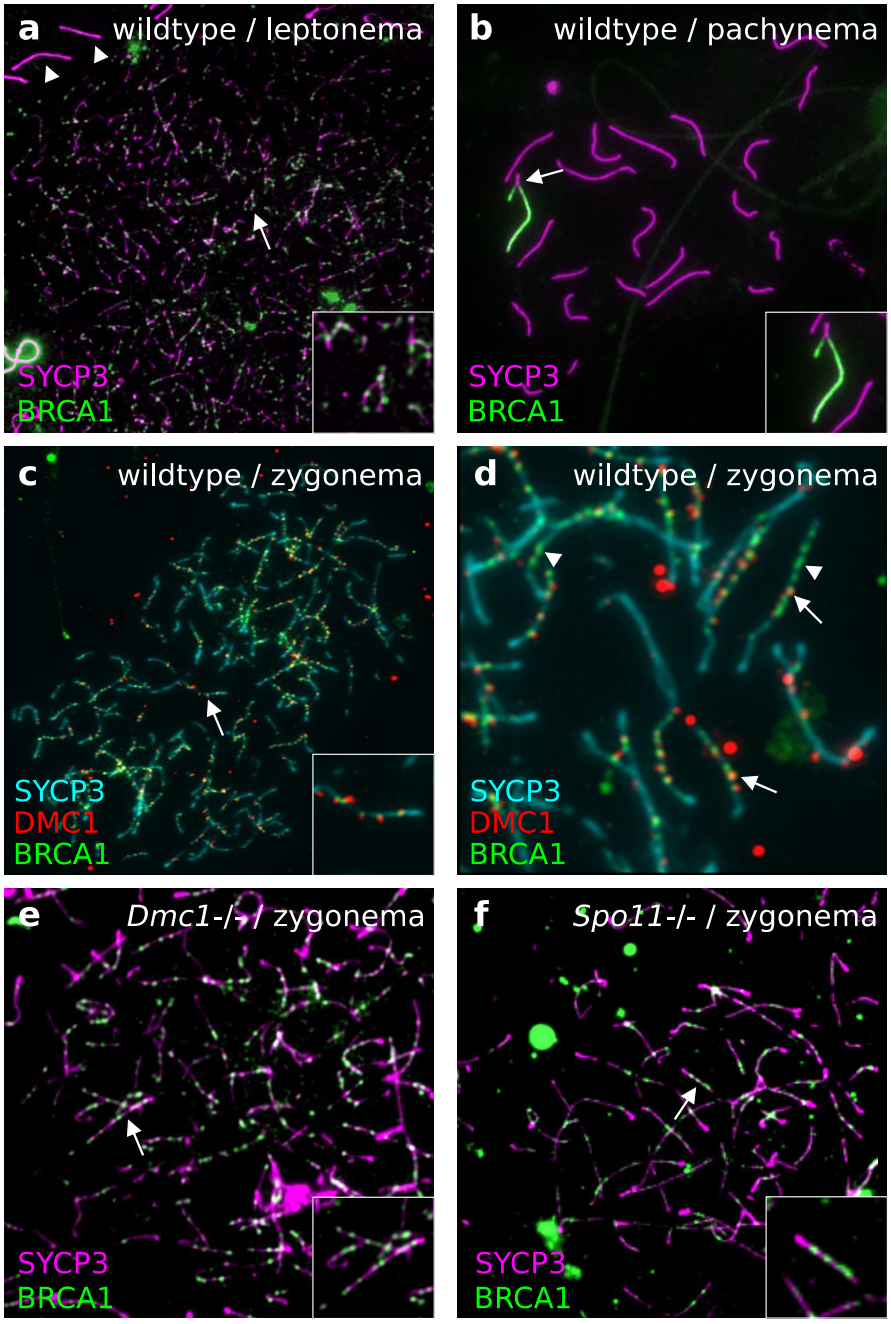

Figure 5.1. BRCA1 localization in wildtype, *Dmc1*-/-, and *Spo11*-/- spermatocytes.

(**a**) Leptotene wildtype spermatocyte immunostained for SYCP3 (magenta) and BRCA1 (green), showing abundant BRCA1 foci associated with pre-synaptic axes. Inset shows magnification of region indicated by arrow. Arrowheads show synapsed chromosomes from nearby nucleus. There are no BRCA1 foci on these synapsed axes. (**b**) Pachytene wildtype spermatocyte showing BRCA1 staining restricted to the non-homologous asynapsed regions of the X and Y chromosomes (inset). The synapsed psuedoautosomal region (arrow) is devoid of BRCA1, as are synapsed autosomes. (**c**) Zygotene wildtype spermatocyte immunostained for SYCP3 (cyan), DMC1 (red), and BRCA1 (green), showing the close proximity of

DMC1 and BRCA1 foci. Inset shows magnification of region indicated by arrow. (**d**) More magnified image of a zygotene wildtype spermatocyte immunostained for SYCP3, DMC1, and BRCA1. Two types of protein complexes are visible: the first type shows co-existence of DMC1 foci and BRCA1 foci (arrows), and the second type contains only BRCA1 foci (arrowhead). (**e**) *Dmc1*-/- zygotene-like spermatocyte immunostained for SYCP3 (magenta) and BRCA1 (green), showing normal BRCA1 foci on asynapsed chromosome axes. Inset shows magnification of region indicated by arrow. (**f**) *Spo11*-/- zygotene-like spermatocyte immunostained for SYCP3 and DMC1, showing BRCA1 foci along DNA DSB-deficient asynaptic cores.

6.1.3 RAD51 localization in *Brca1* mutants

A previous study (Xu et al., 2003) showed impaired loading of RAD51 in *Brca1*Δ11/Δ11 mutants, which suggests that BRCA1 might be required for proficient meiotic DNA DSB repair. A more recent analysis (Broering et al., 2014), however, showed that RAD51 localizes normally in several different *Brca1* mutants. To address these contradictory findings, I assessed the localization of RAD51, using the same antibody used by Xu and colleagues (Xu et al., 2003), in different *Brca1* mutants.

I first examined RAD51 staining in control *Brca1*Δ11/+ *p53*+/- spermatocytes. As expected, RAD51 foci were visible on pre-synaptic chromosomes at zygonema in *Brca1*Δ11/+ *p53*+/- spermatocytes (**Figure 5.2a**). Contrary to the initial report (Xu et al., 2003), RAD51 foci were also visible in *Brca1*Δ11/Δ11 *p53*+/- mutants (**Figure 5.2b**). I verified this finding using a different RAD51 antibody, which has been used in previous meiotic studies (Cole et al., 2012). Using this second antibody, RAD51 foci were also detected in both controls and *Brca1*Δ11/Δ11 *p53*+/- mutants (**Figure 5.2c,d**).

For further verification, I also examined RAD51 staining in a different *Brca1*Δ11 double mutant, namely *Brca1*Δ11/Δ11 *53bp1*-/- males. Using both RAD51 antibodies, RAD51 foci were observed in *Brca1*Δ11/Δ11 *53bp1*-/- spermatocytes (**Figure 5.2e,f**). These data support the more recent report (Becherel et al., 2013) indicating *Brca1* mutation does not affect the loading of RAD51 on pre-synaptic chromosomes during meiotic prophase I.

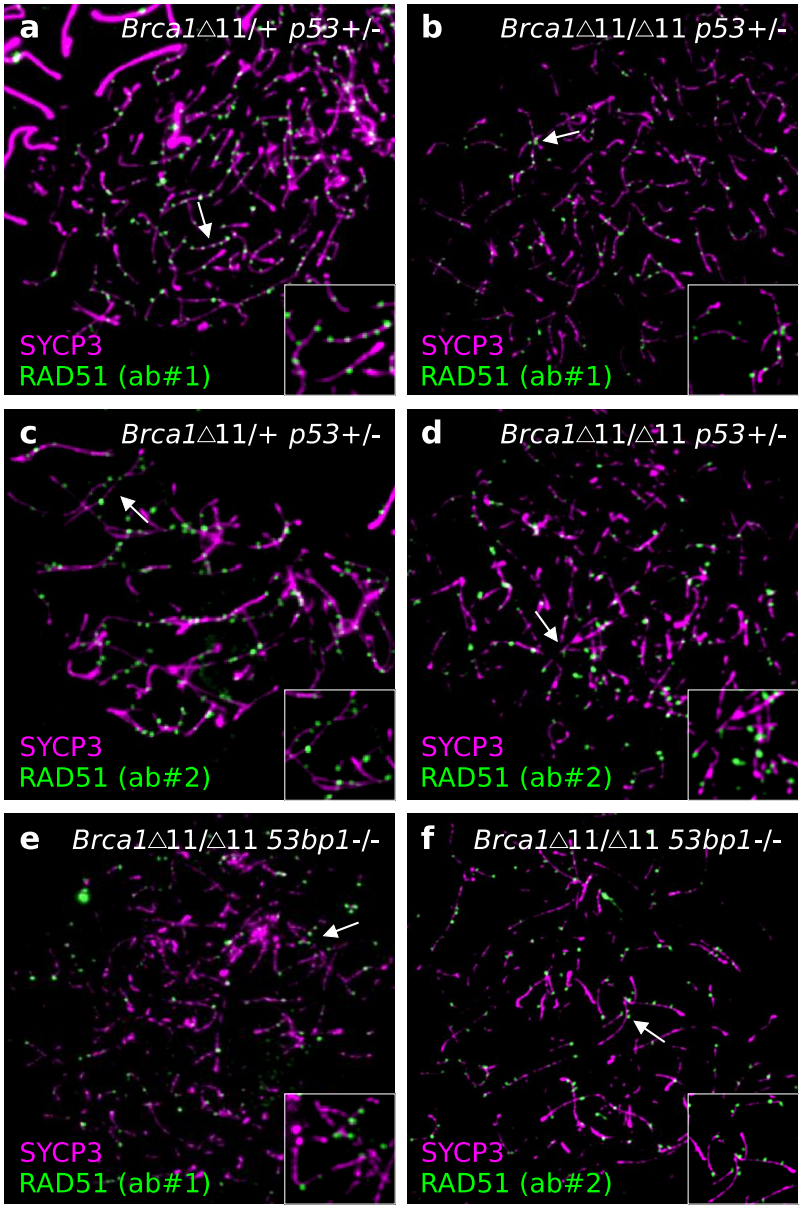

Figure 5.2. RAD51 localization in *Brca1*Δ11/Δ11 mutant spermatocytes.

(**a**) Control *Brca1*Δ11/+ *p53*+/- zygotene spermatocyte immunostained for SYCP3 (magenta) and RAD51 (ab#1, SC-8349, 1:100) (green), showing normal localization of RAD51 on asynapsed chromosome axes. (**b**) *Brca1* Δ11/ Δ11 *p53*+/- zygotene spermatocyte immunostained for SYCP3 and RAD51 (ab#1) showing unimpaired localization of RAD51. (**c**) Control *Brca1* Δ11/+ *p53*+/- zygotene spermatocyte immunostained for SYCP3 (magenta) and RAD51, using a second antibody (ab#2, EMD PC130, 1:250) (green), showing normal localization of RAD51 on asynapsed chromosome axes. (**d**) *Brca1* Δ11/ Δ11 *p53*+/- zygotene spermatocyte immunostained for SYCP3 and RAD51 (ab#2) showing unimpaired localization of RAD51. (**e**) *Brca1* Δ11/ Δ11 *53bp1*-/- zygotene spermatocyte, showing RAD51 foci (ab#1). (**f**) *Brca1* Δ11/ Δ11 *53bp1*-/- zygotene spermatocyte, showing RAD51 foci (ab#2).

6.1.4 ChIP-seq in wildtype spermatocytes

The above data involving the role for BRCA1 in meiotic DNA DSB repair are somewhat paradoxical. I showed that BRCA1 foci are not dependent upon *Spo11*, and that *Brca1* mutants load RAD51 or DMC1 normally. This suggests that BRCA1 is dispensable for DNA DSB repair. This begs the question as to why then BRCA1 localize to meiotic DNA DSB sites.

Given these observations, I wished to examine more closely the location of BRCA1 relative to meiotic DNA DSBs. To address this, I performed anti-BRCA1 chromatin immunoprecipitation followed by deep sequencing (ChIP-seq). This approach has been used previously to generate a detailed map of meiotic DNA DSB hotspots in mice (Smagulova et al., 2011).

As a positive control, I first performed anti-DMC1 ChIP-seq on chromatin from C57Bl/6 wildtype mice testes. A similar experiment was done previously to define hotspots in wildtype spermatocytes (Smagulova et al., 2011). My sequencing data was analyzed by computational biologist Dr. Kevin Brick (National Institutes of Health, USA). In confirmation that my anti-DMC1 ChIP-seq experiment was successful, there was significant enrichment of DMC1 sequencing reads at previously map hotspots in the genome (**Figure 5.3**). Quantitative analysis revealed 19,488 "peaks" of statistically significant DMC1 enrichment, which is similar to the 18,735 hotspots previously identified in the mouse genome (Brick et al., 2012).

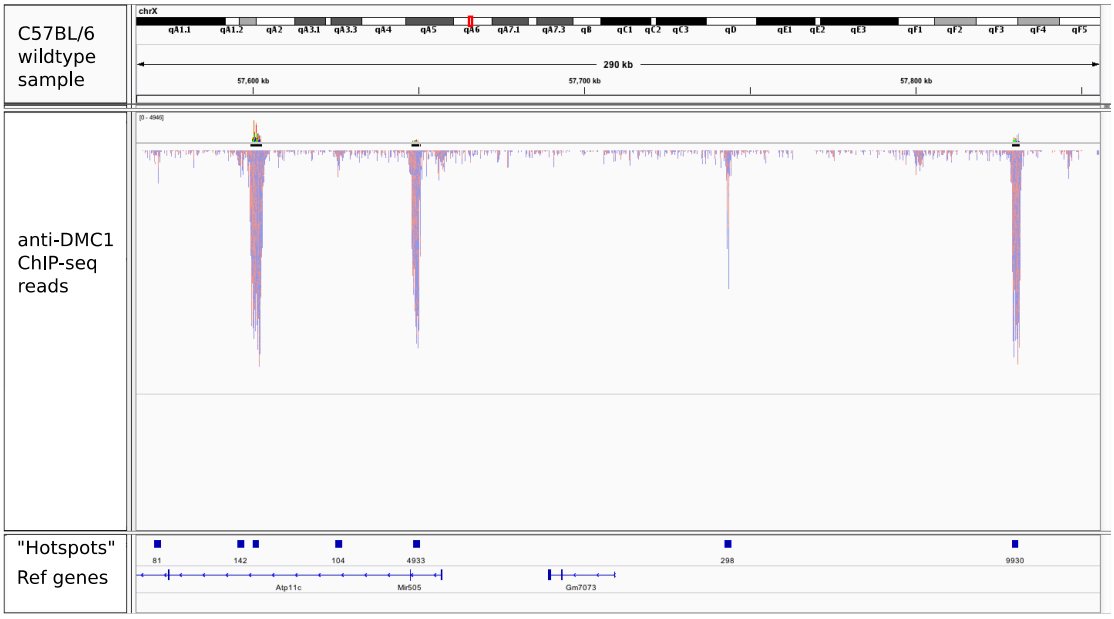

Figure 5.3. Control anti-DMC1 ChIP-seq in wildtype spermatocytes.

Image from Integrative Genome Viewer (IGV) showing representative peaks of DMC1 enrichment within a representative genomic region (a 290kb region on chromosome X) containing several DNA DSB hotspots (blue boxes in "hotspots" row) defined by (Smagulova et al., 2011).

After verifying the efficacy of this approach, I then performed ChIP-seq on C57Bl/6 wildtype spermatocytes using two different anti-BRCA1 antibodies. First, I tested the rabbit polyclonal BRCA1 antibody that I used for chromosome spread experiments, used three different dilutions/conditions (**Figure 5.4a**). I also tested a second BRCA1 antibody that has been used in unpublished ChIP-seq experiments in somatic cells by members of Dr. Andre Nussenzweig's laboratory (NIH) (**Figure 5.4a**).

Compared to my anti-DMC1 ChIP-seq results, enrichment peaks were not as obvious in my anti-BRCA1 ChIP-seq data (**Figure 5.4b**). However, upon comparing the BRCA1 ChIP-seq data to published hotspot data I noticed small peaks of BRCA1 enrichments near a subset of the strongest DMC1-defined hotspots (**Figure 5.4b**). Based on quantitative analysis, BRCA1 enrichment shows positive correlations with hotspot strength, defined by my DMC1 ChIP-seq data (**Figure 5.4c**). For example, anti-BRCA1 sample 3 showed a Pearson's correlation coefficient of 0.70 when compared to C57BL/6 hotspot strength (**Figure 5.4c**). This positive correlation suggests that BRCA1 is enriched at DNA DSB hotpsots, especially at the strongest ones in the genome.

a

Sample	Genotype	ChIP antibody	Protocol	Clusters (PF)
1	C57BL/6 wildtype	anti-BRCA1 polyclonal rabbit, 1.5ul	KE*	17,057, 056
2	C57BL/6 wildtype	anti-BRCA1 polyclonal rabbit, 1.5ul	Standard	27,488,922
3	C57BL/6 wildtype	anti-BRCA1 polyclonal rabbit, 0.75ul	Standard	60,742,753
4	C57BL/6 wildtype	anti-BRCA1 monoclonal mouse, 10ul	Standard	47,241,574

* KE = kinetic enrichment, as described by Khil et al. (2012)

b

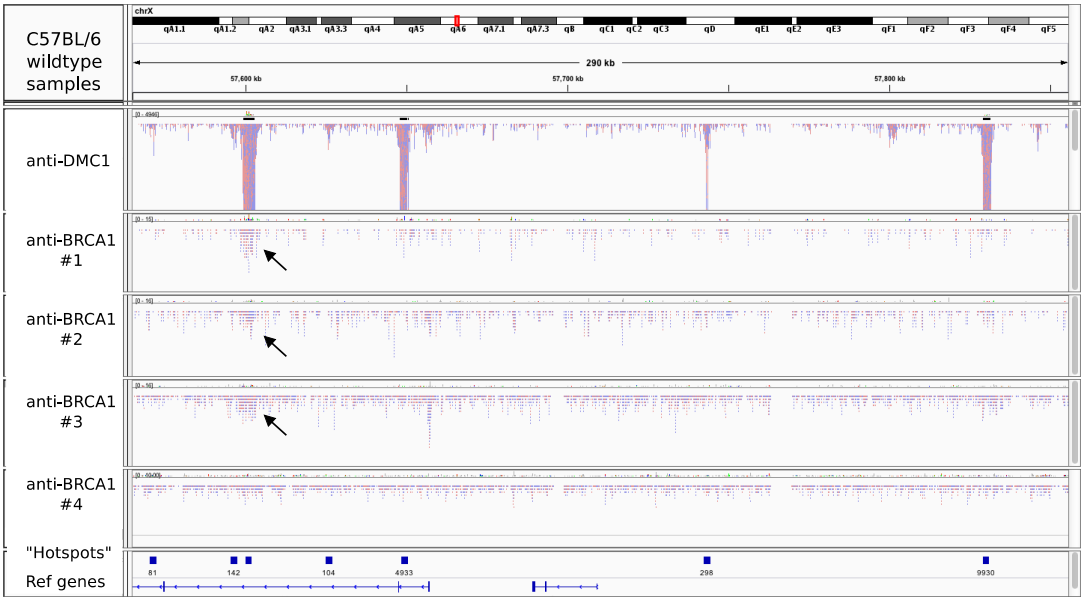

c

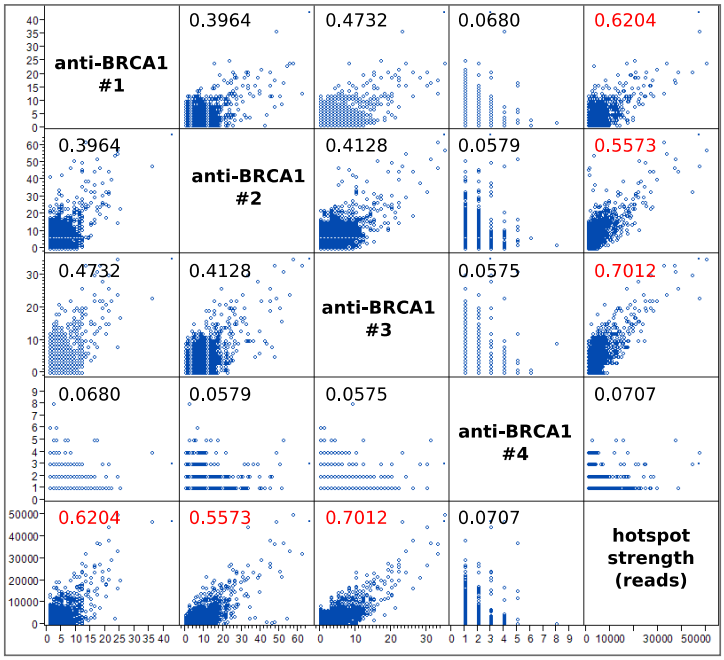

Figure 5.4. Anti-BRCA1 ChIP-seq in wildtype spermatocytes.

(**a**) Summary of anti-BRCA1 ChIP-seq experimental conditions and sequencing results. The standard protocol (Smagulova et al., 2011) and kinetic enrichment (KE) protocol (Khil et al., 2012) was followed as described previously. PF = post filter clusters. (**b**) Representative image showing anti-BRCA1 sequencing reads across the same 290kb region on

chromosome X as shown in Figure 5.3. There is some anti-BRCA1 enrichment compared to background in a minority of DMC1-defined hotspots (arrows, samples #1-3), however the degree of enrichment is small compared to that observed by DMC1 ChIP-seq. (**c**) Correlation plots of anti-BRCA1 read enrichment across the genome between samples compared to hotspot strength (defined by DMC1 enrichment). Number in top left corner of each box is the Pearson's correlation coefficient, where 1.0 indicates a perfect positive linear correlation. Red signifies relatively high positive correlations.

6.1.5 Anti-BRCA1 ChIP-seq in *Spo11*-/- mice

If BRCA1 localizes to meiotic DNA DSB sites, as indicated by my cytological data (Figure 5.1) and ChIP-seq data (Figure 5.4), then why are BRCA1 foci present in DNA DSB-deficient *Spo11*-/- spermatocytes? One possibility is that BRCA1 localizes to chromosomes prior to the formation of DNA DSBs. Under this model, BRCA1 could serve to recruit SPO11 or other DNA DSB machinery to generate DNA DSBs at specific sites. This would predict that BRCA1 would be enriched at hotspots *Spo11*-/- spermatocytes, like in wildtype spermatocytes.

To test this possibility, I performed anti-BRCA1 ChIP-seq on *Spo11*-/- spermatocytes (**Figure 5.5a**). *Spo11*-/- male mice arrest at the mid-pachytene stage of prophase I (Baudat et al., 2000), and are therefore enriched in spermatocytes in early prophase I. To control for this arrest effect, I also performed anti-BRCA1 ChIP-seq using *Dmc1*-/- spermatocytes (**Figure 5.5a**), which also arrest at mid-pachytene (Pittman et al., 1998). I verified earlier that BRCA1 foci are present in *Dmc1*-/- spermatocytes using chromosome spreads (see Figure 5.1e). For these ChIP-seq experiments, I used the same ChIP conditions that were used for sample 3 in the previous experiment (anti-BRCA1, pRb, 0.75ul), since they provided the best results in wildtype spermatocytes (**Figure 5.5a**).

For both *Spo11*-/- and *Dmc1*-/- genotypes, I generated negative control "input" samples. Input samples are made from an aliquot of the sample chromatin before it is subject to immunoprecipitation. Comparing input samples to anti-BRCA1 ChIP samples allow for identification of true peaks of BRCA1 enrichment (Smagulova et al., 2011).

In the control anti-BRCA1 *Dmc1*-/- sample, I observed BRCA1 enrichment at hotspot locations (**Figure 5.5b**). I measured this quantitatively using a metric called Fraction of sequencing Reads In Hotspots (FRIP), which estimates enrichment within hotspots. Importantly, FRIP was significantly higher in the *Dmc1*-/- sample (2.8%) compared to the input sample (1.6%) (**Figure 5.5b**). Furthermore, the FRIP for the *Dmc1*-/- sample was similar to that for the anti-BRCA1 wildtype ChIP sample

produced in my previous experiment (**Figure 5.5b**). These data confirm that BRCA1 is enriched at DNA DSB sites in the *Dmc1*-/- control.

By contrast, there was no significant BRCA1 enrichment at hotspots in the *Spo11*-/- sample (**Figure 5.5b**). The FRIP for the *Spo11*-/- ChIP sample (1.6%) and the *Spo11*-/- input negative control (1.5%) were not significantly different (**Figure 5.5b**). Furthermore, there was no detectable correlation between BRCA1 reads in the *Spo11*-/- sample and hotspot strength (**Figure 5.5c**). This suggests that BRCA1 is not enriched at hotspots in *Spo11*-/- spermatocytes.

To determine if there are any locations in the genome with BRCA1 enrichment, I then looked for BRCA1 peaks outside of hotspot sites. Based on peak calling algorithms, there were only 71 BRCA1 peaks in the *Spo11*-/- ChIP sample, and only three (4%) localized to existing hotspot sites (**Figure 5.5d**). This is in contrast to the *Dmc1*-/- sample, in which 67% of the 79 identified peaks were located within hotspots (**Figure 5.5d**).

Notably, the majority of the 71 peaks identified in the *Spo11*-/- sample were also found in the input control, and thus likely represented mapping artifacts (not shown). Only four peaks in the *Spo11*-/- samples were not in the input negative control, and of these, all were located at transcription start sites (**Figure 5.5e**). This is consistent with a report that suggests a putative role for BRCA1 in transcriptional regulation (Mullan et al., 2006). I confirmed these results with replicate experiments (not shown).

In summary, based on my anti-BRCA1 ChIP-seq data, BRCA1 does not localize to meiotic DNA DSB hotspots in *Spo11*-/- spermatocytes. These data are not consistent with a model whereby BRCA1 is upstream of SPO11 in the meiotic DNA DSB pathway.

a

Sample	Genotype	ChIP antibody	Description	Clusters (PF)
1	*Dmc1-/-*	anti-BRCA1 (pRb)	Standard protocol	118,209,473
2	*Dmc1-/-*	NA	Input	111,231,950
3	*Spo11-/-*	anti-BRCA1 (pRb)	Standard protocol	93,492,664
4	*Spo11-/-*	NA	Input	88,618,480

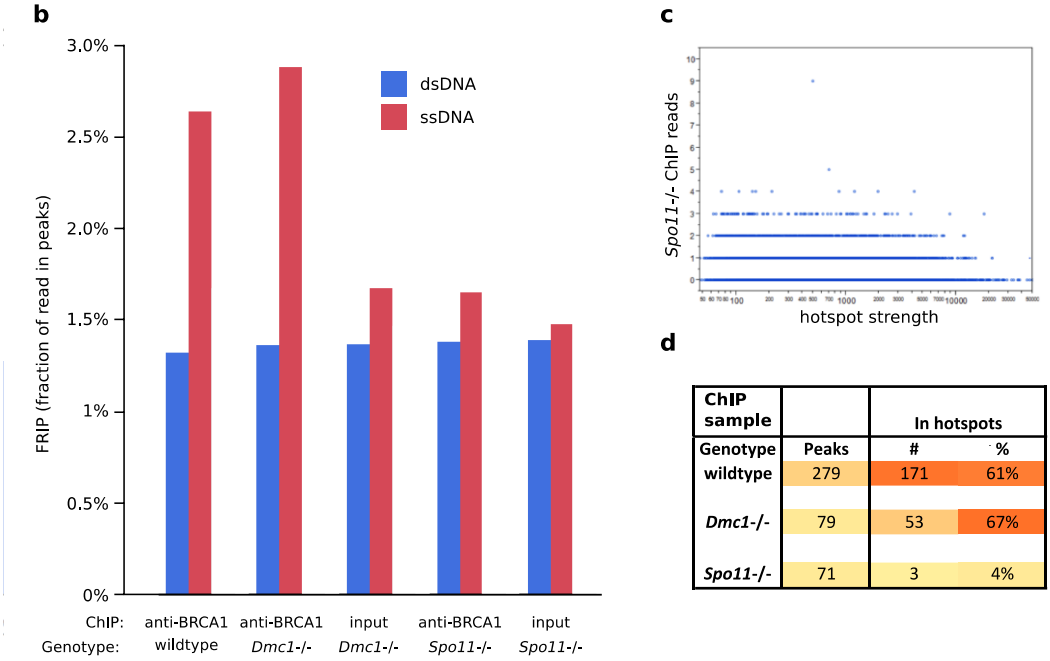

ChIP sample		In hotspots	
Genotype	Peaks	#	%
wildtype	279	171	61%
Dmc1-/-	79	53	67%
Spo11-/-	71	3	4%

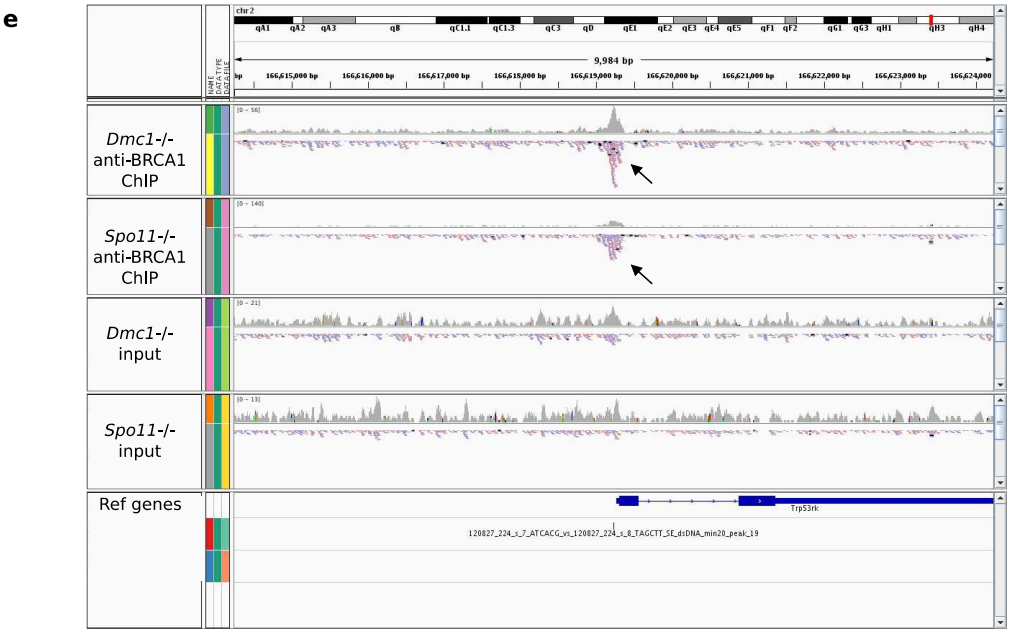

Figure 5.5. Anti-BRCA1 ChIP-seq in *Spo11*-/- spermatocytes.

(**a**) Summary of anti-BRCA1 ChIP-seq experimental conditions and sequencing results. For the two anti-BRCA1 samples (#1,3), I used 0.75ul of pRb antibody, which produced the best results in wildtype spermatocytes (Figure 5.4c). (**b**) Fraction of sequencing reads within hotspot peaks for each sample. If BRCA1 associates with DNA DSBs, anti-BRCA1 ChIP-seq samples should be enriched for DNA fragments (i.e. ssDNA) within hotspots.

The fraction of reads in peaks (i.e. hotspots) (FRIP) is a measure of the percentage of sequencing tags/reads mapping to hotspots. There is enrichment of ssDNA fragments within hotspots in wildtype and *Dmc1*-/- ChIP samples compared to input (negative control), but no significant enrichment of ssDNA fragments within hotspots in the *Spo11*-/- sample compared to input. (**c**) No detectable correlation between anti-BRCA1 ChIP reads and hotspot strength in the absence of *Spo11*. (**d**) Total number of peaks in samples, and the number/percentage of those peaks located within known hotspots. Darker color indicates a higher number/percentage. (**e**) Representative IGV snapshot showing one of four significant peaks of BRCA1 enrichment in the *Spo11*-/- sample (arrow). The peak is located within the promoter region of a gene on chromosome 2, called *Trp53rk*, which encodes a p53 kinase (Abe et al., 2001).

6.1.6 Anti-DMC1 ChIP-seq in *Brca1*-/- spermatocytes

Based on the above results, it seems unlikely that BRCA1 is critical for the designation and/or repair of meiotic DNA DSBs. However, they do not discount the possibility that BRCA1 is involved in positioning/location, or strength of meiotic DNA DSBs. In mammals, PRDM9 is a major determinant of meiotic DNA DSB hotspot location in the genome (Baudat et al., 2010; Brick et al., 2012). However, other currently undefined factors could also be involved in the designation of meiotic DNA DSB hotspot location. If BRCA1 is involved in regulating DNA DSB positioning, then I would expect hotspot locations to be altered in *Brca1* mutant mice, as observed in *Prdm9*-/- mice (Brick et al., 2012).

To test this possibility, I mapped hotspots by anti-DMC1 ChIP-seq in *Brca1*-/- *53bp1*-/- mutants. First, I assessed whether *53bp1* deletion affects hotspot location and strength. There was a strong positive correlation between DMC1 enrichment at hotspots between *Brca1*+/+ *53bp1*-/- controls and wildtype controls (**Figure 5.6a**), suggesting that hotspot location and strength are unaffected on the *53bp1*-/- background.

Next, I analyzed whether hotspot location and strength differed between *Brca1*-/- *53bp1*-/- and littermate *Brca1*+/+ *53bp1*-/- controls. Notably, there was a strong positive correlation in DMC1 enrichment at hotspots between *Brca1*-/- *53bp1*-/- and *Brca1*+/+ *53bp1*-/- littermate controls (Pearson, R=0.8997) (**Figure 5.6b**), and also between *Brca1*-/- *53bp1*-/- and wildtype controls (Pearson, R=0.9228) (**Figure 5.6c**). Based on peak calling algorithms, the number of hotspots in each of our samples ranged from 12,441 to 19,488 depending on the genotype (**Figure 5.6d**). Notably, the vast majority of hotspots overlapped between *Brca1*-/- *53bp1*-/-, *Brca1*+/+ *53bp1*-/-, and wildtype samples (**Figure 5.6e**). This indicates that *Brca1* deletion does not significantly affect hotspot strength or location.

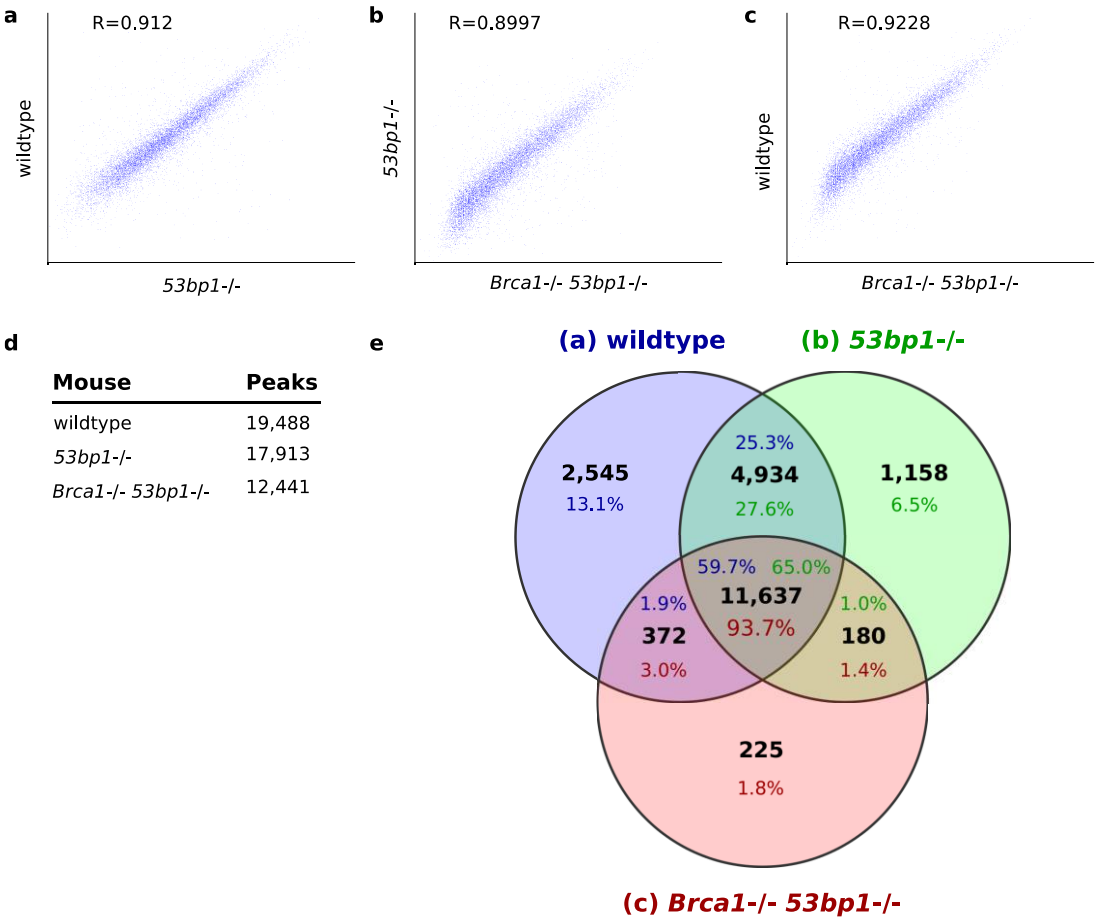

Mouse	Peaks
wildtype	19,488
53bp1-/-	17,913
Brca1-/- 53bp1-/-	12,441

Figure 5.6. Anti-DMC1 ChIP-seq in *Brca1*-/- spermatocytes.

(**a**) Correlation of DMC1 enrichment (i.e. strength) at known DNA DSB hotspot locations between DMC1 ChIP-seq samples. The R value represents the Pearson's correlation coefficient for each comparison. All comparisons showed a significant positive correlation, suggesting that hotspot strength across the genome is largely unchanged by deletion of *Brca1*. (**b**) Number of peaks in DMC1 ChIP-seq samples determined by peak calling algorithms. (**c**) Venn diagram showing the number/percentage of peaks that overlaps between wildtype, *53bp1-/-*, and *Brca1-/- 53bp1-/-* samples. Only overlaps in the central 400bp of hotspots were counted, as described previously (Brick et al., 2012).

6.1.7 ATR localization in *Brca1*-/- spermatocytes

The above analyses suggest that BRCA1 is dispensable for meiotic DNA DSB events. A non-essential role for BRCA1 in meiotic DNA DSB repair is also consistent with the observation that *Brca1* mutant females are fertile (Xu et al., 2003). The *Brca1*-/- male infertility phenotype is therefore due to BRCA1's role in a male-specific process, namely MSCI. This is supported by earlier work on *Brca1*Δ11/Δ11 *p53*+/- mutants, which have defective targeting of ATR to the X and Y chromosome and failed MSCI (Turner et al., 2004).

ATR shows two distinct localization patterns in spermatocytes. In wildtype mice, ATR forms foci on chromosome cores during leptonema and zygonema (Keegan et al., 1996; Moens et al., 1999; Perera et al., 2004) (**Figure 5.7a-b**). At pachynema and diplonema, by contrast, ATR labels the axis and chromatin of the asynapsed X and Y chromosomes (**Figure 5.7c-d**).

While there is evidence that BRCA1 is necessary for recruiting ATR to the sex chromosomes at pachynema (Turner et al., 2004), it is not clear whether BRCA1 is required for targeting of ATR foci to chromosome cores during early meiotic prophase I. To address this, I examined ATR localization at zygonema in *Brca1* mutant spermatocytes. I observed ATR foci on pre-synaptic axes in zygotene spermatocytes in both the control and *Brca1*-/- *53bp1*-/- males (**Figure 5.7e,f**). This indicates that BRCA1 is not required for targeting of ATR foci to chromosomes during early meiotic prophase I.

Next, I studied the localization of ATR at pachynema in the *Brca1*-/- *53bp1*-/- mutant mouse. Previous studies reported failed targeting of ATR to the asynapsed sex chromosomes in the *Brca1*Δ11/Δ11 *p53*+/- mutant (Turner et al., 2004). As expected, ATR localized normally to the asynapsed X-Y chromosomes during pachynema in *Brca1*+/+ *53bp1*-/- control spermatocytes (**Figure 5.7g**). By contrast, in *Brca1*-/- *53bp1*-/- pachytene spermatocytes, I observed disrupted localization of ATR on the asynapsed X-Y (**Figure 5.7h-l**).

There were several different abnormal ATR staining patterns in *Brca1*-/- *53bp1*-/- mutants (**Figure 5.7h-l**). In the majority of mutant

spermatocytes (70%, n=100 cells), ATR localized to the asynapsed sex chromosomes as several foci (**Figure 5.7h**), sometimes involving a large focus near the PAR (**Figure 5.7i**). These ATR foci are reminiscent of the pattern of DNA DSBs proteins on the asynapsed sex chromosomes. In a small percentage of pachytene spermatocytes (10%), ATR accumulated along the length of the asynapsed X-Y chromosomes, but not within the chromatin (**Figure 5.7j**). In another subset of spermatocytes (15%), ATR localized only as a very large and intense focus at the PAR of the X-Y chromosomes (**Figure 5.7k**). In the remaining spermatocytes (5%), ATR was seen within the chromatin of the X-Y chromosomes, but rarely encompassed the entire chromatin domain of the sex chromosomes (**Figure 5.7l**). I also noticed that X-Y pairing was disrupted in a subset of mutant spermatocytes (**Figure 5.7h,j**).

This *Brca1* mutant phenotype is consistent with previously published work on the *Brca1*Δ11/Δ11 mutant (Turner et al., 2004). In conclusion, BRCA1 is dispensable for DNA DSB events during meiosis, but is essential for proper targeting of ATR to the sex chromosomes for meiotic silencing.

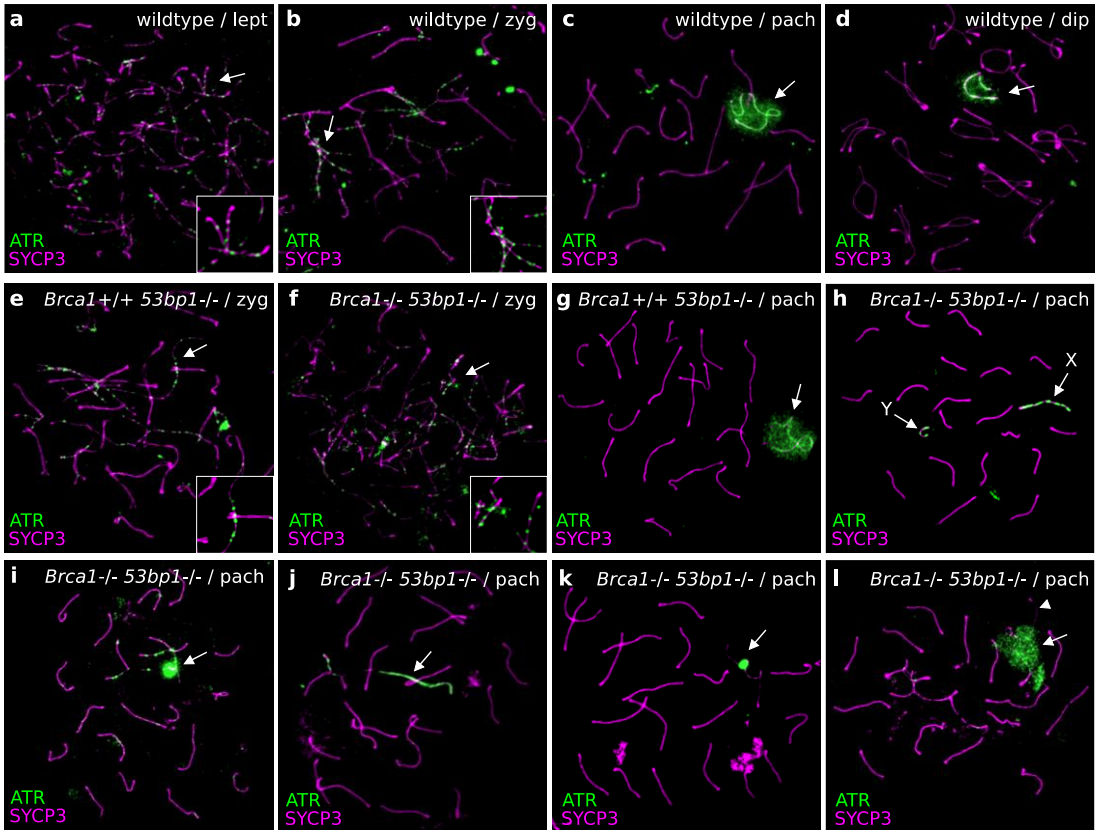

Figure 5.7. ATR localization in wildtype and *Brca1*-/- spermatocytes.

(**a-d**) Wildtype spermatocytes double-immunostained for ATR and SYCP3. (**a,b**) ATR foci are present along presynaptic chromosome cores at leptonema and zygonema. Arrows point to representative regions magnified in inset. (**c**,**d**) ATR labels the XY axis and sex chromatin (arrows) at pachynema and diplonema. (**e**) Control *Brca1*+/+ *53bp1*-/- zygotene spermatocyte, normal ATR foci. (**f**) *Brca1*-/- *53bp1*-/- zygotene spermatocyte, normal ATR foci. (**g**) Control *Brca1*+/+ *53bp1*-/- pachytene spermatocyte, normal ATR staining within the sex chromatin. (**h-l**) Mutant *Brca1*-/- *53bp1*-/- pachytene spermatocytes, showing abnormalities in ATR staining on the X and Y chromosomes. Abnormal XY ATR staining patterns observed include: (**h**) multiple ATR foci (arrows); (**i**) multiple ATR foci with a large ATR signal near the PAR (arrow); (**j**) partial axial ATR staining (arrow); (**k**) a single large ATR focus near the PAR (arrow); (**l**) abnormal chromatin ATR staining (arrow), not encompassing the entire chromatin region of asynapsis (arrowhead).

6.2. Role of *Hormad2* in meiotic silencing

6.2.1 Localization of silencing factors in *Hormad2-/-* mice

To understand the impact of *Hormad2*-deficiency on meiotic silencing, I first examined the localization of several important silencing factors in *Hormad2*-/- mutants, including BRCA1, ATR, and γH2AFX. In *Hormad1*-/- mice, the level of HORMAD2 and BRCA1 and the asynapsed X and Y chromosomes is greatly reduced, suggesting that HORMAD1 is upstream of HORMAD2 and BRCA1 (Daniel et al., 2011). However, the relationship between HORMAD2, BRCA1, and γH2AFX has not been studied.

To address this, I examined *Hormad2*-/- and control wildtype spermatocytes triple-immunstained for SYCP3, BRCA1, and γH2AFX (**Figure 5.8**). As expected, in early pachytene control spermatocytes, BRCA1 localized to the asynapsed X-Y axes and γH2AFX accumulated in the X-Y chromatin (**Figure 5.8a,b**). By contrast, in early pachytene spermatocytes from *Hormad2*-/- mice, X-Y BRCA1 staining was not linear, but foci-like, and did encompass the entire X-Y axes length (**Figure 5.8c**). While γH2AFX was present within the sex chromatin of *Hormad2*-/- spermatocytes, the staining pattern was aberrant, oftentimes not involving all the chromatin (**Figure 5.8d, arrow**). Furthermore, in a subset of *Hormad2*-/- spermatocytes, only a few faint BRCA1 foci were visible on the asynapsed sex chromosomes (**Figure 5.8e**), and this was associated with a drastic reduction in γH2AFX staining (**Figure 5.8f**).

I also noticed that in general that BRCA1 and γH2AFX in *Hormad2*-/- spermatocytes was more prominent near the distal region of the X-Y chromosomes (i.e. near the PAR) (**Figure 5.8g,h, arrows**). In other words, the centromeric region of the X chromosome was not frequently labeled with BRCA1 or γH2AFX (**Figure 5.8g,h, arrowheads**). In summary, targeting and/or accumulation of the silencing factors BRCA1 and γH2AFX is disrupted in the absence of *Hormad2*.

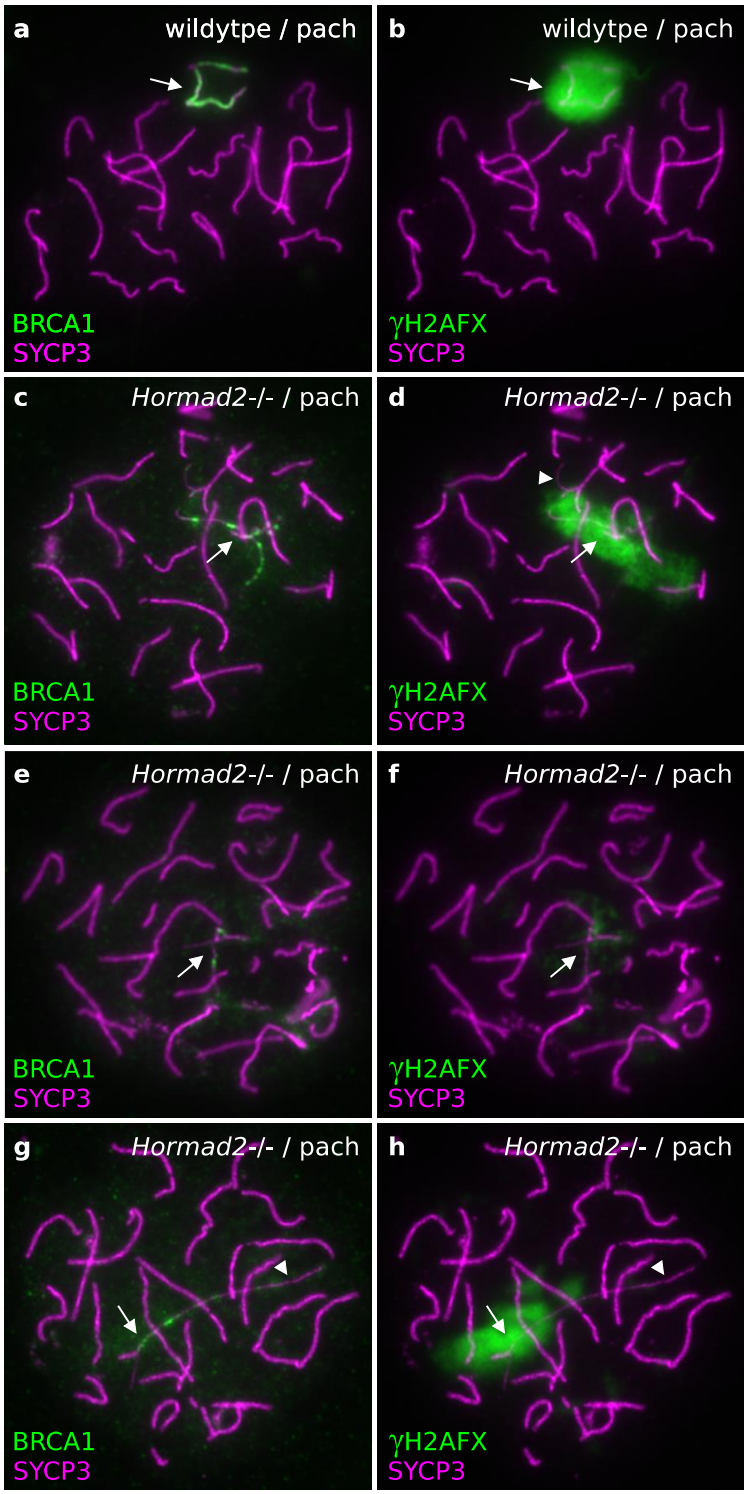

Figure 5.8. Abnormal BRCA1 and γH2AFX staining in *Hormad2*-/- spermatocytes.

(**a,b**) Wildtype pachytene spermatocyte with normal linear localization of BRCA1 along the asynapsed cores of the XY chromosomes. (**b**) Same wildtype spermatocyte showing normal accumulation of γH2AFX within the sex chromatin. (**c**) *Hormad2*-/- pachytene spermatocyte with abnormal BRCA1 staining, characterized by BRCA1 foci, rather than linear BRCA1 staining. (**d**) Same *Hormad2*-/- spermatocyte with diffuse staining of

γH2AFX on the asynapsed sex chromosomes. Arrowhead points to an asynapsed region not labeled with γH2AFX. (**e**) *Hormad2*-/- pachytene spermatocyte with only a few faint BRCA1 foci. (**f**) Same *Hormad2*-/- spermatocyte with drastic reduction in γH2AFX staining. (**g**) *Hormad2*-/- pachytene spermatocyte with few BRCA1 foci near the PAR end of the chromosome (arrow), but none near the centromeric end (arrowhead). (**h**) Same *Hormad2*-/- spermatocyte with γH2AFX staining near the PAR (arrow), but not near the centromeric end (arrowhead).

6.2.2 RNA FISH analysis of X gene transcription in Hormad2-/- mice

The above data suggests that HORMAD2, like HORMAD1, is an important component of the meiotic silencing response. Specifically, HORMAD2 is required for recruiting and/or stabilizing BRCA1. To formally verify a role for HORMAD2 in silencing, I next assessed X chromosome gene transcription in *Hormad2*-/- spermatocytes. If HORMAD2 is a *bona fide* silencing factor, than *Hormad2*-/- spermatocytes should exhibit de-repression of the sex chromosomes, as found in other silencing mutants such as *H2afx*-/- and *Mdc1*-/- mice (Fernandez-Capetillo et al., 2003; Ichijima et al., 2011; Turner et al., 2004).

I assessed X-linked gene transcription in *Hormad2* spermatocytes by gene-specific RNA FISH. I probed for the same three X-linked genes that I studied in my analysis of silencing in XO oocytes and XY spermatocytes, namely *Scml2*, *Utx,* and *Zfx* (see Figure 4.1). I first assessed transcription of *Scml2*, *Utx,* and *Zfx* by RNA FISH in *Hormad2*-/- spermatocytes compared to wildtype spermatocytes (**Figure 5.9a-d**). Using this approach, I found that *Utx* and *Zfx* were expressed in a significantly higher percentage of early pachytene spermatocytes in *Hormad2*-/- mice compared to wildtype controls (**Figure 5.9e,f**). This indicates a silencing defect in *Hormad2*-/- spermatocytes. Interestingly, the frequency of escape from silencing for *Scml2* was not significantly different between wildtype and *Hormad2*-/- mice (**Figure 5.9e,f**).

Next, I compared the level of X de-repression in *Hormad2*-/- mutants to that of *H2afx*-/- mutants, which do not undergo silencing (Fernandez-Capetillo et al., 2003). While the frequency of escape from silencing for *Zfx* was similar between *Hormad2*-/- and *H2afx*-/- mice, the level of escape in *H2afx*-/- compared to *Hormad2*-/- spermatocytes was higher for *Utx* and *Scml2* (**Figure 5.9d,e**). This suggests that a regional disruption of MSCI occurs in *Hormad2*-/- spermatocytes, whereby the centromeric end of the X (i.e. near *Zfx*) is more disrupted than the PAR end (i.e. near *Smcl2*). This is consistent with my earlier observation that γH2AFX in *Hormad2*-/- spermatocytes is more often associated with the PAR end of the X-Y chromosomes.

In summary, *Hormad2*-deficiency leads to at least partial de-repression of the X chromosome. Further characterization of the *Hormad2*-/- mouse, by Attila Tóth and colleagues (Wojtasz et al., 2012), highlighted that MSCI defects are the predominant meiotic phenotype in *Hormad2*-/- mice. This work has revealed that HORMAD2 is an important component of the meiotic silencing pathway in mammals.

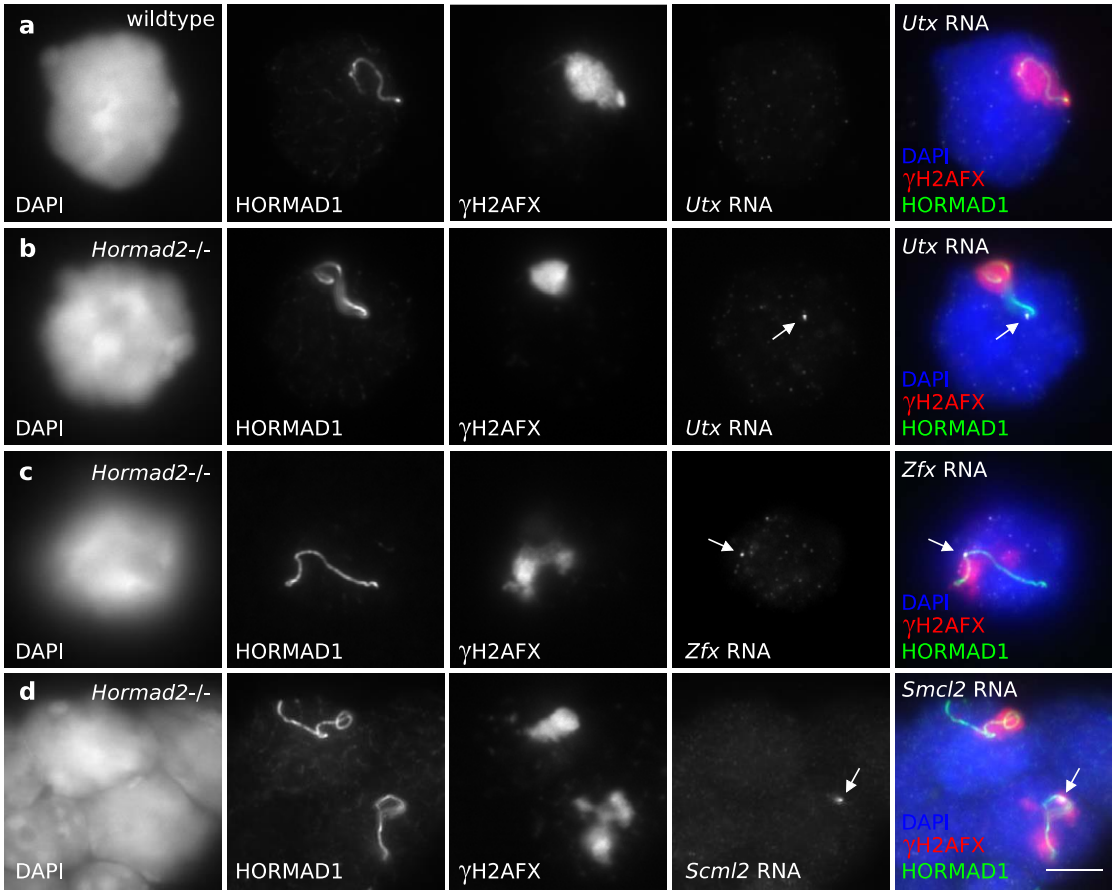

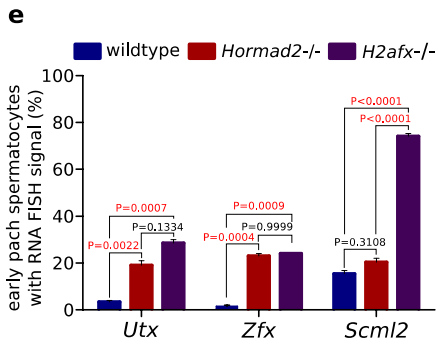

f

Genotype	*Utx*	*Zfx*	*Scml2*
Wildtype #1	4/100	1/100	14/101
Wildtype #2	3/102	2/100	17/101
Hormad2-/- #1	21/100	24/100	22/100
Hormad2-/- #2	17/100	22/100	29/101
H2afx-/- #1	27/101	24/100	76/101
H2afx-/- #2	30/100	24/100	73/100

Figure 5.9. RNA FISH analysis of *Hormad2-/-* spermatocytes.

(**a**) Wildtype early pachytene spermatocyte nucleus subject to RNA FISH for *Utx* (no signal = not expressed), and immunostaining for HORMAD1 and γH2AFX, to identify the asynapsed X chromosome. (**b**) *Hormad2-/-* early pachytene nucleus with an RNA FISH signal for *Utx* (arrow), indicating expression of *Utx* from the asynapsed X chromosome. The region that X chromosome adjacent to the *Utx* RNA FISH signal is devoid of γH2AFX. (**c**) *Hormad2-/-* early pachytene nucleus showing a *Zfx* RNA FISH signal in a region adjacent to an abnormal γH2AFX domain. (**d**) Two *Hormad2-/-* early pachytene nuclei with abnormal γH2AFX domains. The top nucleus is negative for *Scml2* RNA FISH signal, while the bottom nucleus has an *Scml2* RNA FISH signal. (**e**) Percentage of early pachytene spermatocytes with an RNA FISH signal for *Utx*, *Zfx*, and *Scml2* in wildtype, *Hormad2-/-*, and *H2afx-/-* mice. Tukey multiple comparison tests were performed. Red P values are

significant. (**e**) Raw data showing number of early pachytene spermatocytes with an RNA FISH signal for *Utx*, *Zfx*, and *Scml2* in wildtype, *Hormad2*-/-, and *H2afx*-/- mice.

6.3 Discussion

In the final result chapter of my thesis, I provide several lines of evidence that both BRCA1 and HORMAD2 have important roles in the establishment of meiotic silencing in spermatocytes. Furthermore, I showed that BRCA1 is unlikely to be a critical component of the meiotic DNA DSB repair system.

BRCA1 is a multifunctional protein that is important for maintenance of genomic stability in somatic cells (Huen et al., 2010). BRCA1's role as a tumor suppressor its thought to be related to its critical functions in cell cycle checkpoint control and the DNA damage response (Huen et al., 2010). The *Brca1* gene encodes a protein with a RING finger domain, which confers E3 ubiquitin ligase activity to BRCA1, and tandem BRCT domains, which are involved in binding phosphorylated proteins that facilitate the DNA damage response (Huen et al., 2010). Early work revealed that BRCA1 localizes at DNA DSBs in both mitotic and meiotic cells, implicating BRCA1 in the DDR in germ cells (Scully et al., 1997).

A role for BRCA1 in the meiotic DNA DSB repair pathway was supported by meiotic analysis of *Brca1*Δ11/Δ11 mutant mice, which encode a truncated allele of *Brca1* (Xu et al., 2003). This study reported aberrant localization of the DNA repair protein RAD51 in the absence of wildtype BRCA1 (Xu et al., 2003). A subsequent meiotic analysis of *Brca1*Δ11/Δ11 mutant mice uncovered a distinct role for BRCA1 in the meiotic silencing pathway (Turner et al., 2004). In the *Brca1*Δ11/Δ11 spermatocytes, ATR and γH2AFX do not accumulate on the asynapsed X and Y chromosomes at pachynema, leading to failed silencing of the sex chromosomes (Turner et al., 2004). In summary, BRCA1 is thought to have two major functions during meiosis: (1) DNA DSB repair and (2) meiotic silencing.

In wildtype spermatocytes, BRCA1 foci were located on pre-synaptic chromosome axes in leptonema and zygonema and overlapped DMC1 foci. Using ChIP-seq, I showed that the majority of BRCA1 peaks in wildtype spermatocytes are located at sites meiotic DNA DSB hotspots. Furthermore, the level of BRCA1 enrichment at hotspots was positively correlated with

hotspot strength. Together, these data support that BRCA1 associates at DNA DSBs in normal meiosis.

Paradoxically, BRCA1 foci were also observed in programmed DNA DSB-deficient *Spo11*-/- spermatocytes, in agreement with a previous report (Mahadevaiah et al., 2008). This confirms that the initial recruitment of BRCA1 foci onto pre-synaptic chromosome axes is not dependent on DNA DSB formation *per se*. Based on my anti-BRCA1 ChIP-seq data, there was no obvious pattern of BRCA1 enrichment in *Spo11*-/- spermatocytes. This indicates that BRCA1 foci in *Spo11*-/- spermatocytes are not located at hotspot sites, but rather likely bind stochastically to pre-synaptic chromosome axes when DNA DSBs are not present to target BRCA1 to specific sites.

I conclude that BRCA1 does not pre-designate sites of DNA DSBs, and suspect that BRCA1 is actively recruited to DNA DSB sites once formed by SPO11. Like in somatic cells, BRCA1 may be recruited to DNA DSB sites by some early DNA damage response factor, like γH2AFX and/or MDC1 (Lou et al., 2003). Addressing this will involve additional studies of BRCA1 foci localization in other meiotic mutants, e.g. *H2afx*-/-, *Mdc1*-/-, etc.

Impaired loading of RAD51 in *Brca1*Δ11/Δ11 *p53*+/- spermatocytes suggests an important role for RAD51 in meiotic DNA repair events (Xu et al., 2003). However, in my analysis, I observed normal localization of RAD51 in *Brca1*Δ11/Δ11 mutant spermatocytes, which is consistent with a more recent analysis (Broering et al., 2014). This studied also reported normal localization of other homologous recombination factors, such as MSH4 and MLH1 (Broering et al., 2014). Therefore, *Brca1* deficiency has little effect on DNA DSB repair events in spermatocytes.

My subsequent analysis of BRCA1 revolved around the putative role for BRCA1 in meiotic silencing. ATR normally localizes to unrepaired DNA DSBs as foci during early meiotic prophase I (Burgoyne et al., 2007), and spreads along asynapsed axes by pachynema (Turner et al., 2004). Consistent with this early analysis of *Brca1*Δ11/Δ11 mutants (Turner et al., 2004), I observed defective ATR chromatin accumulation in *Brca1*-/- *53bp1*-/- spermatocytes. In this mutant, ATR localized only partially to the

asynapsed X and Y chromosome axes as foci or short stretches, suggesting failure to spread beyond sites of DNA DSBs.

Based on these observations, it is tempting to speculate that BRCA1 is a key factor linking DNA DSBs to meiotic silencing. Historically it has been thought that meiotic silencing occurs independent of DNA DSBs, because γH2AFX domains form in *Spo11*-/- germ cells (Mahadevaiah et al., 2001). However, subsequent experiments showed that meiotic silencing is not correctly targeted to the X and Y chromosomes in *Spo11*-/- spermatocytes (Bellani et al., 2005). My results, and a recently published analysis (Carofiglio et al., 2013)(Carofiglio et al., 2013)(Carofiglio et al., 2013)(Carofiglio et al., 2013)(Carofiglio et al., 2013)(Carofiglio et al., 2013)(Carofiglio et al., 2013)(Carofiglio et al., 2013)(Carofiglio et al., 2013)(Carofiglio et al., 2013), reveal the presence of DNA DSB repair foci within γH2AFX domains of *Spo11*-/- germ cells (**Figure 3.5**), suggesting a potential link between DNA DSBs and meiotic silencing.

Taken together, my BRCA1 results inform an updated model of the meiotic silencing pathway (**Figure 5.10a-b**). During normal meiosis, BRCA1 and ATR localize first to DNA DSBs during early prophase I, and then by pachynema, BRCA1 and ATR spread along the length of the asynapsed axes (Turner et al., 2004). In the absence of BRCA1, ATR cannot efficiently spread between DNA DSBs along the axes or within the chromatin, but is retained at unrepaired DNA DSBs (**Figure 5.10a-b**). Under this model, BRCA1's main meiotic role is to facilitate the spreading of ATR between DNA DSBs on asynapsed chromosomes. This new model places BRCA1 as an important intermediary connecting the DNA DSBs to meiotic silencing (**Figure 5.10a-b**).

The HORMA-domain containing protein HORMAD1 has been implicated in several meiotic processes, including the DNA DSB formation and repair, chromosome synapsis, meiotic silencing, and meiotic surveillance (Daniel et al., 2011; Kogo et al., 2012b; Shin et al., 2010; Shin et al., 2013). Another HORMAD-domain protein, HORMAD2, was recently identified in mammals (Wojtasz et al., 2009). Given that HORMAD1 and HORMAD2 have a similar localization pattern along asynapsed

chromosomes in mammalian germ cells (Fukuda et al., 2009), HORMAD2 may also play a role in meiotic silencing. Consistent with this, I found that BRCA1 accumulation on asynapsed axes is dependent on *Hormad2*.

Aberrant BRCA1 staining was also a feature of *Hormad1*-/- spermatocytes (Daniel et al., 2011), suggesting a potential interdependence between HORMAD1 and HORMAD2. However, HORMAD1 staining was normal in *Hormad2*-/- spermatocytes, indicating that HORMAD1 is upstream of HORMAD2. Indeed, there is reduced HORMAD2 staining in *Hormad1*-/- spermatocytes (Wojtasz et al., 2012), indicating that HORMAD1 recruits HORMAD2 to asynapsed chromosomes. Taken together, these results place HORMAD2 downstream of HORMAD1 and upstream of BRCA1 in the mammalian response to asynapsis (**Figure 5.10a**).

Given that BRCA1 was disrupted by *Hormad2* deletion, I expected downstream silencing factors to also be abnormal. Notably, γH2AFX rarely encompassed the full sex chromatin area in *Hormad2*-/- spermatocytes, and was more frequently associated with the PAR regions of the X-Y chromosomes than the centromeric regions. *Hormad2*-/- spermatocytes therefore show regional disruption of γH2AFX.

Additional work by the Tóth group revealed that *Hormad2* is also required for efficient ATR accumulation on asynapsed chromosomes (Wojtasz et al., 2012). By gene-specific RNA FISH, I observed regional disruption of meiotic silencing, with silencing at the PAR end being relatively intact compared to silencing near the centromere pole. I conclude that efficient meiotic silencing requires *Hormad2*.

Results from my *Brca1* and *Hormad2* mutant analyses, combined with other recent studies (Daniel et al., 2011; Ichijima et al., 2011; Royo et al., 2013), suggest a more detailed model for the meiotic silencing pathway. First, the DNA damage response is activated upon introduction of programmed (i.e. *Spo11*-dependent) or non-programmed (i.e. *Spo11*-independent) DNA DSBs during early meiotic prophase I, resulting in the accumulation of BRCA1, ATR, γH2AFX, and other DDR factors at DNA DSBs (**Figure 5.10b**). Concomitantly, HORMAD1 recruits HORMAD2 to pre-synaptic chromosome axes. Chromosome synapsis during the zygotene-

pachytene transition period facilitates homology-driven repair of DNA DSBs, and the subsequent displacement of BRCA1, ATR, γH2AFX, HORMAD1, and HORMAD2 from chromosomes.

In the absence of a pairing partner, as in the case of the heterologous regions of the X and Y chromosomes, unrepaired DNA DSBs persist into early pachynema, as do their associated DDR factors. At this stage, BRCA1 spreads between DNA DSB sites in a manner that depends upon HORMAD1 (Daniel et al., 2011), HORMAD2 (Wojtasz et al., 2012), and ATR (Royo et al., 2013). Similarly, ATR subsequently accumulates along the length of the asynapsed axes in a HORMAD1/2- and BRCA1-dependent fashion. Finally, ATR spreads from the chromosome axes into the chromatin loops, in a manner that requires MDC1 (Ichijima et al., 2011). Within the chromatin, ATR phosphorylates H2AFX at serine-139 to form γH2AFX (Royo et al., 2013), one of the important effectors of meiotic silencing (Fernandez-Capetillo et al., 2003). Recent work has also revealed that phosphorylation of various chromosome axes components, including HORMAD1, may be important for the silencing (Fukuda et al., 2012).

Similar to the role I ascribed for γH2AFX as a meiotic surveillance factor, subsequent work has revealed that *Hormad2* is required for the elimination of *Spo11*-/- oocytes (Kogo et al., 2012a; Wojtasz et al., 2012). Given the importance of HORMAD2 in the establishment of meiotic silencing, it is possible that HORMAD2's meiotic surveillance function is achieved through meiotic silencing. Alternatively, HORMAD2 could exert its quality control function via ATR, though an otherwise undefined synaptic checkpoint.

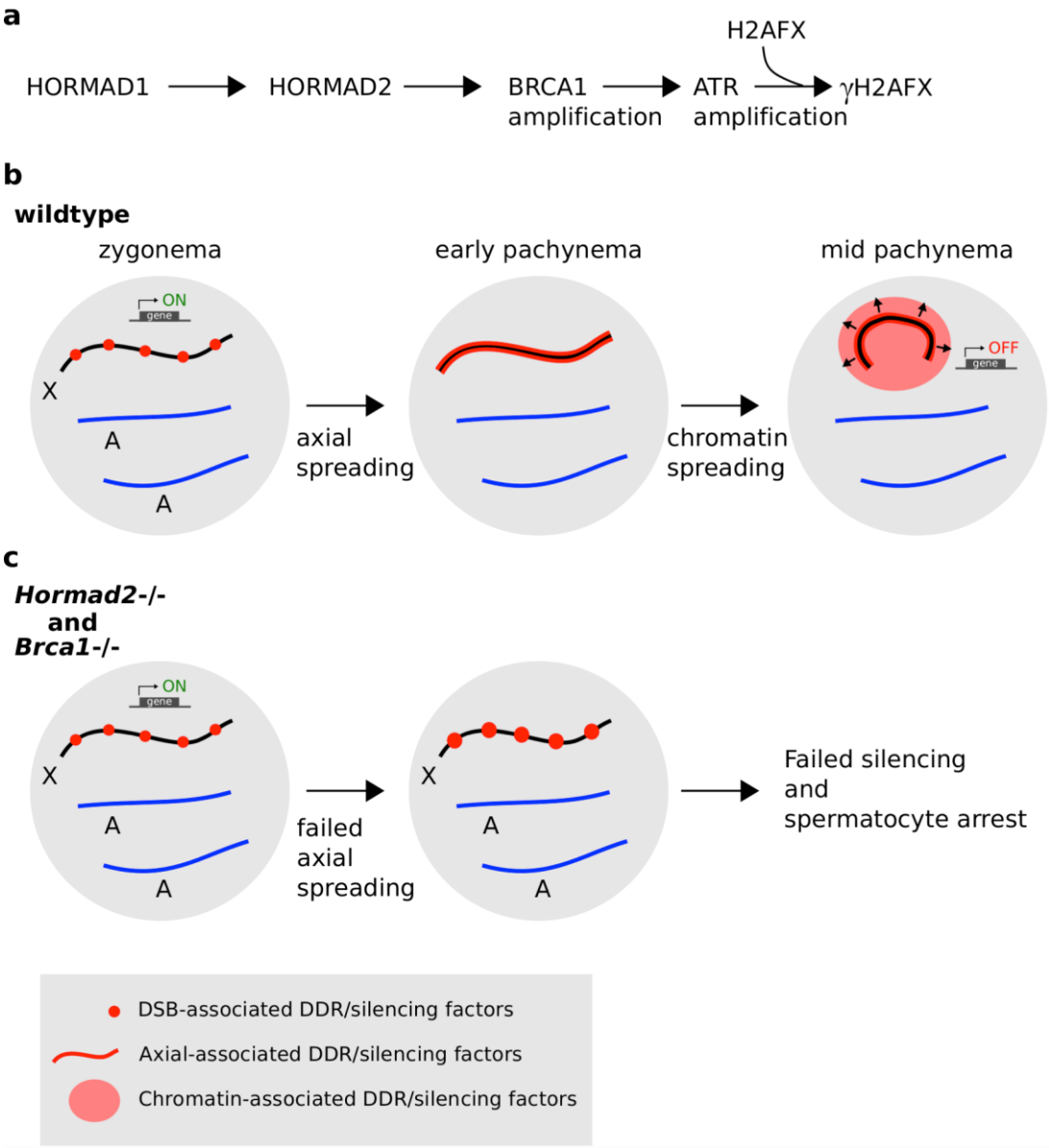

Figure 5.10. Model for mechanism of meiotic silencing in wildtype and mutant meiosis.

(**a**) Proposed sequence of events in meiotic silencing pathway. HORMAD1 binds asynapsed chromosome axes and recruits HORMAD2, which is required for the axial accumulation of BRCA1. BRCA1 then mediates amplification/spreading of ATR throughout the chromatin of the asynapsed chromosome. ATR then phosphorylates H2AFX, forming a γH2AFX silencing domain. (**b**) Proposed events on the asynapsed X chromosome in wildtype spermatocytes. DDR/meiotic silencing factors accumulate as foci near DNA DSBs on asynapsed chromosome axes. These foci are lost once chromosomes synapse, such as on autosomes (A). DDR/meiotic silencing factors, including BRCA1 and ATR, then spread from these DNA DSB-associated foci along the length of the asynapsed chromosome axes. This axial spreading is dependent upon HORMAD1, HORMAD2, BRCA1, and ATR. By mid-pachynema, silencing factors, including MDC1, ATR, and γH2AFX have spread throughout the chromatin, creating a stable silencing state. This

process requires HORMAD1, HORMAD2, BRCA1, ATR, MDC1, and H2AFX. (**c**) Proposed events in *Hormad2*-/- and *Brca1*-/- mice: DDR/meiotic silencing factors do not spread efficiently along the axes, which results in failed chromatin accumulation of silencing factions. Failure to establish a silenced X chromosome in these mutants results in spermatocyte arrest.

7 General discussion

7.1 Overall summary

The prophase I surveillance mechanisms that operate in germ cells have been a topic of considerable interest for decades. In mammals, these mechanisms serve to prevent aneuploidy in embryos by eliminating germ cells with defects. In doing this, however, these mechanisms can also lead to infertility. Despite their clinical importance, limited progress has been made toward understanding the molecular pathways of these surveillance mechanisms. In this thesis, I described and characterized a novel H2AFX-dependent mechanism of meiotic surveillance of asynapsis.

The findings in this thesis challenge the more classical models of meiotic surveillance, which are based on DNA damage and an asynapsis checkpoint, and in doing so they alter the way we think about the pathways that drive germ cell arrest and infertility in mammals. The H2AFX/meiotic silencing-based model is all-encompassing – it unifies existing data in both the male and female germ lines. Importantly, it can easily explain why an asynapsed X chromosome evokes oocyte arrest but not spermatocyte arrest. This paradox of mammalian meiosis is explained by the fact that silencing of important genes on the X chromosome in spermatocytes is compensated for by X-derived autosomal retrogenes, which is not active in oocytes.

In addition, I described a meiotic characterization of two targeted mutant mouse models, *Hormad2*-/- and *Brca1*-/- *53bp1*-/- mice, and in doing so identify new components of the meiotic silencing cascade. My results help clarify the role of BRCA1 in meiosis, and lead us to a simplified model of BRCA1 function in mammalian germ cells, in which BRCA1 functions mainly to facilitate the spreading of ATR along asynapsed chromosomes for silencing. Together, these findings help advance our understanding of mammalian meiosis and fertility. In the following sections, I will discuss outstanding questions and future directions of my work.

7.2 H2AFX-dependent meiotic surveillance

A major finding of this thesis is the role for H2AFX in the diplotene elimination of asynaptic oocytes in mice with chromosome abnormalities. My non-phosphorylatable H2AFX transgene study revealed that serine phosphorylation of H2AFX is the critical epigenetic event responsible for oocyte losses at diplonema. However, these data do not reveal the precise mechanism by which γH2AFX accumulation on asynapsed chromosomes drives oocyte losses.

Evidence that meiotic silencing is the mechanism by which γH2AFX triggers oocyte losses comes from my analysis of accessory chromosome mouse models (i.e. XXY and Tc1). In these models, accumulation of γH2AFX on the accessory asynapsed chromosomes was not associated with oocyte losses. These findings are consistent with the meiotic silencing model of oocyte arrest, but not the checkpoint model. These accessory chromosome results suggest that H2AFX-dependent oocyte losses are dependent on the gene content of asynapsed chromosomes, supporting the meiotic silencing model.

Nevertheless, it is important to acknowledge potential caveats of these experiments. First, it is possible that accessory chromosomes do not mount the same asynapsis response as endogenous chromosomes, and therefore do not trigger a checkpoint. However, I failed to identify any differences in the accumulation of meiotic silencing factors and DNA damage response factors, including BRCA1, ATR, γH2AFX, HORMAD1, and HORMAD2, between accessory and endogenous asynapsed chromosomes. While I cannot discount the possibility that there are unidentified epigenetic differences in the molecular response to asynapsed accessory chromosome, the available data suggests that accessory chromosomes trigger a normal response to asynapsis.

Another potential caveat is that the accessory chromosomes studied are appreciably smaller than the X chromosome in XO oocytes and therefore may not be sufficiently large to trigger oocyte arrest by a putative asynapsis checkpoint. The 171Mb mouse X chromosome is significantly larger than the

42Mb h21 Tc1 chromosome (O'Doherty et al., 2005) and the 91Mb mouse Y chromosome (Ensembl.org). Despite this size difference, however, I measured no significant difference in the intensity of the γH2AFX domain between XO and Tc1 oocytes. This suggests that differences in chromatin γH2AFX signaling are unlikely to contribute to the differential outcome of asynapsis in Tc1 and XO mouse models.

However, it is still possible that there are quantitative differences in other chromatin asynapsis factors, such as ATR, or some axial factors, such as HORMAD1 and HORMAD2, that contribute to oocyte elimination in XO females but not Tc1 females. Additionally, there may be some variations in epigenetic modifications that contribute to the different fates of these oocytes. Future studies should focus on further characterizing the proteins and modifications associated with asynapsed accessory chromosome.

Precisely how meiotic silencing of endogenous asynapsed chromosomes leads to arrest is unclear. The most parsimonious explanation is that the silencing of critical genes starves germ cells of necessary factors, thus leading to oocyte death. Alternatively, it could cause arrest through silencing of non-coding genes or transposons, or through changes in transcription factor binding profiles on asynapsed chromosomes. My data do not allow us to discriminate between these possibilities.

During male meiosis, accumulation of silencing factors, such as HORMAD1, HORMAD2, BRCA1, ATR, MDC1 and γH2AFX, on asynapsed autosomes causes prophase I arrest (Turner et al., 2005), but localization of the same proteins to the asynapsed X chromosome does not. Importantly, the X chromosome does not possess unique properties preventing it from triggering arrest. This is demonstrated by the fact that asynapsed accessory chromosomes, such as in Tc1 males, also fail to trigger prophase I arrest (Mahadevaiah et al., 2008) (unpublished results, Turner lab).

In contrast to the autosomes, however, the X chromosome is dramatically depleted in genes required for male meiosis (Khil et al., 2004; Wang, 2004). Interestingly, silencing of X-linked housekeeping genes is also compensated for by a unique backup system of autosomally-located, X-derived retrogenes that are essential for spermatogenesis (Bradley et al.,

2004; McCarrey and Thomas, 1987; Wang, 2004). The fact that both the X chromosome and accessory chromosomes are deficient in male meiotic genes could explain why H2AFX-induced silencing of these chromosomes does not induce prophase I arrest.

Silencing of the X chromosome in the female, by contrast, is expected to be deleterious, because the X chromosome is enriched for oogenesis genes (Khil et al., 2004), and the autosomal retrogene system that in males compensates for MSCI is not active in the female germ line. In theory, one could test this hypothesis by inserting transgenes for critical X-linked meiotic genes onto autosomes in XO mice and assessing for rescue of oocytes. However, this would be experimentally unrealistic given that the mouse X chromosome contains 940 coding genes, many of which are involved in oogenesis (Khil et al., 2004) such as *Zfx* (Luoh et al., 1997), and 180 long non-coding genes (ensemble.org).

Another important question that should be addressed is whether the rescue in XO *H2afx*-/- oocytes persists into adulthood. While *H2afx* ablation reverses XO perinatal oocyte losses, it is unclear whether the rescue is still evident after prophase I, or whether other surveillance mechanisms act later in development to eliminate those defective oocytes. To examine this, one can count oocytes in wildtype, XO, and XO *H2afx*-/- oocytes at later time points, including several weeks post-partum.

If oocyte numbers are lower in XO *H2afx*-/- females compared to wildtype females at these time points, it is possible that additional quality control mechanisms operate in response to asynapsis. If oocyte numbers remain similar to those found in wildtype females, then it is unlikely that other asynapsis safeguarding mechanisms exist.

7.3 Limitations of an H2AFX-based surveillance mechanism

Based on the work from this thesis, oocytes with an asynapsed X chromosome or an asynapsed autosome are eliminated during diplonema by an H2AFX-dependent mechanism. The limitations of this mechanism are not yet defined. For example, it is unclear whether this surveillance mechanism can function when challenged with larger amounts of asynapsis.

Two independent studies have shown that meiotic silencing breaks down in the presence of more than three pairs of asynapsed chromosomes (Kouznetsova et al., 2009; Mahadevaiah et al., 2008). It has been hypothesized that with more extensive asynapsis, important meiotic silencing factors, such as BRCA1 and ATR, are titrated to unrepaired DNA DSBs, and thus are not available to efficiently facilitate silencing (Kouznetsova et al., 2009; Mahadevaiah et al., 2008). Based upon this observation, I would expect that oocytes with significant levels of asynapsis (>4) would not be eliminated as efficiently as oocytes with fewer asynapsed chromosomes.

Indeed, based on preliminary findings from the Turner laboratory, F1 PWDxB6 oocytes with >4 asynapsed chromosomes show reduced γH2AFX staining and are not eliminated by late diplonema (unpublished results). By contrast, F1 PWDxB6 oocytes with ≤4 asynapsed chromosomes within the same ovaries show normal γH2AFX accumulation and are eliminated by late diplonema (unpublished results). This indicates that the H2AFX-dependent surveillance mechanism breaks down in the face of extensive asynapsis. Furthermore, it suggests that there is not an alternative or compensatory surveillance mechanism to deal with high levels of asynapsis.

To better characterize the limitations of the H2AFX surveillance mechanism, it will be important to determine the total length of asynapsed chromosome axes that causes γH2AFX localization to be disrupted. It will also be of interest to evaluate whether the disruption of meiotic silencing factors is in fact related to titrated at DNA DSBs, as others have suggested (Mahadevaiah et al., 2008).

Interestingly, I showed that DNA repair proteins do not persist on multiple asynapsed chromosomes in PWDxB6 F1 oocytes. To reconcile this, future work should characterize the localization of BRCA1 and ATR, and other factors with a shared role in the DNA damage response and meiotic silencing, on multiple asynapsed chromosomes in PWDxB6 F1 oocytes. Furthermore, it should be examined whether PWDxB6 F1 oocytes give rise to a high proportion of aneuploidy embryos as a result of a relaxed/disrupted prophase I surveillance mechanism.

7.4 DNA DSB repair and the DNA damage checkpoint in mice

Classically, the DNA damage checkpoint has been invoked to explain the elimination of oocytes with persistent DNA damage (Bolcun-Filas et al., 2014; Di Giacomo et al., 2005). In this thesis, I showed that markers of DNA DSB repair, such as RPA/RAD51/DMC1, do not persist on asynapsed chromosomes in chromosomally abnormal mice with competent DNA repair systems. Strikingly, this holds true even when several chromosomes are asynapsed, as in F1 PWDxB6 females, indicating that this repair system is robust. This also suggests that persistent DNA damage is unlikely to be a trigger of oocyte arrest in mice with chromosome abnormalities.

This is in contrast to mice with mutations in DNA repair enzymes, such as *Dmc1*-/- mice, which show signs of persistent DNA damage repair foci. My data question the contribution of the DNA damage checkpoint in normal biology, i.e. outside of situations in which mice have specific mutations or exogenously induced DNA damage. This also emphasises the importance of studying both targeted and non-targeted mouse models to gain a full understanding of the pathways causing prophase oocyte I elimination

My findings of DNA repair on asynapsed chromosomes in oocytes is also consistent with previous work in the male germ line, which showed that DNA DSB markers disappear from the asynapsed X chromosome by mid-late pachynema (Plug et al., 1998). This highlights that DNA repair on asynapsed chromosome is conserved between the sexes.

Mechanistically, it is unclear how DNA DSBs are repaired efficiently on asynapsed chromosomes. RPA turnover on the asynapsed X chromosome occurred with normal kinetics in XO *H2afx*-/- females, indicating that DNA DSB repair on asynapsed chromosomes does not require H2AFX. Additional research is needed to identify the mechanism of DNA DSB repair on asynapsed chromosomes in oocytes.

Studies in yeast have revealed that in addition to the canonical interhomolog (IH) repair pathway, meiotic DNA DSBs can be repaired via alternative pathways, such as intersister (IS) repair (Goldfarb and Lichten, 2010). Normally, to ensure that crossovers are generated during meiosis,

there is a "barrier" that suppresses recombination between sister chromatids to favor repair using homologs (Niu et al., 2005). In yeast meiosis, despite the IH repair bias, IS repair still occurs at substantial levels (Goldfarb and Lichten, 2010; Schwacha and Kleckner, 1997). Recent work suggests that IS repair also occurs in mammals (Li et al., 2011). I suspect that IS recombination is a likely mechanism for the repair of DNA DSBs on asynapsed chromosomes in chromosome variant mice.

Another putative mechanism of DNA DSB repair in the absence of a homologous chromosome is non-homologous end joining (NHEJ), which is a major repair mechanism in somatic cells. Unlike IH and IS repair pathways, which require a homolog (either a homologous chromosome or sister chromatid) for repair, NHEJ does not require any sequence homology. NHEJ involves the direct ligation of broken DNA ends together (Davis and Chen, 2013). NHEJ does not depend upon break resection and 3' ssDNA overhangs, which instead is a feature of HR (Mimitou and Symington, 2009). Since asynapsed chromosomes contained RPA/RAD51/DMC1, which are all proteins that recognize ssDNA, these DNA DSBs have already undergone resection and would no longer be a template for NHEJ. Therefore, NHEJ likely does not contribute to the repair of breaks on asynapsed chromosomes.

Notably, I found that DNA DSB repair takes longer on asynapsed chromosomes compared to synapsed chromosomes in oocytes. This is also consistent with the delayed repaired observed on the asynapsed X chromosome in spermatocytes (Plug et al., 1998). Therefore, the mechanism of repair on asynapsed chromosomes either takes longer or is somewhat delayed in mammalian germ cells. Characterizing this DNA repair mechanism, especially the molecular players involved in it, will be an important area of research for future studies.

7.5 Other factors involved in meiotic silencing and surveillance

In this thesis, I have shown that both BRCA1 and HORMAD2 are essential components of the meiotic silencing pathway in mice. Using a recently generated *Brca1*-/- mutant (Bunting et al., 2012), I verified that

BRCA1 is essential for the accumulation of the silencing factor ATR, consistent with previous reports (Broering et al., 2014; Turner et al., 2004). I also found that HORMAD2 is necessary for the proper axial loading/accumulation of BRCA1 on asynapsed axes. This places HORMAD2 upstream of BRCA1 in the cascade of events leading to silencing.

Recently, the kinase ATR was also shown to be important for meiotic silencing (Royo et al., 2013) and meiotic surveillance in mammals (Wojtasz et al., 2012). In a conditional mouse mutant of *Atr*, the localization of many meiotic silencing components, including BRCA1, ATRIP, TOPBP1, MDC1, γH2AFX, SUMO, and uH2A, is disrupted (Royo et al., 2013). Similarly, *H2afx*-/- mutants show improper loading of ATR and MDC1 (Royo et al., 2013). This indicates an ATR is a critical component of meiotic silencing, and that there is an interdependent relationship between many of the silencing factors.

ATR accumulation at unrepaired DNA DSBs and/or within the chromatin of asynapsed chromatin has been proposed to be a proximal trigger of oocyte arrest in mice with asynapsed chromosomes (e.g. *Spo11*-/-) (Wojtasz et al., 2012). Ablation of *Hormad2* in mice, which results in improper loading of chromatin ATR on asynapsed chromosomes (this thesis), rescues oocyte losses in asynaptic *Spo11*-/- oocytes (Wojtasz et al., 2012). This suggests that chromatin ATR is involved in meiotic surveillance of asynapsis. This is consistent with my model of meiotic surveillance based on meiotic silencing factors. However, these data could also be interpreted as an ATR-dependent checkpoint that functions independent of silencing.

In my XO *H2afx*-/- experiments, the most parsimonious explanation for the rescue of XO oocyte losses is ablation of silencing. However, it is also possible that an ATR-dependent checkpoint was disrupted, and that this contributes to the oocyte rescue phenotype. Indeed, ATR chromatin staining is disrupted in *H2afx*-/- spermatocytes. This possibility of an ATR-dependent checkpoint seems less likely, however, given my accessory chromosome results. In these mouse models, ATR signaling is active but not sufficient to trigger oocyte arrest. If an ATR-dependent checkpoint mechanism operates in mice, then ATR accumulation on asynapsed

accessory chromosomes should induce oocyte losses. Therefore, I favor the model whereby ATR-dependent oocyte losses occur via ATR's direct role in meiotic silencing (Royo et al., 2013).

It is also possible that ATR plays an important role in a DNA DSB dependent checkpoint. To assess for a potential role for ATR in a meiotic DNA DSB checkpoint, it will be important to examine oocyte numbers in *Atr* mutant females. The effect of *Atr* ablation should be studied in the context of mouse models with persistent unrepaired DNA DSBs (i.e. *Dmc1*-/-). If ATR is involved in a DNA DSB checkpoint pathway, *Atr* ablation should increase oocyte numbers in *Dmc1*-/- mutants, and other mutants with persistent unrepaired DNA DSBs phenotypes (Di Giacomo et al., 2005).

Whether any other downstream effectors are involved in H2AFX-mediated oocyte losses remains unclear. A recent study reported a role for the checkpoint kinase protein CHK2 in the DNA damage checkpoint in oocytes (Bolcun-Filas et al., 2014). While *Chk2* ablation reversed oocyte losses in DNA DSB repair defective oocytes (i.e. *Dmc1*-/- and *Trip13* mutants), it is unknown whether it has a role in regulating the elimination of oocytes with asynapsed chromosomes. It seems unlikely that CHK2 would be directly involved in H2AFX-dependent oocyte losses because they seem to be involved in distinct pathways. CHK2 seems to function predominately in DNA damage-induced oocyte losses (Bolcun-Filas et al., 2014; Livera et al., 2008), whereas H2AFX is not involved in the DNA damage checkpoint (this thesis).

It is will also be important to test for a role for apoptosis in H2AFX-dependent oocyte losses. This can be assessed by genetically ablating the apoptosis pathway in mice with chromosome abnormalities (e.g. XO mice). For example, oocyte numbers can be counted in XO mice with a mutation in key apoptosis regulators, such as *p53* or its paralog *p63*, both of which have been shown to be involved in DNA damage-induced apoptosis in oocytes (Bolcun-Filas et al., 2014). XO oocyte rescue by *p53*/*63* deletion would implicate a role for apoptotic cell death in XO oocyte losses. Another way to examine for a role for apoptosis is to examine the localization of apoptotic

pathway proteins (e.g. cleaved caspases, p53, p63, etc.) by immunofluorescence in XO ovary sections.

In summary, much remains to be discovered about the downstream effectors involved in the elimination of oocytes with asynapsis. Characterizing this pathway is important because it may provide targets with which to interfere with oocyte elimination

7.6 Sexual dimorphism in meiotic silencing

Another important conclusion from my thesis is that silencing is sexually dimorphic in mammals. Numerous previous studies have shown that meiotic silencing in spermatocytes is very robust, leading to the complete inactivation of X-linked coding genes at pachynema (Khil et al., 2004; Turner et al., 2005). While there have been reports that X-linked miRNAs escape meiotic silencing in spermatocytes, new work is challenging these results, showing that miRNAs are also subject to silencing (Turner lab, unpublished results).

Previous studies in the female germ line have shown that the major silencing factors BRCA1, ATR, γH2AFX, and ubi-H2A all localize to asynapsed chromosomes (Baarends et al., 2005; Turner et al., 2005). These marks coincided with an absence of Cot1 RNA and RNA polymerase II immunostaining, indicative of silencing (Baarends et al., 2005; Turner et al., 2005). Based on these studies, meiotic silencing was expected to be proficient in oocytes, similar to spermatocytes. However, until now, studies of gene specific RNA FISH studies, the gold standard for analyzing nascent transcription in germ cells, were lacking.

My RNA FISH analyses have unequivocally shown that meiotic silencing is less robust in oocytes compared to spermatocytes. Furthermore, simultaneous three-gene RNA FISH showed that within individual oocytes, genes on asynapsed chromosomes are silenced in a stochastic manner. In other words, the combination of genes that are silenced on a given asynapsed chromosome differs between individual oocytes. This mosaicism could create distinct gene expression profiles that disturb different biological pathways. Thus, in XO females, and other chromosomally

abnormal mouse models exhibiting prophase I germ cell losses, the precise cause of arrest could differ from oocyte to oocyte depending on the suite of genes that are silenced, as discussed above.

Why is meiotic silencing more robust in males than in females? While most major components of silencing (e.g. BRCA1, ATR, γH2AFX) are present on asynapsed chromosomes in oocytes, it is possible that other contributors of meiotic silencing are absent or not expressed appropriately in oocytes. Consistent with this idea, a recent study (Taketo and Naumova, 2013) revealed that the repressive histone modification H3K9me3 is not present on asynapsed chromosomes in oocytes like it is in spermatocytes. The Turner lab has also independently verified this finding (unpublished). This indicates that there are epigenetic differences in the response to asynapsed chromosome in oocytes. Furthermore, this suggests that H3K9me3 is required for stable and complete silencing of meiotic chromosomes. Identification of the histone methyltransferases that catalyze H3K9 methylation on asynapsed chromosomes represents an important challenge in the future for understanding sex differences in the prophase I response to asynapsis.

There are likely important clinical implications of the reduced efficiency of silencing in the female germ line. In general, chromosome abnormalities confer greater germ cell losses in males than in females (Burgoyne et al., 2009). This is due in part to the reduced stringency of the metaphase I spindle checkpoint in females (LeMaire-Adkins et al., 1997; Nagaoka et al., 2011), but is also thought to reflect ill-defined sex differences in the efficacy of the prophase I response to asynapsis (Hunt and Hassold, 2002; Morelli and Cohen, 2005; Nagaoka et al., 2012). A decreased efficiency of meiotic silencing may help explain the reduced efficiency of the prophase I surveillance response.

For example, it is possible that oocytes with prophase I defects are able to avoid elimination if its asynapsed chromosome are replete of essential genes or if not enough critical genes are silenced. Therefore, the sexual dimorphism in silencing may provide an explanation to why chromosome abnormalities cause more severe germ cell loss in males than

in females, and also why most cases of human aneuploidy arise from maternal meiotic errors (Morelli and Cohen, 2005).

Evolutionarily, is there a reason for the sexual dimorphism in silencing efficiency? Insight into this intriguing question may come from the recent confirmation that robust XY silencing in spermatocytes is critical for spermatocyte survival (Royo et al., 2010). Defects in silencing of the X and Y chromosomes in spermatocytes (i.e. MSCI) cause midpachytene arrest, and this has been linked to the misexpression of toxic sex-linked genes (Royo et al., 2010). It is therefore possible that meiotic silencing in males must be highly efficient in order to prevent the mis-expression of these "toxic" XY-encoded genes during normal male meiosis. In the female germ line, by contrast, there is little selective pressure for a robust meiotic silencing response, since incomplete silencing does not negatively impact oocyte survival.

References

Abe, K., Naruse, C, Kato, T, Nishiuchi, T, Saitou, M, Asano, M. (2011). Loss of heterochromatin protein 1 gamma reduces the number of primordial germ cells via impaired cell cycle progression in mice. Biol Reprod *85*, 1013-1024.

Abe, Y., Matsumoto, S., Wei, S., Nezu, K., Miyoshi, A., Kito, K., Ueda, N., Shigemoto, K., Hitsumoto, Y., Nikawa, J.*, et al.* (2001). Cloning and characterization of a p53-related protein kinase expressed in interleukin-2-activated cytotoxic T-cells, epithelial tumor cell lines, and the testes. J Biol Chem *276*, 44003-44011.

Adelman, C.A., and Petrini, J.H. (2008). ZIP4H (TEX11) deficiency in the mouse impairs meiotic double strand break repair and the regulation of crossing over. PLoS Genet *4*, e1000042.

Agger, K., Cloos, P.A., Christensen, J., Pasini, D., Rose, S., Rappsilber, J., Issaeva, I., Canaani, E., Salcini, A.E., and Helin, K. (2007). UTX and JMJD3 are histone H3K27 demethylases involved in HOX gene regulation and development. Nature *449*, 731-734.

Aguilera, A. (2002). The connection between transcription and genomic instability. EMBO J *21*, 195-201.

Alexander, W.G., Raju, N.B., Xiao, H., Hammond, T.M., Perdue, T.D., Metzenberg, R.L., Pukkila, P.J., and Shiu, P.K. (2008). DCL-1 colocalizes with other components of the MSUD machinery and is required for silencing. Fungal Genet Biol *45*, 719-727.

Alton, M., Lau, M.P., Villemure, M., and Taketo, T. (2008). The behavior of the X- and Y-chromosomes in the oocyte during meiotic prophase in the B6.Y(TIR)sex-reversed mouse ovary. Reproduction *135*, 241-252.

An, J.Y., Kim, E.A., Jiang, Y., Zakrzewska, A., Kim, D.E., Lee, M.J., Mook-Jung, I., Zhang, Y., and Kwon, Y.T. (2010). UBR2 mediates transcriptional silencing during spermatogenesis via histone ubiquitination. Proc Natl Acad Sci U S A *107*, 1912-1917.

Andersen, S.L., and Sekelsky, J. (2010). Meiotic versus mitotic recombination: two different routes for double-strand break repair: the different functions of meiotic versus mitotic DSB repair are reflected in different pathway usage and different outcomes. Bioessays *32*, 1058-1066.

Aravin, A.A., Sachidanandam, R., Girard, A., Fejes-Toth, K., and Hannon, G.J. (2007). Developmentally regulated piRNA clusters implicate MILI in transposon control. Science *316*, 744-747.

Ashley, T., Plug, A.W., Xu, J., Solari, A.J., Reddy, G., Golub, E.I., and Ward, D.C. (1995). Dynamic changes in Rad51 distribution on chromatin during meiosis in male and female vertebrates. Chromosoma *104*, 19-28.

Baarends, W.M., Hoogerbrugge, J.W., Roest, H.P., Ooms, M., Vreeburg, J., Hoeijmakers, J.H., and Grootegoed, J.A. (1999). Histone ubiquitination and chromatin remodeling in mouse spermatogenesis. Dev Biol *207*, 322-333.

Baarends, W.M., Wassenaar, E., van der Laan, R., Hoogerbrugge, J., Sleddens-Linkels, E., Hoeijmakers, J.H., de Boer, P., and Grootegoed, J.A. (2005). Silencing of unpaired chromatin and histone H2A ubiquitination in mammalian meiosis. Mol Cell Biol *25*, 1041-1053.

Baker, S.M., Plug, A.W., Prolla, T.A., Bronner, C.E., Harris, A.C., Yao, X., Christie, D.M., Monell, C., Arnheim, N., Bradley, A.*, et al.* (1996). Involvement

of mouse Mlh1 in DNA mismatch repair and meiotic crossing over. Nat Genet *13*, 336-342.
Barchi, M., Mahadevaiah, S., Di Giacomo, M., Baudat, F., de Rooij, D.G., Burgoyne, P.S., Jasin, M., and Keeney, S. (2005). Surveillance of different recombination defects in mouse spermatocytes yields distinct responses despite elimination at an identical developmental stage. Mol Cell Biol *25*, 7203-7215.
Barlow, A.L., Benson, F.E., West, S.C., and Hultén, M.A. (1997). Distribution of the Rad51 recombinase in human and mouse spermatocytes. EMBO J *16*, 5207-5215.
Bartek, J., and Lukas, J. (2007). DNA damage checkpoints: from initiation to recovery or adaptation. Curr Opin Cell Biol *19*, 238-245.
Bassing, C.H., Chua, K.F., Sekiguchi, J., Suh, H., Whitlow, S.R., Fleming, J.C., Monroe, B.C., Ciccone, D.N., Yan, C., Vlasakova, K.*, et al.* (2002). Increased ionizing radiation sensitivity and genomic instability in the absence of histone H2AX. Proc Natl Acad Sci U S A *99*, 8173-8178.
Baudat, F., Buard, J., Grey, C., Fledel-Alon, A., Ober, C., Przeworski, M., Coop, G., and de Massy, B. (2010). PRDM9 is a major determinant of meiotic recombination hotspots in humans and mice. Science *327*, 836-840.
Baudat, F., Imai, Y., and de Massy, B. (2013). Meiotic recombination in mammals: localization and regulation. Nat Rev Genet *14*, 794-806.
Baudat, F., Manova, K., Yuen, J.P., Jasin, M., and Keeney, S. (2000). Chromosome synapsis defects and sexually dimorphic meiotic progression in mice lacking Spo11. Mol Cell *6*, 989-998.
Bean, C.J., Schaner, C.E., and Kelly, W.G. (2004). Meiotic pairing and imprinted X chromatin assembly in Caenorhabditis elegans. Nat Genet *36*, 100-105.
Becherel, O.J., Yeo, A.J., Stellati, A., Heng, E.Y., Luff, J., Suraweera, A.M., Woods, R., Fleming, J., Carrie, D., McKinney, K.*, et al.* (2013). Senataxin plays an essential role with DNA damage response proteins in meiotic recombination and gene silencing. PLoS Genet *9*, e1003435.
Bekker-Jensen, S., Lukas, C., Melander, F., Bartek, J., and Lukas, J. (2005). Dynamic assembly and sustained retention of 53BP1 at the sites of DNA damage are controlled by Mdc1/NFBD1. J Cell Biol *170*, 201-211.
Bellani, M.A., Boateng, K.A., McLeod, D., and Camerini-Otero, R.D. (2010). The expression profile of the major mouse SPO11 isoforms indicates that SPO11beta introduces double strand breaks and suggests that SPO11alpha has an additional role in prophase in both spermatocytes and oocytes. Mol Cell Biol *30*, 4391-4403.
Bellani, M.A., Romanienko, P.J., Cairatti, D.A., and Camerini-Otero, R.D. (2005). SPO11 is required for sex-body formation, and Spo11 heterozygosity rescues the prophase arrest of Atm-/- spermatocytes. Journal of cell science *118*, 3233-3245.
Bender, L.B., Cao, R., Zhang, Y., and Strome, S. (2004). The MES-2/MES-3/MES-6 complex and regulation of histone H3 methylation in C. elegans. Curr Biol *14*, 1639-1643.
Bennett, M.D. (1977). The time and duration of meiosis. Philos Trans R Soc Lond B Biol Sci *277*, 201-226.

Bhalla, N., and Dernburg, A.F. (2005). A conserved checkpoint monitors meiotic chromosome synapsis in Caenorhabditis elegans. Science *310*, 1683-1686.
Bhattacharyya, T., Gregorova, S., Mihola, O., Anger, M., Sebestova, J., Denny, P., Simecek, P., and Forejt, J. (2013). Mechanistic basis of infertility of mouse intersubspecific hybrids. Proc Natl Acad Sci U S A *110*, E468-477.
Bishop, C.E., and Hatat, D. (1987). Molecular cloning and sequence analysis of a mouse Y chromosome RNA transcript expressed in the testis. Nucleic Acids Res *15*, 2959-2969.
Bishop, D.K., Park, D., Xu, L., and Kleckner, N. (1992). DMC1: a meiosis-specific yeast homolog of E. coli recA required for recombination, synaptonemal complex formation, and cell cycle progression. Cell *69*, 439-456.
Bolcun-Filas, E., Costa, Y., Speed, R., Taggart, M., Benavente, R., De Rooij, D.G., and Cooke, H.J. (2007). SYCE2 is required for synaptonemal complex assembly, double strand break repair, and homologous recombination. J Cell Biol *176*, 741-747.
Bolcun-Filas, E., Hall, E., Speed, R., Taggart, M., Grey, C., de Massy, B., Benavente, R., and Cooke, H.J. (2009). Mutation of the mouse Syce1 gene disrupts synapsis and suggests a link between synaptonemal complex structural components and DNA repair. PLoS Genet *5*, e1000393.
Bolcun-Filas, E., Rinaldi, V.D., White, M.E., and Schimenti, J.C. (2014). Reversal of female infertility by Chk2 ablation reveals the oocyte DNA damage checkpoint pathway. Science *343*, 533-536.
Bolcun-Filas, E., and Schimenti, J.C. (2012). Genetics of meiosis and recombination in mice. Int Rev Cell Mol Biol *298*, 179-227.
Borde, V., Goldman, A.S., and Lichten, M. (2000). Direct coupling between meiotic DNA replication and recombination initiation. Science *290*, 806-809.
Boulton, S.J. (2006). Cellular functions of the BRCA tumour-suppressor proteins. Biochem Soc Trans *34*, 633-645.
Bourc'his, D., and Bestor, T.H. (2004). Meiotic catastrophe and retrotransposon reactivation in male germ cells lacking Dnmt3L. Nature *431*, 96-99.
Bradley, J., Baltus, A., Skaletsky, H., Royce-Tolland, M., Dewar, K., and Page, D.C. (2004). An X-to-autosome retrogene is required for spermatogenesis in mice. Nat Genet *36*, 872-876.
Brick, K., Smagulova, F., Khil, P., Camerini-Otero, R.D., and Petukhova, G.V. (2012). Genetic recombination is directed away from functional genomic elements in mice. Nature *485*, 642-645.
Broering, T.J., Alavattam, K.G., Sadreyev, R.I., Ichijima, Y., Kato, Y., Hasegawa, K., Camerini-Otero, R.D., Lee, J.T., Andreassen, P.R., and Namekawa, S.H. (2014). BRCA1 establishes DNA damage signaling and pericentric heterochromatin of the X chromosome in male meiosis. J Cell Biol *205*, 663-675.
Brown, E.J., and Baltimore, D. (2000). ATR disruption leads to chromosomal fragmentation and early embryonic lethality. Genes Dev *14*, 397-402.
Bunting, S.F., Callén, E., Kozak, M.L., Kim, J.M., Wong, N., López-Contreras, A.J., Ludwig, T., Baer, R., Faryabi, R.B., Malhowski, A., *et al.* (2012). BRCA1

functions independently of homologous recombination in DNA interstrand crosslink repair. Mol Cell *46*, 125-135.
Burgoyne, P.S. (1979). Evidence for an association between univalent Y chromosomes and spermatoycte loss in XYY mice and men. Cytogenet Cell Genet *23*, 84-89.
Burgoyne, P.S. (1982). Genetic homology and crossing over in the X and Y chromosomes of Mammals. Human genetics *61*, 85-90.
Burgoyne, P.S., and Baker, T.G. (1981). Oocyte depletion in XO mice and their XX sibs from 12 to 200 days post partum. J Reprod Fertil *61*, 207-212.
Burgoyne, P.S., and Baker, T.G. (1984). Meiotic pairing and gametogenic failure. Symp Soc Exp Biol *38*, 349-362.
Burgoyne, P.S., and Baker, T.G. (1985). Perinatal oocyte loss in XO mice and its implications for the aetiology of gonadal dysgenesis in XO women. J Reprod Fertil *75*, 633-645.
Burgoyne, P.S., and Biddle, F.G. (1980). Spermatocyte loss in XYY mice. Cytogenetics and cell genetics *28*, 143-144.
Burgoyne, P.S., Mahadevaiah, S.K., and Turner, J.M. (2007). The management of DNA double-strand breaks in mitotic G2, and in mammalian meiosis viewed from a mitotic G2 perspective. Bioessays *29*, 974-986.
Burgoyne, P.S., Mahadevaiah, S.K., and Turner, J.M. (2009). The consequences of asynapsis for mammalian meiosis. Nat Rev Genet *10*, 207-216.
Burma, S., Chen, B.P., Murphy, M., Kurimasa, A., and Chen, D.J. (2001). ATM phosphorylates histone H2AX in response to DNA double-strand breaks. The Journal of biological chemistry *276*, 42462-42467.
Bähler, J. (2005). Cell-cycle control of gene expression in budding and fission yeast. Annu Rev Genet *39*, 69-94.
Cabrero, J., Teruel, M., Carmona, F.D., and Camacho, J.P. (2007a). Histone H2AX phosphorylation is associated with most meiotic events in grasshopper. Cytogenet Genome Res *116*, 311-315.
Cabrero, J., Teruel, M., Carmona, F.D., Jiménez, R., and Camacho, J.P. (2007b). Histone H3 lysine 9 acetylation pattern suggests that X and B chromosomes are silenced during entire male meiosis in a grasshopper. Cytogenet Genome Res *119*, 135-142.
Caestecker, K.W., and Van de Walle, G.R. (2013). The role of BRCA1 in DNA double-strand repair: past and present. Exp Cell Res *319*, 575-587.
Capel, B., Rasberry, C., Dyson, J., Bishop, C.E., Simpson, E., Vivian, N., Lovell-Badge, R., Rastan, S., and Cattanach, B.M. (1993). Deletion of Y chromosome sequences located outside the testis determining region can cause XY female sex reversal. Nat Genet *5*, 301-307.
Carballo, J.A., Johnson, A.L., Sedgwick, S.G., and Cha, R.S. (2008). Phosphorylation of the axial element protein Hop1 by Mec1/Tel1 ensures meiotic interhomolog recombination. Cell *132*, 758-770.
Carballo, J.A., Panizza, S., Serrentino, M.E., Johnson, A.L., Geymonat, M., Borde, V., Klein, F., and Cha, R.S. (2013). Budding Yeast ATM/ATR Control Meiotic Double-Strand Break (DSB) Levels by Down-Regulating Rec114, an Essential Component of the DSB-machinery. PLoS Genet *9*, e1003545.
Carofiglio, F., Inagaki, A., de Vries, S., Wassenaar, E., Schoenmakers, S., Vermeulen, C., van Cappellen, W.A., Sleddens-Linkels, E., Grootegoed, J.A., Te

Riele, H.P.*, et al.* (2013). SPO11-Independent DNA Repair Foci and Their Role in Meiotic Silencing. PLoS Genet *9*, e1003538.
Carrel, L., and Willard, H.F. (2005). X-inactivation profile reveals extensive variability in X-linked gene expression in females. Nature *434*, 400-404.
Catlett, M.G., and Forsburg, S.L. (2003). Schizosaccharomyces pombe Rdh54 (TID1) acts with Rhp54 (RAD54) to repair meiotic double-strand breaks. Mol Biol Cell *14*, 4707-4720.
Celeste, A., Difilippantonio, S., Difilippantonio, M.J., Fernandez-Capetillo, O., Pilch, D.R., Sedelnikova, O.A., Eckhaus, M., Ried, T., Bonner, W.M., and Nussenzweig, A. (2003a). H2AX haploinsufficiency modifies genomic stability and tumor susceptibility. Cell *114*, 371-383.
Celeste, A., Fernandez-Capetillo, O., Kruhlak, M.J., Pilch, D.R., Staudt, D.W., Lee, A., Bonner, R.F., Bonner, W.M., and Nussenzweig, A. (2003b). Histone H2AX phosphorylation is dispensable for the initial recognition of DNA breaks. Nature cell biology *5*, 675-679.
Celeste, A., Petersen, S., Romanienko, P.J., Fernandez-Capetillo, O., Chen, H.T., Sedelnikova, O.A., Reina-San-Martin, B., Coppola, V., Meffre, E., Difilippantonio, M.J.*, et al.* (2002). Genomic instability in mice lacking histone H2AX. Science *296*, 922-927.
Checchi, P.M., and Engebrecht, J. (2011). Caenorhabditis elegans histone methyltransferase MET-2 shields the male X chromosome from checkpoint machinery and mediates meiotic sex chromosome inactivation. PLoS Genet *7*, e1002267.
Checchi, P.M., Lawrence, K.S., Van, M.V., Larson, B.J., and Engebrecht, J. (2014). Pseudosynapsis and Decreased Stringency of Meiotic Repair Pathway Choice on the Hemizygous Sex Chromosome of Caenorhabditis elegans Males. Genetics *197*, 543-560.
Chowdhury, D., Keogh, M.C., Ishii, H., Peterson, C.L., Buratowski, S., and Lieberman, J. (2005). gamma-H2AX dephosphorylation by protein phosphatase 2A facilitates DNA double-strand break repair. Mol Cell *20*, 801-809.
Chu, S., and Herskowitz, I. (1998). Gametogenesis in yeast is regulated by a transcriptional cascade dependent on Ndt80. Mol Cell *1*, 685-696.
Cloud, V., Chan, Y.L., Grubb, J., Budke, B., and Bishop, D.K. (2012). Rad51 is an accessory factor for Dmc1-mediated joint molecule formation during meiosis. Science *337*, 1222-1225.
Cloutier, J.M., and Turner, J. (2010). Meiotic sex chromosome inactivation. Current Biology *20*, R962-R963.
Cohen, P.E., Pollack, S.E., and Pollard, J.W. (2006). Genetic analysis of chromosome pairing, recombination, and cell cycle control during first meiotic prophase in mammals. Endocr Rev *27*, 398-426.
Cohen, P.E., and Pollard, J.W. (2001). Regulation of meiotic recombination and prophase I progression in mammals. Bioessays *23*, 996-1009.
Cole, F., Kauppi, L., Lange, J., Roig, I., Wang, R., Keeney, S., and Jasin, M. (2012). Homeostatic control of recombination is implemented progressively in mouse meiosis. Nat Cell Biol *14*, 424-430.
Collins, I., and Newlon, C.S. (1994). Meiosis-specific formation of joint DNA molecules containing sequences from homologous chromosomes. Cell *76*, 65-75.

Costa, Y., Speed, R., Ollinger, R., Alsheimer, M., Semple, C.A., Gautier, P., Maratou, K., Novak, I., Höög, C., Benavente, R.*, et al.* (2005). Two novel proteins recruited by synaptonemal complex protein 1 (SYCP1) are at the centre of meiosis. J Cell Sci *118*, 2755-2762.
Cuddihy, A.R., and O'Connell, M.J. (2003). Cell-cycle responses to DNA damage in G2. Int Rev Cytol *222*, 99-140.
Daniel, K., Lange, J., Hached, K., Fu, J., Anastassiadis, K., Roig, I., Cooke, H.J., Stewart, A.F., Wassmann, K., Jasin, M.*, et al.* (2011). Meiotic homologue alignment and its quality surveillance are controlled by mouse HORMAD1. Nature cell biology *13*, 599-610.
Davis, A.J., and Chen, D.J. (2013). DNA double strand break repair via non-homologous end-joining. Transl Cancer Res *2*, 130-143.
de Boer, P., Giele, M., Lock, M.T., de Rooij, D.G., Giltay, J., Hochstenbach, R., and te Velde, E.R. (2004). Kinetics of meiosis in azoospermic males: a joint histological and cytological approach. Cytogenet Genome Res *105*, 36-46.
De La Fuente, R., Baumann, C., Fan, T., Schmidtmann, A., Dobrinski, I., and Muegge, K. (2006). Lsh is required for meiotic chromosome synapsis and retrotransposon silencing in female germ cells. Nat Cell Biol *8*, 1448-1454.
de Vries, F.A., de Boer, E., van den Bosch, M., Baarends, W.M., Ooms, M., Yuan, L., Liu, J.G., van Zeeland, A.A., Heyting, C., and Pastink, A. (2005). Mouse Sycp1 functions in synaptonemal complex assembly, meiotic recombination, and XY body formation. Genes Dev *19*, 1376-1389.
de Vries, M., Vosters, S., Merkx, G., D'Hauwers, K., Wansink, D.G., Ramos, L., and de Boer, P. (2012). Human male meiotic sex chromosome inactivation. PLoS One *7*, e31485.
de Vries, S.S., Baart, E.B., Dekker, M., Siezen, A., de Rooij, D.G., de Boer, P., and te Riele, H. (1999). Mouse MutS-like protein Msh5 is required for proper chromosome synapsis in male and female meiosis. Genes Dev *13*, 523-531.
Deng, C.X., and Brodie, S.G. (2000). Roles of BRCA1 and its interacting proteins. Bioessays *22*, 728-737.
Dernburg, A.F., McDonald, K., Moulder, G., Barstead, R., Dresser, M., and Villeneuve, A.M. (1998). Meiotic recombination in C. elegans initiates by a conserved mechanism and is dispensable for homologous chromosome synapsis. Cell *94*, 387-398.
Di Giacomo, M., Barchi, M., Baudat, F., Edelmann, W., Keeney, S., and Jasin, M. (2005). Distinct DNA-damage-dependent and -independent responses drive the loss of oocytes in recombination-defective mouse mutants. Proc Natl Acad Sci U S A *102*, 737-742.
Donehower, L.A., Harvey, M., Slagle, B.L., McArthur, M.J., Montgomery, C.A., Butel, J.S., and Bradley, A. (1992). Mice deficient for p53 are developmentally normal but susceptible to spontaneous tumours. Nature *356*, 215-221.
Downs, J.A., Allard, S., Jobin-Robitaille, O., Javaheri, A., Auger, A., Bouchard, N., Kron, S.J., Jackson, S.P., and Côté, J. (2004). Binding of chromatin-modifying activities to phosphorylated histone H2A at DNA damage sites. Mol Cell *16*, 979-990.
Edelmann, W., Cohen, P.E., Kane, M., Lau, K., Morrow, B., Bennett, S., Umar, A., Kunkel, T., Cattoretti, G., Chaganti, R.*, et al.* (1996). Meiotic pachytene arrest in MLH1-deficient mice. Cell *85*, 1125-1134.

Edelmann, W., Cohen, P.E., Kneitz, B., Winand, N., Lia, M., Heyer, J., Kolodner, R., Pollard, J.W., and Kucherlapati, R. (1999). Mammalian MutS homologue 5 is required for chromosome pairing in meiosis. Nat Genet *21*, 123-127.
Eicher, E.M., Hale, D.W., Hunt, P.A., Lee, B.K., Tucker, P.K., King, T.R., Eppig, J.T., and Washburn, L.L. (1991). The mouse Y* chromosome involves a complex rearrangement, including interstitial positioning of the pseudoautosomal region. Cytogenet Cell Genet *57*, 221-230.
Ellis, N., and Goodfellow, P.N. (1989). The mammalian pseudoautosomal region. Trends Genet *5*, 406-410.
Evans, E.P., and Phillips, R.J. (1975). Inversion heterozygosity and the origin of XO daughters of Bpa/+female mice. Nature *256*, 40-41.
Falck, J., Coates, J., and Jackson, S.P. (2005). Conserved modes of recruitment of ATM, ATR and DNA-PKcs to sites of DNA damage. Nature *434*, 605-611.
Farah, J.A., Cromie, G.A., and Smith, G.R. (2009). Ctp1 and Exonuclease 1, alternative nucleases regulated by the MRN complex, are required for efficient meiotic recombination. Proc Natl Acad Sci U S A *106*, 9356-9361.
Fernandez-Capetillo, O., Mahadevaiah, S.K., Celeste, A., Romanienko, P.J., Camerini-Otero, R.D., Bonner, W.M., Manova, K., Burgoyne, P., and Nussenzweig, A. (2003). H2AX is required for chromatin remodeling and inactivation of sex chromosomes in male mouse meiosis. Developmental Cell *4*, 497-508.
Fillingham, J., Keogh, M.C., and Krogan, N.J. (2006). GammaH2AX and its role in DNA double-strand break repair. Biochem Cell Biol *84*, 568-577.
Finn, K., Lowndes, N.F., and Grenon, M. (2012). Eukaryotic DNA damage checkpoint activation in response to double-strand breaks. Cell Mol Life Sci *69*, 1447-1473.
Ford, C.E., and Evands, E.P. (1964). A reciprocal translocation in the mouse between the x chromosome and a short autosome. Cytogenetics *3*, 295-305.
Ford, C.E., Jones, K.W., Polani, P.E., De Almeida, J.C., and Briggs, J.H. (1959). A sex-chromosome anomaly in a case of gonadal dysgenesis (Turner's syndrome). Lancet *1*, 711-713.
Forejt, J. (1976). Spermatogenic failure of translocation heterozygotes affected by H-2-linked gene in mouse. Nature *260*, 143-145.
Forejt, J., Capkova, J., and Gregorova, S. (1980). T(16: 17)43H translocation as a tool in analysis of the proximal part of chromosome 17 (including T-t gene complex) of the mouse. Genetical research *35*, 165-177.
Fraune, J., Schramm, S., Alsheimer, M., and Benavente, R. (2012). The mammalian synaptonemal complex: protein components, assembly and role in meiotic recombination. Exp Cell Res *318*, 1340-1346.
Fukuda, T., Daniel, K., Wojtasz, L., Toth, A., and Hoog, C. (2009). A novel mammalian HORMA domain-containing protein, HORMAD1, preferentially associates with unsynapsed meiotic chromosomes. Exp Cell Res *316*, 158-171.
Fukuda, T., Pratto, F., Schimenti, J.C., Turner, J.M., Camerini-Otero, R.D., and Höög, C. (2012). Phosphorylation of chromosome core components may serve as axis marks for the status of chromosomal events during mammalian meiosis. PLoS Genet *8*, e1002485.
Futcher, B. (1996). Cyclins and the wiring of the yeast cell cycle. Yeast *12*, 1635-1646.

Garcia-Cruz, R., Roig, I., Robles, P., Scherthan, H., and Garcia, M. (2009). ATR, BRCA1 and gammaH2AX localize to unsynapsed chromosomes at the pachytene stage in human oocytes. Reprod BioMed Online *18*, 37-44.
Gartner, A., Milstein, S., Ahmed, S., Hodgkin, J., and Hengartner, M.O. (2000). A conserved checkpoint pathway mediates DNA damage--induced apoptosis and cell cycle arrest in C. elegans. Mol Cell *5*, 435-443.
Ghabrial, A., and Schüpbach, T. (1999). Activation of a meiotic checkpoint regulates translation of Gurken during Drosophila oogenesis. Nat Cell Biol *1*, 354-357.
Gill, G. (2005). Something about SUMO inhibits transcription. Curr Opin Genet Dev *15*, 536-541.
Goedecke, W., Eijpe, M., Offenberg, H.H., van Aalderen, M., and Heyting, C. (1999). Mre11 and Ku70 interact in somatic cells, but are differentially expressed in early meiosis. Nat Genet *23*, 194-198.
Goldfarb, T., and Lichten, M. (2010). Frequent and efficient use of the sister chromatid for DNA double-strand break repair during budding yeast meiosis. PLoS biology *8*, e1000520.
Gondos, B., Bhiraleus, P., and Hobel, C.J. (1971). Ultrastructural observations on germ cells in human fetal ovaries. Am J Obstet Gynecol *110*, 644-652.
González-González, E., López-Casas, P.P., and del Mazo, J. (2008). The expression patterns of genes involved in the RNAi pathways are tissue-dependent and differ in the germ and somatic cells of mouse testis. Biochim Biophys Acta *1779*, 306-311.
Goodier, J.L., and Kazazian, H.H. (2008). Retrotransposons revisited: the restraint and rehabilitation of parasites. Cell *135*, 23-35.
Gottlieb, T.M., and Jackson, S.P. (1993). The DNA-dependent protein kinase: requirement for DNA ends and association with Ku antigen. Cell *72*, 131-142.
Greaves, I.K., Rangasamy, D., Devoy, M., Marshall Graves, J.A., and Tremethick, D.J. (2006). The X and Y chromosomes assemble into H2A.Z-containing [corrected] facultative heterochromatin [corrected] following meiosis. Mol Cell Biol *26*, 5394-5405.
Grey, C., Barthès, P., Chauveau-Le Friec, G., Langa, F., Baudat, F., and de Massy, B. (2011). Mouse PRDM9 DNA-binding specificity determines sites of histone H3 lysine 4 trimethylation for initiation of meiotic recombination. PLoS Biol *9*, e1001176.
Gribble, S.M., Wiseman, F.K., Clayton, S., Prigmore, E., Langley, E., Yang, F., Maguire, S., Fu, B., Rajan, D., Sheppard, O*., et al.* (2013). Massively parallel sequencing reveals the complex structure of an irradiated human chromosome on a mouse background in the Tc1 model of Down syndrome. PLoS One *8*, e60482.
Guillon, H., Baudat, F., Grey, C., Liskay, R.M., and de Massy, B. (2005). Crossover and noncrossover pathways in mouse meiosis. Mol Cell *20*, 563-573.
Guioli, S., Lovell-Badge, R., and Turner, J.M. (2012). Error-prone ZW pairing and no evidence for meiotic sex chromosome inactivation in the chicken germ line. PLoS Genet *8*, e1002560.

Hall, H., Hunt, P., and Hassold, T. (2006). Meiosis and sex chromosome aneuploidy: how meiotic errors cause aneuploidy; how aneuploidy causes meiotic errors. Curr Opin Genet Dev *16*, 323-329.
Hall, J.M., Lee, M.K., Newman, B., Morrow, J.E., Anderson, L.A., Huey, B., and King, M.C. (1990). Linkage of early-onset familial breast cancer to chromosome 17q21. Science *250*, 1684-1689.
Hamer, G., Gell, K., Kouznetsova, A., Novak, I., Benavente, R., and Höög, C. (2006). Characterization of a novel meiosis-specific protein within the central element of the synaptonemal complex. J Cell Sci *119*, 4025-4032.
Hamer, G., Wang, H., Bolcun-Filas, E., Cooke, H.J., Benavente, R., and Höög, C. (2008). Progression of meiotic recombination requires structural maturation of the central element of the synaptonemal complex. J Cell Sci *121*, 2445-2451.
Han, L., Hu, Z., Liu, Y., Wang, X., Hopkins, K.M., Lieberman, H.B., and Hang, H. (2010). Mouse Rad1 deletion enhances susceptibility for skin tumor development. Mol Cancer *9*, 67.
Handel, M.A., and Schimenti, J.C. (2010). Genetics of mammalian meiosis: regulation, dynamics and impact on fertility. Nat Rev Genet *11*, 124-136.
Harper, J.W., and Elledge, S.J. (2007). The DNA damage response: ten years after. Mol Cell *28*, 739-745.
Harrison, J.C., and Haber, J.E. (2006). Surviving the breakup: the DNA damage checkpoint. Annu Rev Genet *40*, 209-235.
Hartsuiker, E., Mizuno, K., Molnar, M., Kohli, J., Ohta, K., and Carr, A.M. (2009). Ctp1CtIP and Rad32Mre11 nuclease activity are required for Rec12Spo11 removal, but Rec12Spo11 removal is dispensable for other MRN-dependent meiotic functions. Mol Cell Biol *29*, 1671-1681.
Hartwell, L.H., and Weinert, T.A. (1989). Checkpoints: controls that ensure the order of cell cycle events. Science *246*, 629.
Hassold, T., and Hunt, P. (2001). To err (meiotically) is human: the genesis of human aneuploidy. Nat Rev Genet *2*, 280-291.
Heard, E., and Turner, J. (2011). Function of the sex chromosomes in mammalian fertility. Cold Spring Harb Perspect Biol *3*, a002675.
Henderson, S. (1964). RNA synthesis during male meiosis and spermiogenesis. (Chromosoma), pp. 345-366.
Herbert, M., Kalleas, D., Cooney, D., Lamb, M., and Lister, L. (2015). Meiosis and maternal aging: insights from aneuploid oocytes and trisomy births. Cold Spring Harb Perspect Biol *7*, a017970.
Hochwagen, A., and Amon, A. (2006). Checking your breaks: surveillance mechanisms of meiotic recombination. Curr Biol *16*, R217-228.
Hodges, C.A., LeMaire-Adkins, R., and Hunt, P.A. (2001). Coordinating the segregation of sister chromatids during the first meiotic division: evidence for sexual dimorphism. J Cell Sci *114*, 2417-2426.
Homolka, D., Ivanek, R., Capkova, J., Jansa, P., and Forejt, J. (2007). Chromosomal rearrangement interferes with meiotic X chromosome inactivation. Genome Res *17*, 1431-1437.
Homolka, D., Jansa, P., and Forejt, J. (2012). Genetically enhanced asynapsis of autosomal chromatin promotes transcriptional dysregulation and meiotic failure. Chromosoma *121*, 91-104.

Hong, E.J., and Roeder, G.S. (2002). A role for Ddc1 in signaling meiotic double-strand breaks at the pachytene checkpoint. Genes Dev *16*, 363-376.
Hopkins, K.M., Auerbach, W., Wang, X.Y., Hande, M.P., Hang, H., Wolgemuth, D.J., Joyner, A.L., and Lieberman, H.B. (2004). Deletion of mouse rad9 causes abnormal cellular responses to DNA damage, genomic instability, and embryonic lethality. Mol Cell Biol *24*, 7235-7248.
Horejsí, Z., Falck, J., Bakkenist, C.J., Kastan, M.B., Lukas, J., and Bartek, J. (2004). Distinct functional domains of Nbs1 modulate the timing and magnitude of ATM activation after low doses of ionizing radiation. Oncogene *23*, 3122-3127.
Hornecker, J.L., Samollow, P.B., Robinson, E.S., Vandeberg, J.L., and McCarrey, J.R. (2007). Meiotic sex chromosome inactivation in the marsupial Monodelphis domestica. Genesis *45*, 696-708.
Hoyer-Fender, S., Costanzi, C., and Pehrson, J.R. (2000). Histone macroH2A1. 2 is concentrated in the XY-body by the early pachytene stage of spermatogenesis. Experimental Cell Research *258*, 254-260.
Hoyle, H.D., Hutchens, J.A., Turner, F.R., and Raff, E.C. (1995). Regulation of beta-tubulin function and expression in Drosophila spermatogenesis. Dev Genet *16*, 148-170.
Huen, M.S., Sy, S.M., and Chen, J. (2010). BRCA1 and its toolbox for the maintenance of genome integrity. Nat Rev Mol Cell Biol *11*, 138-148.
Hunt, P.A., and Hassold, T.J. (2002). Sex matters in meiosis. Science *296*, 2181-2183.
Hunt, P.A., and Hassold, T.J. (2008). Human female meiosis: what makes a good egg go bad? Trends Genet *24*, 86-93.
Hunter, N., and Kleckner, N. (2001). The single-end invasion: an asymmetric intermediate at the double-strand break to double-holliday junction transition of meiotic recombination. Cell *106*, 59-70.
Ichijima, Y., Ichijima, M., Lou, Z., Nussenzweig, A., Camerini-Otero, R.D., Chen, J., Andreassen, P.R., and Namekawa, S.H. (2011). MDC1 directs chromosome-wide silencing of the sex chromosomes in male germ cells. Genes & development *25*, 959-971.
Inagaki, A., Schoenmakers, S., and Baarends, W.M. (2010). DNA double strand break repair, chromosome synapsis and transcriptional silencing in meiosis. Epigenetics *5*, 255-266.
Inagaki, A., van Cappellen, W.A., van der Laan, R., Houtsmuller, A.B., Hoeijmakers, J.H., Grootegoed, J.A., and Baarends, W.M. (2009). Dynamic localization of human RAD18 during the cell cycle and a functional connection with DNA double-strand break repair. DNA Repair (Amst) *8*, 190-201.
Jan, S.Z., Hamer, G., Repping, S., de Rooij, D.G., van Pelt, A.M., and Vormer, T.L. (2012). Molecular control of rodent spermatogenesis. Biochim Biophys Acta *1822*, 1838-1850.
Jang, J.K., Sherizen, D.E., Bhagat, R., Manheim, E.A., and McKim, K.S. (2003). Relationship of DNA double-strand breaks to synapsis in Drosophila. J Cell Sci *116*, 3069-3077.
Jaramillo-Lambert, A., and Engebrecht, J. (2010). A single unpaired and transcriptionally silenced X chromosome locally precludes checkpoint signaling in the Caenorhabditis elegans germ line. Genetics *184*, 613-628.

Jaramillo-Lambert, A., Harigaya, Y., Vitt, J., Villeneuve, A., and Engebrecht, J. (2010). Meiotic errors activate checkpoints that improve gamete quality without triggering apoptosis in male germ cells. Curr Biol *20*, 2078-2089.
Jones, K.T., and Lane, S.I. (2013). Molecular causes of aneuploidy in mammalian eggs. Development *140*, 3719-3730.
Joyce, E.F., Pedersen, M., Tiong, S., White-Brown, S.K., Paul, A., Campbell, S.D., and McKim, K.S. (2011). Drosophila ATM and ATR have distinct activities in the regulation of meiotic DNA damage and repair. J Cell Biol *195*, 359-367.
Kauppi, L., Barchi, M., Baudat, F.d.r., Romanienko, P.J., Keeney, S., and Jasin, M. (2011). Distinct Properties of the XY Pseudoautosomal Region Crucial for Male Meiosis. Science *331*, 916-920.
Kauppi, L., Barchi, M., Lange, J., Baudat, F., Jasin, M., and Keeney, S. (2013). Numerical constraints and feedback control of double-strand breaks in mouse meiosis. Genes Dev *27*, 873-886.
Keegan, K.S., Holtzman, D.A., Plug, A.W., Christenson, E.R., Brainerd, E.E., Flaggs, G., Bentley, N.J., Taylor, E.M., Meyn, M.S., Moss, S.B*., et al.* (1996). The Atr and Atm protein kinases associate with different sites along meiotically pairing chromosomes. Genes Dev *10*, 2423-2437.
Keeney, S. (2008). Spo11 and the Formation of DNA Double-Strand Breaks in Meiosis. Genome Dyn Stab *2*, 81-123.
Keeney, S., Giroux, C.N., and Kleckner, N. (1997). Meiosis-Specific DNA Double-Strand Breaks Are Catalyzed by Spo11, a Member of a Widely Conserved Protein Family. Cell *88*, 375-384.
Kelly, W.G., Schaner, C.E., Dernburg, A.F., Lee, M.H., Kim, S.K., Villeneuve, A.M., and Reinke, V. (2002). X-chromosome silencing in the germline of C. elegans. Development *129*, 479-492.
Keogh, M.C., Kim, J.A., Downey, M., Fillingham, J., Chowdhury, D., Harrison, J.C., Onishi, M., Datta, N., Galicia, S., Emili, A*., et al.* (2006). A phosphatase complex that dephosphorylates gammaH2AX regulates DNA damage checkpoint recovery. Nature *439*, 497-501.
Khalil, A.M., Boyar, F.Z., and Driscoll, D.J. (2004). Dynamic histone modifications mark sex chromosome inactivation and reactivation during mammalian spermatogenesis. Proceedings of the National Academy of Sciences of the United States of America *101*, 16583.
Khil, P.P., Smagulova, F., Brick, K.M., Camerini-Otero, R.D., and Petukhova, G.V. (2012). Sensitive mapping of recombination hotspots using sequencing-based detection of ssDNA. Genome Res *22*, 957-965.
Khil, P.P., Smirnova, N.A., Romanienko, P.J., and Camerini-Otero, R.D. (2004). The mouse X chromosome is enriched for sex-biased genes not subject to selection by meiotic sex chromosome inactivation. Nature genetics *36*, 642-646.
Kierszenbaum, A.L., and Tres, L.L. (1974). Transcription sites in spread meiotic prophase chromosomes from mouse spermatocytes. J Cell Biol *63*, 923-935.
Kneitz, B., Cohen, P.E., Avdievich, E., Zhu, L., Kane, M.F., Hou, H., Kolodner, R.D., Kucherlapati, R., Pollard, J.W., and Edelmann, W. (2000). MutS homolog 4 localization to meiotic chromosomes is required for chromosome pairing during meiosis in male and female mice. Genes Dev *14*, 1085-1097.

Koehler, K.E., Cherry, J.P., Lynn, A., Hunt, P.A., and Hassold, T.J. (2002). Genetic control of mammalian meiotic recombination. I. Variation in exchange frequencies among males from inbred mouse strains. Genetics *162*, 297-306.
Koehler, K.E., Millie, E.A., Cherry, J.P., Schrump, S.E., and Hassold, T.J. (2004). Meiotic exchange and segregation in female mice heterozygous for paracentric inversions. Genetics *166*, 1199-1214.
Kogo, H., Tsutsumi, M., Inagaki, H., Ohye, T., Kiyonari, H., and Kurahashi, H. (2012a). HORMAD2 is essential for synapsis surveillance during meiotic prophase via the recruitment of ATR activity. Genes Cells *17*, 897-912.
Kogo, H., Tsutsumi, M., Ohye, T., Inagaki, H., Abe, T., and Kurahashi, H. (2012b). HORMAD1-dependent checkpoint/surveillance mechanism eliminates asynaptic oocytes. Genes Cells *17*, 439-454.
Kolas, N.K., Svetlanov, A., Lenzi, M.L., Macaluso, F.P., Lipkin, S.M., Liskay, R.M., Greally, J., Edelmann, W., and Cohen, P.E. (2005). Localization of MMR proteins on meiotic chromosomes in mice indicates distinct functions during prophase I. J Cell Biol *171*, 447-458.
Kouznetsova, A., Wang, H., Bellani, M., Camerini-Otero, R.D., Jessberger, R., and Hoog, C. (2009). BRCA1-mediated chromatin silencing is limited to oocytes with a small number of asynapsed chromosomes. J Cell Sci *122*, 2446-2452.
Kuramochi-Miyagawa, S., Watanabe, T., Gotoh, K., Totoki, Y., Toyoda, A., Ikawa, M., Asada, N., Kojima, K., Yamaguchi, Y., Ijiri, T.W.*, et al.* (2008). DNA methylation of retrotransposon genes is regulated by Piwi family members MILI and MIWI2 in murine fetal testes. Genes Dev *22*, 908-917.
La Salle, S., Sun, F., Zhang, X.D., Matunis, M.J., and Handel, M.A. (2008). Developmental control of sumoylation pathway proteins in mouse male germ cells. Dev Biol *321*, 227-237.
Lammers, J.H., Offenberg, H.H., van Aalderen, M., Vink, A.C., Dietrich, A.J., and Heyting, C. (1994). The gene encoding a major component of the lateral elements of synaptonemal complexes of the rat is related to X-linked lymphocyte-regulated genes. Mol Cell Biol *14*, 1137-1146.
Lange, J., Pan, J., Cole, F., Thelen, M.P., Jasin, M., and Keeney, S. (2011). ATM controls meiotic double-strand-break formation. Nature *479*, 237-240.
Lee, D.W., Pratt, R.J., McLaughlin, M., and Aramayo, R. (2003). An argonaute-like protein is required for meiotic silencing. Genetics *164*, 821-828.
Lees-Murdock, D.J., and Walsh, C.P. (2008). DNA methylation reprogramming in the germ line. Adv Exp Med Biol *626*, 1-15.
LeMaire-Adkins, R., Radke, K., and Hunt, P.A. (1997). Lack of checkpoint control at the metaphase/anaphase transition: a mechanism of meiotic nondisjunction in mammalian females. J Cell Biol *139*, 1611-1619.
Leu, J.Y., and Roeder, G.S. (1999). The pachytene checkpoint in S. cerevisiae depends on Swe1-mediated phosphorylation of the cyclin-dependent kinase Cdc28. Mol Cell *4*, 805-814.
Li, X.C., Bolcun-Filas, E., and Schimenti, J.C. (2011). Genetic evidence that synaptonemal complex axial elements govern recombination pathway choice in mice. Genetics *189*, 71-82.

Li, X.C., and Schimenti, J.C. (2007). Mouse pachytene checkpoint 2 (trip13) is required for completing meiotic recombination but not synapsis. PLoS genetics *3*, e130.
Libby, B.J., De La Fuente, R., O'Brien, M.J., Wigglesworth, K., Cobb, J., Inselman, A., Eaker, S., Handel, M.A., Eppig, J.J., and Schimenti, J.C. (2002). The mouse meiotic mutation mei1 disrupts chromosome synapsis with sexually dimorphic consequences for meiotic progression. Dev Biol *242*, 174-187.
Lifschytz, E., and Lindsley, D.L. (1972). The role of X-chromosome inactivation during spermatogenesis (Drosophila-allocycly-chromosome evolution-male sterility-dosage compensation). Proc Natl Acad Sci U S A *69*, 182-186.
Lim, D.S., and Hasty, P. (1996). A mutation in mouse rad51 results in an early embryonic lethal that is suppressed by a mutation in p53. Mol Cell Biol *16*, 7133-7143.
Lima-de-Faria, A., and Borum, K. (1962). The period of DNA synthesis prior to meiosis in the mouse. J Cell Biol *14*, 381-388.
Lipkin, S.M., Moens, P.B., Wang, V., Lenzi, M., Shanmugarajah, D., Gilgeous, A., Thomas, J., Cheng, J., Touchman, J.W., Green, E.D.*, et al.* (2002). Meiotic arrest and aneuploidy in MLH3-deficient mice. Nat Genet *31*, 385-390.
Liu, J.G., Yuan, L., Brundell, E., Björkroth, B., Daneholt, B., and Höög, C. (1996). Localization of the N-terminus of SCP1 to the central element of the synaptonemal complex and evidence for direct interactions between the N-termini of SCP1 molecules organized head-to-head. Exp Cell Res *226*, 11-19.
Livera, G., Petre-Lazar, B., Guerquin, M.J., Trautmann, E., Coffigny, H., and Habert, R. (2008). p63 null mutation protects mouse oocytes from radio-induced apoptosis. Reproduction *135*, 3-12.
Lou, Z., Chini, C.C., Minter-Dykhouse, K., and Chen, J. (2003). Mediator of DNA damage checkpoint protein 1 regulates BRCA1 localization and phosphorylation in DNA damage checkpoint control. J Biol Chem *278*, 13599-13602.
Lou, Z., Minter-Dykhouse, K., Franco, S., Gostissa, M., Rivera, M.A., Celeste, A., Manis, J.P., van Deursen, J., Nussenzweig, A., Paull, T.T.*, et al.* (2006). MDC1 maintains genomic stability by participating in the amplification of ATM-dependent DNA damage signals. Mol Cell *21*, 187-200.
Lovejoy, C.A., and Cortez, D. (2009). Common mechanisms of PIKK regulation. DNA Repair (Amst) *8*, 1004-1008.
Lu, L.Y., Xiong, Y., Kuang, H., Korakavi, G., and Yu, X. (2013). Regulation of the DNA damage response on male meiotic sex chromosomes. Nat Commun *4*, 2105.
Ludwig, T., Chapman, D.L., Papaioannou, V.E., and Efstratiadis, A. (1997). Targeted mutations of breast cancer susceptibility gene homologs in mice: lethal phenotypes of Brca1, Brca2, Brca1/Brca2, Brca1/p53, and Brca2/p53 nullizygous embryos. Genes Dev *11*, 1226-1241.
Lukas, C., Melander, F., Stucki, M., Falck, J., Bekker-Jensen, S., Goldberg, M., Lerenthal, Y., Jackson, S.P., Bartek, J., and Lukas, J. (2004). Mdc1 couples DNA double-strand break recognition by Nbs1 with its H2AX-dependent chromatin retention. EMBO J *23*, 2674-2683.

Luoh, S.W., Bain, P.A., Polakiewicz, R.D., Goodheart, M.L., Gardner, H., Jaenisch, R., and Page, D.C. (1997). Zfx mutation results in small animal size and reduced germ cell number in male and female mice. Development *124*, 2275-2284.
Lydall, D., Nikolsky, Y., Bishop, D.K., and Weinert, T. (1996). A meiotic recombination checkpoint controlled by mitotic checkpoint genes. Nature *383*, 840-843.
Lynn, A., Ashley, T., and Hassold, T. (2004). Variation in human meiotic recombination. Annu Rev Genomics Hum Genet *5*, 317-349.
MacQueen, A.J., and Hochwagen, A. (2011). Checkpoint mechanisms: the puppet masters of meiotic prophase. Trends Cell Biol *21*, 393-400.
MacQueen, A.J., Phillips, C.M., Bhalla, N., Weiser, P., Villeneuve, A.M., and Dernburg, A.F. (2005). Chromosome sites play dual roles to establish homologous synapsis during meiosis in C. elegans. Cell *123*, 1037-1050.
MacQueen, A.J., and Villeneuve, A.M. (2001). Nuclear reorganization and homologous chromosome pairing during meiotic prophase require C. elegans chk-2. Genes Dev *15*, 1674-1687.
Mahadevaiah, S.K., Bourc'his, D., de Rooij, D.G., Bestor, T.H., Turner, J.M., and Burgoyne, P.S. (2008). Extensive meiotic asynapsis in mice antagonises meiotic silencing of unsynapsed chromatin and consequently disrupts meiotic sex chromosome inactivation. J Cell Biol *182*, 263-276.
Mahadevaiah, S.K., Costa, Y., and Turner, J.M. (2009a). Using RNA FISH to study gene expression during mammalian meiosis. Methods Mol Biol *558*, 433-444.
Mahadevaiah, S.K., Evans, E.P., and Burgoyne, P.S. (2000). An analysis of meiotic impairment and of sex chromosome associations throughout meiosis in XYY mice. Cytogenetics and cell genetics *89*, 29-37.
Mahadevaiah, S.K., Lovell-Badge, R., and Burgoyne, P.S. (1993). Tdy-negative XY, XXY and XYY female mice: breeding data and synaptonemal complex analysis. Journal of Reproduction and Fertility *97*, 151-160.
Mahadevaiah, S.K., Odorisio, T., Elliott, D.J., Rattigan, A., Szot, M., Laval, S.H., Washburn, L.L., McCarrey, J.R., Cattanach, B.M., Lovell-Badge, R.*, et al.* (1998). Mouse homologues of the human AZF candidate gene RBM are expressed in spermatogonia and spermatids, and map to a Y chromosome deletion interval associated with a high incidence of sperm abnormalities. Hum Mol Genet *7*, 715-727.
Mahadevaiah, S.K., Royo, H., VandeBerg, J.L., McCarrey, J.R., Mackay, S., and Turner, J.M. (2009b). Key features of the X inactivation process are conserved between marsupials and eutherians. Curr Biol *19*, 1478-1484.
Mahadevaiah, S.K., Turner, J.M., Baudat, F., Rogakou, E.P., de Boer, P., Blanco-Rodriguez, J., Jasin, M., Keeney, S., Bonner, W.M., and Burgoyne, P.S. (2001). Recombinational DNA double-strand breaks in mice precede synapsis. Nat Genet *27*, 271-276.
Maine, E.M. (2010). Meiotic silencing in Caenorhabditis elegans. Int Rev Cell Mol Biol *282*, 91-134.
Malki, S., van der Heijden, G.W., O'Donnell, K.A., Martin, S.L., and Bortvin, A. (2014). A role for retrotransposon LINE-1 in fetal oocyte attrition in mice. Dev Cell *29*, 521-533.

Marahrens, Y., Panning, B., Dausman, J., Strauss, W., and Jaenisch, R. (1997). Xist-deficient mice are defective in dosage compensation but not spermatogenesis. Genes Dev *11*, 156-166.
Margolin, G., Khil, P.P., Kim, J., Bellani, M.A., and Camerini-Otero, R.D. (2014). Integrated transcriptome analysis of mouse spermatogenesis. BMC Genomics *15*, 39.
Marston, A.L., and Amon, A. (2004). Meiosis: cell-cycle controls shuffle and deal. Nat Rev Mol Cell Biol *5*, 983-997.
Mazeyrat, S., Saut, N., Grigoriev, V., Mahadevaiah, S.K., Ojarikre, O.A., Rattigan A, Bishop, C., Eicher, E.M., Mitchell, M.J., and Burgoyne, P.S. (2001). A Y-encoded subunit of the translation initiation factor Eif2 is essential for mouse spermatogenesis. Nat Genet *29*, 49-53.
McCarrey, J.R., and Thomas, K. (1987). Human testis-specific PGK gene lacks introns and possesses characteristics of a processed gene. Nature *326*, 501-505.
McKee, B.D., and Handel, M.A. (1993). Sex chromosomes, recombination, and chromatin conformation. Chromosoma *102*, 71-80.
McMahill, M.S., Sham, C.W., and Bishop, D.K. (2007). Synthesis-dependent strand annealing in meiosis. PLoS Biol *5*, e299.
Meiklejohn, C.D., Landeen, E.L., Cook, J.M., Kingan, S.B., and Presgraves, D.C. (2011). Sex chromosome-specific regulation in the Drosophila male germline but little evidence for chromosomal dosage compensation or meiotic inactivation. PLoS Biol *9*, e1001126.
Metzler-Guillemain, C., and de Massy, B. (2000). Identification and characterization of an SPO11 homolog in the mouse. Chromosoma *109*, 133-138.
Metzler-Guillemain, C., Luciani, J., Depetris, D., Guichaoua, M.R., and Mattei, M.G. (2003). HP1beta and HP1gamma, but not HP1alpha, decorate the entire XY body during human male meiosis. Chromosome Res *11*, 73-81.
Meuwissen, R.L., Offenberg, H.H., Dietrich, A.J., Riesewijk, A., van Iersel, M., and Heyting, C. (1992). A coiled-coil related protein specific for synapsed regions of meiotic prophase chromosomes. EMBO J *11*, 5091-5100.
Mihola, O., Trachtulec, Z., Vlcek, C., Schimenti, J.C., and Forejt, J. (2009). A mouse speciation gene encodes a meiotic histone H3 methyltransferase. Science *323*, 373-375.
Mikhaylova, L.M., and Nurminsky, D.I. (2011). Lack of global meiotic sex chromosome inactivation, and paucity of tissue-specific gene expression on the Drosophila X chromosome. BMC Biol *9*, 29.
Milman, N., Higuchi, E., and Smith, G.R. (2009). Meiotic DNA double-strand break repair requires two nucleases, MRN and Ctp1, to produce a single size class of Rec12 (Spo11)-oligonucleotide complexes. Mol Cell Biol *29*, 5998-6005.
Mimitou, E.P., and Symington, L.S. (2009). DNA end resection: many nucleases make light work. DNA Repair (Amst) *8*, 983-995.
Minkovsky, A., Sahakyan, A., Rankin-Gee, E., Bonora, G., Patel, S., and Plath, K. (2014). The Mbd1-Atf7ip-Setdb1 pathway contributes to the maintenance of X chromosome inactivation. Epigenetics Chromatin *7*, 12.

Modzelewski, A.J., Holmes, R.J., Hilz, S., Grimson, A., and Cohen, P.E. (2012). AGO4 regulates entry into meiosis and influences silencing of sex chromosomes in the male mouse germline. Dev Cell *23*, 251-264.
Moens, P.B., Chen, D.J., Shen, Z., Kolas, N., Tarsounas, M., Heng, H.H., and Spyropoulos, B. (1997). Rad51 immunocytology in rat and mouse spermatocytes and oocytes. Chromosoma *106*, 207-215.
Moens, P.B., Kolas, N.K., Tarsounas, M., Marcon, E., Cohen, P.E., and Spyropoulos, B. (2002). The time course and chromosomal localization of recombination-related proteins at meiosis in the mouse are compatible with models that can resolve the early DNA-DNA interactions without reciprocal recombination. J Cell Sci *115*, 1611-1622.
Moens, P.B., Tarsounas, M., Morita, T., Habu, T., Rottinghaus, S.T., Freire, R., Jackson, S.P., Barlow, C., and Wynshaw-Boris, A. (1999). The association of ATR protein with mouse meiotic chromosome cores. Chromosoma *108*, 95-102.
Monesi, V. (1965). Differential rate of ribonucleic acid synthesis in the autosomes and sex chromosomes during male meiosis in the mouse. Chromosoma *17*, 11-21.
Monk, M., and McLaren, A. (1981). X-chromosome activity in foetal germ cells of the mouse. J Embryol Exp Morphol *63*, 75-84.
Montini, E., Buchner, G., Spalluto, C., Andolfi, G., Caruso, A., den Dunnen, J.T., Trump, D., Rocchi, M., Ballabio, A., and Franco, B. (1999). Identification of SCML2, a second human gene homologous to the Drosophila sex comb on midleg (Scm): A new gene cluster on Xp22. Genomics *58*, 65-72.
Morelli, M.A., and Cohen, P.E. (2005). Not all germ cells are created equal: aspects of sexual dimorphism in mammalian meiosis. Reproduction *130*, 761-781.
Moynahan, M.E., Chiu, J.W., Koller, B.H., and Jasin, M. (1999). Brca1 controls homology-directed DNA repair. Mol Cell *4*, 511-518.
Mueller, J.L., Mahadevaiah, S.K., Park, P.J., Warburton, P.E., Page, D.C., and Turner, J.M. (2008). The mouse X chromosome is enriched for multicopy testis genes showing postmeiotic expression. Nat Genet *40*, 794-799.
Mullan, P.B., Quinn, J.E., and Harkin, D.P. (2006). The role of BRCA1 in transcriptional regulation and cell cycle control. Oncogene *25*, 5854-5863.
Murakami, H., and Keeney, S. (2008). Regulating the formation of DNA double-strand breaks in meiosis. Genes Dev *22*, 286-292.
Nagaoka, S.I., Hassold, T.J., and Hunt, P.A. (2012). Human aneuploidy: mechanisms and new insights into an age-old problem. Nat Rev Genet *13*, 493-504.
Nagaoka, S.I., Hodges, C.A., Albertini, D.F., and Hunt, P.A. (2011). Oocyte-specific differences in cell-cycle control create an innate susceptibility to meiotic errors. Curr Biol *21*, 651-657.
Namekawa, S.H., Park, P.J., Zhang, L.F., Shima, J.E., McCarrey, J.R., Griswold, M.D., and Lee, J.T. (2006). Postmeiotic sex chromatin in the male germline of mice. Current Biology *16*, 660-667.
Namekawa, S.H., VandeBerg, J.L., McCarrey, J.R., and Lee, J.T. (2007). Sex chromosome silencing in the marsupial male germ line. Proc Natl Acad Sci U S A *104*, 9730-9735.

Neale, M.J., and Keeney, S. (2006). Clarifying the mechanics of DNA strand exchange in meiotic recombination. Nature *442*, 153-158.
Neale, M.J., Pan, J., and Keeney, S. (2005). Endonucleolytic processing of covalent protein-linked DNA double-strand breaks. Nature *436*, 1053-1057.
Niu, H., Wan, L., Baumgartner, B., Schaefer, D., Loidl, J., and Hollingsworth, N.M. (2005). Partner choice during meiosis is regulated by Hop1-promoted dimerization of Mek1. Mol Biol Cell *16*, 5804-5818.
O'Carroll, D., Scherthan, H., Peters, A.H., Opravil, S., Haynes, A.R., Laible, G., Rea, S., Schmid, M., Lebersorger, A., Jerratsch, M.*, et al.* (2000). Isolation and characterization of Suv39h2, a second histone H3 methyltransferase gene that displays testis-specific expression. Mol Cell Biol *20*, 9423-9433.
O'Connell, M.J., and Cimprich, K.A. (2005). G2 damage checkpoints: what is the turn-on? J Cell Sci *118*, 1-6.
O'Doherty, A., Ruf, S., Mulligan, C., Hildreth, V., Errington, M.L., Cooke, S., Sesay, A., Modino, S., Vanes, L., Hernandez, D.*, et al.* (2005). An aneuploid mouse strain carrying human chromosome 21 with Down syndrome phenotypes. Science *309*, 2033-2037.
Offenberg, H.H., Schalk, J.A., Meuwissen, R.L., van Aalderen, M., Kester, H.A., Dietrich, A.J., and Heyting, C. (1998). SCP2: a major protein component of the axial elements of synaptonemal complexes of the rat. Nucleic Acids Res *26*, 2572-2579.
Oliver, T.R., Feingold, E., Yu, K., Cheung, V., Tinker, S., Yadav-Shah, M., Masse, N., and Sherman, S.L. (2008). New insights into human nondisjunction of chromosome 21 in oocytes. PLoS Genet *4*, e1000033.
Ollinger, R., Alsheimer, M., and Benavente, R. (2005). Mammalian protein SCP1 forms synaptonemal complex-like structures in the absence of meiotic chromosomes. Mol Biol Cell *16*, 212-217.
Ollinger, R., Childs, A.J., Burgess, H.M., Speed, R.M., Lundegaard, P.R., Reynolds, N., Gray, N.K., Cooke, H.J., and Adams, I.R. (2008). Deletion of the pluripotency-associated Tex19.1 gene causes activation of endogenous retroviruses and defective spermatogenesis in mice. PLoS Genet *4*, e1000199.
Ollinger, R., Reichmann, J., and Adams, I.R. (2010). Meiosis and retrotransposon silencing during germ cell development in mice. Differentiation *79*, 147-158.
Pacheco, S., Marcet-Ortega, M., Lange, J., Jasin, M., Keeney, S., and Roig, I. (2015). The ATM signaling cascade promotes recombination-dependent pachytene arrest in mouse spermatocytes. PLoS Genet *11*, e1005017.
Paigen, K., and Petkov, P. (2010). Mammalian recombination hot spots: properties, control and evolution. Nat Rev Genet *11*, 221-233.
Parikh, R.A., White, J.S., Huang, X., Schoppy, D.W., Baysal, B.E., Baskaran, R., Bakkenist, C.J., Saunders, W.S., Hsu, L.C., Romkes, M.*, et al.* (2007). Loss of distal 11q is associated with DNA repair deficiency and reduced sensitivity to ionizing radiation in head and neck squamous cell carcinoma. Genes Chromosomes Cancer *46*, 761-775.
Parvanov, E.D., Petkov, P.M., and Paigen, K. (2010). Prdm9 controls activation of mammalian recombination hotspots. Science *327*, 835.

Paull, T.T., Rogakou, E.P., Yamazaki, V., Kirchgessner, C.U., Gellert, M., and Bonner, W.M. (2000). A critical role for histone H2AX in recruitment of repair factors to nuclear foci after DNA damage. Curr Biol *10*, 886-895.
Pepling, M.E., and Spradling, A.C. (2001). Mouse ovarian germ cell cysts undergo programmed breakdown to form primordial follicles. Dev Biol *234*, 339-351.
Perera, D., Perez-Hidalgo, L., Moens, P.B., Reini, K., Lakin, N., Syväoja, J.E., San-Segundo, P.A., and Freire, R. (2004). TopBP1 and ATR colocalization at meiotic chromosomes: role of TopBP1/Cut5 in the meiotic recombination checkpoint. Mol Biol Cell *15*, 1568-1579.
Perry, J., Palmer, S., Gabriel, A., and Ashworth, A. (2001). A short pseudoautosomal region in laboratory mice. Genome Res *11*, 1826-1832.
Peters, A.H., Plug, A.W., van Vugt, M.J., and de Boer, P. (1997). A drying-down technique for the spreading of mammalian meiocytes from the male and female germline. Chromosome Res *5*, 66-68.
Petersen, S., Casellas, R., Reina-San-Martin, B., Chen, H.T., Difilippantonio, M.J., Wilson, P.C., Hanitsch, L., Celeste, A., Muramatsu, M., Pilch, D.R.*, et al.* (2001). AID is required to initiate Nbs1/gamma-H2AX focus formation and mutations at sites of class switching. Nature *414*, 660-665.
Pilch, D.R., Sedelnikova, O.A., Redon, C., Celeste, A., Nussenzweig, A., and Bonner, W.M. (2003). Characteristics of gamma-H2AX foci at DNA double-strand breaks sites. Biochem Cell Biol *81*, 123-129.
Pittman, D.L., Cobb, J., Schimenti, K.J., Wilson, L.A., Cooper, D.M., Brignull, E., Handel, M.A., and Schimenti, J.C. (1998). Meiotic prophase arrest with failure of chromosome synapsis in mice deficient for Dmc1, a germline-specific RecA homolog. Molecular cell *1*, 697-705.
Plug, A.W., Peters, A.H., Keegan, K.S., Hoekstra, M.F., de Boer, P., and Ashley, T. (1998). Changes in protein composition of meiotic nodules during mammalian meiosis. J Cell Sci *111 (Pt 4)*, 413-423.
Plug, A.W., Peters, A.H., Xu, Y., Keegan, K.S., Hoekstra, M.F., Baltimore, D., de Boer, P., and Ashley, T. (1997). ATM and RPA in meiotic chromosome synapsis and recombination. Nat Genet *17*, 457-461.
Pérez-Hidalgo, L., Moreno, S., and San-Segundo, P.A. (2003). Regulation of meiotic progression by the meiosis-specific checkpoint kinase Mek1 in fission yeast. J Cell Sci *116*, 259-271.
Redon, C., Pilch, D., Rogakou, E., Sedelnikova, O., Newrock, K., and Bonner, W. (2002). Histone H2A variants H2AX and H2AZ. Curr Opin Genet Dev *12*, 162-169.
Refolio, E., Cavero, S., Marcon, E., Freire, R., and San-Segundo, P.A. (2011). The Ddc2/ATRIP checkpoint protein monitors meiotic recombination intermediates. J Cell Sci *124*, 2488-2500.
Reinholdt, L.G., and Schimenti, J.C. (2005). Mei1 is epistatic to Dmc1 during mouse meiosis. Chromosoma *114*, 127-134.
Reini, K., Uitto, L., Perera, D., Moens, P.B., Freire, R., and Syväoja, J.E. (2004). TopBP1 localises to centrosomes in mitosis and to chromosome cores in meiosis. Chromosoma *112*, 323-330.
Revenkova, E., Eijpe, M., Heyting, C., Hodges, C.A., Hunt, P.A., Liebe, B., Scherthan, H., and Jessberger, R. (2004). Cohesin SMC1 beta is required for

meiotic chromosome dynamics, sister chromatid cohesion and DNA recombination. Nat Cell Biol *6*, 555-562.
Reynolds, A., Qiao, H., Yang, Y., Chen, J.K., Jackson, N., Biswas, K., Holloway, J.K., Baudat, F., de Massy, B., Wang, J.*, et al.* (2013). RNF212 is a dosage-sensitive regulator of crossing-over during mammalian meiosis. Nat Genet *45*, 269-278.
Roeder, G.S., and Bailis, J.M. (2000). The pachytene checkpoint. Trends Genet *16*, 395-403.
Rogakou, E.P., Boon, C., Redon, C., and Bonner, W.M. (1999). Megabase chromatin domains involved in DNA double-strand breaks in vivo. J Cell Biol *146*, 905-916.
Rogakou, E.P., Pilch, D.R., Orr, A.H., Ivanova, V.S., and Bonner, W.M. (1998). DNA double-stranded breaks induce histone H2AX phosphorylation on serine 139. J Biol Chem *273*, 5858-5868.
Rogers, R.S., Inselman, A., Handel, M.A., and Matunis, M.J. (2004). SUMO modified proteins localize to the XY body of pachytene spermatocytes. Chromosoma *113*, 233-243.
Roig, I., Dowdle, J.A., Toth, A., de Rooij, D.G., Jasin, M., and Keeney, S. (2010). Mouse TRIP13/PCH2 Is Required for Recombination and Normal Higher-Order Chromosome Structure during Meiosis. PLoS Genet *6*, e1001062.
Romanienko, P.J., and Camerini-Otero, R.D. (2000). The mouse Spo11 gene is required for meiotic chromosome synapsis. Mol Cell *6*, 975-987.
Royo, H., Polikiewicz, G., Mahadevaiah, S.K., Prosser, H., Mitchell, M., Bradley, A., de Rooij, D.G., Burgoyne, P.S., and Turner, J.M. (2010). Evidence that meiotic sex chromosome inactivation is essential for male fertility. Curr Biol *20*, 2117-2123.
Royo, H., Prosser, H., Ruzankina, Y., Mahadevaiah, S.K., Cloutier, J.M., Baumann, M., Fukuda, T., Höög, C., Tóth, A., de Rooij, D.G.*, et al.* (2013). ATR acts stage specifically to regulate multiple aspects of mammalian meiotic silencing. Genes Dev *27*, 1484-1494.
Sachs, L. (1954). Sex-linkage and the sex chromosomes in man. Ann Eugen *18*, 255-261.
Sakaguchi, K., Ishibashi, T., Uchiyama, Y., and Iwabata, K. (2009). The multi-replication protein A (RPA) system--a new perspective. FEBS J *276*, 943-963.
Salido, E.C., Li, X.M., Yen, P.H., Martin, N., Mohandas, T.K., and Shapiro, L.J. (1996). Cloning and expression of the mouse pseudoautosomal steroid sulphatase gene (Sts). Nat Genet *13*, 83-86.
San-Segundo, P.A., and Roeder, G.S. (1999). Pch2 Links Chromatin Silencing to Meiotic Checkpoint Control. Cell *97*, 313-324.
Schimenti, J. (2005). Synapsis or silence. Nat Genet *37*, 11-13.
Schoenmakers, S., Wassenaar, E., Hoogerbrugge, J.W., Laven, J.S., Grootegoed, J.A., and Baarends, W.M. (2009). Female meiotic sex chromosome inactivation in chicken. PLoS Genet *5*, e1000466.
Schoenmakers, S., Wassenaar, E., Laven, J.S., Grootegoed, J.A., and Baarends, W.M. (2010). Meiotic silencing and fragmentation of the male germline restricted chromosome in zebra finch. Chromosoma *119*, 311-324.
Schoenmakers, S., Wassenaar, E., van Cappellen, W.A., Derijck, A.A., de Boer, P., Laven, J.S., Grootegoed, J.A., and Baarends, W.M. (2008). Increased frequency of asynapsis and associated meiotic silencing of heterologous

chromatin in the presence of irradiation-induced extra DNA double strand breaks. Dev Biol *317*, 270-281.
Schramm, S., Fraune, J., Naumann, R., Hernandez-Hernandez, A., Höög, C., Cooke, H.J., Alsheimer, M., and Benavente, R. (2011). A novel mouse synaptonemal complex protein is essential for loading of central element proteins, recombination, and fertility. PLoS Genet *7*, e1002088.
Schwacha, A., and Kleckner, N. (1994). Identification of joint molecules that form frequently between homologs but rarely between sister chromatids during yeast meiosis. Cell *76*, 51-63.
Schwacha, A., and Kleckner, N. (1995). Identification of double Holliday junctions as intermediates in meiotic recombination. Cell *83*, 783-791.
Schwacha, A., and Kleckner, N. (1997). Interhomolog bias during meiotic recombination: meiotic functions promote a highly differentiated interhomolog-only pathway. Cell *90*, 1123-1135.
Sciurano, R., Rahn, M., Rey-Valzacchi, G., and Solari, A.J. (2007). The asynaptic chromatin in spermatocytes of translocation carriers contains the histone variant gamma-H2AX and associates with the XY body. Hum Reprod *22*, 142-150.
Scully, R., Chen, J., Plug, A., Xiao, Y., Weaver, D., Feunteun, J., Ashley, T., and Livingston, D.M. (1997). Association of BRCA1 with Rad51 in mitotic and meiotic cells. Cell *88*, 265-275.
Searle, A.G., Beechy , C. V. and Evans, E. P . (1978). Meiotic effects in chromosomally derived sterility of mice. (*Annales de Biologie animale Biochemie et Biophysique*), pp. 391-398.
Shannon, M., Richardson, L., Christian, A., Handel, M.A., and Thelen, M.P. (1999). Differential gene expression of mammalian SPO11/TOP6A homologs during meiosis. FEBS Lett *462*, 329-334.
Shimada, M., Nabeshima, K., Tougan, T., and Nojima, H. (2002). The meiotic recombination checkpoint is regulated by checkpoint rad+ genes in fission yeast. EMBO J *21*, 2807-2818.
Shin, M., Besser, L.M., Kucik, J.E., Lu, C., Siffel, C., Correa, A., and Collaborative, C.A.M.P.a.S. (2009). Prevalence of Down syndrome among children and adolescents in 10 regions of the United States. Pediatrics *124*, 1565-1571.
Shin, Y.H., Choi, Y., Erdin, S.U., Yatsenko, S.A., Kloc, M., Yang, F., Wang, P.J., Meistrich, M.L., and Rajkovic, A. (2010). Hormad1 mutation disrupts synaptonemal complex formation, recombination, and chromosome segregation in Mammalian meiosis. PLoS Genet *6*, e1001190.
Shin, Y.H., McGuire, M.M., and Rajkovic, A. (2013). Mouse HORMAD1 is a meiosis i checkpoint protein that modulates DNA double- strand break repair during female meiosis. Biol Reprod *89*, 29.
Shiu, P.K., Raju, N.B., Zickler, D., and Metzenberg, R.L. (2001). Meiotic silencing by unpaired DNA. Cell *107*, 905-916.
Shrivastava, V., Pekar, M., Grosser, E., Im, J., and Vigodner, M. (2010). SUMO proteins are involved in the stress response during spermatogenesis and are localized to DNA double-strand breaks in germ cells. Reproduction *139*, 999-1010.
Shroff, R., Arbel-Eden, A., Pilch, D., Ira, G., Bonner, W.M., Petrini, J.H., Haber, J.E., and Lichten, M. (2004). Distribution and dynamics of chromatin

modification induced by a defined DNA double-strand break. Current biology : CB *14*, 1703-1711.
Smagulova, F., Gregoretti, I.V., Brick, K., Khil, P., Camerini-Otero, R.D., and Petukhova, G.V. (2011). Genome-wide analysis reveals novel molecular features of mouse recombination hotspots. Nature *472*, 375-378.
Solari, A.J. (1964). THE MORPHOLOGY AND ULTRASTRUCTURE OF THE SEX VESICLE IN THE MOUSE. Exp Cell Res *36*, 160-168.
Solari, A.J. (1974). The behavior of the XY pair in mammals. Int Rev Cytol *38*, 273-317.
Song, R., Ro, S., Michaels, J.D., Park, C., McCarrey, J.R., and Yan, W. (2009). Many X-linked microRNAs escape meiotic sex chromosome inactivation. Nature genetics *41*, 488-493.
Soper, S.F., van der Heijden, G.W., Hardiman, T.C., Goodheart, M., Martin, S.L., de Boer, P., and Bortvin, A. (2008). Mouse maelstrom, a component of nuage, is essential for spermatogenesis and transposon repression in meiosis. Dev Cell *15*, 285-297.
Speed, R.M. (1982). Meiosis in the foetal mouse ovary. I. An analysis at the light microscope level using surface-spreading. Chromosoma *85*, 427-437.
Speed, R.M. (1986). Oocyte development in XO foetuses of man and mouse: the possible role of heterologous X-chromosome pairing in germ cell survival. Chromosoma *94*, 115-124.
Srivastava, N., Gochhait, S., de Boer, P., and Bamezai, R.N. (2009). Role of H2AX in DNA damage response and human cancers. Mutat Res *681*, 180-188.
Srivastava, N., Gochhait, S., Gupta, P., and Bamezai, R.N. (2008). Copy number alterations of the H2AFX gene in sporadic breast cancer patients. Cancer Genet Cytogenet *180*, 121-128.
Stergiou, L., and Hengartner, M.O. (2004). Death and more: DNA damage response pathways in the nematode C. elegans. Cell Death Differ *11*, 21-28.
Stewart, G.S., Wang, B., Bignell, C.R., Taylor, A.M., and Elledge, S.J. (2003). MDC1 is a mediator of the mammalian DNA damage checkpoint. Nature *421*, 961-966.
Stracker, T.H., Usui, T., and Petrini, J.H. (2009). Taking the time to make important decisions: the checkpoint effector kinases Chk1 and Chk2 and the DNA damage response. DNA Repair (Amst) *8*, 1047-1054.
Stucki, M., Clapperton, J.A., Mohammad, D., Yaffe, M.B., Smerdon, S.J., and Jackson, S.P. (2005). MDC1 directly binds phosphorylated histone H2AX to regulate cellular responses to DNA double-strand breaks. Cell *123*, 1213-1226.
Sun, H., Treco, D., and Szostak, J.W. (1991). Extensive 3'-overhanging, single-stranded DNA associated with the meiosis-specific double-strand breaks at the ARG4 recombination initiation site. Cell *64*, 1155-1161.
Sun, S.C., and Kim, N.H. (2012). Spindle assembly checkpoint and its regulators in meiosis. Hum Reprod Update *18*, 60-72.
Takai, H., Naka, K., Okada, Y., Watanabe, M., Harada, N., Saito, S., Anderson, C.W., Appella, E., Nakanishi, M., Suzuki, H.*, et al.* (2002). Chk2-deficient mice exhibit radioresistance and defective p53-mediated transcription. EMBO J *21*, 5195-5205.

Taketo, T., and Naumova, A.K. (2013). Oocyte heterogeneity with respect to the meiotic silencing of unsynapsed X chromosomes in the XY female mouse. Chromosoma *122*, 337-349.
Tarsounas, M., Morita, T., Pearlman, R.E., and Moens, P.B. (1999). RAD51 and DMC1 form mixed complexes associated with mouse meiotic chromosome cores and synaptonemal complexes. J Cell Biol *147*, 207-220.
Tarsounas, M., Pearlman, R.E., Gasser, P.J., Park, M.S., and Moens, P.B. (1997). Protein-protein interactions in the synaptonemal complex. Mol Biol Cell *8*, 1405-1414.
Tease, C., and Fisher, G. (1986). Further examination of the production-line hypothesis in mouse foetal oocytes. I. Inversion heterozygotes. Chromosoma *93*, 447-452.
Thacker, D., Mohibullah, N., Zhu, X., and Keeney, S. (2014). Homologue engagement controls meiotic DNA break number and distribution. Nature *510*, 241-246.
Traven, A., and Heierhorst, J. (2005). SQ/TQ cluster domains: concentrated ATM/ATR kinase phosphorylation site regions in DNA-damage-response proteins. Bioessays *27*, 397-407.
Tsubouchi, T., Zhao, H., and Roeder, G.S. (2006). The meiosis-specific zip4 protein regulates crossover distribution by promoting synaptonemal complex formation together with zip2. Dev Cell *10*, 809-819.
Tung, K.S., Hong, E.J., and Roeder, G.S. (2000). The pachytene checkpoint prevents accumulation and phosphorylation of the meiosis-specific transcription factor Ndt80. Proc Natl Acad Sci U S A *97*, 12187-12192.
Turner, J.M. (2007). Meiotic sex chromosome inactivation. Development *134*, 1823-1831.
Turner, J.M., Aprelikova, O., Xu, X., Wang, R., Kim, S., Chandramouli, G.V., Barrett, J.C., Burgoyne, P.S., and Deng, C.X. (2004). BRCA1, histone H2AX phosphorylation, and male meiotic sex chromosome inactivation. Curr Biol *14*, 2135-2142.
Turner, J.M., Mahadevaiah, S.K., Ellis, P.J., Mitchell, M.J., and Burgoyne, P.S. (2006). Pachytene asynapsis drives meiotic sex chromosome inactivation and leads to substantial postmeiotic repression in spermatids. Dev Cell *10*, 521-529.
Turner, J.M., Mahadevaiah, S.K., Fernandez-Capetillo, O., Nussenzweig, A., Xu, X., Deng, C.X., and Burgoyne, P.S. (2005). Silencing of unsynapsed meiotic chromosomes in the mouse. Nat Genet *37*, 41-47.
Unal, E., Arbel-Eden, A., Sattler, U., Shroff, R., Lichten, M., Haber, J.E., and Koshland, D. (2004). DNA damage response pathway uses histone modification to assemble a double-strand break-specific cohesin domain. Molecular cell *16*, 991-1002.
van Attikum, H., and Gasser, S.M. (2009). Crosstalk between histone modifications during the DNA damage response. Trends Cell Biol *19*, 207-217.
van der Heijden, G.W., Derijck, A.A., Posfai, E., Giele, M., Pelczar, P., Ramos, L., Wansink, D.G., van der Vlag, J., Peters, A.H., and de Boer, P. (2007). Chromosome-wide nucleosome replacement and H3.3 incorporation during mammalian meiotic sex chromosome inactivation. Nat Genet *39*, 251-258.

Vernet, N., Mahadevaiah, S.K., Ojarikre, O.A., Longepied, G., Prosser, H.M., Bradley, A., Mitchell, M.J., and Burgoyne, P.S. (2011). The Y-encoded gene zfy2 acts to remove cells with unpaired chromosomes at the first meiotic metaphase in male mice. Current biology : CB *21*, 787-793.
Vibranovski, M.D. (2014). Meiotic sex chromosome inactivation in Drosophila. J Genomics *2*, 104-117.
Vibranovski, M.D., Lopes, H.F., Karr, T.L., and Long, M. (2009). Stage-specific expression profiling of Drosophila spermatogenesis suggests that meiotic sex chromosome inactivation drives genomic relocation of testis-expressed genes. PLoS Genet *5*, e1000731.
Viera, A., Rufas, J.S., Martínez, I., Barbero, J.L., Ortega, S., and Suja, J.A. (2009). CDK2 is required for proper homologous pairing, recombination and sex-body formation during male mouse meiosis. J Cell Sci *122*, 2149-2159.
Vigodner, M. (2009). Sumoylation precedes accumulation of phosphorylated H2AX on sex chromosomes during their meiotic inactivation. Chromosome Res *17*, 37-45.
Vigodner, M., and Morris, P.L. (2005). Testicular expression of small ubiquitin-related modifier-1 (SUMO-1) supports multiple roles in spermatogenesis: silencing of sex chromosomes in spermatocytes, spermatid microtubule nucleation, and nuclear reshaping. Dev Biol *282*, 480-492.
Wallace, B.M., and Hultén, M.A. (1985). Meiotic chromosome pairing in the normal human female. Ann Hum Genet *49*, 215-226.
Wang, H., and Hoog, C. (2006). Structural damage to meiotic chromosomes impairs DNA recombination and checkpoint control in mammalian oocytes. J Cell Biol *173*, 485-495.
Wang, H., Wang, M., Böcker, W., and Iliakis, G. (2005a). Complex H2AX phosphorylation patterns by multiple kinases including ATM and DNA-PK in human cells exposed to ionizing radiation and treated with kinase inhibitors. J Cell Physiol *202*, 492-502.
Wang, L., Liu, W., Zhao, W., Song, G., Wang, G., Wang, X., and Sun, F. (2014). Phosphorylation of CDK2 on Threonine 160 Influences Silencing of Sex Chromosome During Male Meiosis. Biol Reprod *90*, 138.
Wang, P.J. (2004). X chromosomes, retrogenes and their role in male reproduction. Trends Endocrinol Metab *15*, 79-83.
Wang, P.J., Page, D.C., and McCarrey, J.R. (2005b). Differential expression of sex-linked and autosomal germ-cell-specific genes during spermatogenesis in the mouse. Human molecular genetics *14*, 2911.
Wang, W.H., and Sun, Q.Y. (2006). Meiotic spindle, spindle checkpoint and embryonic aneuploidy. Front Biosci *11*, 620-636.
Wang, X., and Haber, J.E. (2004). Role of Saccharomyces single-stranded DNA-binding protein RPA in the strand invasion step of double-strand break repair. PLoS Biol *2*, E21.
Ward, I.M., Minn, K., van Deursen, J., and Chen, J. (2003). p53 Binding protein 53BP1 is required for DNA damage responses and tumor suppression in mice. Mol Cell Biol *23*, 2556-2563.
Weinert, T.A., and Hartwell, L.H. (1988). The RAD9 gene controls the cell cycle response to DNA damage in Saccharomyces cerevisiae. Science *241*, 317-322.

Weiss, R.S., Enoch, T., and Leder, P. (2000). Inactivation of mouse Hus1 results in genomic instability and impaired responses to genotoxic stress. Genes Dev *14*, 1886-1898.
Wojtasz, L., Cloutier, J.M., Baumann, M., Daniel, K., Varga, J., Fu, J., Anastassiadis, K., Stewart, A.F., Reményi, A., Turner, J.M.*, et al.* (2012). Meiotic DNA double-strand breaks and chromosome asynapsis in mice are monitored by distinct HORMAD2-independent and -dependent mechanisms. Genes Dev *26*, 958-973.
Wojtasz, L., Daniel, K., Roig, I., Bolcun-Filas, E., Xu, H., Boonsanay, V., Eckmann, C.R., Cooke, H.J., Jasin, M., Keeney, S.*, et al.* (2009). Mouse HORMAD1 and HORMAD2, two conserved meiotic chromosomal proteins, are depleted from synapsed chromosome axes with the help of TRIP13 AAA-ATPase. PLoS Genet *5*, e1000702.
Wold, M.S. (1997). Replication protein A: a heterotrimeric, single-stranded DNA-binding protein required for eukaryotic DNA metabolism. Annu Rev Biochem *66*, 61-92.
Wu, H.Y., and Burgess, S.M. (2006). Two distinct surveillance mechanisms monitor meiotic chromosome metabolism in budding yeast. Curr Biol *16*, 2473-2479.
Xu, X., Aprelikova, O., Moens, P., Deng, C.X., and Furth, P.A. (2003). Impaired meiotic DNA-damage repair and lack of crossing-over during spermatogenesis in BRCA1 full-length isoform deficient mice. Development *130*, 2001-2012.
Xu, X., Qiao, W., Linke, S.P., Cao, L., Li, W.M., Furth, P.A., Harris, C.C., and Deng, C.X. (2001). Genetic interactions between tumor suppressors Brca1 and p53 in apoptosis, cell cycle and tumorigenesis. Nat Genet *28*, 266-271.
Xu, X., Wagner, K.U., Larson, D., Weaver, Z., Li, C., Ried, T., Hennighausen, L., Wynshaw-Boris, A., and Deng, C.X. (1999). Conditional mutation of Brca1 in mammary epithelial cells results in blunted ductal morphogenesis and tumour formation. Nat Genet *22*, 37-43.
Yang, F., De La Fuente, R., Leu, N.A., Baumann, C., McLaughlin, K.J., and Wang, P.J. (2006). Mouse SYCP2 is required for synaptonemal complex assembly and chromosomal synapsis during male meiosis. J Cell Biol *173*, 497-507.
Yang, F., Gell, K., van der Heijden, G.W., Eckardt, S., Leu, N.A., Page, D.C., Benavente, R., Her, C., Höög, C., McLaughlin, K.J.*, et al.* (2008). Meiotic failure in male mice lacking an X-linked factor. Genes Dev *22*, 682-691.
Yoshida, K., Kondoh, G., Matsuda, Y., Habu, T., Nishimune, Y., and Morita, T. (1998). The mouse RecA-like gene Dmc1 is required for homologous chromosome synapsis during meiosis. Molecular cell *1*, 707-718.
Yuan, L., Liu, J.G., Hoja, M.R., Wilbertz, J., Nordqvist, K., and Hoog, C. (2002). Female germ cell aneuploidy and embryo death in mice lacking the meiosis-specific protein SCP3. Science *296*, 1115-1118.
Yuan, L., Liu, J.G., Zhao, J., Brundell, E., Daneholt, B., and Hoog, C. (2000). The murine SCP3 gene is required for synaptonemal complex assembly, chromosome synapsis, and male fertility. Mol Cell *5*, 73-83.
Yuen, B.T., Bush, K.M., Barrilleaux, B.L., Cotterman, R., and Knoepfler, P.S. (2014). Histone H3.3 regulates dynamic chromatin states during spermatogenesis. Development *141*, 3483-3494.

Zhang, L., Kim, K.P., Kleckner, N.E., and Storlazzi, A. (2011). Meiotic double-strand breaks occur once per pair of (sister) chromatids and, via Mec1/ATR and Tel1/ATM, once per quartet of chromatids. Proc Natl Acad Sci U S A *108*, 20036-20041.
Zhao, H., Watkins, J.L., and Piwnica-Worms, H. (2002). Disruption of the checkpoint kinase 1/cell division cycle 25A pathway abrogates ionizing radiation-induced S and G2 checkpoints. Proc Natl Acad Sci U S A *99*, 14795-14800.
Zhou, B.B., and Bartek, J. (2004). Targeting the checkpoint kinases: chemosensitization versus chemoprotection. Nat Rev Cancer *4*, 216-225.
Zou, L., and Elledge, S.J. (2003). Sensing DNA damage through ATRIP recognition of RPA-ssDNA complexes. Science *300*, 1542-1548.